VERLAG DER TECHNISCHEN UNIVERSITÄT GRAZ

Andreas Hackl

Enhanced Tyre Modelling for Vehicle Dynamics Control Systems

Experimental Validation of Transient and Temperature Influences on Tyre Force Behaviour

FTG 8

MONOGRAPHIC SERIES TU GRAZ
REIHE FAHRZEUGTECHNIK

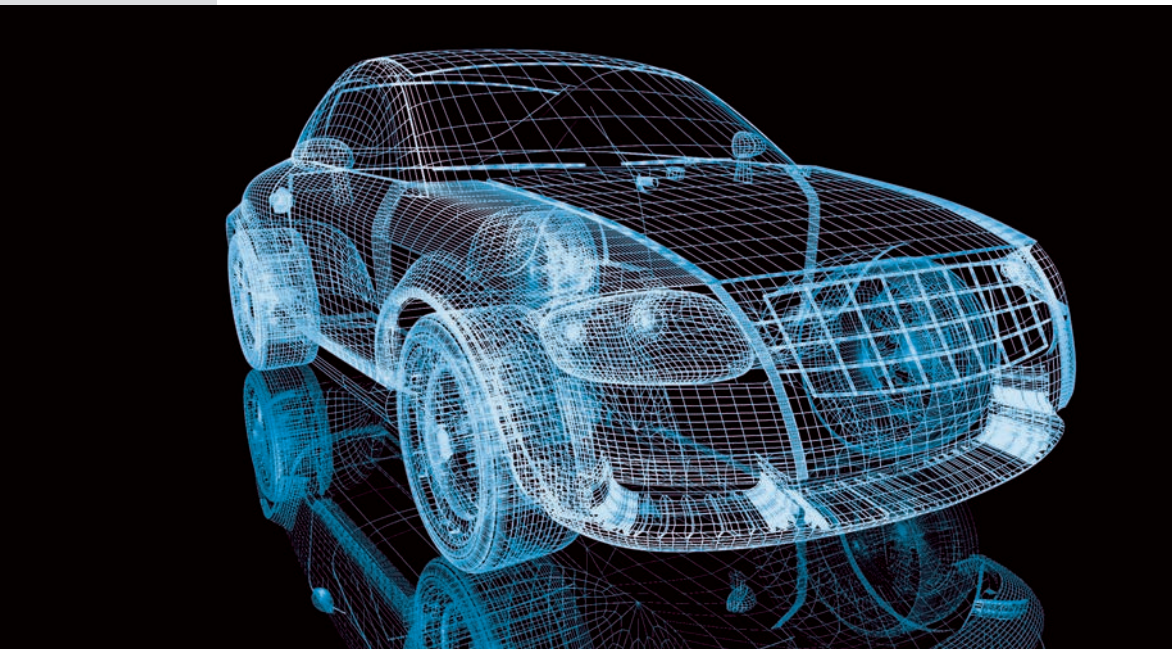

Andreas Hackl

Enhanced Tyre Modelling for Vehicle Dynamics Control Systems

Experimental Validation of Transient and Temperature Influences on Tyre Force Behaviour

Monographic Series TU Graz

Reihe Fahrzeugtechnik

Series Editor:

Institute of Automotive Engineering

Monographic Series TU Graz

Reihe Fahrzeugtechnik Volume 8

Andreas Hackl

Enhanced Tyre Modelling for Vehicle Dynamics Control Systems

Experimental Validation of Transient and Temperature Influences on Tyre Force Behaviour

This work is based on the dissertation *"Enhanced Tyre Modelling for Vehicle Dynamics Control Systems: Experimental Validation of Transient and Temperature Influences on Tyre Force Behaviour"*, presented at Graz University of Technology, Institute of Automotive Engineering in October 2019.

Assessment:
Wolfgang Hirschberg (Graz University of Technology)
Ralph Mayer (Chemnitz University of Technology)

Supervision:
Wolfgang Hirschberg (Graz University of Technology)
Georg Rill (Ostbayerische Technische Hochschule Regensburg)

Cover photo	'concept car' von ArchMen (modified) Fotolia / Adobe Stock
Cover layout	Christina Fraueneder, TU Graz Stefan Schleich, TU Graz
Print	DATAFORM Media Ges.m.b.H.

Print
ISBN 978-3-85125-728-1

E-Book
ISBN 978-3-85125-729-8
DOI 10.3217/978-3-85125-728-1

Acknowledgement

This thesis was produced during my work as a scientific assistant at the Institute of Automotive Engineering at Graz University of Technology. Here, I want to thank the persons who have significantly supported my work on this project over the last few years.

My most sincere thanks go to my supervisor Univ.-Prof.i.R. Dr. techn. Wolfgang Hirschberg. Not only for his valuable technical advice and precise scientific direction, but also for our many open and fruitful discussions. His encouraging words helped me through the hard times while completing this work. Furthermore, I also would like to thank Prof. Dr.-Ing. Georg Rill, Professor Emeritus at OTH Regensburg, who acted as second supervisor during the thesis, not only for providing me with the TMeasy tyre model, but also for all the overall support in scientific, technical and non-technical matters.

I would also like to thank Univ.-Prof. Dr.-Ing. Ralph Mayer, head of the Institute of Vehicle System Design at Chemnitz University of Technology, for his decision to serve as second assessor of my work, for his interest in the thesis and for our related discussions.

A special thanks also goes to all of my colleagues at the institute, especially those within the department of Vehicle Dynamics and Tyres: Martin Schabauer, Dr. Liang Shao and Christoph Scherndl under direction of Ass.Prof. Dr.techn. Cornelia Lex. The interesting discussions and the subsequent suggestions resulted in the continuous evolution of this thesis.

A special thanks also to our cooperation partner ThyssenKrupp Presta AG. It is only with their cooperation that the quite costly tyre measurements on an industrial flat track test bench were possible. Special thanks to the Vehicle Dynamics and Testing Group under the direction of Kristof Polmans.

Another industrial partner that I would like to thank is AVL List GmbH and the departmental group working with Lead Engineer Rupert Scheucher. With their support and the possibility to do measurements on their tyre section prototype test bench, fundamental knowledge of rubber physics was gained.

A special thank you goes to my family. I am very grateful to my parents, Friedrich and Brigitte Hackl, for enabling me to study, as well as my brother Stefan Hackl who will always be there to encourage me when needed. Finally, my heartfelt appreciation goes to my domestic partner Manuela Kirchengast, thank you for all the emotional and mental support throughout the duration of the project.

Last but not least, my gratitude goes to all of my friends, each of whom contributed in their own way to helping me to keep an eye on the goal, find new motivation and finish this work.

Thank you all for your support!

Andreas Hackl
Graz, August 2019

Abstract

Modelling and simulation of safety-related *advanced driver assistance systems* (ADAS) and *vehicle dynamics controller* (VDC) have become a state of the art tool to reduce development time and save costs. In order to meet the ever growing demands for shorter calculation time, higher accuracy and greater ease in setting parameters not only increases expectations in terms of vehicle and environment models, but also the demands for increased accuracy in tyre modelling. Therefore, this work deals with the influences of tyre temperature as well as modelling of the transient tyre forces which are acting during interactions of safety relevant ADAS and VDC operations. Special focus is held on handling and semi-physical tyre model approaches which are widely being applied in the field of ADAS and VDC.

The first part of the thesis addresses how the effects of transient force transmission and tyre temperature are interacting concerning the overall tyre behaviour. A literature review shows that first-order approaches to the description of the transient behaviour are widely used in this field. However, most of these approaches are connected to steady-state tyre force characteristics. Based on the property that steady-state characteristics are affected by external influences, transient tyre force transmissions are linked to tyre temperature.

The second part of the thesis deals with the modelling of the tyre temperature, including the effects on steady-state force characteristics. To handle different tyre layer temperatures, a multi-layer model is presented and evaluated using an industrial flat track test bench with two different types of tyres. After modelling the temperature behaviour, the focus shifts to the influences of lateral and longitudinal tyre force direction. Relatedly, an extension based on TMeasy, the tyre model used, is presented which is able to integrate the steady-state tyre characteristics based on different tyre layer temperatures. Consequently, by validating the overall tyre model, a significant increase in model accuracy can be demonstrated.

By using the extended temperature model, the focus is transient tyre modelling in the final part of the thesis. Through validating the well-known first-order Voigt-Kelvin model approach, described by a spring and damper element, suitability around fixed operating points is shown, but inaccuracies for a wide frequency working range do occur. Therefore, in order to model the effect of dynamic frequency dependent hardening of elastomers, an extended Maxwell model approach is presented. Via validation with measurement data, it is shown that the extended Maxwell model gains in accuracy in comparison to the standard Voigt-Kelvin approach, especially within higher frequency areas. In summary, this confirms the overall statement of the thesis: A model which is able to describe the dynamic hardening effect of the tyre delivers better performance, especially in relation to high frequency manoeuvres. Nevertheless, the improvements based on the enhanced modelling approaches depend significantly on the accuracy and validity of the fundamental steady-state tyre force model.

Kurzfassung

Durch den vermehrten Einsatz von Fahr- und Fahrerassistenzsystemen wurde die Modellbildung und Simulation zu einem wichtigen Werkzeug der heutigen Zeit. Dabei werden immer höhere Anforderungen wie kürzere Rechenzeit, höhere Genauigkeit oder einfachere Parametrierbarkeit an die hinterlegten mathematischen Modelle gestellt. So genügt es heutzutage auch nicht mehr, Simulationen rein auf fahrzeugbasierten Modelle durchzuführen, Einflüsse der Umwelt als auch die Interaktion über Reifenmodelle werden immer wichtiger. Somit beschäftigt sich die vorliegende Arbeit mit der Modellbildung und Simulation von semi-physikalischen Reifenmodellen, welche im Bereich von Fahr- und Fahrerassistenzsysteme weit verbreitet sind. Spezieller Fokus wird hierbei auf den Einfluss der Reifentemperatur sowie das Verhalten der transienten Reifenkraft gelegt.

Der erste Teil der Arbeit befasst sich somit mit der Frage, wie diese beiden Effekte in Bezug auf das Reifenverhalten zusammenwirken. Basierend auf einer Literaturrecherche wird gezeigt, dass Modellansätze erster Ordnung in diesem Bereich weit verbreitet sind, jedoch darüber hinaus mit der stationären Reifencharakteristik gekoppelt sind. Durch die Eigenschaft, dass sich ändernde Temperaturen ein verändertes stationäres Reifenverhalten mit sich bringen, kann eine Interaktion gezeigt werden.

Somit beschäftigt sich der zweite Teil der Arbeit mit der Modellbildung und Simulation der Reifentemperatur einschließlich ihrer Auswirkungen auf die stationären Reifenkraftcharakteristiken. Basierend auf verschiedenen Temperaturen im Lagenaufbau wird ein Mehrschichtmodell präsentiert, mittels zwei Reifentypen parametriert und anhand Messungen validiert. Nach dem Temperaturverhalten selbst wird Fokus auf Einflüsse in Quer- und Längskraftrichtung gelegt. Dabei wird eine Erweiterung des verwendeten Reifenmodells TMeasy vorgestellt, mit welchem es möglich ist, die stationäre Reifenkraft an unterschiedliche Temperaturen anzupassen. Durch die abschließende Validierung des erweiterten Reifenmodells kann eine signifikante Erhöhung der Modellgenauigkeit nachgewiesen werden.

Unter Verwendung des erweiterten Temperaturmodells liegt der Schwerpunkt im letzten Teil der Arbeit auf der Modellierung des transienten Reifenkraftverhaltens. Beginnend mit der Validierung des Voigt-Kelvin Modellansatzes, bestehend aus einem Feder- und Dämpferelement, kann von einer guten Übereinstimmung in einem definierten Arbeitspunkt, jedoch von deutlichen Abweichungen in erweiterten Frequenzbereichen ausgegangen werden. Um diesen typischen Effekt der dynamischen frequenzabhängigen Verhärtung von Elastomeren modellieren zu können, wird ein erweiterter Maxwell Modellansatz vorgestellt. Bei der Validierung mittels Messdaten kann eine verbesserte Modellgenauigkeit erreicht werden. Zusammenfassend kann somit gezeigt werden, dass ein Modellansatz, welcher in der Lage ist, die dynamische Verhärtung des Reifens abzubilden, eine erhöhte Modellierungsgenauigkeit insbesondere bei hochfrequenten Manövern mit sich bringt. Jedoch bringt eine Erweiterung nur dann zufriedenstellendes Verbesserungspotential, wenn bereits ein gutes Basismodell für stationäre Reifenkräfte vorhanden ist.

Contents

Abbreviations

ABS Antilock braking system

ADAS Advanced driver assistance systems

CA Collision avoidance

DE Differential equation

DMA Dynamic mechanical analyses

EPS Electric power steering

FEM Finite element model

FFT Fast Fourier transformation

IR Infrared

ISO International Organisation for Standardisation

LTI Linear time invariant

MBS Multi-body system

ODE Ordinary differential equation

PP0 Pirelli Pzero 245/40 R20 99W

RMS Root mean square

SAE Society of Automotive Engineers

SBR Styrene-butadiene rubber

SBW Steer-by-wire

STI Standard tyre interface

TCS Traction control system

TIME Tyre measurement

TMPT Tyre model performance test

UR3 Uniroyal Rainsport3 255/50 R19 107Y

VDC Vehicle dynamics controller

VSC Vehicle stability controller

WFT Wheel force transducer

WLF Williams Landel Ferry model

Symbols

In this work, variables and parameters are noted using

$$ {}^{4}_{1}x^{3}_{2,5} , $$

where the mathematical objects have been designated as

x, X	scalar	and		
$\boldsymbol{x}, \boldsymbol{X}$	vector	or	matrix.	

The indices describe the following:

1. The coordinate system in which the quantity is defined, e.g. 0 for global
2. A description or distinction, e.g. r_e for effective tyre radius or an index for coordinate direction, e.g. a_y for lateral acceleration
3. The exponent, the transposition operator $\boldsymbol{x}^\mathrm{T}$ or an additional assignment, e.g. x^max for the maximum value of x
4. The relative relation for switching the representation in different coordinate systems; the relative reference indicates to which direction the transformation applies, e.g. ${}^{wc}\boldsymbol{x}$ from wheel centre to wheel coordinate system
5. Any further information which are not given in 1 to 4

Coordinate systems

$({}_0x,\ {}_0y,\ {}_0z)$	The *global coordinate system*, defined by its origin on the ground plane and the ${}_0z$-axis running perpendicular to it.
$({}_cx,\ {}_cy,\ {}_cz)$	The *wheel centre coordinate system*, defined by its origin in the wheel *c*-point. The ${}_cy$-axis is in the direction of the rotation axis of the wheel and the ${}_cx$-axis is parallel to the ground plane. It uses the same additional indices for the position of the wheels mounted on the vehicle as the wheel coordinate system.
$({}_wx,\ {}_wy,\ {}_wz)$	The *wheel coordinate system*, defined by its origin in the tyre *w*-point where the ${}_wz$-axis is parallel to the ${}_0z$-axis. The ${}_wx$ and ${}_wy$-axes are the projections of the ${}_cx$ and ${}_cy$-axes along the ${}_wz$ direction on the ground plane.

Note: If no coordinate system is specified in the variable, the wheel coordinate system is used.

Coordinate transformation

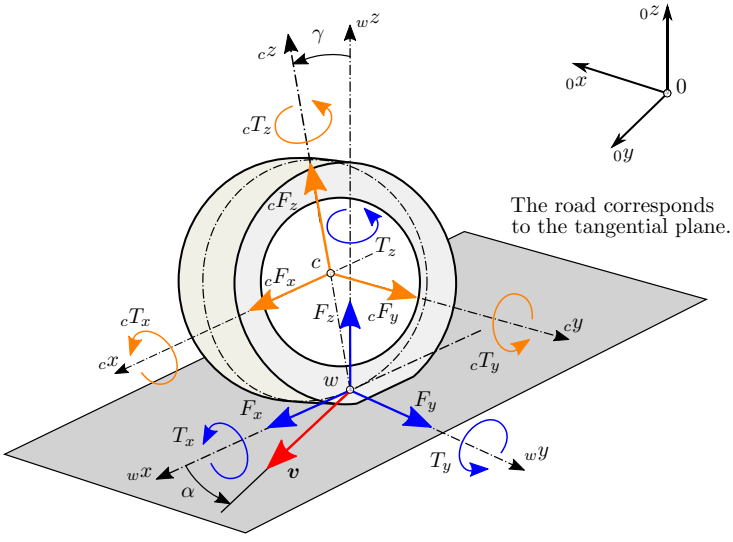

Figure 0.1.: Wheel centre c-coordinate and wheel w-coordinate system according to *International Organisation for Standardisation* (ISO) 8855, [ISO Central Secretary, 2011], adapted from [Hirschberg & Waser, 2012] and based on [Van Oosten et al., 1997]

Regarding stationary conditions, forces and torques measured inside the c-axis system can be transformed into the w-axis system, see Figure 0.1. Forces from wheel centre ${}_c\boldsymbol{F} = [{}_cF_x\ {}_cF_y\ {}_cF_z]^{\mathrm{T}}$ are converted to the wheel coordinate system ${}_w\boldsymbol{F} = [{}_wF_x\ {}_wF_y\ {}_wF_z]^{\mathrm{T}}$ by using Equation 0.1 and torques from ${}_c\boldsymbol{T}$ to ${}_w\boldsymbol{T}$ by means of Equation 0.2.

Hence, transformation of the **tyre forces** is defined by

$$ {}_w\boldsymbol{F} = {}^{wc}\boldsymbol{M}\ {}_c\boldsymbol{F} + m_{\mathrm{w}}\, g\ {}_w\mathbf{e}_{\mathrm{z}}\,, \tag{0.1} $$

with the transformation matrix

$$ {}^{wc}\boldsymbol{M} = \begin{bmatrix} 1 & 0 & 0 \\ 0 & \cos\gamma & -\sin\gamma \\ 0 & \sin\gamma & \cos\gamma \end{bmatrix}, $$

where m_{w} is the wheel's mass, g is the gravitational acceleration and γ is the inclination angle.

Equivalent to the respective forces, **tyre torques** are given by

$$ {}_w\boldsymbol{T} = {}^{wc}\boldsymbol{M}\left({}_c\boldsymbol{T} - {}_c\boldsymbol{r}_{wc} \times {}_c\boldsymbol{F}\right), \tag{0.2} $$

with radius vector ${}_c\boldsymbol{r}_{wc}$

$$ {}_c\boldsymbol{r}_{wc} = \begin{bmatrix} 0 \\ 0 \\ -r_\mathrm{s} \end{bmatrix}, $$

thus $r_\mathrm{s} = \overline{cw}$ defines the static tyre radius.

Parameters and scalar variables

a	Acceleration
c	Stiffness
c_p	Specific heat capacity
c_α	Cornering stiffness
d	Damper
e	Error
f	Frequency
g	Gravitational acceleration
g_f	Groove factor
l	Length
m	Mass
n	Number, pneumatic trail
p	Pressure
q	Heat or thermal flux
r	Radius
s	Slip, distance
t	Time
v	Speed, velocity
w	Wear, width
x	Longitudinal deflection
y	Lateral deflection
z	Relative sensitivity
A	Contact area, amplitude
F	Force
G	Frequency based transfer function
I	Moment of inertia
M	Magnitude
$\dot{Q}$	Rate of heat flow
P	Power

R	Resistance
T	Torque, periodic time, temperature
α	Tyre slip angle
γ	Inclination angle
δ	Thickness
λ	Thermal conductivity
μ	Road friction
ρ	Mass density
σ	Relaxation length
τ	Time constant
ω	Rotational speed
Δ	Interval between two discrete time steps
Ψ	Twist angle

Vectors and matrices

$\boldsymbol{a}$	Acceleration vector
$\boldsymbol{f}$	Vector with partial derivatives
$\boldsymbol{n}$	Normal vector
$\boldsymbol{p}$	Sensitivity vector
$\boldsymbol{q}$	Tyre contact force and torque vector
$\boldsymbol{v}$	Speed vector
$\boldsymbol{F}$	Force vector
$\boldsymbol{T}$	Torque vector
$\boldsymbol{J}$	Jacobian matrix
$\boldsymbol{M}$	Coordinate system transformation matrix

Indices

0	Initial condition
∞	Infinity
a	Ambient
ad	Adhesive
b	Bore, bulk, belt
c	Carcass, centre, contact
circ	Circumference
cond	Conduction

conv	Convection
cp	Contact path
e	Effective
f	Friction, filter
gf	Groove factor
h	Hysteresis
i	Inner
init	Initialisation
k	Time step
long	Longitudinal
lat	Lateral
m	Mean
meas	Measured
max	Maximum
min	Minimum
opt	Optimised
p	Particle, peak
r	Road
rad	Radial
s	Static, sliding, surface, sample rate
sbr	Styrene-butadiene rubber
sim	Simulated
t	Tension, travel, tread
tar	Target
th	Thermal
u	Particle deflection
v	Velocity
w	Wheel, worst, width
D	Dynamic
G	Generalised
M	Maxwell
N	Nominal
S	Steady-state
T	Temperature based
i	Index variable
x	x-direction
y	y-direction
z	z-direction

1

Introduction

Today, the technology in automotive engineering is undergoing constant evolution. Key factors like *digitalisation*, *electro mobility* and *autonomous driving* are making steady progress during our lifetimes. Not only statements from companies like Daimler at the International Motor Show in Frankfurt in 2017, that they will invest an additional 10 billion Euro in the field of electric vehicles in the next few years, or from Volkswagen that they will have 80 new electrified vehicles on the market by 2025 confirm the trend, [Müller-Wondorf, 2017]. Even a simple look around while driving is enough to make clear the increase in hybrid or fully electric vehicles as well as vehicles with a high level of driver assistance systems. Taking this one step further, pioneers in the automotive industry have already been talking about autonomously driving vehicles in the coming years.

The systems already available on the market thus present an alternative viewpoint, but within the same future based result. It all started with *antilock braking system* (ABS) as an early active safety system in the 1970s, followed by *traction control system* (TCS) in the late 1980s and the first *vehicle stability controller* (VSC) in the mid 1990s. Furthermore, over the last ten to twenty years, *electric power steering* (EPS), *steer-by-wire* (SBW) or *collision avoidance* (CA) are just a few examples which represent the trend that even more and more electronic systems are becoming state of the art within shorter periods of time. In summary, trends towards *advanced driver assistance systems* (ADAS) and *vehicle dynamics controller*s (VDCs) are clearly moving in the direction of autonomous driving, as can be seen in Figure 1.1.

However, the motivations to continue these trends are different for final customers, businesses and researchers. For end-users, properties like comfort, fuel consumption, driving range and even just the price are hard facts when it comes to deciding to purchase a vehicle. In contrast, for business and research, such trends usually bring very different questions and requirements. With a focus on autonomous driving, automated functions show additional demand in terms of predicting and monitoring a vehicle's behaviour in real time along with increasing levels of automation. For driving functions with *Society of Automotive Engineers* (SAE) automation levels of 3 and higher, the responsibility is transferred from drivers to the automated system, also including legal responsibility, [SAE, 2014]. This is why the demand on safety-relevant systems like ADAS and VDC with their focus on autonomous driving, are becoming more and more important.

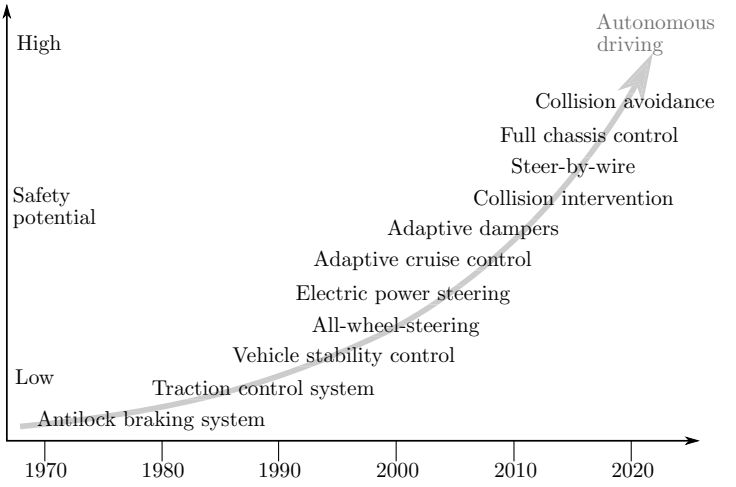

Figure 1.1.: Technology roadmap for *advanced driver assistance systems* (ADAS) and *vehicle dynamics controller* (VDC), adapted from [Seewald, 2000]

The question is how can the increased requirements be met within shorter development timeframes? The answer to this question leads us to virtual product development. The goal of this trend is to bring a larger part of the development process into the virtual world of modelling, simulation and testing. Starting from problem description, up to controller design and then testing, validation and tuning of ADAS and VDCs all should be done in the virtual world, see e.g. [Van der Auweraer et al., 2013] or [Bernsteiner, 2016]. This brings the advantage that physical testing can be done in less time and under different conditions. In particular, validation and testing at the limit of vehicle stability and under extreme conditions can be done without any safety risks and repeated over and over again. Furthermore, all possible traffic and environmental scenarios can be generated to evaluate the programmed algorithms under every feasible condition.

Nonetheless, the practicality and applicability of these simulations are reflected in model accuracy, or rather how good such models represent real world behaviour. Therefore, an increase in virtual world complexity, which is synonymous with a more detailed modelling process, adds to these challenges. However, a more detailed modelling process does not automatically increase the computation accuracy. More often, it only leads to a more complicated parameterisation process, which brings with it greater computational effort. Finally, higher model accuracy is only valid with accurate model parameters and more calculation power. To summarise, in most technical and economic cases, a trade-off between model accuracy, parameterisation and computation time has to be resolved.

1.1. Significance of tyre modelling for ADAS and VDC

A vehicle model itself is hardly capable of describing real world conditions on its own. In addition to a realistic vehicle model, an environment description and a driver behaviour are needed as well. Going one step further, one has to ask what use does an accurate vehicle and environmental model have when interaction between both cannot be represented well enough.

This leads us to the point that a tyre model is needed to model the interaction between the vehicle and environment. Furthermore, especially in handling and safety situations like steering precision tests and driving stability, or in bad road conditions like snow or ice, the tyre's influence on the overall vehicle behaviour is higher than that of the vehicle properties itself, see Figure 1.2 based on [Braess & Seiffert, 2013]. This leads us to the final conclusion that a more detailed vehicle model tends to place a higher accuracy demand on tyre modelling and vice versa.

State of the art semi-physical tyre models are already able to describe real world behaviour in a more or less accurate way within a short calculation time. In addition to the steady-state behaviour, self-aligning torque, rolling resistance, bore torque or the influences of toe and camber are just a few more examples of time-invariant behaviours that can be modelled with semi-physical approaches.

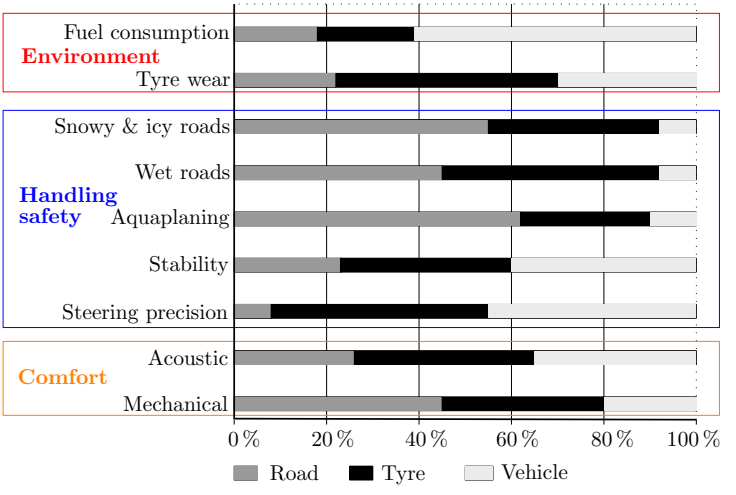

Figure 1.2.: Influence of road, tyre and vehicle on the overall driving behaviour based on environment, handling safety and comfort, based on [Braess & Seiffert, 2013]

However, the focus here is the application field of ADAS and VDCs, which are normally working in time critical situations and usually close to the stability limit of the vehicle. This means semi-physical tyre models without the inclusion of time-dependent tyre behaviour are hardly able to handle such user cases sufficiently. In summary, modelling and simulation of safety-relevant ADAS and VDCs, which act in standard and limit driving situations, lead to increasing accuracy demands in the description of dynamic reactions of tyre contact forces, e.g. [Hirschberg et al., 2000], [Rauh & Mössner-Beigel, 2008] and [Lex & Eichberger, 2011]. Furthermore, a new algorithm working with even shorter calculation times leads to a higher frequency responsibility of the testing environment in general, [Lugner et al., 2005].

For that purpose, basic first-order approaches are state of the art and widely applied in the field of vehicle dynamics and handling. Basic investigations were already taking place in the early 1940s from [Schlippe & Dietrich, 1942] were modified and refined, see for example [Pacejka, 2012], [Rill, 2006] and [Rill, 2012]. However, this simple but effective implementation for transient tyre behaviour is still being included in research investigations in the area of monitoring and observer design, e.g. [Baffet et al., 2006], [Lundahl et al., 2011] or [Lex, 2015], as well as further basic tyre investigations, e.g. [Hackl et al., 2016a] and [Rill, 2017].

Research is nonetheless still continuing to validate and enhance these applications. In [Einsle, 2010] a second-order approach, described as lag element application (PT2), generates higher accuracy with respect to vehicle-specific applications. Alternatively, in [Pacejka, 2012] a second-order semi-physical approach is given, which may result in high calculation time if inaccurate parameters are provided. More detail is presented in Chapter 2 concerning the mentioned as well as some additional applications.

Finally, various earlier transient approaches are being implemented in tyre modelling applications, but investigations have shown that basic first-order approaches work well around a fixed operating point, although during manoeuvres with higher manoeuvre frequency ranges and large slip values, a more detailed model is recommended. This means that further effort has to be made in order to cover the targeted range of model application, [Hackl et al., 2016a]. Furthermore, second-order approaches which are often implemented by adding a tyre mass are more time sensitive to low masses and moreover sensitive to parameter values in terms of accuracy, [Hackl et al., 2016c].

In summary, implementations like these are either difficult to simulate well in critical driving situations, which means for high frequency demand, or they are just mathematical approaches without the physical background for practical application, or they may be too costly in terms of labour for semi-physical and real time operations. To conclude, in the field of semi-physical tyre modelling, more intensive investigation and focus first has to be given to a model description that is able to cover transient influences within high frequency areas, and second, which is able to handle the conditions of short calculation time, parameterability and physical background. Furthermore, to guarantee a realistic model interaction between the tyre and the road, external influences like tyre temperature or wear should be taken into account when achieving these goals.

1.2. Thesis contribution and outline

Modelling and simulation of safety-relevant ADAS and VDCs have become a state of the art tool to reduce development time and risk as well as save costs. In order to meet the ever-growing demands for shorter calculation times, greater accuracy and easier parameterisation, increasing demands on tyre modelling is necessarily one of the outcomes. Especially for highly dynamic applications and critical driving situations, a high need for accuracy in the description of transient reactions of tyre contact forces is required. For that purpose, basic approaches need to be refined, which are widely applied in the field of vehicle dynamics and handling modelling.

Therefore, the goal of this thesis is to develop an extended implementation for modelling transient tyre behaviour for semi-physical tyre model approaches. In particular, the model should be able to describe frequency variant manoeuvre inputs, which leads to improvements in high level, highly transient applications while retaining the properties of semi-physical modelling. Additionally, an implementation in the most common semi-physical tyre models should be possible.

Furthermore, in most real operational tyre applications, an interaction of various external influences like tyre speed, internal pressure changes and temperature influences affect the behaviour of the steady-state characteristics and furthermore the overall tyre behaviour in specific ways. Hence, before deeper focus is given to tyre dynamics, basic research into external influences on fundamental tyre behaviour is carried out. Therefore, impacts which cannot be ignored have to be taken into account during the parameterisation and validation process in order to avoid external effects.

Finally, the enhanced tyre model implementations, based on semi-physical approaches, are implemented in a widely used tyre model and validated with measurement data from an industrial test bench. For a wide application range, two different types of tyres from two different manufacturer are used, one sports car tyre *Pirelli Pzero 245/40 R20 99W* (PP0) and one luxury vehicle tyre *Uniroyal Rainsport3 255/50 R19 107Y* (UR3).

In order to achieve these goals, the presented thesis is structured as follows:

Chapter 1 provides an overview about the significance of modelling and simulation for safety relevant ADAS and VDCs. Whereby, fundamentals between vehicle, environment and tyre modelling are presented. Furthermore, special focus is given on the importance of transient tyre models, especially under extreme driving conditions. Finally an outlook showing that external influences have to be taken into account for detailed investigations.

Chapter 2 begins with basic tyre properties that serve as the basis for the interface between roadways and vehicles and this is followed by a typical tyre model interface description. In the next part, a common literature based classification of different types of tyre models is presented, wherein the focus is handling and structural models. Moreover, greater focus is given to various transient tyre force approaches that are semi-physical, whereby common applications are presented in more detail.

Finally, the chapter ends with a state of the art model evaluation and a transition to the next chapters.

Chapter 3 starts with a parameter sensitivity analysis based on the evaluation results from Chapter 2. The results show how external influences affect the force behaviour. Subsequently, literature investigations on various external influences were done. In the second part, special focus is held on temperature, which turned out to be the main external influencing factor. Therefore, first a detailed literature study concerning state of the art temperature models is presented, followed by fundamental tyre section investigations. The outcome of these tyre section measurements, in which the behaviour of only a small section of the tyre tread is investigated, is used as the basis for the temperature model application in Chapter 5.

Chapter 4 begins with an overview of different tyre test bench applications, including advantages and disadvantages, before details about temperature and semi-physical based transient force modelling are presented. Afterwards, basic information about the TMeasy tyre model, which is used for further extensions, is given. Relatedly, a stepwise parameterisation process for the standard model version is presented. Special focus is given to measurement manoeuvres for parameterisation of the steady-state characteristics.

Chapter 5 contains the temperature modelling approach related to investigations in Chapter 3. In the first step, the temperature modelling procedure based on different tyre layers is explained, parameterised and validated. As further step, focus is given to temperature influences on the steady-state tyre characteristics. Therefore, the objective to implement a semi-physical model approach is defined; one which is able to integrate the steady-state behaviour based on different tyre layer temperatures. Finally, this extended model approach is evaluated and validated with measurements from an industrial flat track test bench.

Chapter 6 describes the validation of a standard transient model approach and presents an extended semi-physical based transient model approach based on the application developed in Chapter 5. First, a detailed model validation of the state of the art model approach is given for a non-rolling tyre. Based on the knowledge gained, an extended model approach that is able to describe the dynamic hardening effect of the tyre is presented, parameterised and validated with two different types of tyres using the measurement data.

Chapter 7 summarises the main findings of this thesis and provides a final statement.

2

Tyre model approaches and semi-physical transient force modelling

A basic tyre model forms the foundation for the implementation of the transient tyre behaviour. In addition, all tyre model parameters are dependent on the basic properties of a tyre. Therefore, this chapter starts with the main tyre materials followed by the essential functions of a tyre as an introduction. In the next step, the *standard tyre interface* (STI) is presented, which serves as an interface for linking the respective tyre and road model to the vehicle model.

Furthermore, to fulfil all mentioned requirements in the virtual world while keep the trade-offs in mind, various tyre model applications are already available. Therefore, a common literature-based classification of different types of tyre models is given in the following section. A subdivision into handling and structural applications is used and the main known tyre models are presented.

In the second part of the chapter, greater focus is put on transient force modelling. Starting from historical research, a further description of the state of the art implementation in mainly semi-physical approaches is provided. Additionally, different first order and higher model applications are discussed in more detail.

Finally, the chapter ends with a state of the art model evaluation and a discussion of the similarities of these approaches. This validation leads into the next chapters.

2.1. Tyre modelling as one basis for vehicle simulation

As the only interface between road and vehicle, the tyre is clearly an indispensable component of a vehicle overall. The main functions range from longitudinal - i.e. driving, braking and climbing - to lateral functions like steering characteristics, controllability and driving stability. A tyre also has vertical functionality, e.g. riding comfort, safety and durability, [Lex & Hirschberg, 2015].

To handle this broad range of tasks, the structure of a tyre consists of 150 to 200 different components and many different materials, [Lex & Hirschberg, 2015]. There are several layers of elastomer and polymer, different types of fillers, reinforcements, softeners and

Table 2.1.: Tyre material components in percentage mass, adapted from [Lex & Hirschberg, 2015] and [Rill, 2012]

Component	Material	Mass (approx.)
Elastomer	Natural and synthetic	38 %
Filler materials	Carbon, silica, chalk	30 %
Reinforcements	Steel, rayon, nylon	16 %
Softener	Oil, synthetic resin	10 %
Vulcanisation	Sulphur, zinc oxide	4 %
Miscellaneous		2 %

additional materials that are bonded together into a matrix of polymeric material, see Table 2.1. However, the components presented in Table 2.1 physically make up the tyre, but the potential tyre-road contact forces depend on the tyre-road grip, which is influenced by many parameters [Lex & Hirschberg, 2015]:

Tyre characteristics like tyre type and dimension, tyre tread pattern, internal pressure, tyre wear or use history

Kinematics of tyre motion like sliding velocities, tyre deflection and camber

Roadway characteristics like material (asphalt, concrete), road texture (microscopic and macroscopic), environmental temperature and tyre-road intermediary layers, e.g. water or snow

In summary, the tyre is a complex vehicle component with a broad range of functions. Nonetheless, as in the real world where various types of tyres are available for different use cases, a lot of tyre models are already available on the market or published scientifically dependent on the demand.

Therefore, for the use of a tyre model in a virtual product environment or within a simulation algorithm, the interaction between road and vehicle has to be defined. A tyre model has to convert the tyre-road grip potential into tyre-road forces and torques depending on the influencing parameters that were mentioned above. As the exact interface between tyre and road is defined by the contact patch, detailed definitions become more difficult. Still, in order to guarantee a strict fit between tyre and vehicle model, standardised input and output values as well as coordinate systems are used. Therefore, an interface based on the *standard tyre interface* (STI), as referred to in [Van Oosten et al., 1997], is used in this project.

In Figure 2.1 the basic tyre-road-vehicle simulation model interface based on a STI is given. Both the tyre and road model have two main input aspects. The first part, the tyre and road parameters, are constant values and are defined as time-independent parameters or functions. In most cases, tyre information is generated from test bench measurements while road parameters describe normal road conditions, like makeup or texture. The second inputs are defined based on the time-dependent values.

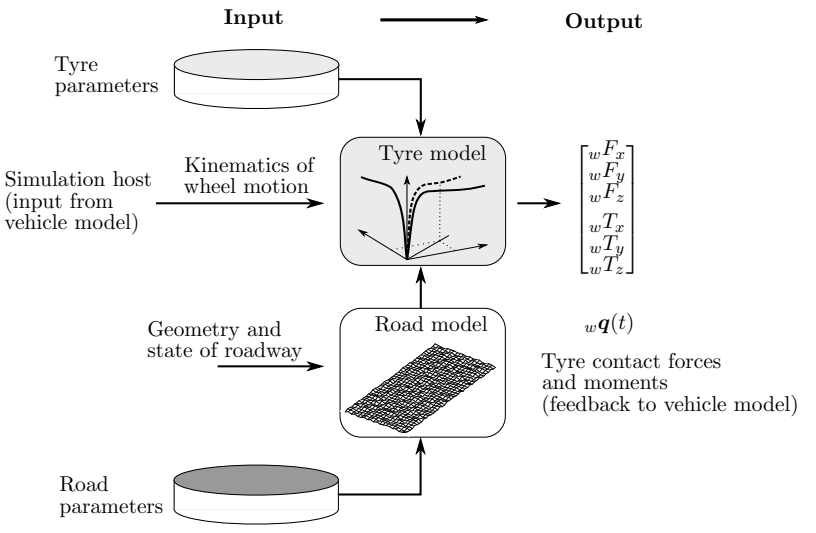

Figure 2.1.: Tyre, road and vehicle simulation model interface, based on a *standard tyre interface* (STI), referred to [Van Oosten et al., 1997]

For the tyre model, this information is about the kinematic motion of the wheel, like camber and vertical displacements. Time dependent characteristics for the road model include surface temperature and road friction. Obviously, if the conditions or surface texture are changing over time, these count as varying time inputs as well.

Depending on these intermittent and continuous characteristics as well as on the interaction between tyre and road model, time dependent tyre contact forces and torques, denoted as generalised forces $_w\boldsymbol{q}(t)$ are calculated. Based on the transformation matrix $^{wc}\boldsymbol{M}$, forces from the wheel centre c- can be transformed into the wheel w-coordinate system and vice versa, see Section Coordinate transformation in Chapter Symbols.

In summary, to mathematically describe the behaviour of a tyre and use it within an interaction with the vehicle and environment application, a tyre model is needed. Depending on the specific application, calculation time and complexity, a number of tyre model approaches already exist on the market. In Section 2.2 an overview of different model applications and classifications are given.

2.2. Classification of tyre models

In a time in which modelling and simulation are becoming more and more important in the automotive industry, several tyre model applications defined for different use cases are already available. Commercial models like **FTire** [cosin, 2018a], [cosin, 2018b], **RMOD-K** [Oertel & Fandre, 2001], [Oertel, 2018], [IAT Dynamics mbH, 2018], the **Magic Formula Tyre Model MF-Tyre** [Pacejka & Bakker, 1992], [Pacejka, 2012] and its extension **MF-Swift** [Schmeitz et al., 2007], [Pacejka, 2012], [TNO Delft Tyre, 2013], [TNO Automotive Safety Sol., 2018], **CDTire** [Gallrein & Bäcker, 2007], [Frauenhofer-Institut, 2018], **TameTire** [Pearson et al., 2016] and **TMeasy** [Rill, 2012], [Rill, 2018] are the most common for automotive applications.

Furthermore, tyre models like **TMsimple** [Hirschberg, 2009], **Dugoff tyre model** [Dugoff et al., 1970], [Ding & Taheri, 2010], **UniTire Model** [Guo et al., 2005b], [Dang & Guo, 2011] and [Xu et al., 2016], or the **Three-dimensional Ring Model** from [Kindt et al., 2008] and [Kindt et al., 2009] are just a few more which are often used for automotive applications.

Additionally, special tyre models like **Hohenheimer Reifenmodell** (engl. *Hohenheim tyre model*) [Witzel & Böttinger, 2014], [Böttinger, 2018]or the tyre model used in the PhD thesis from [Lines, 1991], which are specifically for agricultural vehicles and construction machinery, are available.

However, strictly subdividing these models into categories proves to be difficult. One possibility is segmentation into fields of application, or how the contact patch is mathematically modelled, for example with a contact point, a contact area or a three dimensional approach. Independently of these distributions, a trade-off between accuracy, parameter flexibility and calculation time is given in each application. Therefore, subdivision into physical structure, which just means model complexity, is more common. Nonetheless as mentioned above, strict subdivision is difficult and therefore different category levels are found in the literature.

A simple segmentation is found in [Rill, 2012], where only two groups are identified: handling and structural models, also known as high frequency models. Structural models are defined as complex approaches for which multi-track contact and pressure distribution across the belt width are taken into account. Comparatively, handling models provide for vehicle dynamics simulation.

A distinction between three main aspects is given in [Lex & Hirschberg, 2015], wherein a smooth transition from mathematical-empirical to semi-physical and beyond to physical tyre models is defined. In this consideration, a more detailed subdivision of handling models is used. A similar definition is stated in [Acosta et al., 2018] and also [Pacejka, 2012]. Thereby, an unbroken transition from three major groups is given between physical, simple physical and empirical models.

A more detailed segmentation is presented with five or more groups in [Zegelaar, 1998], [Rauh, 2003], [Einsle, 2010] or [Kerschbaumer, 2017]. All four of these literature sources

divide the simple physical model into more detailed groups, and additionally they include a mathematical-empirical and a complex physical model, such as a *finite element model* (FEM).

In summary, different definitions of tyre model classification, going from two up to five or more groups, are given in the literature. Furthermore, because of a fluid categorisation transition, a strict classification of the models is not entirely suitable. Nevertheless, a literature-based classification with two main groups as well as several subgroups is used for further investigations in this thesis by

- **Handling tyre models** and
- **Structural tyre models** .

2.2.1. Handling models (HM)

Handling tyre models are presented here as the main group used for vehicle dynamics simulation. With the exception of some elastic characteristics for the description of transient force, the tyre structure can be viewed as rigid. In most cases, the force application is limited to one single point with its centre in the contact patch. Description of forces and torques rely on the laws of physics, in contrast to mathematical functions, and are parameterised from measurement data as seen in Figure 2.2. Therefore, these model applications are characterised by a useful compromise between user-friendliness, model complexity and accuracy. Furthermore, a subdivision among tyre models with pure mathematical implementation, called mathematical-empirical, and models with more focus on physical parameterisation, called semi-physical, is often used in the literature, for example in [Lex & Hirschberg, 2015].

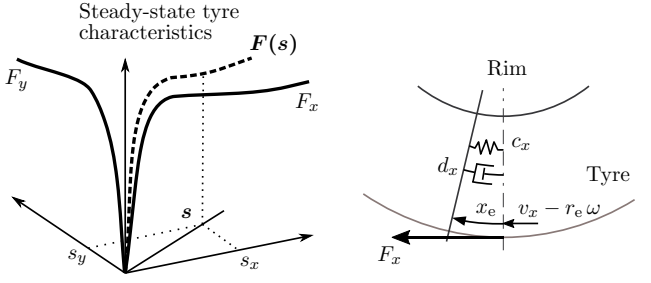

Figure 2.2.: Structure examples for handling tyre models; mathematical and semi-physical steady-state tyre characteristics based on measurement data on the left, and a common model approach for the longitudinal transient tyre force on the right, adapted from [Rill, 2012]

Simple mathematical implementations do have linear or hyperbolic tangent (tanh) dependencies of slip to tyre force characteristics. Hence, these applications only apply for small slip angles and longitudinal slip values and are often used in model-based observation design and basic vehicle investigations.

A well-known empirical tyre model application is the **Dugoff tyre model** from [Dugoff et al., 1970]. This model uses mathematical functions to calculate the longitudinal and lateral force depending on vertical load, slip angle, longitudinal slip, maximum road friction and the velocity components in the wheel plane. This model has already been on the market for a long time, but it is still used in modern research investigations due to its simplicity, e.g. [Ding & Taheri, 2010] and [Bhoraskar & Sakthivel, 2017].

Possibly the most popular model in this group is the commercial **Magic Formula Tyre Model MF-Tyre**, based on the standard Pacejka formulation, see [Pacejka & Bakker, 1992], [Pacejka, 2012]. The tyre behaviour is modelled on non-linear functions and based on the parameterisation of experimental data. Different variations and extensions of this model have been proposed in last years. Not only the in-house extensions are on the market, **MF-Swift** [Schmeitz et al., 2007], [TNO Delft Tyre, 2013] and [TNO Automotive Safety Sol., 2018]; enhancements from external developers that also include temperature influences are available, for example [Calabrese et al., 2015].

A further handling model that already has a high degree of real-world applicability is the **TMeasy-Tire Model**, [Hirschberg et al., 2002], [Rill, 2012] or [Rill, 2018]. The idea of TMeasy goes back to an industrial project involving agricultural tractor tyres where no tyre measurement data were available. TMeasy is a constantly evolving tyre model; the last version is based on a three-dimensional slip approach and is valid for different kinds of tyres including motorcycle and special purposed tyres. The physical parameters allow a skilled engineer to parameterise TMeasy from a technical point of view. Of course, setting parameters from test bench or vehicle measurements is possible as well.

A further common tyre model in this group is **UniTire**, see for example [Guo et al., 2005a], [Guo et al., 2005b], [Dang & Guo, 2011] or [Xu et al., 2016]. UniTire is a unified non-linear and non-steady-state tyre model for dynamic vehicle simulation control investigations with complex wheel motion inputs. Based on early research in 1973, UniTire has been further developed by several extensions, for example in 1995 combined slip was improved upon and in 1998 further extreme operating conditions such as steering with sharp angles or low speed starting and braking were included. Implementation in *multi-body system* (MBS) software like MSC.ADAMS or in the driving simulator at Jilin University in China are further considerable successes, [Guo & Lu, 2007].

Additional tyre models in this category are the tyre model from [Lines, 1991], developed for agricultural tractor tyres and the **TMsimple** tyre model tied to physical parameters and used for longitudinal, lateral and combined steady-state investigations, [Hirschberg, 2009].

2.2.2. Structural models (SM)

The structural tyre models are defined as complex approaches where multi-track contact and pressure distribution across the belt are taken into account. Depending on the model, modifications such as rigid or flexible belt and different tyre pressure distributions within the contact patch are used, as can be seen in Figure 2.3. Furthermore, depending on the field of application, some simplifications regarding force and torque generation mechanisms are given. The structural tyre models need a lot of material data and a higher computing time as well. Moreover they are used in a broad field of application so different subgroups are defined in the literature.

The first subgroup is called brush model. It represents the intermediate step between a semi-physical and a simple physical model. Brush models describe the contact between the tyre belt and the roadway using individual frictional bristle elements. In most cases, the tyre belt is assumed to be rigid. Under load, they become deformed and thereby transmission power is transferred in a longitudinal and lateral direction from the road to the belt. An implementation is given as an example in the tyre model called **BRIT** (Brush and Ring Tire Model) from [Gipser et al., 1997], or as extension with increasing flexibility in [Svendenius & Wittenmark, 2003].

A common subgroup of structural tyre models are rigid belt models, which are often also called shell models. The tyre belt modelled as a rigid ring is a characteristic of this type of model. The rigid belt is coupled to various non-linear spring damper mass elements on the rim bodies. Therefore, the displacements of the ring are used as separate degrees of freedom. When driving over short-wave lanes, multiple contact zones are formed. Well-known model examples are **CDTire** [Gallrein & Bäcker, 2007], [Frauenhofer-Institut, 2018], **RMOD-K** [Oertel & Fandre, 2001], [IAT Dynamics mbH, 2018] and [Oertel, 2018] and the Magic Formula Tyre Model MF-Tyre extension **MF-Swift** [Schmeitz et al., 2007], see also [Pacejka, 2012], [TNO Delft Tyre, 2013] and [TNO Automotive Safety Sol., 2018].

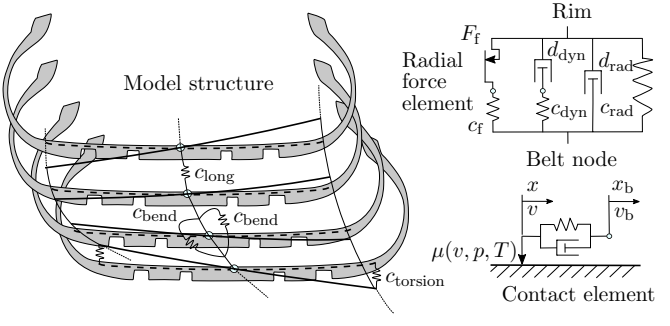

Figure 2.3.: Modelling approach for structural tyre models based on the FTire tyre model, adapted from [Rill, 2012] and related to [cosin, 2018a]

The next step toward fully physical approaches is a flexible belt model in two dimensions (2D), e.g. **RMOD-K 7 FB** [Oertel, 2018]. The characteristics of an elastic belt ring allow comfort application in longitudinal and vertical directions. Hence, due to the reduction of the centre plane, only simplified lateral force transmissions are suitable. Extensions bring the flexible belt models into three dimensions. They have multiple elastic belt rings coupled via non-linear force elements. With high numbers of belt rings, detailed lateral belt mechanics can be characterised as well. Due to the precise lateral properties, comfort and rough road investigations in all directions are possible as well. Representatives of this group are **FTire** [cosin, 2018a], [cosin, 2018b] and the **Three-dimensional Ring Model** from [Kindt et al., 2008] and [Kindt et al., 2009].

A further subgroup of structural model applications are finite element models, which are also called complex physical models. These approaches are based on detailed tyre structure descriptions and try to characterise the behaviour of the tyre-road contact analytically using physical equations. The tyre force and torque generation are based on physical principles like elastic deformation, adhesion and sliding. Furthermore, behaviour is usually included as a combination of static friction, coulomb friction and Stribeck effects. Also, non-linear material properties and a tyre's composite structure are taken into account, [Acosta et al., 2018]. Analysis through driving across obstacles with various velocities, investigation of tyre tread modelling or simulation of high frequency modes are the main fields of application. Nonetheless, depending on the elements included and the computation power, the main disadvantage is the calculation time. In summary, FEMs represent a tyre in a realistic way, but it is hardly suitable for usage in real time application fields like *advanced driver assistance systems* (ADAS) and *vehicle dynamics controller*s (VDCs). The main representatives in this group are presented in [Chae, 2006], [Ghoreishy, 2006], [Ghoreishy, 2009] and [Brinkmeier et al., 2008], whereby a schematic representation is given in Figure 2.4.

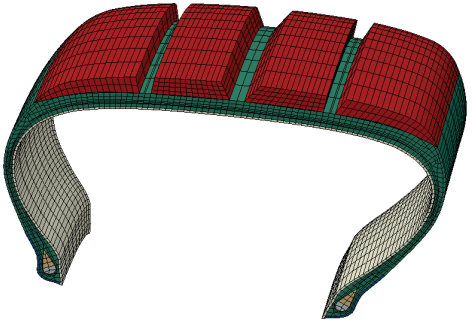

Figure 2.4.: Schematic representation of a *finite element model* (FEM) structure

Table 2.2.: Classification of tyre model approaches

Name	**Type**[(1)] **& approach**	**References**
Linear model	HM - mathematical	
Dugoff	HM - mathematical	[Dugoff et al., 1970] [Ding & Taheri, 2010] [Bhoraskar & Sakthivel, 2017]
Lines	HM - mathematical	[Lines, 1991]
TMsimple	HM - semi-physical	[Hirschberg, 2009]
MF-Tyre	HM - semi-physical	[Pacejka & Bakker, 1992] [Pacejka, 2012]
TMeasy	HM - semi-physical	[Hirschberg et al., 2002] [Rill, 2012] [Rill, 2018]
UniTire	HM - semi-physical	[Guo et al., 2005a] [Guo et al., 2005b] [Dang & Guo, 2011] [Xu et al., 2016]
Brush model	SM - brush approach	[Gipser et al., 1997] [Svendenius & Wittenmark, 2003]
TameTire	SM - brush approach	[Pearson et al., 2016]
CDTire 20	SM - rigid belt	[Gallrein & Bäcker, 2007] [Frauenhofer-Institut, 2018]
RMOD-K 7 RB	SM - rigid belt	[Oertel & Fandre, 2001] [Oertel, 2018] [IAT Dynamics mbH, 2018]
MF-Swift	SM - rigid belt	[Schmeitz et al., 2007] [TNO Delft Tyre, 2013] [TNO Automotive Safety Sol., 2018]
FTire	SM - flexible belt	[cosin, 2018a] [cosin, 2018b]
3D-Ring model	SM - flexible belt	[Kindt et al., 2008] [Kindt et al., 2009]
Finite element models	SM - FEM	[Chae, 2006] [Ghoreishy, 2006] [Ghoreishy, 2009] [Brinkmeier et al., 2008]

[(1)] HM . . . Handling model with **low** to **moderate** computation effort
SM . . . Structure model with **moderate** to **high** computation effort

In summary, it was shown that many different types of model approaches are commercially available or have been published scientifically. A uniform subdivision turns out to be difficult, but it is also not always necessary. Furthermore, a trade-off between accuracy, calculation time and parameterability is present and depends on the specific application. Table 2.2 presents a summarised list of the mentioned tyre model approaches.

However, vehicle and tyre model application for ADAS and VDC have specification requirements concerning parameterisation and calculation time. Depending on the literature noted in Table 2.2, a differentiated compromise between the mentioned properties is achieved by using handling (i.e. semi-physical) tyre models. An overview on transient tyre force modelling for semi-physical approaches is presented in the next section.

2.3. Semi-physical based transient force modelling

Based on considerations from Section 2.2 above, it has been shown that many different types of tyre model applications are already commercially available or have been published in scientific literature. Furthermore, a good trade-off between model accuracy, calculation time and parameterability is given for handling and semi-physical based tyre model approaches, which seems to be the reason why they are still widely applied in the field of ADAS and VDC. Therefore, a detailed literature overview of semi-physical based transient force modelling is given in this section.

2.3.1. Historical overview

The research into transient tyre behaviour goes back several years. The first to investigate and model the transient lateral force behaviour of tyres were [Schlippe & Dietrich, 1942]. Based on the considerations of the belt mechanical properties, they developed a stretched string approach, which forms the basis for a lot of other research, as described below in Subsection 2.3.2.

In [Weber & Persch, 1976] experimental validations of different tyre speed and slip angle frequency simulations are presented. Results of their investigations have shown phase delays higher than 90 deg degrees between input and output on manoeuvres at low speed and frequencies $f > 4\,\mathrm{Hz}$, which corresponds to dynamic characteristics higher than first-order in this field of application. Furthermore, by using a constant slip angle manoeuvre amplitude, an increasing force behaviour on higher speed and frequency showed early tyre hardening effects.

Investigations on parameter influences like tyre load, tyre pressure and slip angle with a focus on the relaxation length are presented in [Laermann, 1986]. The investigations of *Laermann* reveal that the dynamic response of the tyre force shows a typical relaxation behaviour. However, the description of self-aligning torque reveals a more complex behaviour. From these results, the transient tyre model approach is modelled with a first-order model coupled with a rigid ring model.

Further investigations on influences of speed and tyre load on transient behaviour are presented in [Holtschulze, 2000]. The special focus is amplitudes and phase response influences during slip angle sine manoeuvres. In comparison to [Weber & Persch, 1976] only phase delays up to 60 deg were reached by using a tyre speed higher than 30 km/h and manoeuvre frequency with $f < 5\,\text{Hz}$. Therefore, a first-order *differential equation* (DE) based on cornering stiffness, lateral stiffness and tyre speed is sufficient to model the transient behaviour.

A very detailed experimental investigation into parameter sensitivities on the transient lateral force behaviour is presented in [Einsle, 2010]. Influences of wheel load, pressure and camber on lateral tyre stiffness are investigated, and moreover influences of cornering stiffness and furthermore relaxation length are presented. All investigations were carried out and evaluated with four different types of tyres. As the basis for simulation evaluations, a first-order approach was used. Furthermore, an extended second-order approximation was developed and evaluated, see Subsection 2.3.4.

In summary, based on investigations conducted as long ago as the early 1940s, research on transient tyre characteristics is still on-going, whereby for a detailed timeline Chapter 5 of [Pacejka, 2012] is recommended.

Hence, three trends to model the transient behaviour of the horizontal tyre forces and torques in a semi-physical approach can be recognised. First, there is the stretched string model in which the tyre belt is simplified to a string, and this forms the historical foundation for the others. The second approach is based on a single-contact point, where the position of the force application point changes in terms of physical parameters, and third, mathematical approaches based on DE, which are transformed into frequency domain. A detailed description of these three model applications is given in the next subsections.

2.3.2. Stretched string model

In 1941, *Von Schlippe* and *Dietrich* introduced the concept of a stretched string with a finite contact length to describe the transient behaviour of a rolling tyre, [Schlippe & Dietrich, 1942]. Here, the main goal was to analyse the shimmy characteristics of tyres. These investigations formed the foundation of nearly all stretched string models. Therefore, in this chapter a summary of the stretched string model based on [Besselink, 2000] and [Pacejka, 2012] is presented.

The basis is a massless string under a constant pretension force F_y, which is uniformly and elastically supported in a lateral direction, as seen in Figure 2.5. As a further simplification, no sliding between road and finite contact surface is assumed. Basic research conducted by *Von Schlippe* started from a non-rolling tyre in which a plane description of a stretched string was considered, as can be seen Figure 2.6. Two assumptions were given. First, for points in the contact region, no sliding occurs with respect to the road, and second, only small deflections were considered. After considering a lateral force at the centre, two main regions were formed. The first one is designated as the contact

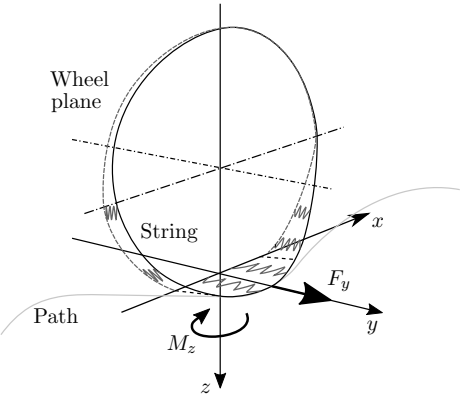

Figure 2.5.: Massless tyre string model under a constant pre-tension force F_y, which is uniformly and elastically supported in lateral direction, based on [Pacejka, 2012]

patch, with the length $2a$ starting from s_1 and ending with s_2, where the string is in contact with the road. The second one connects the length σ of the lateral deflection of the string as an exponential function and is defined with

$$\sigma = \sqrt{\frac{F_\mathrm{t}}{c_\mathrm{c}}}\,, \tag{2.1}$$

where F_t denotes the tension force and c_c the carcass stiffness which is evenly distributed over the length of the string.

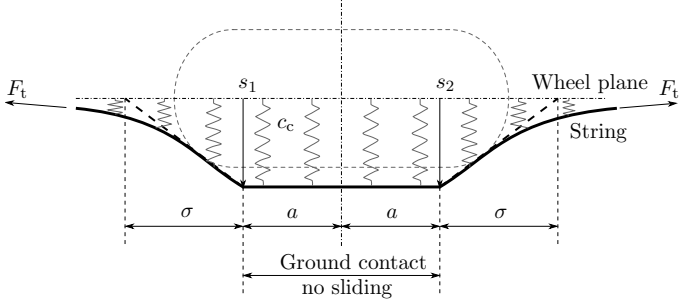

Figure 2.6.: Deflection of a non-rolling string application with a lateral displacement of the wheel centre (top view), based on [Schlippe & Dietrich, 1942] and adapted from [Besselink, 2000]

In a next step, a rolling tyre is considered. Therefore, when driving along with a defined slip angle α, a point on the circumference of the tyre will enter the contact patch, travel through it and leave it afterwards, see Figure 2.7.

The point going through the patch will enter at a lateral deflection s_1 with zero sliding conditions, follow the manoeuvre path and leave with a displacement defined with s_2. Using a global coordinate system, the location of the entry point at y_1 is defined with

$$y_1 = y_c + a\,\Psi + s_1\,, \tag{2.2}$$

where y_c defines the distance to the location of the wheel centre and Ψ the tyre rotation with respect to the global coordinate system. If the slope of the string deflections remains continuous at the leading edge, Equation (2.2) can be derived with respect to the travelled distance s_t with

$$\frac{\mathrm{d}s_1}{\mathrm{d}s_t} = \Psi - \frac{s_1}{\sigma} - \frac{\mathrm{d}y_c}{\mathrm{d}s_t} - a\,\frac{\mathrm{d}\Psi}{\mathrm{d}s_t}\,. \tag{2.3}$$

By using the time t and assuming a constant tyre velocity v with $s_t = v \cdot t$ Equation (2.3) can be written as follows

$$\dot{s}_1 = v\left(\Psi - \frac{s_1}{\sigma}\right) - \dot{y}_c - a\,\dot{\Psi}\,. \tag{2.4}$$

Furthermore, by using Equation (2.2) and its time derivative, assuming a constant contact length and by implementing Equation (2.4), the DE for the global position of the leading edge is given by

$$\frac{\sigma}{v}\,\dot{y}_1 + y_1 = y_c + \Psi\,(\sigma + a)\,. \tag{2.5}$$

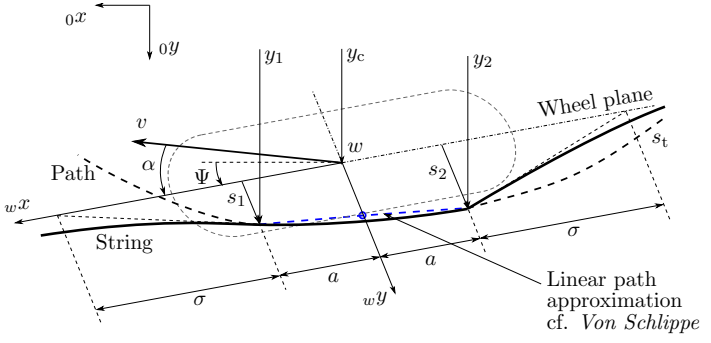

Figure 2.7.: Deflection of a string application for a rolling tyre (top view), based on [Schlippe & Dietrich, 1942] and adapted from [Besselink, 2000]

As no sliding is assumed in the contact area, *Von Schlippe* points out that the line path follows the leading contact point, whereby the lateral position of the leading point with respect to the ground is defined by Equation (2.5). After leaving point s_2, the lateral string deflection will gradually tend to approach zero again. Because the string has no bending stiffness, in most cases a kink occurs at the run out area. Hence, the lateral force applied on the rim can be calculated by integrating the deflection of the carcass stiffness times the deflection over the string length. But Equation (2.5) only describes the leading point and the retardation behaviour of the points on the ground contact string line leads to mathematical difficulties. This property limits the usage of such string models in general in time domain simulations.

However, in [Sharp & Jones, 1980] a discretised string model with about 50 elements in the contact path is developed. This method seems to be close to exact but it also very time consuming. Therefore, approximating the characteristics of the particle path in an easier way has prevailed.

The most obvious and maybe simplest approximation has already been defined by *Von Schlippe*, [Schlippe & Dietrich, 1942]. In the approach the path is considered to be a straight contact line connecting the entry and exit of the patch, as seen in Figure 2.7 (cf. the linear path approximation). Since a non-sliding region and a constant contact length are given, the characteristics of the linear approximation can be mathematically described by a time shift with

$$y_2(t) = y_1\left(t - \frac{2a}{v}\right) . \tag{2.6}$$

Thus the lateral force can be determined from the deflection of the contact patch with respect to the wheel centre by

$$F_y = c_y\left(\frac{y_1 + y_2}{2} - y_\mathrm{c}\right) = c_y\left(\frac{s_1 + s_2}{2}\right) , \tag{2.7}$$

where c_y is the lateral tyre stiffness in the centre contact point with respect to the rim. For a straight contact line the interaction with the evenly distributed carcass stiffness c_c is given with $c_y = 2\,c_\mathrm{c}\,(\sigma + a)$.

By using the time derivative of Equation (2.7) and by implementing Equation (2.4) at position s_1 and s_2, a first-order DE for the lateral force is given with

$$\dot{F}_y + \frac{v}{\sigma}\,F_y = c_y\left(v\,\Psi - \dot{y}_\mathrm{c} - a\,\dot{\Psi}\right) . \tag{2.8}$$

In summary, based on a stretched string tyre model together with an assumption of contact patch characteristics, a DE of the lateral tyre force is given. Hence, the main simplification is given in the contact patch characteristics. If a more detailed description is needed, a parabolic approximation is recommended, but this also brings the negative of additional calculation time, see [Pacejka, 2012] or [Besselink, 2000].

A modified version from *Von Schlippe* is given in [Holtschulze, 2000]. Based on Equation (2.8), he describes the transient tyre force in the wheel centre coordinate system. By implementing the relaxation length with $\sigma = c_\alpha / c_y$, where c_α defines the cornering stiffness and α the slip angle of the tyre, the equation simplifies to

$$\frac{c_\alpha}{v\, c_y} \dot{F}_y + F_y = c_\alpha\, \alpha\,. \tag{2.9}$$

Further mathematical transformation by defining $\tau = c_\alpha \,/\, (v\, c_y)$ as a time velocity dependent constant and $F_y^{\mathrm{S}} = c_\alpha\, \alpha$ for the steady-state tyre characteristics brings us to the well-known first-order DE within its initial condition. This equation defined by

$$\tau_{x,y}\, \dot{F}_{x,y}^{\mathrm{D}} + F_{x,y}^{\mathrm{D}} = F_{x,y}^{\mathrm{S}} \qquad \text{with} \qquad F_{x,y}^{\mathrm{D}}(t_0 = 0) = 0\,, \tag{2.10}$$

is often used in tyre transient implementations and can generally be used both laterally and longitudinally, see for example in [Rill, 2012]. The superscripts D and S distinguish between transient and steady-state tyre forces and the subscripts x and y indicate the longitudinal and lateral directions of the tyre contact forces F. Note that if no indices are specified in the variable, the transient force F^{D} is used in this thesis.

2.3.3. Single contact point tyre model

A simplification of the stretched string model is given by the single contact point tyre model, based on [Pacejka, 2012]. In this implementation, the whole contact patch is merged into one single point. Therefore, this approach is less complex and needs significantly less computing time. According to *Pacejka*, this model can be enhanced for simulations, starting from standstill, in order to investigate the influence of camber and turn slip and for the simulation of fully non-linear combined tyre forces. In the following subsection, a linear version of this model with two enhancements up to a full non-linear implementation is presented.

2.3.3.1. Linear based single contact point model

Within this application, the contact patch is simplified to a single point w' which is elastically attached to the wheel plane point w, as shown in Figure 2.8. The superscript $'$ indicates the variables regarding the single contact point. The compliance of the carcass is modelled by a longitudinal and a lateral spring. Due to a difference in the velocities of point w' and w, the contact point w' moves in a lateral and longitudinal direction with respect to the wheel rim and this deflects the tyre carcass. For further mathematical descriptions, the focus is on the lateral directions.

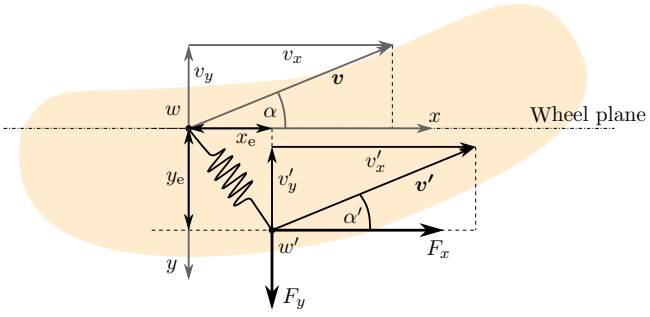

Figure 2.8.: Force application point displacement of a single contact point tyre model in a lateral and longitudinal direction (top view), adapted from [Pacejka, 2012]

Based on the difference in the velocities of point w' and w, the time dependent deflection rates in lateral direction can be defined as

$$\frac{\mathrm{d}y_\mathrm{e}}{\mathrm{d}t} = -(v_y - v'_y)\,, \tag{2.11}$$

where y_e is defined as lateral deflection and $v_y - v'_y$ as the difference between sliding velocities. Note that camber influence is not included, wherein $v_y = v_{\mathrm{sy}}$ and $v'_y = v'_{\mathrm{sy}}$ applies. For small slip values, the lateral slip force is defined as

$$F_y = c_\alpha\,\alpha' = -\,c_\alpha\,\frac{v'_y}{|v_x|}\,, \tag{2.12}$$

where α' refers to the contact point slip angle or transient slip angle. It is assumed that the difference between the longitudinal velocity of the contact centre and the wheel centre longitudinal velocity is negligible. By calculating v'_y from Equation (2.11), implementing it in Equation (2.12) and calculating the internal spring force with $F_y = c_y\,y_\mathrm{e}$ the equation for the lateral deflection is defined by

$$\frac{\mathrm{d}y_\mathrm{e}}{\mathrm{d}t} + \frac{c_y}{c_\alpha}\,|v_x|\,y_\mathrm{e} = -v_y = |v_x|\,\alpha\,, \tag{2.13}$$

where $\alpha \approx -v_y/|v_x|$ describes the slip angle of point w. By solving the DE, the lateral force can be calculated with the internal spring force.

Alternative definition in point w' For linear and small slip condition, the transient slip angle is calculated as

$$\alpha' \approx \tan\alpha' = \frac{y_\mathrm{e}}{\sigma}\,, \tag{2.14}$$

where $\sigma = c_\alpha / c_y$ is defined as relaxation length. After rearranging the time derivative of Equation (2.14) reads

$$\frac{\mathrm{d}y_\mathrm{e}}{\mathrm{d}t} = \frac{\mathrm{d}\sigma}{\mathrm{d}t}\,\alpha' + \frac{\mathrm{d}\alpha'}{\mathrm{d}t}\,\sigma\,. \tag{2.15}$$

Combining Equation (2.15) with Equation (2.13) and assuming that the relaxation length σ is constant leads to

$$\sigma\,\frac{\mathrm{d}\alpha'}{\mathrm{d}t} + |v_x|\,\alpha' = |v_x|\,\alpha = -v_y\,, \tag{2.16}$$

whereby the lateral force can be calculated with $F_y = c_\alpha\,\alpha'$. If only small changes in α' and F_z are considered, the influence of changing wheel loads F_z on the relaxation length can be taken into account by combining Equation (2.15) and (2.13) with

$$\sigma\,\frac{\mathrm{d}\alpha'}{\mathrm{d}t} + \left(|v_x| + \frac{\mathrm{d}\sigma}{\mathrm{d}F_z}\,\frac{\mathrm{d}F_z}{\mathrm{d}t}\right)\,\alpha' = |v_x|\,\alpha = -v_y\,. \tag{2.17}$$

Combining $F_y = c_y\,y$ with Equation (2.13) and assuming that the lateral tyre stiffness c_y is independent of the wheel load while taking the linear steady-state lateral force $F_y^\mathrm{S} = c_\alpha\,\alpha$ into account, the transient force F_y^D yields

$$\sigma\,\frac{\mathrm{d}F_y^\mathrm{D}}{\mathrm{d}t} + |v_x|\,F_y^\mathrm{D} = |v_x|\,F_y^\mathrm{S}\,, \tag{2.18}$$

which is similar to Equation (2.9) and (2.10).

2.3.3.2. Semi non-linear single contact point application

The objective of this semi non-linear model is to enhance the linear model for large slip values. According to [Pacejka, 2012], it is possible to substitute the linear steady-state force F_y^S in Equation (2.18) with the Magic Formula and use the wheel slip angle α as input. However *Pacejka* points out that this might lead to incorrect tyre behaviour because the simulation might still show adhesion in the contact patch, where in reality the tyre is already fully sliding. The more appropriate method is to compute the transient slip angle α' from Equation (2.14) with Equation (2.13) in a first step. From this, the tyre force is computed with the Magic-Formula and the transient slip angle is used as input, like

$$F_y^\mathrm{S} = f(\alpha', F_z, \dots)\,. \tag{2.19}$$

It is important to note that although the linear tyre force is substituted with non-linear

characteristics, the decrease of the relaxation length with increasing slip values is not taken into account with this approach.

2.3.3.3. Non-linear single contact point application

Up to this point, the relaxation length has been defined by

$$\sigma = \frac{c_\alpha}{c_y} \quad \text{and} \quad c_\alpha = \left.\frac{\partial F_y}{\partial \alpha}\right|_{\alpha=0}, \tag{2.20}$$

whereby this is only applicable for small slip values. With increasing slip, the slope of the tyre force characteristics decreases until it gets to zero at the force maximum. Under realistic conditions, the relaxation length also decreases with increasing slip values. To take this behaviour into account, *Pacjeka* introduces the intersection length σ^* in the single contact point model, which is defined as the ratio of the lateral deflection y_e and the transient lateral slip α' with

$$\sigma^* = \frac{y_\mathrm{e}}{\tan\alpha'}, \tag{2.21}$$

and concerning this, Equation (2.13) yields

$$\frac{\mathrm{d}y_\mathrm{e}}{\mathrm{d}t} + \frac{1}{\sigma^*}\,|v_x|\,y_\mathrm{e} = -v_y = |v_x|\,\tan\alpha\,, \tag{2.22}$$

where σ is replaced with σ^*. Writing Equation (2.22) more directly is possible by eliminating σ^* from Equation (2.21) with

$$\frac{\mathrm{d}y_\mathrm{e}}{\mathrm{d}t} + |v_x|\,\tan\alpha' = -v_y = |v_x|\,\tan\alpha\,. \tag{2.23}$$

Writing Equation (2.23) completely in terms of transient slip angle by using the relationship $F_y = c_y\,y_\mathrm{e}$ and remembering $F_y = f(\alpha', F_z)$ yields

$$\frac{1}{c_y}\,\frac{\partial F_y}{\partial \tan\alpha'}\,\frac{\mathrm{d}\tan\alpha'}{\mathrm{d}t} + |v_x|\,\tan\alpha' = -v_y - \frac{1}{c_y}\,\frac{\partial F_y}{\partial F_z}\,\frac{\mathrm{d}F_z}{\mathrm{d}t}\,, \tag{2.24}$$

where the input $\mathrm{d}F_z\,/\,\mathrm{d}t$ requires the slope $\partial F_y\,/\,\partial F_z$ at given slip angle values. By assuming the wheel load F_z as constant, the second term on the right side of Equation (2.24) vanishes and the first-order DE as well as the restricted version of this model can be written as

$$\sigma_\alpha\,\frac{\mathrm{d}\tan\alpha'}{\mathrm{d}t} + |v_x|\,\tan\alpha' = -v_y\,, \tag{2.25}$$

with

$$\sigma_\alpha = \frac{1}{c_y}\,\frac{\partial F_y}{\partial \tan\alpha'}\,. \tag{2.26}$$

In summary, within this model, the relaxation length depends on the slope of the tyre force characteristics. *Pacejka* points out that beyond the force maximum, the value of the relaxation length might become negative. Therefore, the solution to Equation (2.25) is unstable beyond the peak of the tyre force.

2.3.3.4. Enhanced non-linear transient tyre model

This transient tyre model is an important part of the widely known tyre models MF-Tyre and MF-Swift. Up to this point, the time delay of the tyre force was modelled by means of the relaxation length. In the previous investigations, even the decrease of the relaxation length with increasing slip values was taken into account, as can be seen in Equation (2.26). According to [Pacejka, 2012], this approach leads to a complex description of combined slip conditions as well as to possible computation problems. Therefore, *Pacejka* presents a different approach to model the transient behaviour of the tyre forces and torques. For this approach, the compliance of the tyre carcass is modelled explicitly by springs. This enables the separation of the slip properties of the contact patch and the deformation of the tyre carcass without the relaxation length.

Two main enhancements of this model in comparison to the previously presented versions of the single contact point model are given. First, the contact point is represented by a small mass m_c and second, in addition to the carcass springs, a longitudinal and lateral damper is introduced. The contact mass increases the order of the system by one. Referring to *Pacejka*, the introduction of the small contact mass brings the disadvantage of a new natural frequency, but it facilitates the computation.

Based on *Newton's 2nd law*, the equation of motion regarding the mass point applies in a longitudinal direction with

$$m_\mathrm{c}\,\dot{v}^*_{sx} + d_x\,\dot{x}_\mathrm{e} + c_{\mathrm{c}x}\,x_\mathrm{e} = F_x^\mathrm{S}\left(s'_x, \alpha', F_z\right)\,, \tag{2.27}$$

and in lateral direction by

$$m_\mathrm{c}\,\dot{v}^*_{sy} + d_y\,\dot{y}_\mathrm{e} + c_{cy}\,y_\mathrm{e} = F_y^\mathrm{S}\left(s'_x, \alpha', \gamma, F_z\right) - F_{y,\mathrm{NL}}\,. \tag{2.28}$$

Within Equation (2.27) and (2.28), d_x and d_y denote the damping properties, $c_{\mathrm{c}x}$ and c_{cy} indicate the carcass stiffnesses and $\dot{v}^*_{sx}$ and $\dot{v}^*_{sy}$ specifies the derivatives of the contact patch sliding velocities. On the right side of these equations, the steady-state tyre forces F_x^S and F_y^S, which are computed using the Magic Formula, act as inputs. The transient longitudinal slip s'_x, the transient lateral slip angle α', the camber angle γ and the tyre load F_z are used as inputs for the Magic Formula. The part $F_{y,\mathrm{NL}}$ indicates the non-lagging camber force. Referring to *Pacejka*, this force has to be taken into account if the influence of tyre camber is of interest. For more information, see Section 7.3 in [Pacejka, 2012].

Again, the deflection rates $\dot{x}_\mathrm{e}$ and $\dot{y}_\mathrm{e}$ can be derived from the differences of the sliding velocities by

$$\dot{x}_\mathrm{e} = v_{sx}^* - v_{\mathrm{s}x} \quad \text{and} \quad \dot{y}_\mathrm{e} = v_{sy}^* - v_{\mathrm{s}y}\,, \tag{2.29}$$

whereby, the sliding velocities of the wheel point w are given by

$$v_{\mathrm{s}x} = v_x - r_\mathrm{e}\,\omega \quad \text{and} \quad v_{\mathrm{s}y} = v_y - r_\mathrm{s}\,\dot{\gamma}\,, \tag{2.30}$$

where r_e indicates the effective rolling radius, ω the wheel speed of revolution, r_s the static radius and $\dot{\gamma}$ the camber rate. However, *Pacejka* again introduces the relaxation length σ_c to enable computations for near or at standstill. Therefore, the following first-order DE for the transient lateral slip is defined by

$$\sigma_\mathrm{c}\,\frac{\mathrm{d}\alpha'}{\mathrm{d}t} + |v_x|\,\alpha' = -v_{sy}^*\,. \tag{2.31}$$

According to *Pacejka*, the relaxation length σ_c can be given as a small finite value like half of the contact patch length, or it can be set to zero if simulations near or at standstill are irrelevant. Therefore, Equation (2.31) does not take wheel load changes into account. However, a simple approach to adapt this relaxation length to respond to load changes is given in [Pacejka, 2012]. Furthermore, it is important to note that $c_{\mathrm{c}x,y}$ denotes the lateral or longitudinal stiffness of the carcass and not the overall tyre stiffness $c_{x,y}$. Hence, *Pacejka* indicates a way to derive the carcass stiffness from the measured relaxation length.

Finally, the transient tyre forces at the wheel rim can be computed in a longitudinal direction by

$$F_x = d_x\,\dot{x}_\mathrm{e} + c_{\mathrm{c}x}\,x_\mathrm{e}\,, \tag{2.32}$$

and in lateral direction respectively by

$$F_y = d_y\,\dot{y}_\mathrm{e} + c_{\mathrm{c}y}\,y_\mathrm{e} + F_{y,NL}\,. \tag{2.33}$$

It is important to note that this transient tyre model is not just implemented in MF-Tyre, but also in the MF-Swift tyre model. In Chapter 9 and 10 of [Pacejka, 2012], the MF-Swift tyre model is discussed in detail. Within MF-Swift, the previously presented model for the transient horizontal tyre forces is enhanced for turn slip and the relaxation length σ_c plays an important role. *Pacejka* uses a Brush Model to determine the relaxation length, which is used as the contact patch slip model in MF-Swift. The contact mass is enhanced by additional tread elements. Therefore, the relaxation length is determined by means of this model. According to [Kuiper & Van Oosten, 2007] and [TNO Delft Tyre, 2013], this version of the transient tyre model is also implemented in MF-Tyre to simulate the non-linear relaxation behaviour. *Kuiper* gives a short overview regarding the two approaches to simulate the transient tyre forces within MF-Tyre. A former version of this model can also be found in [Pacejka & Besselink, 1997].

2.3.3.5. First-order tyre dynamics according to Rill

A further well-known single contact point transient tyre model application is based on a non-linear first-order tyre dynamics approach developed by *Rill* and implemented in the TMeasy tyre model. In comparison to the model application mentioned in the previous subsections, this implementation is based on a first-order Taylor expansion. The explanation is adapted from [Hackl et al., 2016a], whereby a detailed model description is given in [Rill, 2012] and [Rill, 2006].

The tyre forces F_x, F_y and the turn torque $T_z = r_\mathrm{b}\, F_\Psi$ are operating in the contact patch and deflecting the tyre in the longitudinal, lateral and circumferential directions, as seen in Figure 2.9. In this approach, the turn torque is modelled via a sliding contact ring with radius r_b where the sliding force F_Ψ is calculated via an appropriate bore motion. The transient tyre force in lateral direction is given by

$$F_y^\mathrm{D} \;=\; c_y\, y_\mathrm{e} \;+\; d_y\, \dot{y}_\mathrm{e}\,, \tag{2.34}$$

which is often referred as Voigt-Kelvin model in literature. Thereby, c_y and d_y describe the stiffness and damping properties of the tyre in the lateral direction. Due to the time derivative $\dot{y}_\mathrm{e}$ of the lateral tyre deflection y_e, the contact point velocity changes from v_y to $v_y + \dot{y}_\mathrm{e}$, which is derived from the rim motion.

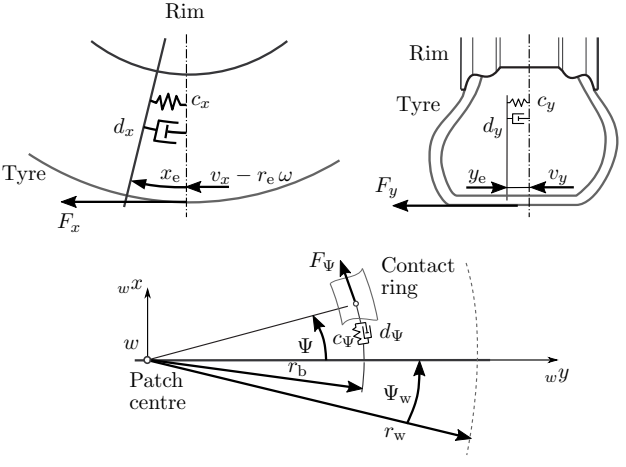

Figure 2.9.: Tyre deflection in the longitudinal direction (upper left) and lateral direction (upper right) as well as bore rotation around the ${}_w z$ axis (below) according to the first-order tyre dynamics and implemented as a Voigt-Kelvin model approach in the TMeasy tyre model, adapted from [Hackl et al., 2016a] and based on [Rill, 2006]

A first-order Taylor expansion is then applied to the non-linear tyre force characteristics $F_y = F_y(s_y)$ delivers the transient lateral force as

$$F_y^{\mathrm{D}} \;=\; F_y\left(v_y + \dot{y}_{\mathrm{e}}\right) \;\approx\; F_y\left(v_y\right) \;+\; \frac{\partial F_y}{\partial v_y}\,\dot{y}_{\mathrm{e}} \;=\; F_y^{\mathrm{S}} \;+\; \frac{\partial F_y}{\partial s_y^{\mathrm{N}}}\,\frac{\partial s_y^{\mathrm{N}}}{\partial v_y}\,\dot{y}_{\mathrm{e}}\,, \tag{2.35}$$

where F_y^{S} names the steady-state lateral tyre force. A normalised lateral slip is used within the tyre model TMeasy that is defined by

$$s_y^{\mathrm{N}} \;=\; \frac{-v_y}{r_{\mathrm{e}}\,|\omega|\,\hat{s}_y + v_{\mathrm{N}}}\,, \tag{2.36}$$

where v_y represents the lateral component of the contact point velocity derived from the rim motions, r_{e} describes the dynamic rolling radius of the tyre, ω defines the angular velocity of the wheel around the wheel rotation axis and $\hat{s}_y$ is a named slip normalisation factor, [Rill, 2012]. In addition, a small fictitious velocity $v_{\mathrm{N}} > 0$ was added in the denominator to avoid singularities in the lateral slip for $\omega = 0$, which will occur with a locked wheel or at standstill.

The TMeasy tyre model introduces a generalised three-dimensional tyre slip s_{G} wherein the normalised longitudinal and lateral slips as well as the bore slip are vectorially added. Then, a generalised tyre characteristic $F_{\mathrm{G}} = F_{\mathrm{G}}\left(s_{\mathrm{G}}\right)$ is used to describe the steady-state tyre behaviour. As a consequence, the steady-state lateral tyre force and its partial derivative with respect to the normalised lateral slip is given by

$$F_y^{\mathrm{S}} \;=\; \frac{F_{\mathrm{G}}}{s_{\mathrm{G}}}\,s_y^{\mathrm{N}} \;=\; f_{\mathrm{G}}\,s_y^{\mathrm{N}} \quad\text{and}\quad \frac{\partial F_y}{\partial s_y^{\mathrm{N}}} \;\approx\; f_{\mathrm{G}}\,, \tag{2.37}$$

where f_{G} characterises the global derivative of the tyre characteristics F_{G} with respect to the generalised slip s_{G}.

Combining Equation (2.34) with (2.35) and taking Equations (2.37) and (2.36) into account results in

$$c_y\,y_{\mathrm{e}} \;+\; d_y\,\dot{y}_{\mathrm{e}} \;=\; f_{\mathrm{G}}\,\frac{-v_y}{r_{\mathrm{e}}\,|\omega|\,\hat{s}_y + v_{\mathrm{N}}} \;+\; f_{\mathrm{G}}\,\frac{-1}{r_{\mathrm{e}}\,|\omega|\,\hat{s}_y + v_{\mathrm{N}}}\,\dot{y}_{\mathrm{e}}\,. \tag{2.38}$$

By introducing the abbreviation $v_{Ty}^{*} = r_{\mathrm{e}}\,|\omega|\,\hat{s}_y + v_{\mathrm{N}}$ for the travel speed one finally gets

$$\left(v_{Ty}^{*}\,d_y \;+\; f_{\mathrm{G}}\right)\,\dot{y}_{\mathrm{e}} \;=\; -\,v_{Ty}^{*}\,c_y\,y_{\mathrm{e}} \;-\; f_{\mathrm{G}}\,v_y\,. \tag{2.39}$$

This first-order DE describes the dynamics of the lateral tyre deflection and together with Equation (2.34) this defines the dynamics of the lateral tyre force. Similar relations are applied for the longitudinal force F_x^{D} and the dynamic turn torque T_z^{D} within the TMeasy tyre model. The first-order dynamics of the lateral tyre deflection and hence the dynamics of the lateral tyre force can be characterised using a time coefficient τ_y or

the corresponding relaxation length σ_y. Therefore, Equation (2.39) gets

$$\tau_y \;=\; \frac{v_{Ty}^{*}\, d_y \;+\; f_{\mathrm{G}}}{v_{Ty}^{*}\, c_y} \qquad \text{and} \qquad \sigma_y \;=\; \tau_y\, r_{\mathrm{e}}\, |\omega| \;\approx\; \frac{v_{Ty}^{*}\, d_y \;+\; f_{\mathrm{G}}}{c_y}\,. \tag{2.40}$$

The time constant as well as the relaxation length depend on the modified transport velocity v_{Ty}^{*}, the stiffness c_y and damping d_y properties of the tyre and the global derivative of the generalised steady-state tyre characteristics f_{G}. This automatically results in a dependency on the wheel load F_z and the generalised slip s_{G}.

2.3.4. Mathematical based approach

A more mathematical based approach to investigate the transient behaviour brings us to the transfer functions. For these investigations, a first-order or higher DE that describes the transient tyre behaviour has to be defined and then transformed from the time to the frequency domain. Following from this, the system function can be reshaped as a ratio of the frequency dependent output, e.g. the lateral tyre force $F_y(s)$ and the input, e.g. slip angle $\alpha(s)$, like

$$G(s) \;=\; \frac{F_y(s)}{\alpha(s)}\,, \tag{2.41}$$

where $G(s)$ represents the frequency-based transfer function of the system. Hence, based on the mathematical *System Theory* a frequency response or so called *Bode diagram* can be generated for detailed investigations. A *Bode diagram* is usually a combination of a *Bode magnitude plot*, which represents the magnitude of the frequency response influences and a *Bode phase plot* which describes the phase response between input and output. Note that most common methods dealing with *Bode diagram* are only permitted for *linear time invariant* (LTI) systems. Hence, for investigations within nonlinear models, a numerical method based on sine signal input has to be used. For further theoretical details, see for example [Horn & Doudoumas, 2004].

2.3.4.1. Approach based on semi-physical fundamentals

Based on the fundamentals derived in the previous subsection, Equation (2.9) is given with

$$\tau\, \dot{F}_y + F_y = c_\alpha\, \alpha\,, \tag{2.42}$$

where the time constant is defined by $\tau = c_\alpha/(v\, c_y)$.

After transforming Equation (2.42) into the frequency domain, the system function $G(s)$, which is defined as the ratio of the transient lateral force $F_y(s)$ and the side slip angle α, reads

$$G(s) = \frac{F_y(s)}{\alpha(s)} = \frac{c_\alpha}{1 + \tau\, s}\,. \tag{2.43}$$

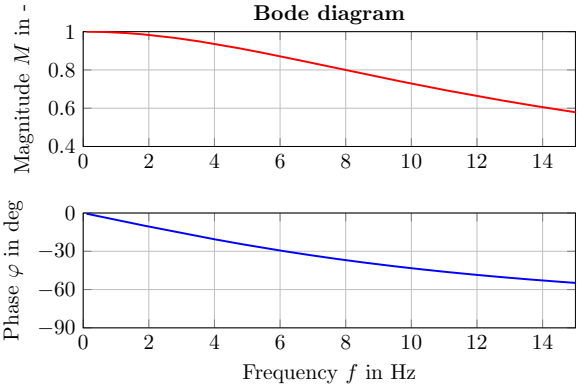

Figure 2.10.: Magnitude and phase response of a first-order lag element (PT1), wherein the upper plot presents the magnitude ratio by $M = F_y^{\mathrm{D}}/F_y^{\mathrm{S}}$ and the lower one the phase response between F_y^{D} and F_y^{S} for a time constant of $\tau = 0.015$

According to a graphic representation of the system responses, as shown in Figure 2.10, the system behaviour can be described. The upper plot shows that an increasing manoeuvre frequency causes a reduction in the output magnitude. Furthermore, an increasing phase delay between the two signals with increasing frequency is presented in the bottom plot. This simple example thus shows that a *Bode diagram* is a useful tool to describe system behaviour.

The first tyre dynamic behaviour investigations with *Bode diagrams* were done by [Nast et al., 1991]. They investigated the tyre transfer behaviour in terms of the lateral force and the self-aligning torque by means of Gaussian noise on a drum test bench. The measurements carried out show the influence of the tyre velocity on the frequency responses. A lower tyre velocity leads to a stronger decrease in the phase response. To approximate the measured frequency responses, a second-order DE was used.

A very detailed investigation into transient tyre modelling based on the frequency domain is given in [Besselink, 2000]. After a detailed explanation of different types of dynamic tyre models, the focus was on the shimmy stability based on the frequency response.

2.3.4.2. Second-order extension according to Einsle

Additionally [Einsle, 2010] investigated the transfer behaviour and the frequency responses of tyres. He used a measurement procedure with a slip angle sine at different frequencies on a flat track test bench. The results show that the tyre force amplitude

decreases and the phase lag increases with rising input frequency. He points out that at about $f \approx 4\,\mathrm{Hz}$ and $v_x \approx 20\,\mathrm{km/h}$, a phase lag of $\varphi \geq 90\,\mathrm{deg}$ can occur. This phase lag can also be seen in the *Bode diagrams* for the measurement results of different tyres. *Einsle* also points out that the decrease in the lateral tyre force amplitude can already take up to 85 % of the maximum value at about $f \approx 5\,\mathrm{Hz}$. Furthermore, he notes that the frequency responses show a typical behaviour of a lag element of first or higher order (PTx).

After analysing a large series of measurements, *Einsle* concludes that the modelling of the transient behaviour of the tyre using the widely applied first-order approach (PT1) is not sufficient at low velocities. A transfer system with PT1 behaviour can only account for a maximum phase lag of 90 deg. Therefore, the description of the transient lateral tyre force using a second-order approach (PT2) is seen as necessary. In conclusion, a mathematical description of a second-order DE was defined by

$$\tau^2\,\ddot{F}_y^{\mathrm{D}} \;+\; \frac{\sigma_\alpha}{v_x}\,\dot{F}_y^{\mathrm{D}} \;+\; F_y^{\mathrm{D}} \;=\; F_y^{\mathrm{S}} \tag{2.44}$$

with

$$\tau \;=\; \frac{\sigma_\alpha}{2\,D_\alpha\,v_x} \qquad \text{and} \qquad F_y^{\mathrm{S}} = c_\alpha\,\alpha\,. \tag{2.45}$$

In his implementation, τ denotes the time constant, σ_α names the relaxation length, v_x indicates the longitudinal tyre velocity, c_α denotes the cornering stiffness and α names the slip angle. Typical for a PT2 element, the damping parameter D_α occurs. *Einsle* labels this variable as relaxation damping. Furthermore, investigations into influences of the wheel load, inflation pressure, tyre camber, tyre velocity and the slip angle on this damping parameter were carried out.

Finally, a performance comparison of the well-known first-order approach and its extension given in Equation (2.44) is presented in this thesis, where the major difference occurs in the phase response. He points to the modelling of the transient lateral force by the PT2 approach as the best solution. It is important to note that, due to a high value for the damping parameter $D_\alpha > 1$, the value of the time constant τ is very small. This leads to an overcritical damping of the PT2-element. Therefore, the step response of the lateral tyre force is similar to the step response of a PT1, but a different phase response can be recognised.

2.4. Comparative conclusion of the investigated model approaches

After starting with a short description of physical tyre components, followed by basic tyre functions and a presentation of the STI, the focus of the chapter was the classification of tyre models and transient tyre model applications based on semi-physical approaches.

In the first part of this chapter, a broad overview of already existing tyre model approaches for application in the automotive industry was presented. Based on an already large selection of various models, it was shown that different model classifications, from two up to five or more different groups with fluid transition, are already existent in the literature. Finally, a subdivision into handling models and structural models was made and presented in more detail.

As a result of the literature research, semi-physical based handling models turned out to offer a good trade-off between accuracy, parameter specification and calculation time for further transient tyre investigations based on ADAS and VDC application. For experimental research in the next chapters, the decision to use the tyre model **TMeasy** was made. TMeasy fulfils all the requirements as a semi-physical handling model and additionally it already has a fundamental transient model implemented. Furthermore, through cooperation with its creator, Georg Rill, the open source code was provided for investigations during this thesis project.

In the second part, the focus was semi-physical transient tyre model approaches. Based on stretched string tyre research from *Von Schlippe*, which forms the basis of the majority of later research, state of the art applications are presented in more detail. It was shown that first-order approaches in particular deal with the implementation of the relaxation length σ, which depends on the cornering stiffness c_α and the lateral stiffness c_y, or the time constant τ which is related to σ and the longitudinal velocity v_x. Regardless, stretched string and single contact point application leads to this semi-physical approach, which is mathematically summarised by Equation (2.10) with

$$\tau_{x,y}\,\dot{F}^{\mathrm{D}}_{x,y} + F^{\mathrm{D}}_{x,y} = F^{\mathrm{S}}_{x,y} \qquad \text{with} \qquad F^{\mathrm{D}}_{x,y}(t_0 = 0) = 0\,. \tag{2.46}$$

Differences in this first-order application are mostly given in the value τ, e.g. with

$$\frac{d_y}{c_y} + \frac{1}{|v|}\,\frac{c_\alpha}{c_y} = \tau_{\mathrm{Rill}} > \tau_{\mathrm{Pacejka}} = \frac{1}{|v|}\,\frac{c_\alpha}{c_y}\,, \tag{2.47}$$

where an additional term d_y/c_y is given in the application of *Rill*, or in the implementation of the steady-state characteristics $F^{\mathrm{S}}_{x,y}$ with different linear and non-linear applications.

A possible extension involves the implementation of relaxation length that is dependent on wheel load, see Equation (2.17) or (2.24). This implementation makes sense from a technical point of view, but the parameterisation process seems to be complicated because of the interaction of the lateral and the cornering stiffness.

Common state of the art modelling approaches are second-order non-linear applications using tyre mass. An advantage of this approach is the implementation of tyre damping, but a small tyre particle mass is not easy to define and furthermore influences the simulation time in a critical way. Results in [Hackl et al., 2016c] show that the second-order

application does not really improve the accuracy, but it does influence the simulation time negatively.

Finally, different transient approaches are already being implemented in tyre modelling applications. Still, these implementations are either hardly able to handle the simulation of critical driving situations, which means a high frequency demand, they are just mathematical approaches without the physical background for practical applications, or they are still too time consuming for semi-physical and real time operations. In conclusion, in the field of semi-physical tyre modelling, on the one hand a model is needed that is able to cover transient influences within high frequency areas, and on the other hand a model is needed that is able to adhere to the conditions of short calculation time, parameterability and physical background. Therefore, further focus should be on the following:

- Wheel load dependent model parameter research to increase accuracy and represent the vertical force dependency in critical driving situations
- The influence of the manoeuvre frequency to model the viscoelastic mechanism of tyre deformation

However, before the parameters of a basic model can be specified, with a special focus on transient investigations, another main aspect has to be taken into account. Looking at Equation (2.46), it is obvious that three variables are included in the equation. The main part is the transient force $F_{x,y}^{\mathrm{D}}$ and its derivative $\dot{F}_{x,y}^{\mathrm{D}}$, the second is $\tau_{x,y}$, which is constant in basic applications or speed and physical rubber dependent in extended implementations. There is also a third part which is neglected in most investigations: inaccuracies in the steady-state characteristic $F_{x,y}^{\mathrm{S}}$.

This leads to the result that the dynamic behaviour is not only dependent on parameters which are represented by the transient time constant $\tau_{x,y}$, but also that steady-state tyre implementation is able to influence the transient force behaviour. This means inaccuracies in steady-state characteristics influence the parameterisation and evaluation process of the dynamic behaviour.

Because the steady-state characteristic is implemented in most transient model applications, the relation to the time constant influence has to be investigated first. Therefore, how inaccuracies can influence the transient characteristics will be investigated in the beginning of the next chapter. Furthermore, what leads to these inaccuracies and how they have to be taken into account is described.

3

External influences on steady-state tyre characteristics

The transient model behaviour not only depends on parameters which are represented by the transient time constant, but also on the accuracy of the steady-state implementation, as is presented in the comparative conclusion of Chapter 2. A sensitivity analysis based on Equation (2.46) to evaluate the influence of the time constant τ in comparison to the steady-state characteristics on the transient force behaviour is presented in the first part of this chapter. Specifically, the statement that inaccuracies in the steady-state influence the transient force behaviour is mathematically proven. This leads to the point that accurate steady-state characteristics form the foundation for transient force investigations.

While the presentation of an accurate parameterisation process based on measurement data will be subject of the next chapter, some attention is also paid to the effects that influence the steady-state behaviour. Therefore, a literature review concerning effects like changes in road condition, tyre velocity, tyre wear or temperature, including their influences, are investigated in more detail. As a result of this study, external effects that cannot be reduced in size have to be taken into account during further investigations and parameterisation processes in order to avoid influencing effects.

The special focus is tyre temperature, which turned out to be the main influencing factor. Since these effects should not be neglected, possible model implementations and their influences on the tyre force behaviour are considered more closely in the second part of this chapter. Specifically, possible temperature model implementations and the effects on steady-state properties are presented based on a review of the literature.

For experimental purposes, a small section of the tyre tread is cut out and examined in detail on a prototype test bench. The objective of these section measurements is to reach a theoretical understanding of rubber physics with respect to external influences. Finally, starting from a literature review and followed by basic and practical experimental validations, a temperature model structure is presented as a foundation for further investigations.

3.1. Sensitivity analysis - Basic examination of tyre dynamics

Sensitivity analyses are often used for parameter studies when values or initial conditions of systems are not accurately known in order to evaluate which effects can be ignored in the specification of the model, [Campolongo et al., 2000], [Waser, 2009]. A parameter is defined as being sensitive when small changes to the value lead to big changes in the results. Therefore, to calculate the sensitivity of the two parameters of the first-order *differential equation* (DE) presented in Section 2.4 with

$$\tau_{x,y}\,\dot{F}^{\mathrm{D}}_{x,y} + F^{\mathrm{D}}_{x,y} = F^{\mathrm{S}}_{x,y}\,, \tag{3.1}$$

is the goal for this section.

To achieve this goal, a local method worked out in [Lex, 2015] with the mathematical foundation from [Dickinson & Gelinas, 1976] is chosen. This method is particularly suitable for sensitivity analyses of parameters and state vectors in DEs. Basis of this method forms the equation

$$\dot{\boldsymbol{p}} = \boldsymbol{f}_c + \boldsymbol{J}\cdot\boldsymbol{p}\,, \tag{3.2}$$

where $\boldsymbol{p} = \partial\boldsymbol{z}/\partial\boldsymbol{c}_m$ defines the linear sensitivities of the given model with respect to a parameter c_m, $\boldsymbol{f}_c$ being the sensitivity of the right-hand side of the DE $\boldsymbol{f}$ with respect to c_m and $\boldsymbol{J}$ defines the Jacobian matrix of the DE based on the state vector, [Dickinson & Gelinas, 1976]. Therefore, to calculate the sensitivity from Equation (3.1), the first derivative must be formed at the beginning and the sensitivity has to be resolved by using Equation (3.2) afterwards. A mathematical theory concerning this is given in Appendix A. For a detailed description and further use cases, please reference [Lex, 2015].

The solution to the sensitivity analysis of a practical step steering input manoeuvre by using Equation (3.1) is presented in Figure 3.1. Whereas, F^{S} represents the steady-state and F^{D} the resulting dynamic force behaviour. In the upper plot, a steady-state force step from $F^{\mathrm{S}} = 0\,\mathrm{N}$ to $F^{\mathrm{S}} = 2000\,\mathrm{N}$ is given at the time $t_0 = 0.1\,\mathrm{sec}$ with a time step of $\Delta t = 0.01\,\mathrm{sec}$. In addition, the transient force F^{D} using a time constant $\tau = 0.05$ is presented as a result after solving the DE.

In the second plot below, the relative sensitivities with respect to the steady-state force $z_{F^{\mathrm{S}}}$ and furthermore with respect to the time constant z_τ is presented. In addition, the total sensitivity, as a result of both with $z_{F^{\mathrm{S}}} + z_\tau$, is given. It is apparent that $z_{F^{\mathrm{S}}}$ has a relative linear sensitivity influence in all areas when $F^{\mathrm{S}} \neq 0$. This corresponds to the fact that the accuracy of the steady-state characteristics directly influences the accuracy of the transient behaviour in a linear way.

Alternatively, the relative sensitivity of the value τ only influences the results in dynamic time, corresponding to Equation (3.1) when $F^{\mathrm{S}}_{x,y} - F^{\mathrm{D}}_{x,y} \neq 0$. Furthermore, the highest sensitivity of z_τ is given after a time period of $t \approx t_0 + \tau$ within this example. Moreover, a relative sensitivity relationship of $|z_\tau| < |z_{F^{\mathrm{S}}}|$ is given for most τ and ΔF^{S} value combinations. See characteristics $z_{F^{\mathrm{S}}} + z_\tau$ in Figure 3.1 below.

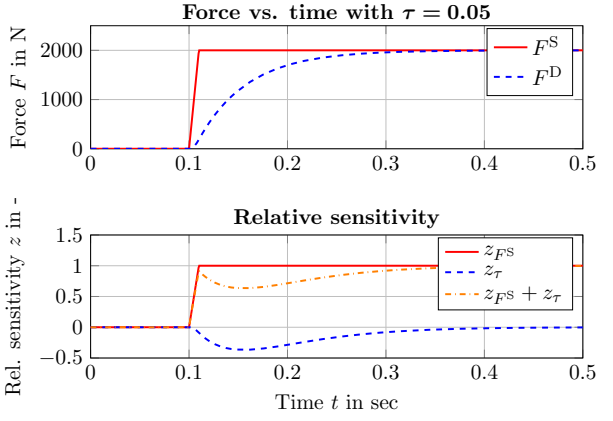

Figure 3.1.: Sensitivity analysis in order to evaluate the influence of the steady-state characteristics F^{S} in relation to the influence of the time constant τ, based on Equation 3.1; in the upper plot a step steer input manoeuvre F^{S} and the transient force F^{D} by solving the DE, with $\tau = 0.05$ is presented, and in the plot below, the sensitivities of the steady-state force $z_{F^{\mathrm{S}}}$ and the time constant z_τ is presented; moreover, the total sensitivity, as a result $z_{F^{\mathrm{S}}} + z_\tau$, is given

As a further step, a more detailed investigation by including the influence on the dynamic force behaviour and on the relative sensitivity, based on the results from Figure 3.1, is presented in Figure 3.2. A variance of $\tau = \tau \pm 20\,\%$ is given in the three plots in the left and a variance of $F^{\mathrm{S}} = F^{\mathrm{S}} \pm 20\,\%$ is presented in the three plots on the right. In the two upper plots, the influence on the transient force behaviour is given. On the upper left plot, it is apparent that a higher time constant τ represents a more sluggish behaviour for the force and vice versa. On the right upper plot, a variation of the value F^{S} is presented. As was already seen in the results from Figure 3.1, a direct change in the steady-state force results. Furthermore, a larger gradient is given around t_0 in order to reach the higher values of F^{S}.

In the middle two plots the sensitivities relative to the initial conditions are given. On the left side, a variance of the value τ leads directly to an influence in the relative sensitivity within a transient timeframe. Meanwhile, a change of the steady-state value F^{S} leads to a linear offset.

Furthermore, the interaction between both sensitivities is given in the two plots below. Overall, it is shown that changes in both values directly influence the behaviour of the dynamic characteristics, which is also evident in the sensitivity behaviour. Subsequently, inaccuracies in the steady-state characteristics lead to parameterisation errors in the

value of the time constant and vice versa. Therefore, accuracy in steady-state characteristics is required for further investigations of the dynamic behaviour.

In summary, looking at Equation (3.1) from a technical point of view, the two variables implemented $\tau_{x,y}$ and $F^{\mathrm{S}}_{x,y}$ influence the transient behaviour of the force $F^{\mathrm{D}}_{x,y}$. This assumption has been confirmed by a mathematical investigation using a sensitivity analysis in this section. In a next step, the possibility for a precise model description of the steady-state characteristics therefore has to be investigated.

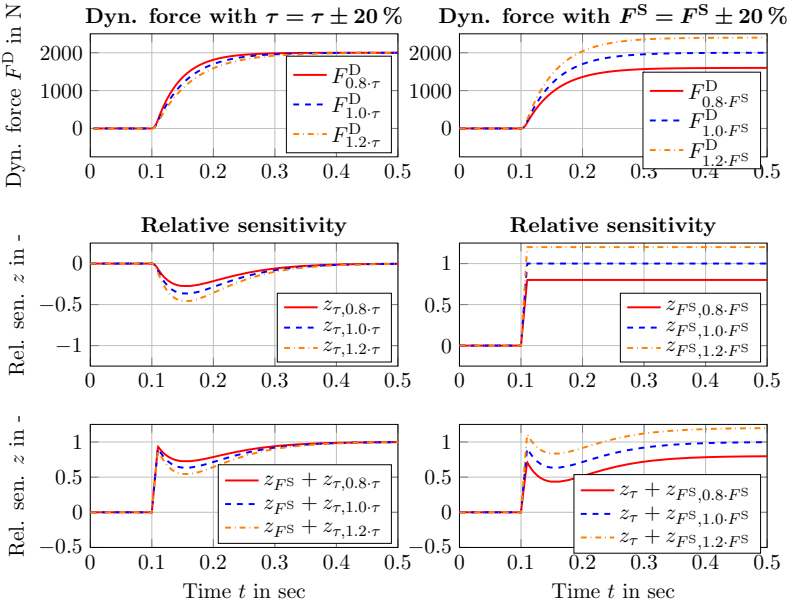

Figure 3.2.: Sensitivity analysis with a variance of $\tau = \tau \pm 20\,\%$ and $F^{\mathrm{S}} = F^{\mathrm{S}} \pm 20\,\%$; the two upper plots represent the parameter influences on the dynamic force behaviour F^{D}; the middle plots show the influences on the relative sensitivity based on the initial results, as presented in Figure 3.1 and the superimposed results are given in the two bottom plots

3.2. Steady-state tyre behaviour as a basis for transient investigations

Steady-state tyre modelling forms the basis for handling tyre models, and it also affects transient force modelling when its behaviour is implemented as it's been done in Equation (3.1). Therefore, two main points for modelling the steady-state tyre behaviour as well as further tyre implementations in an accurate way are obvious:

1. Basic mathematical equations, which are able to emulate the physical tyre characteristics
2. Specific measurement data for parameterisation and validation of the model

Basic model A model can only be as accurate as the mathematical implementation behind it. This brings once again to a fundamental conflict. In detail, a model description should be as accurate as necessary but as simple as possible. As an example, a linear model is never able to describe non-linear behaviour. Therefore, the trade-off always points to the problem formulation.

Measurement data The desire for measurement data without uncertainties, perfectly filtered and without external influences is always given but never achievable. This is a fact, but experience has shown that often less attention is paid to it. Defining a suitable measurement procedure and evaluating the measured data are the first steps in an adequate modelling process.

The two main points mentioned above are the foundation of modelling processes. Nonetheless, beside model accuracy and measurement data being taken for granted, external influences additionally affect the results in terms of characteristics and thus also parameterisation.

While attention goes to the measurement data and the parameterisation process, which will be part of the next chapter. Influences that cannot be reduced in size and influence further investigations on transient behaviour have to be taken into account during the parameterisation and validation process in order to avoid external effects.

To evaluate these external influences, a literature study centred on basic tyre rubber properties and steady-state characteristics was carried out and summarised in Table 3.1. Beside the main parameters which influence the steady-state characteristics, like vertical load F_z, longitudinal slip s_x and lateral slip s_y, focus was on longitudinal velocity v_x, tyre pressure p, tyre temperatures T, maximum road friction coefficient $\mu^{\max}$ and tyre wear w.

Longitudinal velocity Investigations into tyre velocity correspond closely with research on tyre tread compounds. Thus different velocity characteristics influence the maximum coefficient of friction.
As stated in [Lang & Klueppel, 2017] and [Hou et al., 2018], it can be shown that

Table 3.1.: External influences which effect basic tyre rubber properties and steady-state tyre characteristics - literature overview

Influence	**Symbol**	**Source**
Longitudinal velocity	v_x	[Février & Fandard, 2008] [Guo et al., 2005b] [Hou et al., 2018] [Lang & Klueppel, 2017]
Tyre pressure	p	[Angrick et al., 2014] [Braghin et al., 2006] [Parczewski, 2013]
Tyre temperatures	T	[Angrick et al., 2014] [Anupam et al., 2013] [Corollaro, 2014] [Février & Fandard, 2008] [Hou et al., 2018]
Maximum road friction coefficient	$\mu^{\max}$	[Angrick et al., 2014] [Anupam et al., 2013] [Giashi et al., 2015] [Hirschberg et al., 2009] [Hou et al., 2018] [Lang & Klueppel, 2017]
Tyre wear	w	[Braghin et al., 2006] [Tremlett & Limebeer, 2016]

the maximum coefficient of friction is velocity dependent and therefore also the maximal achievable tangential forces. The friction increases with increasing velocity until a certain limit is reached, while it decreases after this point with a lower gradient than when moving towards the maximum.
Alternatively, the effect that force and torque of a tyre vary with the travelling speed, especially when they nearly saturated, are demonstrated in [Guo et al., 2005b] and [Février & Fandard, 2008]. Furthermore, speed-dependent effects were incorporated into semi-physical tyre model approaches and validated with measurement data.

Tyre pressure In [Parczewski, 2013] the focus is on longitudinal, lateral and vertical tyre stiffness. It is noted that they are strongly affected by the inflation pressure, although it has to be stated that each direction is influenced in a different manner. The main focus of [Angrick et al., 2014] is to investigate temperature dependencies of tyre characteristics and the lateral coefficient of friction. In addition, the effects

of internal pressure are examined in more detail, in which a dependency of cornering stiffness on internal pressure is given. Furthermore, the maximum coefficient of friction shows sensitivity to pressure changes as well.

Tyre temperature Tyre temperature investigations often correspond to tyre tread compound investigations, for example research of the velocity influence and maximum road friction. In this case, focus on tyre tread section investigations and their influences on road friction is given in [Anupam et al., 2013] and [Hou et al., 2018]. In [Anupam et al., 2013], experimental observations show that a higher road, ambient or inner temperature resulted in a lower hysteresis friction for a given tyre slip ratio.
As an alternative to compound investigations, [Angrick et al., 2014] and [Corollaro, 2014] show a strong temperature dependence for both the cornering stiffness and the maximum coefficient of friction. Specifically, in [Angrick et al., 2014] an experimental dependency involving cornering stiffness, relaxation length and lateral coefficient of friction on core and surface temperature is presented.

Maximum coefficient of friction The literature description of external influences is given in Table 3.1; there is a strong interaction. Therefore, the maximum coefficient of friction itself is influenced by various effects, e.g. velocity and temperature. Additionally, it can be stated that the lateral and longitudinal stiffness of a tyre is, to a certain degree, dependent on the achieved adhesive friction between the tyre and the road.

Tyre wear Most state of the art tyre wear investigations focus on predicting global tyre wear. In [Braghin et al., 2006] for example, a tool to numerically predict global tyre wear as well as to qualitatively determine the wear distribution is presented. A direct implementation of tyre wear and the corresponding forces is given in [Tremlett & Limebeer, 2016]. Here, a friction power dependency on wear rate and surface temperature is shown.

As a review of the summary given in Table 3.1, in most real tyre operating applications an interaction of various external influences affect the behaviour of the steady-state characteristics and furthermore the overall tyre behaviour in a certain way. To carry out a detailed investigation, for example in the field of tyre dynamics in this thesis, external influences should be reduced or taken into account.

As basis for further investigations, one goal of this thesis is to evaluate the transient tyre characteristics for handling models under test bench conditions. In this case, most of the external influences can be controlled, e.g. longitudinal velocity, tyre pressure and road friction. Furthermore, the information that the time constant of changing tyre wear is small in comparison to the time constant of the dynamic behaviour was a result of investigation of the measurement data. In addition, the changes in tyre wear can be kept small by defining a suitable measurement procedure.

Finally, to guarantee a realistic model interaction between tyre and road, the effect of changing temperature during highly dynamic measurement manoeuvres should not be neglected. In this case, a temperature model including the effects on the steady-state characteristics has to be implemented in the basic version of TMeasy first in order to make sure that all further effects are represented correctly. This task thus forms a further main part of this thesis.

Before an implementation can be performed, a temperature model that meets the requirements has to be found. Therefore, a literature study of common state of the art tyre temperature model approaches is given in Section 3.3 as a first step. To validate influences of different layer temperatures on tyre behaviour, an investigation on main steady-state parameter influences is carried out as a further step in Section 3.4.

As not just analyses of tyre tests are common nowadays, research results on tyre tread section measurements are also used to gain experience in this field. After presenting literature-based results, basic section measurements on a prototype test bench to reach a theoretical understanding of rubber physics based on external influences were done together with an industrial partner, see Subsection 3.4.2.

Finally, these theoretical and experimental investigations form the foundation of the development of a temperature model that can be implemented in the tyre model used, TMeasy, or any other appropriate model. After presenting the structure of the temperature model at the end of this chapter, details on model design, the parameterisation process and validation is given in Chapter 5.

3.3. Literature based temperature model approaches

As a basis for the model design an overview of different literature-based tyre temperature model approaches is given in the following section and summarised in Table 3.2. A listing of simplified stationary heat conduction approaches based on the *first law of thermodynamics* and application implemented by the *Fourier heat equation* is done as well, and thermal effects and discretisation properties are presented. From this listing, approaches that have the potential to interacting with the TMeasy tyre model in the best practical way are considered in the next subsections in more detail.

3.3.1. Temperature model according to Mizuno

The temperature model developed from [Mizuno et al., 2005] is characterised by an empirical approach with the aim of describing the surface temperature of a tyre and considering its effects on the tyre characteristics via a force model based on MF-Tyre. In a first step, the surface temperature is calculated based on a thermodynamic model approach, and in a second step, the force model is achieved by modifying the lateral and longitudinal tyre force parameters.

Table 3.2.: Classification of tyre temperature model approaches

Name/source	Appr.[1]	Thermal effects[2]	Discretisation
[Mizuno et al., 2005]	SSHC	HE: ambient air HG: friction & hysteresis HC: radial direction	Not discretised, math. approach
[Sorniotti, 2009]	FLT	HE: amb. air & cont. patch HG: friction & hysteresis HC: radial direction	Tyre modelled as one/two point masses
[Kelly & Sharp, 2012]	FLT	HE: amb. air & cont. patch HG: friction & hysteresis HC: radial direction	Tyre divided into point masses
[Büttner et al., 2015]	FLT	HE: amb. air & cont. patch HG: friction & hysteresis HC: radial direction	Tyre divided into three point masses
ThermoTyre [De Rosa et al., 2008]	FHE	HE: amb. air & cont. patch HG: friction HC: two-dimensional	Tyre modelled as infinitesimal element
[Calabrese et al., 2015]	FHE	HE: amb., cont. p. & rim HG: friction & hysteresis HC: three-dimensional	Three-dim. finite element model

[1] SSHC ... Simplified stationary heat conduction with **low** calculation time
FLT ... First law of thermodynamics with **low** calculation time
FHE ... Fourier heat equation with **moderate** calculation time

[2] HE ... Heat exchange
HG ... Heat generation
HC ... Heat conduction

Thermal model

The thermal model approach is based on the assumptions that input and output only occurs in the contact area between road and tyre. Therefore, the tyre surface temperature T_s of the tyre can be described as

$$m\, c_p \frac{\mathrm{d}T_\mathrm{s}}{\mathrm{d}t} \;=\; P_\mathrm{f} - \lambda \frac{A_\mathrm{t}}{\delta_\mathrm{t}} \left(T_\mathrm{s} - T_\mathrm{r}\right), \tag{3.3}$$

where m is defined as mass, c_p as specific heat capacity, λ as thermal conductivity, A_t as contact area of the tread, δ_t the tread thickness and T_r as road surface temperature. Furthermore, P_f represents the induced thermal energy from frictional power and is

calculated using the combined tyre forces $\boldsymbol{F}$ and the sliding velocities $\boldsymbol{v}_\mathrm{s}$, with

$$P_\mathrm{f} = \boldsymbol{F} \cdot \boldsymbol{v}_\mathrm{s} \,. \tag{3.4}$$

To fully define Equation (3.3), the parameters m, c_p and λ have to be set from rubber characteristic tables or parameterised from measurement data. Because m and c_p are hard to separate during the parameterisation process via measurement data, in most approaches they are parameterised in combination with $c_p' = m\, c_p$.

Tyre force model

To generate a magic formula approach that is temperature dependent, the parameters corresponding to the longitudinal and lateral force are modified. Here, in the *Mizuno*, linear approaches to the parameters that represent the steady-state force characteristics are adapted. Specifically, this means the parameters D_i, C_i, B_i and E_i, where i is used for longitudinal x and lateral y direction, from the *Magic formula* equation

$$F_i(i) \;=\; D_i \,\sin\left(C_i \,\arctan\left[B_i\, i - E_i \left(B_i\, i - \arctan\left[B_i\, i\right]\right)\right]\right) \tag{3.5}$$

have to be adapted. As an example, the modification of the parameter D_i, which means the maximum value of the force in Equation (3.5), is extended by

$$D_i'(T_\mathrm{s}) = D_i \left[1 + a_i \left(T_\mathrm{s} - T_0\right)\right] \,, \tag{3.6}$$

where a_i defines the linear temperature dependency and T_0 sets an initial value.

The same procedure is carried out for the further parameters C_i, B_i and E_i and for both longitudinal and lateral characteristics. In [Mizuno et al., 2005] simulation results are compared to measured data from an indoor testing facility. In summary, the model is characterised as being a simple concept - one that is easy to use and offers a wide range for adaption.

3.3.2. Temperature model according to Sorniotti

The main goal of the approach from *Sorniotti* is an adequate temperature simulation while keeping the computational effort as low as possible. For this purpose, the model applies the first law of thermodynamics to a tyre. Therefore, two different approaches are presented in [Sorniotti, 2009]. The first one considers the tyre as a whole with combined thermal properties, whereas the second one divides the tyre into two regions, the carcass and the tread, each with distinct thermal capacities. Both temperature model approaches are combined with a brush model in which the cornering stiffness and the friction coefficient are controlled by the temperatures predicted from the thermal models.

Thermal model

For this application, the second model approach is presented in detail as an example. Therefore, the first law of thermodynamics is used to calculate tyre temperature changes in the carcass T_c and in the tread T_t from an initial value, defined by

$$c_{p,\mathrm{c}} \frac{\mathrm{d}T_\mathrm{c}}{\mathrm{d}t} = P_\mathrm{h} + \dot{Q}_\mathrm{cond} + \dot{Q}_\mathrm{c\text{-}a} \quad \text{and} \tag{3.7}$$

$$c_{p,\mathrm{t}} \frac{\mathrm{d}T_\mathrm{t}}{\mathrm{d}t} = P_{F_x} + P_{F_y} - \dot{Q}_\mathrm{cond} + \dot{Q}_\mathrm{t\text{-}a}\,, \tag{3.8}$$

where $c_{p,\mathrm{c}}$ and $c_{p,\mathrm{t}}$ represent the specific heat capacity in the carcass and the tread for the mass of one kilogram. The following thermal effects are considered and shown graphically in Figure 3.3:

- Heat generation from hysteresis effect (rolling resistance) P_h
- Conduction of the heat flow through the tyre $\dot{Q}_\mathrm{cond}$
- Convection related to the cooling flux in relation to the external ambient air, proportional to the differences between carcass and ambient air $\dot{Q}_\mathrm{c\text{-}a}$ or tread and ambient air $\dot{Q}_\mathrm{t\text{-}a}$
- Heat generation from frictional forces in longitudinal P_{F_x} and lateral P_{F_y} direction

In this approach the tyre is discretised by its overall thermal heat capacities $c_{p,\mathrm{c}}$ and $c_{p,\mathrm{t}}$, and therefore temperature changes are calculated without the need for information regarding the geometrical properties or mass distribution. The friction power $P_{F_{x/y}}$ is calculated by means of the longitudinal and lateral forces that occur and their respective sliding velocities. This frictional energy is distributed between the tyre and the road with an additional coefficient. The internal heating from hysteresis effects inside the carcass is related to the tyre rolling resistance and can be computed as a polynomial function of tyre velocity.

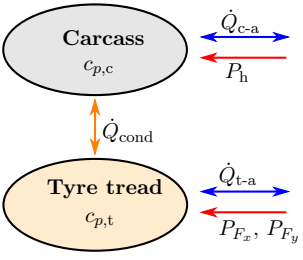

Figure 3.3.: Schematic heat flow of the second approach from *Sorniotti*, where the thermal tyre model is split into two parts, the carcass and the tyre tread, adapted from [Sorniotti, 2009]

The heat exchange with the surroundings $\dot{Q}_{\text{c/t-a}}$ is calculated from the temperature difference between the ambient air T_{a}, the respective area $A_{i\text{-}j}$ and a heat convection coefficient h_i by

$$\dot{Q}_{\text{c-a}} = h_{\text{c}} \cdot A_{\text{c-a}} \cdot (T_{\text{a}} - T_{\text{c}}) , \tag{3.9}$$

$$\dot{Q}_{\text{t-a}} = h_{\text{t}} \cdot A_{\text{t-a}} \cdot (T_{\text{a}} - T_{\text{t}}) \quad \text{and} \tag{3.10}$$

$$\dot{Q}_{\text{cond}} = h_{\text{cond}} \cdot A_{\text{c-t}} \cdot (T_{\text{c}} - T_{\text{t}}) . \tag{3.11}$$

In [Sorniotti, 2009], the thermal model has been validated through measurement data from infrared sensors along the width of the tyre. As expected, the approach without discretisation of the tyre cannot cope with the quick temperature changes that a tyre is experiencing. The second implementation brings improvements that can be represented by the two degrees of freedom model.

Tyre force model

The brush model implemented by the author was expanded to consider the temperatures generated by the thermal models. In the case of the two degrees of freedom model, the friction coefficient is considered as a linear function of the tread temperature, whereas the tyre stiffness is a linear function of the tyre carcass temperature. For the one degree of freedom model, only one temperature is available for the tyre model.

A comparison between the brush model, the extended temperature dependent brush model and a magic formula application shows that the temperature dependent approach fits the measurement data in a satisfactory way. In contrast, the brush model and the magic formula can produce a significant deviation from the measurement data, depending on the temperature changes that the tyre is experiencing.

3.3.3. Temperature model according to Büttner

The goal of the model approach from [Büttner et al., 2015] is to cover a wide field of applications in terms of vehicle-tyre combinations. This model was developed for implementation in Porsche's control systems in order to further improve them by including the tyre temperature. Due to the large number of tyres used on the wide vehicle range the company is producing, the model describes the tyre via its thermal rather than it's geometric properties. To do so, the tyre is split into three different regions or layers with individual thermal properties and representative heat mechanisms.

These layers are defined as the surface layer, the bulk layer and the inner liner. In this approach, the sidewalls as well as the filling medium are not taken into account. Because of the chosen discretisation, the model is designed to calculate an average surface temperature along the width and circumference. For each layer, an energy balance via the first law of thermodynamics is performed using the following thermal effects:

- Heat generation from hysteresis effect in longitudinal x, lateral y and vertical z directions $P_{\mathrm{h},i}$
- Heat generation from frictional forces in longitudinal P_{F_x} and lateral P_{F_y} direction
- Conduction in the non-sliding region of the contact patch between tyre surface and road $\dot{Q}_{\mathrm{s\text{-}r}}$
- Convection related to the cooling flux toward the external ambient air, proportional to the differences between tyre surface and ambient air $\dot{Q}_{\mathrm{s\text{-}a}}$
- Conduction of the heat flow through the tyre, e.g. from surface to the bulk $\dot{Q}_{\mathrm{b\text{-}s}}$

As a characteristics representation for one of the layers, Figure 3.4 displays the energy balance of the surface layer, where both heating from friction as well as hysteresis effects are taking place. The induced energy from friction power $P_{F_{x/y}}$ is calculated by using the acting forces in lateral and longitudinal directions along with the corresponding sliding velocities. The heat released through hysteresis is considered as a product of all measured or estimated forces $F_{x/y/z}$ and the current travel velocity in longitudinal direction v_x. Additionally, heat is exchanged with the surroundings.

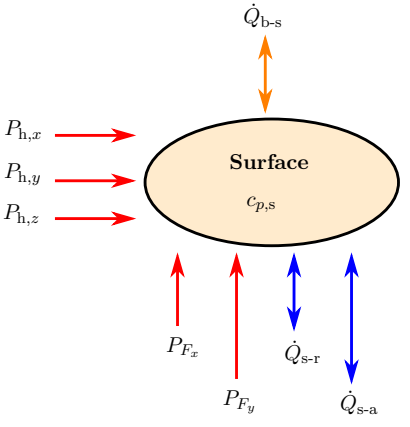

Figure 3.4.: Schematic heat flow of the surface layer from the model approach based on *Büttner*, where power generation is given through the hysteresis effect $P_{\mathrm{h},x/y/z}$ and from friction power $P_{F_{x/y}}$ and heat flow arises between tyre surface and road $\dot{Q}_{\mathrm{s\text{-}r}}$, surface and ambient air $\dot{Q}_{\mathrm{s\text{-}a}}$ and between bulk and surface layers $\dot{Q}_{\mathrm{b\text{-}s}}$, based on [Büttner et al., 2015]

Convection is influenced by the temperature difference between the surface T_s and the ambient air T_a, the area of the tyre surface and a supplementary coefficient. This coefficient in turn is dependent on various factors like longitudinal velocity v_x, length of the carcass l_c, the thermal conductivity λ, the density ρ as well as the specific heat capacity c_p of the ambient air and calculated by

$$\dot{Q}_\mathrm{conv} \approx f(v_x^{k_\mathrm{conv}}, l_\mathrm{c}, \lambda_\mathrm{a}, \rho_\mathrm{a}, c_{p,\mathrm{a}}) \cdot A \cdot (T_\mathrm{a} - T_\mathrm{s})\,. \tag{3.12}$$

To consider the different airflow conditions, the empirical constant parameter k_conv is included and optimised in the course of the fitting process. The same procedure is applied for the thermal resistance R_th of the compound due to the lack of information on the material properties for every region of the tyre. With this approach, the different layers can be coupled with

$$\dot{Q}_\mathrm{cond} = \frac{1}{R_\mathrm{th}} \cdot \Delta T\,, \tag{3.13}$$

and therefore temperature changes can be calculated for each layer depending on the behaviour of adjacent regions. In summary, the energy balance for the surface layer can be expressed for each time step Δt as

$$\Delta T_\mathrm{s} = \frac{\Delta t}{m_i \cdot c_{p,\mathrm{s}}} \left(\sum P_{\mathrm{h},x/y/z} + \sum P_{F_{x/y}} + \dot{Q}_\mathrm{s\text{-}r} + \dot{Q}_\mathrm{s\text{-}a} - \dot{Q}_\mathrm{b\text{-}s} \right) \tag{3.14}$$

where in [Büttner et al., 2015] a layer mass of m_i is considered for each layer. Therefore, all information needed for modelling a tyre, can be found in its designation. The fitting process is carried out by comparing the simulation results to the measurement data generated using infrared sensors mounted on a testing vehicle. Overall, this approach delivers good accuracy with low computational load and offers a wide range of applications.

3.3.4. ThermoTyre temperature model

The ThermoTyre model is based on a one dimensional, partial differential Fourier heat equation, see [De Rosa et al., 2008]. This equation is applied to an infinitesimal element revolving around the wheel axis at the current angular velocity of the tyre, as mathematically described by

$$\lambda \frac{\partial^2 T}{\partial \delta^2} = \rho\, c_p \frac{\partial T}{\partial t} \tag{3.15}$$

and displayed in Figure 3.5. The term $\partial^2 T / \partial \delta^2$ represents the directional derivative of the temperature T over tyre thickness δ. This leads to the advantage of this approach that temperature can be modelled depending on the circumferential position and for any point along the depth of the tyre.

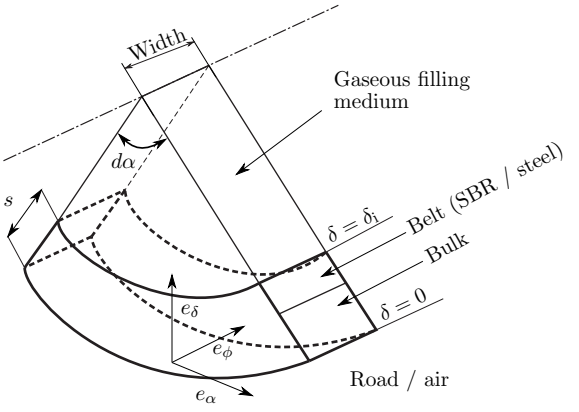

Figure 3.5.: Infinitesimal element spinning around the tyre axis, adapted from [Hackl et al., 2018] and based on [De Rosa et al., 2008]

Here, the following thermal effects are considered:

- Heat generation from frictional forces in longitudinal q_{F_x} and lateral q_{F_y} directions
- Conduction in the non-sliding region of the contact patch between tyre and road q_{cond}
- Convection related to the cooling flux toward the external ambient air, proportional to the differences between ambient air inside and outside the tyre and the tyre itself q_{conv}
- Conduction of the heat flow through the tyre directly based on Equation (3.15)

To calculate Equation (3.15) depending on time and around the circumference at each revolution, the infinitesimal element traverses through three distinctive areas, namely the generation zone, the convection zone and the conduction zone. When the element is in contact with the ambient air or the road, convective or conductive heat transfer is a given. Furthermore, heat transfer based on temperature differences between the inner layer at $\delta = \delta_\text{i}$ and the filling medium can be calculated in the same matter. In summary, heat transfer is described by

$$q_{\text{conv}} = -\lambda \left.\frac{\partial T}{\partial \delta}\right|_{\delta=0/\delta_\text{i}} = h_i \cdot \left[T_\infty - T(0/\delta_\text{i}, t)\right], \tag{3.16}$$

where T_∞ describes the constant temperature based on the position for ambient T_a, road T_r and inner filling medium T_i. Because these mechanisms of heat exchange are described as boundary conditions on the inner and outer surface, the area of heat transfer is

generated via the integration over the circumference. For the same reason, the frictional power generated inside the sliding region of the contact patch $A_{\mathrm{cp,s}}$ has to be divided by the sliding area inside the contact patch with

$$q_{F_{x/y}} = -\lambda \left.\frac{\partial T}{\partial \delta}\right|_{\delta=0} \cong \frac{1}{A_{\mathrm{cp,s}}} \cdot F_{x/y} \cdot v_{\mathrm{s},x/y}\,. \tag{3.17}$$

To activate the needed boundary condition, the current angular position is derived by means of the wheel rotational speed and is then compared with the corresponding zone angles. Therefore, just one boundary condition is active at any given time. Consequently, this model is characterised by distinctive temperature behaviour. At each revolution, when the wheel enters the sliding region of the contact patch, the temperature rises in an almost stepwise way because of the short but high intensity of the frictional heating. After passing through this zone, the element enters the convective zone followed by the conductive zone, where in both the temperature decreases continuously throughout the remaining rotation until the sliding region is reached again.

Although the computational time is high, this model delivers quite accurate temperature simulations. Because of the partial access, material properties can be changed arbitrarily along the tyre depth, thus modelling the tyre structure as well as possible. This means that the temperature distribution over the tyre thickness and the circumference can be displayed in detail.

3.4. Temperature influence on tyre characteristics

After presenting the main thermal model approaches for handling applications, a short literature overview covering the temperature influence on tyre characteristics is given in this section. For that purpose, two different research methods are common today. Firstly, the field of investigation describes the temperature influence on steady-state tyre force versus slip characteristics through the use of test bench measurement data. The second part uses tyre tread section measurements for a detailed investigation of rubber behaviour. In particular for the first field, only a few results containing detailed descriptions regarding influences on tyre characteristics have already been published. Nevertheless, an overview of both research possibilities is given in this section, followed by the author's own basic section measurements on a prototype test bench to confirm the statements in the literature.

3.4.1. Temperature influences on steady-state characteristics

Analyses of temperature influences on steady-state behaviour are laborious and not easy to perform. Investigations are thus carried out under test bench conditions in nearly all cases. Furthermore, two main factors are presented in the literature that are influenced by the temperature. The first parameter is cornering stiffness c_α laterally respectively

slip stiffness c_s longitudinally. Because nearly no results are found concerning the longitudinal direction, the focus is on lateral investigations. The second factor that is influenced by the temperature is the maximum tyre force, which is based on the coefficient of friction.

Cornering stiffness

The cornering stiffness of a tyre is mainly governed by the bending and shear stiffness of the tread in contact with the road and the rigidity of the supporting structure, mainly the tyre's sidewall. To investigate the temperature influence on this tyre property, a differentiation has to be made between the effects of temperature and the pressure of the filling medium. Under real-life driving conditions, both are interconnected. In very simple terms, it can be stated that with rising temperature the shear modulus of the supporting structure is decreasing and therefore the rigidity present is decreasing as well. Simultaneously, the internal tyre pressure is rising, which partly compensates for this loss.

To determine the individual influence of those effects, in the course of the work of [Angrick et al., 2014], specific operating conditions had to be introduced. Here special focus is on test bench measurement conditions in which tyre pressure is kept constant along with a focus on tyre temperature. The outcome shows that with increasing temperature, a significant loss in cornering stiffness can be observed. While results are presented from *Angrick* with three temperature values, the decrease happens at a rate of approximately 3 to 4 % per 10 degC at the beginning, whereby with higher temperature a saturation occurs, represented schematically in Figure 3.6 on the left. Further investigations of inflation pressure seem to be less pronounced, and additionally the observed effects differ for the investigated wheel loads. At low loads, the cornering stiffness is reduced whereas at higher loads the identified curves coincide with the tyre becoming stiffer with increasing pressure.

An additional wide range of experimental investigation into the influence of temperature on tyre behaviour is given in [Corollaro, 2014]. By measuring the surface and inner layer temperature during test bench measurements, a three-layer model (surface, bulk and inner layer) is developed and validated as a first step. Furthermore, the influences of the bulk temperature on the cornering stiffness were investigated with a special measurement procedure. Therein, a three phase warm-up setting is presented to saturate the bulk temperature at fixed levels by keeping the surface conditions as constant as possible. After reaching the specified temperature, a constant slip angle under various normal forces was applied and cornering stiffness was measured. The results of these investigations clearly show that the cornering stiffness is directly influenced by the bulk temperature of the tyre.

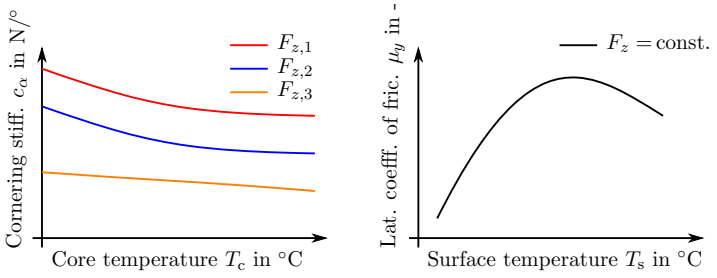

Figure 3.6.: Schematic representation of the influence of temperature on tyre characteristics: left shows cornering stiffness in relation to core temperature with $F_{z,1} > F_{z,2} > F_{z,3}$ and right shows the lateral coefficient of friction versus the surface temperature, adapted from [Angrick et al., 2014]

Coefficient of friction

In general, the overall friction coefficient μ is a combination of various mechanisms. The most pronounced of these are adhesion and hysteresis. As a rubber section enters the contact patch, *van der Waals* binding between the tyre and the road start to form, representing the adhesive part. As the deflection between the rubber and the road molecules increases, these bindings start to break loose, generating a difference in velocity. This relative speed governs the hysteresis part of the friction. To distinguish between those two effects is a challenging task, because under real driving conditions they work in a coupled manner. For this reason, most studies focus on the friction characteristics as a whole.

In the course of the work of [Angrick et al., 2014], which investigated the temperature dependence of the friction coefficient, specific measurement procedures were conducted. To identify the effects of the internal pressure and the temperature separately, one measurement routine includes heating the tyre while keeping the initial tyre pressure constant. The authors state that the friction potential is mainly dependent on processes occurring in the tyre surface. Therefore, the friction coefficient is considered a function of the surface temperature rather than the core temperature of the tyre, with changes up to 5 % per 10 degC.

Investigations indicate that characteristics show small sensitivity to pressure changes. Therefore the focus is on the influence of temperature, which is displayed on the right in Figure 3.6. Starting at an initial condition, for the observed tyre, the friction coefficient rises until it reaches its maximum at around 65 degC to 75 degC. At higher temperatures a decrease can be seen, however with a slope significantly lower than at lower temperatures.

In contrast to *Angrick*, a similar investigation of road friction depending on tyre temperature is given in [Tremlett & Limebeer, 2016]. One goal of this article was to investigate temperature influences on road friction and furthermore on lap time simulation of a race car. Based on a single-layer temperature model and various heat generation and exchange phenomena, the value of the tyre tread temperature is calculated. The sensitivity of the tyre friction to tread temperature is represented by a grip factor λ_g, which depends on the tread temperature. The characteristics of the grip factor are parameterised based on measurement data. In the application from *Tremlett & Limebeer*, the grip factor looks similar to the results from *Angrick* in Figure 3.6 right. This means that increasing grip behaviour is anticipated, followed by a maximum area and resulting in a decreasing grip effect.

Overall temperature influence investigations

A further common possibility in terms of the temperature influence on tyre characteristics is to evaluate force versus slip behaviour. [Sorniotti, 2009] for example presents the temperature influence on combined tyre force by using measurement manoeuvres. He notes that under combined longitudinal and lateral force conditions, an error of about 25 % can be occur if no temperature effect is considered.

Alternatively, [Février & Fandard, 2008] and [Calabrese et al., 2015] present the influence of the thermal effects on the lateral grip (F_y/F_z) during slip angle sweeps at different tyre loads. Large influences are mainly present at high slip angle values in relation to a hysteresis effect.

In summary, investigations into the temperature influence on tyre characteristics seems to be an important topic, but further research has to be carried out in order to understand these effects in greater detail. The already published literature divides the temperature influences into effects on cornering stiffness and maximum friction coefficient, which are both implemented in the steady-state tyre characteristics. Literature-based force errors of up to 25 % by ignoring the temperature confirm the results from the sensitivity analysis in Section 3.1. As detailed investigations are mainly possible on tyre test benches, financing is often a limiting factor. Therefore, to evaluate influences of temperature, an additional common method is also used in investigations of tyre tread section measurements.

3.4.2. Temperature influences on tyre tread section measurements

Another possibility concerning the influence of temperature, especially on rubber behaviour, is to investigate tyre tread sections. To do this, just a small part of the tyre tread is used. The section is cut out of the tread and clamped into the test bench. For the most part, two different types of test bench movements are common: circular and linear shifts. Dependent on speed, temperature, tyre load and surface, the responsible

forces in horizontal and vertical directions are measured. Section investigations are thus analyses of the coefficient of friction μ as well.

In general, as stated in Section 3.4.1, the coefficient of friction μ is composed of various mechanisms, with adhesion and hysteresis being the most dominant ones. As concluded by [Persson et al., 2005], *van der Waals* binding and therefore adhesion occurs when the effective distances between rubber and road surface is below 10^{-6} m. This mechanism is dependent on the true contact area between the tyre and the road. [Klueppel et al., 2011] shows that this contact area is strongly influenced by the contact pressure and the sliding velocity. The former leads to an increase in the effective contact area with rising pressure due to a better filling of the available cavities of the surface texture. An increase in the latter, i.e. sliding velocity, leads to a decrease in the useable contact patch because of the time-span becoming too short for the rubber sections to fully enter these cavities. Additionally, this ratio between the contact patch and the true contact area is temperature dependent due to material softening, leading to a deeper penetration of the rubber into the road surface.

On the contrary, hysteresis is governed by deformations of the viscoelastic material and the rate of their excitation. This happens inside the contact patch at all times due to the vertical load and the lateral and longitudinal sliding forces acting on the tyre. At high levels of slip when the rubber sections travel through the contact patch, the maximum shear stress allowed by adhesion is exceeded within a fraction of the length of the contact patch. Therefore, under these conditions, the resulting shear stress from hysteresis is more distinct than the adhesion component. In the work of [Lang & Klueppel, 2017], the correlation between adhesion and hysteresis is shown for variations in speed and contact pressure, illustrating the basic composition of friction curves. It can be seen that the initial friction build-up is governed by adhesion, while the contribution of hysteresis becomes dominant with increasing velocity.

To investigate the temperature dependence of friction from hysteresis, excitation frequencies should mainly be dependent on the sliding velocity. Therefore, a well-defined testing surface is needed to exclude the effect of different excitation frequencies from varying sizes of road cavities. In the course of the work from [Angrick et al., 2014], P120 sandpaper is used as this grit size is common on most test rigs. Other authors, for example [Lang & Klueppel, 2017], use real-world road surfaces like granite to perform measurements. In this case, the asperities of the surface are measured via white light interferometry to determine the roughness of the used substrates. Under these conditions, the dissipation factor $\tan\delta$, which is often defined as a loss factor, can be seen as a function of the excitation frequency and can be adjusted depending on the temperature. This temperature-frequency shift is described by Williams, Landel and Ferry via their *Williams Landel Ferry model* (WLF) equation, [Williams et al., 1955]. To conclude, the main factor governing friction from hysteresis is $\tan\delta$, which in turn is very dependent on frequency. Additionally, this characteristic can be shifted along the frequency plane with changing temperature, as can be seen on the left in Figure 3.7.

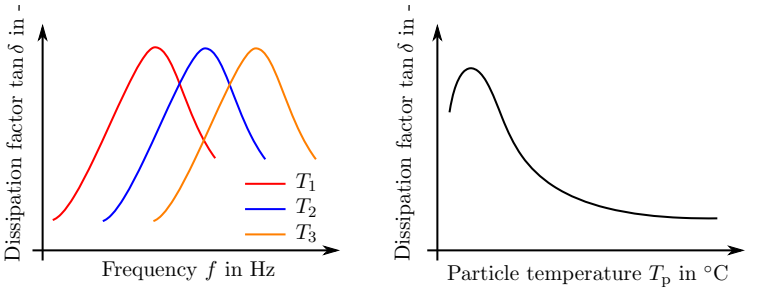

Figure 3.7.: Dissipation factor dependency on frequency and section temperature; left, temperature-frequency shift described by the WLF equation with $T_1 < T_2 < T_3$, based on [Williams et al., 1955]; right, section temperature influences on the loss factor, adapted from [Angrick et al., 2014]

Laboratory tests were performed on a hydro-pulsar test rig by [Angrick et al., 2014] to calculate the dissipation factor $\tan\delta$. This factor is mathematically described by

$$\tan\delta = \frac{E''}{E'} \tag{3.18}$$

and can be seen as the quotient of loss modulus E'' and storage modulus E' and furthermore defines the energy dissipation within the rubber material. It thus describes the behaviour of the material between viscous fluid ($\tan\delta = 1$) and ideal elastic ($\tan\delta = 0$), or in other words, the relation of inner damping against outer deformation.

The measurements, as well as similar *dynamic mechanical analyses* (DMA) carried out by [Lang & Klueppel, 2017], indicate a peak in the loss factor at very low temperatures, i.e. below 0 degC. With increased temperatures, the loss factor decreases rapidly with a declining slope towards higher temperatures, reaching its lower limit at temperatures above 70 degC. A schematic representation of the observed characteristics is given in Figure 3.7 on the right.

Measurements carried out by [Klueppel et al., 2011] indicated that this behaviour is applicable for different elastomers used in tyre production. Although having different absolute values regarding $\tan\delta$ and the corresponding position on the frequency plane, the friction characteristics correlate to the $\tan\delta$ characteristics for all tested elastomers.

Aside from the horizontal WLF shift in the work of [Lang & Klueppel, 2017], an additional vertical shift factor is introduced for highly filled rubbers. This vertical shift is based on the differences in the viscoelastic response of the filler network in comparison to the rubber matrix when undergoing temperature changes. This shift can be observed for the elastomers tested in [Klueppel et al., 2011], but it is of minor importance compared to the horizontal shift factor since exact material composition is an unknown in most cases.

In general, as shown by [Giashi et al., 2015], the achievable friction increases with increasing velocity while decreasing with increasing contact pressure. In terms of temperature influence, a distinction has to be made. In the work of [Anupam et al., 2013], the authors show the effect of different pavement and ambient temperatures on friction characteristics for different road surfaces. It can be seen that for every surface with increasing pavement temperature as well as ambient temperature, the coefficient of friction decreases for all velocities tested. Therefore, it can be concluded that the decisive temperature regarding friction is the temperature of the rubber bulk rather than the surface temperature of the tyre. While for DMA measurements these temperatures are generated in a coupled manner since the samples are heated until a target temperature is reached, for a tyre in use the temperature distribution can vary drastically over the tyre depth. It can be concluded that the surface temperature affects the adhesive component of the friction curve, while the rubber's internal temperature is responsible for the hysteretic component.

This is one of the reasons for the deviation between the tyre and the material sample measurements. Additionally, uncertainties regarding the coefficients of the WLF transformation, a wider range of excitation frequencies as well as differences in the effective contact area cause the optimum temperature to appear lower under real road conditions in comparison to the test bench measurements.

3.4.3. Tyre tread section measurements & laboratory testing

As part of the research for this thesis project, the possibility arose to do tyre tread section measurements on a prototype test bench belonging to the industry partner AVL List GmbH, [AVL, 2019]. However, because no measurement data on special test benches is desired for parameterising the enhanced model application in this thesis, the basic investigations are not focused on receiving parameter information, but are rather used to validate results from literature and confirm information for the modelling process, especially on the temperature model.

The main goal of these measurements was therefore to identify temperature-dependent characteristics of the observed sections. The measurements include variations in tyre and road temperature as well as velocity and wheel load and were carried out on different road textures. The testing sample used was from a Continental EcoContact 3 tyre of type 145/65 R15 72T.

Test bench setup and measurement procedure

The test rig prototype consists of a linear actuator, a load cell as well as a heated carrier board and surface board, see Figure 3.8. Measurements can be carried out under various loads by adding boards with fixed weight. In addition to a solid aluminium surface plate with one millimetre roughness, measurements were carried out on P120 sandpaper.

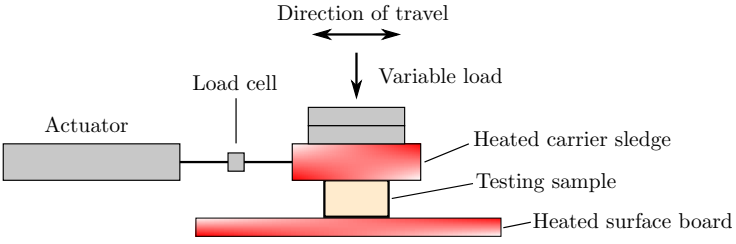

Figure 3.8.: Schematic representation of the tyre section test rig of the industry partner AVL List GmbH, [AVL, 2019]; degrees of freedom are represented by the variable load, actuator settings, e.g. manoeuvre speed and temperature variation of the surface and the carrier board

Table 3.3.: Measurement procedure for the tyre section tests using a sample of Continental EcoContact 3 tyre of type 145/65 R15 72T

Influence	**Symbol & unit**	**Testing range**
Sample velocity	v in mm/s	0 - 150
Surface temperature	T_s in degC	30 - 90
Section temperature	T_p in degC	20 - 70

Figure 3.9.: Cut out tyre tread samples for section investigations in lateral (top) and longitudinal (bottom) direction as used on the prototype test rig

The procedure was carried out using a fixed manoeuvre matrix with varying movement velocity, track temperature and tyre temperature, see Table 3.3. The maximum velocity feasible with the linear actuator is 150 mm/s. The temperature of the surface board corresponds to the track temperature, wherein as a special advantage of this test bench, heating of the carrier plate was adjusted to reach the tested tyre temperatures inside the tread block. This was done to ensure that tyre temperatures correlate to the average temperature of the rubber part of the sample.

Investigations on longitudinal as well on lateral samples were done - the tyre sections are represented in Figure 3.9. The results of those investigations are presented in the next section.

Tyre tread section analysis

The chosen vertical loads during the section measurements correspond to the loads for a tyre at normal pressure when mounted on an average subcompact car. When the actuator starts moving, force and therefore friction build up until the section starts moving, as can be seen on the top and middle plots in Figure 3.10.

Depending on various conditions like section geometry, vertical load or actuator velocity and acceleration, peak behaviour can occur before it converges to its steady-state sliding friction μ_s. This peak μ_p is composed of adhesive forces with additional frequency induced hardening of the tread block through hysteresis. In steady-state motion, the friction is governed solely by hysteresis, indicated by lower values than peak friction. When the actuator stops its motion around $t = 12\,\text{sec}$, the molecules inside the section stop oscillating and the friction decreases while creeping up until it reaches it's adhesive steady-state value μ_{ad}. In this state, friction is governed by adhesive forces without additional influence from hysteresis.

In summary, during this process three friction areas are recognisable, first the peak area around $t = 4\,\text{sec}$ where the highest value is given in most of the cases, second a mean area around $t = 5$ up to $t = 12\,\text{sec}$ in which at constant speed, a value lower than the peak value changes and finally an adhesive area around $t = 15$ up to $t = 22\,\text{sec}$ where no movement of the section is given. Based on these ranges, three different types of friction coefficients are given, namely peak μ_p, slide μ_s and adhesive friction μ_{ad}.

The same procedure can be seen when the actuator moves the section back into it's starting position, allowing for anisotropic characteristics to be analysed. Furthermore, the bottom plot in Figure 3.10 shows the course of friction over section load for peak, mean and adhesive values. A decreasing behaviour with increasing section load is plain to see for all three of the friction components. Moreover, at high section load, the peak characteristics shifts to the mean value of the friction due to saturation. Hence, this behaviour is dependent on the state parameters like speed, temperature and surface roughness.

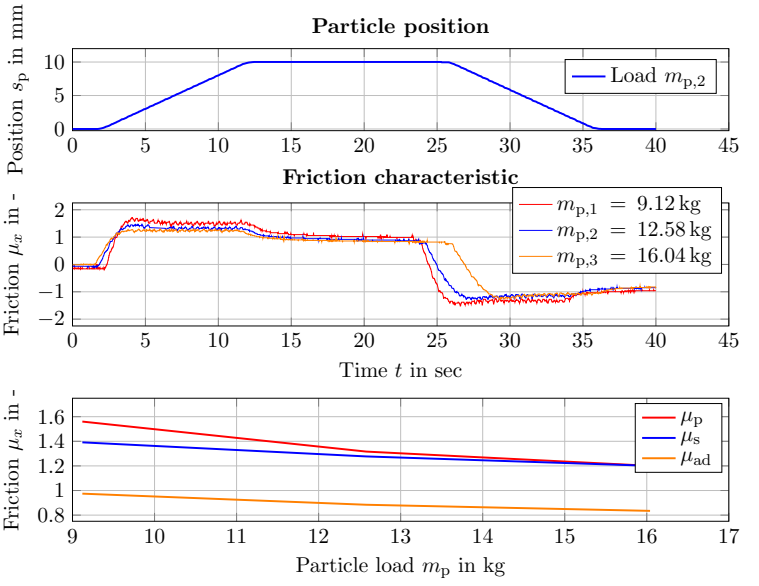

Figure 3.10.: Exemplary section measurement procedure over time at surface temperature $T_s = 30\,\text{degC}$ and section temperature $T_p = 20\,\text{degC}$ and three different loads; the three friction areas peak μ_p around $t = 4\,\text{sec}$, slide μ_s around $t = 5$ up to $t = 12\,\text{sec}$ and adhesive μ_{ad} around $t = 15$ up to $t = 22\,\text{sec}$ are clearly recognisable; the bottom graph shows the three friction areas dependent on the section load

Looking at load and section temperature, a detailed investigation of the adhesive friction is given in Figure 3.11. With increasing load, a decreasing effect on friction is shown for all temperatures. This correlates quite well with the well-known behaviour with tyre-road contact. Furthermore, the frictional coefficient increases with rising temperature until a maximum is reached, after which time a decreasing effect is given for any load. This behaviour indicates that the available cavities of the sandpaper are not filled to their full extent at lower temperatures. With increasing temperature, the material softens and the effective area for adhesion grows. After the optimum temperature is reached and all available contact areas are used, the on-going decrease in storage modulus leads to a decrease in achievable friction.

Because of differences in surface texture and related varying excitation frequencies, the achievable friction varies significantly between the rough surface plate and the sandpaper

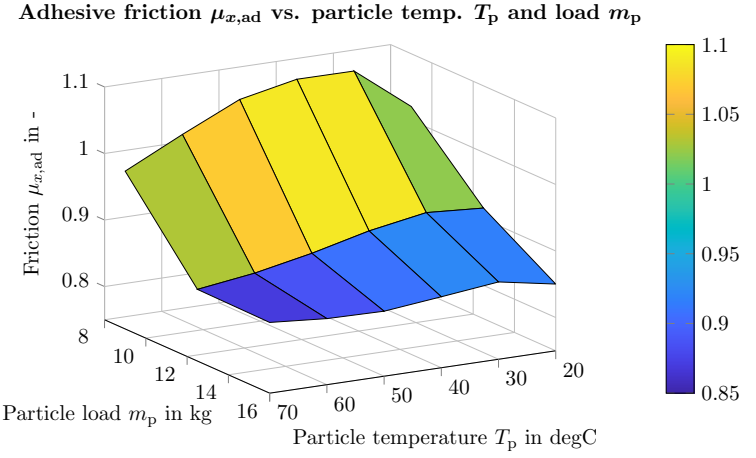

Figure 3.11.: Longitudinal coefficient of friction $\mu_{x,\mathrm{ad}}$ over section temperature T_p and load m_p on **P120 sandpaper** with track temperature $T_\mathrm{s} = 30\,\mathrm{degC}$ and measurement speed $v = 1\,\mathrm{mm/s}$

surface. Figure 3.12 shows the coefficient of mean friction over tyre temperature and velocity. The maximum friction is situated between $T_\mathrm{p} = 50 - 60\,\mathrm{degC}$ and a sliding velocity of $v \approx 100\,\mathrm{mm/s}$. At velocities $v < 100\,\mathrm{mm/s}$ the friction is decreases, indicating that the tested velocity range is suitable for identifying friction master curves. Because of the rough surface of the aluminium board, the amount of friction is governed by interlocking mechanisms between the tyre and the surface cavities. This results in high absolute values, and additionally it can be seen that the friction is not decreasing significantly in the range of its maximum.

The same measurements were carried out on P120 grit sandpaper to exclude the mentioned interlocking mechanisms. As expected, Figure 3.13 shows values much lower compared to measurements on the rough aluminium surface. The maximum is located around $T_\mathrm{p} \approx 50\,\mathrm{degC}$ and a velocity of $v \approx 100\,\mathrm{mm/s}$ and appears more pronounced than on the aluminium plate in terms of both temperature and velocity range. Additionally, it can be seen that the value range of the coefficient of friction is wider than on the rough surface.

To identify the influence of the road temperature, measurements were carried out with varying track temperature while keeping tyre temperature constant. Figure 3.14 shows the results of these measurements on the rough aluminium surface. It can be seen that starting from the low values, friction decreases as temperature rises. When the effect of hysteresis is held constant due to fixed tyre temperature, material softening and related

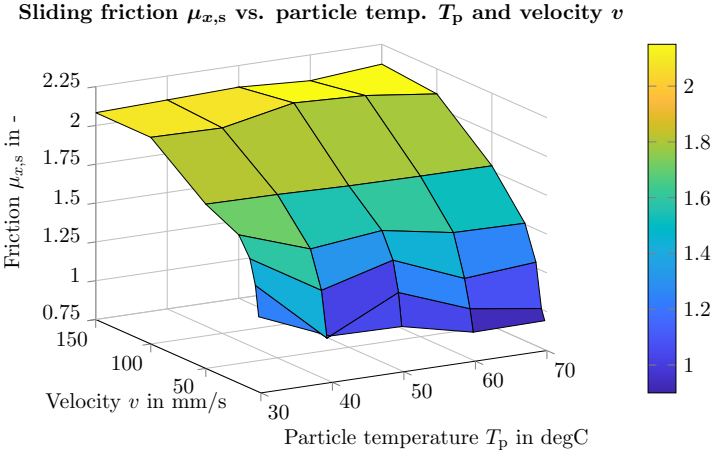

Figure 3.12.: Longitudinal coefficient of friction $\mu_{x,s}$ over section temperature T_p and velocity v on a **rough aluminium surface** with track temperature $T_s = 50\,\text{degC}$ and section load $m_p = 9.12\,\text{kg}$

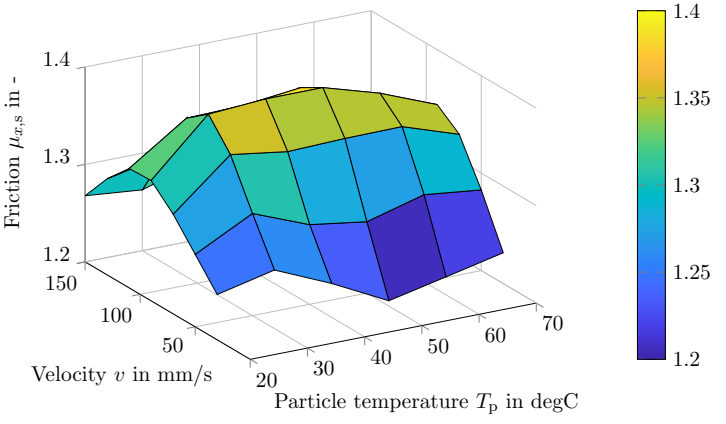

Figure 3.13.: Longitudinal coefficient of friction $\mu_{x,s}$ over section temperature T_p and velocity v on **P120 sandpaper** surface with track temperature $T_s = 30\,\text{degC}$ and section load $m_p = 12.58\,\text{kg}$

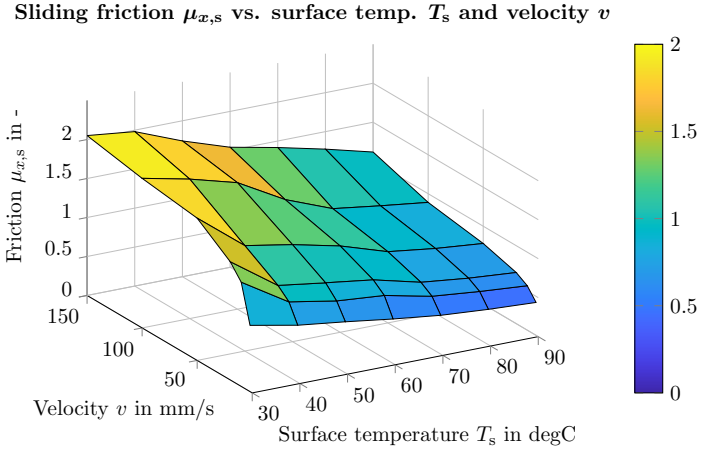

Figure 3.14.: Longitudinal coefficient of friction $\mu_{x,s}$ over surface temperature T_s and velocity v on a **rough aluminium surface** with section temperature $T_p = 50$ degC and section load $m_p = 9.12\,kg$

enhanced contact area does not compensate for the loss in adhesive forces from the increasing temperature on this surface. In reality, the surface and bulk temperature come in a coupled manner, with hysteresis effects outweighing adhesion and thus generating an optimum temperature window. The distinctiveness of this correlation is dependent on the size of the cavities of the road surface as well as the rubber's capacity to fill them.

When comparing the peak and sliding friction characteristics, it can be seen that the temperature dependent behaviour is almost identical. On average, peak friction is $15 - 20\,\%$ higher than mean friction for all measurements on the longitudinal sample. Regarding the lateral sample, the difference is not as pronounced, with sliding and peak friction coinciding in most cases. Additionally it can be observed that with increasing vertical load, the difference between peak and mean friction is decreasing for both samples. In general, both samples show a distinct temperature dependent behaviour with optimum friction at approximately $T_p \approx 50\,degC$ and a velocity of $v = 100\,mm/s$.

In summary, measurements carried out on the section test rig show good results regarding both qualitative and quantitative dependencies. It could be shown that hysteresis, and therefore the inner temperature, is the governing factor regarding friction. Rising surface temperature comes with a decline in the achievable friction in all cases for both samples. It has to be stated that these measurements are not suitable for specifying characteristics like cornering stiffness or transient behaviour due to the lack of tyre rotation. Nonetheless, this approach does make for an affordable way to gain rubber information in a fast and easy manner.

3.5. Comparative conclusion of external influences, especially tyre temperature

In the final comparative conclusion of Chapter 2, the steady-state characteristics represent not only a main part of handling tyre models - it also affects the transient behaviour in many model applications. This chapter thus began with a sensitivity analysis, which demonstrated mathematically how inaccuracies in steady-state behaviour influence dynamics modelling.

Based on a literature study, it was shown that nearly all external influences interact and furthermore affect the steady-state characteristics in some way. Therefore, to guarantee a realistic model interaction between tyre and road, the impact of external influences has to be reduced or taken into account. As the focus of this thesis is test bench investigations, most of the external influences can be controlled, but temperature effects during highly dynamic measurement manoeuvres should not be neglected and have to be taken into account. In this case, to define a suitable temperature model for handling application, an overview of common approaches was given. Aside from the general requirements, i.e being able to run with short calculation time and the possibility to define physical parameters, an approach based on the first law of thermodynamics seems to be the best compromise for further steps.

As concluded in Section 3.4, different tyre layer temperatures influence various tyre properties, for example cornering stiffness and maximum force. Therefore, the chosen thermal approach should provide temperatures for regions of the tyre where most influence on the tyre coefficient of friction as well as the cornering stiffness is predicted. Concerning stiffness, both the rubber bulk as well as the supporting structure (carcass, sidewall) are expected to be of major importance. Since the thermal model should not reference the tyre's sidewalls, the governing temperature influence inside the tyre tread region is the decrease in the rubber's storage modulus. Additionally, the temperature-dependent ratio between storage and loss modulus $\tan\delta$ in this rubber belt region is a dominant factor in terms of hysteresis friction. The reliable prediction of the temperature inside this rubber bulk is therefore of great importance. To achieve this, different authors use varying subdivisions of the tyre, as can be seen in Section 3.3.

It was concluded that the most useful sectioning of a tyre is by dividing it into a bulk layer and a belt layer. The former corresponds to the rubber mass and the latter to the supporting structure inside the tread. With this approach, the high density and therefore high mass of the belt layer and the resulting sluggish thermal behaviour does not inhibit the relatively quick temperature changes inside the bulk layer.

Furthermore, the parameterisation of the model is mostly carried out using measurements from infrared sensors. These sensors only scan the outermost region of the tyre, hence measuring extreme temperature changes. For this reason, a very reactive layer at the tyre surface is needed, which can be achieved through the separation between bulk layer and surface layer. Therefore, a thin rubber surface layer had to be implemented.

This surface temperature can also be used to manipulate the adhesive component of friction separately from the hysteresis component.

In summary, all relevant temperatures of the tyre regarding validation and parameterisation can be shown and used for the corresponding tyre characteristics by means of this approach. Before presenting the temperature model used, including the impact on tyre behaviour in Chapter 5, the parameterisation process of the basis TMeasy tyre model from an industrial flat track test bench is presented in the next Chapter 4.

4

TMeasy tyre model setup and parameterisation process

After theoretical investigations of basic tyre behaviour, general tyre modelling, and transient tyre characteristics in Chapter 2 and analysis on external influences, with special attention on the influence of temperature on steady-state behaviour in Chapter 3, the next three chapters primarily deal with practical implementation.

Before the focus shifts to temperature and then extended dynamic implementations, the standard TMeasy model is presented as the foundation for next investigations in this chapter. Relatedly, the details of an overall process for setting the parameters as part of the standard setup of the TMeasy tyre model are presented.

Since this process starts by defining a feasible test bench, including suitable manoeuvres, and is followed by measurement data acquisition, the focus first goes to various test bench applications, including their advantages and disadvantages. After defining a test rig system, attention goes to the manoeuvre decision as a basis for the parameterisation process. Additionally, various information regarding problems during the general tyre parameterisation process are given, including filtering and optimisation tools. Finally, the first part of this chapter ends with a summary statement regarding the parameterisation process.

The second part focuses on the parameterisation process of the standard TMeasy model by using two different types of tyres. For broader application range, two different manufacturers and two tyre types are used; one sports car tyre *Pirelli Pzero 245/40 R20 99W* (PP0) and one luxury vehicle tyre *Uniroyal Rainsport3 255/50 R19 107Y* (UR3). In summary, presentation of the test bench used, followed by some general information about the TMeasy tyre model and results of the parameterisation process are the main goals of this part of the thesis.

Due to the amount of literature that already describes the stepwise parameterisation process of the TMeasy tyre model, the focus is on the main areas of interests of this work. Therefore, detailed attention is given to parameterising the steady-state characteristics of the standard model. This includes manoeuvre selection, filtering, the parameter identification process, analysis, and of course model evaluation. Relatedly, a detailed overall model validation for both types of tyres is given in Appendix B. The chapter ends with a conclusion covering the overall parameterisation process.

4.1. Tyre modelling based on measurement data

Tyre modelling and simulation deals with various interactions and non-linear effects; this has already been shown as an outcome of previous chapters. This means that a precise description of the tyre properties is essential for the realistic modelling of force transmission behaviour.

As was already mentioned in Section 3.2, more than just a mathematical description is needed to model a system's behaviour in an accurate way. Additionally, finding the parameters that are mostly defined using measurement data plays a main role in the overall process.

In detail, model behaviour is first characterised using mathematical equations, and also described with parameter values, whereby both aspects have the same weight. Furthermore, measurement data that is utilised in the carrying out of the parameterisation process are as important as the model description using equations. Nonetheless measurement data are manoeuvre-dependent and can be generated from different types of test benches. This leads to the statement that an accurate model starts from the manoeuvre selected and not from measurement data.

In summary, the stepwise process from manoeuvre selection and definition, as well as test bench choice and parameterisation, is discussed in detail in the next subsections.

4.1.1. Manoeuvre selection as the first step in the parameterisation process

The process of selecting manoeuvres tends to be the first step in model parameterisation. Because different types of models have various structures and parameters implemented, this part depends on the approach and the model itself. Whereby physical models are more related to geometry and material parameters, handling models are more represented by mathematical values or parameters with physical meaning.

A further consideration that has to be taken into account is the manoeuvre design itself. For example, by using a very slow manoeuvre to keep the dynamic influences as low as possible, tyre temperature increases and changing the tyre properties. On the contrary, if we try to keep the tyre temperature low by using a manoeuvre with short measuring time but with high dynamic changes, transient forces occur. This mentioned trade-off is a given due to the measurement procedure for the steady-state tyre characteristics, as described in detail in Subsection 4.2.3.

In summary, depending on the tyre model approach, the requirements surrounding the tyre model and relevant knowledge are required to define a suitable list of manoeuvres. An example of a schematic listing tyre data and manoeuvre conditions, based on information from [Van Oosten, 2003] and [Ammon, 2005], is given in Table 4.1.

Table 4.1.: Exemplary manoeuvre requirements for tyre data, based on [Van Oosten, 2003] and [Ammon, 2005]

Type of data	**Measurement/manoeuvre**
Geometry and material	Size of tyre and rim Mass and moment of inertia Tread height and width Tread stiffness ratio and friction Belt dimension
Stationary test data	Vertical stiffness Steady-state tyre force and torques Self-aligning torque
Dynamic test data	Long. & lateral stiffness and damping Transient side-slip or slip excitations Eigen frequencies and modal damping
Data on road surface excitations	Single obstacle or vertical step Durability test

4.1.2. Tyre test bench systems

To generate measurement data for parameterising tyre models, two different categories, with each having two different types, have prevailed in the past years. To generate measurement data on a laboratory test bench, the tyre is operated on an artificially produced surface road, which may be rounded or flat. Due to their design, a distinction between internal drum, external drum and flat track test benches is made, see Figure 4.1 a.) and Figure 4.1 b.). In addition to the original laboratory test benches, mobile testing facilities like tyre trucks and data acquisition under real driving conditions have often been used and validated in recent years, and are represented schematically in Figure 4.1 c.) and Figure 4.1 d.).

To evaluate these four systems, an overview of the properties, advantages and disadvantages is given in the following descriptions.

Drum test rigs Depending on the application, drum test rigs are divided into inner and outer drum test benches, as seen in Figure 4.1 on the top left. For inner drum applications, it's easy to change ambient conditions or road surfaces. By using roadway constructions like asphalt, safety walking surfaces or sandpaper with various grain sizes, different tyre-road contact is provided for. Furthermore, temperature variations are possible with little effort. This means that both summer and winter environmental conditions can be set. By adding water or snow inside the drum, extreme conditions can also be investigated, see e.g. [Gnadler et al., 2005].

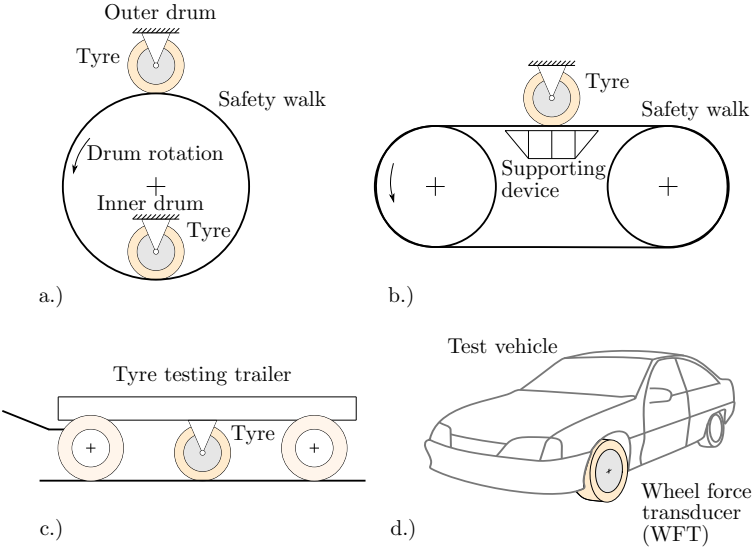

Figure 4.1.: Schematic representation of common tyre test bench systems adapted from [Rill, 2012]; upper left, inner and outer drum applications; upper right, flat track tyre test bench; bottom left, tyre trailer system; bottom right, schematic representation of tyre measurements under real driving operation

The second approach for drum test rigs is outer applications. In contrast to the inner drum test bench, no real concrete or asphalt road surfaces can be applied at higher speeds due to the centrifugal forces. Therefore either a metallic surface or sandpaper is used, whereby a variation in the coefficient of friction is possible with appropriate grain sizes as well. For small drum sizes, outside approaches provide the advantage of a simple and robust design.
Overall, for both inner and outer applications, the main disadvantages are the curvature of the surface and the related artificial tyre contact area conditions. Especially for smaller drum diameters, curvature influences in force and self-aligning torque measurements are present. A further limitation is given by the fact that a few systems only allow braking and non-transient manoeuvres. The main advantages are the economical and robust construction, the wide field of application and the simplicity of investigating different surface conditions. This approach is therefore common for high wheel loads and rolling resistance investigations, especially for truck tyres.

Flat track test benches Compared to drum applications, flat track test benches bring the main advantage of even surface, as seen in Figure 4.1 on the top right. Thus, negative influences in relation to the reaction forces and torques due to a curved road can be excluded, which delivers highly precise measurement data; for details see [Hüsemann, 2011] or [Unrau, 2013].
Further advantages are present for testing that is not steady-state, and dry and wet conditions are possible. This means that fast changes in normal force, longitudinal slip and lateral slip can be applied separately and combined as well. Also, a broad range of camber applications is possible under various loads. The limitation in terms of extreme load approaches, for example for truck tyre research, and additionally high costs are named as disadvantages of these rig systems. Moreover, like drum test rigs, applying real road surface conditions is not possible. For this reason, some kind of adapted sandpaper or safety walkway is normally used.

Tyre measuring truck or trailer Truck or trailers equipped to measure tyres offer the possibility to measure the tyre properties on real roads and surfaces, see Figure 4.1 on the bottom left. In this case, the test tyre is carried as an additional wheel on a truck or trailer. By undergoing manoeuvres, the testing wheel is deflected, driven or braked relative to the carrier vehicle and the applied forces and torques are measured via a measurement rim. Depending on the actuators, testing and combined tyre forces that are not steady-state are available as well. Because real tyre-road conditions are used, this method delivers very precise measurement data. Furthermore, different road conditions like dry, wet, snowy or icy can be used and investigated. Nevertheless, this can also count as a disadvantage. Changing environmental conditions such as road, surface, temperature or weather makes the reproducibility of the data difficult. Nonetheless, even and long test tracks are necessary for carrying out manoeuvres under constant conditions. In addition, testing speed and high loads, for example for truck tyres, are limited due to the limitations of the test trailer.

Real driving operation Another alternative to laboratory test benches is to ascertain tyre characteristics in real driving conditions, see [Nuessle, 2003], [Kollreider, 2009] or [Kerschbaumer, 2017]. To do so, a dynamic driving manoeuvre is used to gain information from the carrier vehicle, in particular high amounts of lateral acceleration or side slip angle. Based on the vehicle behaviour and the measured or calculated data, the tyre force and furthermore tyre characteristics are observed. To generate a tyre model from driving, in addition to an advanced observer design, parameter information from the test vehicle also has to be known. Fixed operating point measuring technology has to be set up, for example a ground-speed sensor for exact speed as well as wheel position sensors to measure the wheels relative to the road surface, and this has to be mounted onto the test vehicle. For detailed applications, *wheel force transducer*s (WFTs) are additionally assembled on the test vehicle. They measure the intersection forces and torques between rim and wheel hub, which have to then be transformed into wheel contact forces and torques, as can be seen Figure 4.1 on the bottom right.

The main advantage of real driving operation compared to laboratory test benches is testing under real tyre-road surface conditions. Like using a tyre measuring truck or trailer, testing on wet, snowy or icy surfaces can be done without changing the test setup. In addition, the need for even roads, changing conditions and reproducibility are difficulties related to this method. In addition, during defined driving conditions, only a mixture of different behaviours that influence tyre forces are available, e.g. camber, slip angle, longitudinal slip and furthermore steady-state and transient operating points. Overall, to generate a tyre model by driving delivers realistic tyre-road surface conditions, but also a lot of calculation effort and less reproducibility.

In summary, various requirements demand different tyre operating applications. Drum tests represent advantages in terms of compact construction and price, whereas outdoor approaches are used for more accurate tyre-road-surface investigations. Nevertheless, for a detailed study of reproducible results on transient tyre behaviour and temperature influences, measurements on flat track test benches are recommended for the present objective and are used in this project.

4.1.3. Parameterisation process

In order to meet the high accuracy demands of vehicle dynamic simulations, parameterisation is an important part of the overall modelling process. Therefore the adaption of tyre parameters is an optimisation process in combination with technical knowledge. Before focussing on the parameterisation process, measurement data evaluation and validation is necessary. Hence, various warm up procedures and different slip definitions are just a few examples that influence measurement results in a critical way. This additionally means that tyre characteristics are influenced for manoeuvre and test bench setups, wherein a detailed investigation is presented in [Zamow, 1995].

In this study, a measurement programme of 27 manoeuvres was performed on seven different test benches with various changes in pressure, tyre velocity and normal force. While in some investigations small deviations have occurred, larger discrepancies have come up in the measurements of longitudinal and lateral force characteristics, which specifically yield deviations of about 25 %. Also, the effect of various changes on external influences like speed, normal force and pressure show different changes in tyre behaviour. The conclusion is that considerable differences have occurred in the results of various test benches.

To conclude these investigations, a European Union research project named *tyre measurement* (TIME) was founded, see [Klaas et al., 1999]. The goal of the programme was to generate comparable tyre test bench results under vehicle-relevant conditions. This means that a measurement procedure can be designed in such a way that a few measurements have to be carried out in the defined range of realistic combinations. Furthermore, short-duration manoeuvres were intended to minimise influences on temperature and tyre wear. In summary, the TIME procedure does not prevent the fact that measurements on different test benches lead to differing results. It merely represents a standardisation of

the measurement procedure, which at least reduces the differences in the test procedure and presents a foundation for detailed investigations.

In summary, the combination of the measurement procedure and the test bench system forms the basis for the parameterisation process. Hence, for most commercial applications, the evaluation and parameter fitting process is carried out by a defined manufacturer software tool, where a parameter file for the desired model is generated as a final output.

By using industrial software products, knowledge transfer about the overall modelling and parameterisation process is rarely given in most cases. Particularly for research, black-box systems are neither useful for detailed investigations in tyre modelling nor in overall vehicle simulations. The parameterisation from measurement data thus leads to a part of the overall process that cannot be ignored. Some key information and properties concerning this are noted in the following description.

Data generation versus parameterisation process Normally, the sequence is defined by manoeuvre selection, data generation and the parameterisation process. Hence, this order makes sense from a technical point of view and should normally be carried out by one department. But in some cases, these parts are split up among two or more parties, which results in an additional time delay. This means that model parameterisation without information about detailed manoeuvre or test bench properties are usually associated with additional problems. As an example, parameterising driving characteristics when only braking data are available is a common example, see [Rill & Hirschberg, 2012]. Thus, missing measurement data, manoeuvre information, test bench information or data filtering information are just a few examples. In summary, well-founded parameterisation from weakly defined measurement data is indeed a difficult hurdle.

Optimisation versus parameterisation Often, parameterisation tools only define model values or implement a spline in measurement data by solving a minimisation problem. Hence, investigation of outliers or influences like temperature and pressure changes is not to be taken into account. Therefore, investigations of raw measurement data as well as on model parameterisation always have to be checked from an engineering point of view. In other words, data behaviour has to be understood, correctly filtered, parameterised and validated in a stepwise way. To be sure, using physical-based models simplifies this step immensely. Likewise, a stepwise parameterisation process is recommended.

Test bench data versus vehicle application When using tyre models parameterised from test bench data under real vehicle conditions, the difference in the friction coefficient has to be taken into account. While most test benches have some kind of safety walkway or sandpaper surface, road friction on asphalt is different. Therefore, defined road measurements for the reference vehicle have to be carried out by adapting a road friction coefficient. A detailed description of the procedure is given in [Hirschberg et al., 2009].

In conclusion, the tyre parameterisation process is an ambitions and expensive part of the overall simulation process, needing knowledge and experience. This level of effort may be underestimated in some cases.

4.1.4. Parameterisation process conclusion

The parameterisation process is a major part of the overall modelling operation. This includes manoeuvre definition, test bench knowledge and correct parameterisation. Experiments have shown that only good accuracy in the parameter selection process can be guaranteed if the focus is on all parts. Therefore, a detailed description of this process is given in the next section, based on the TMeasy tyre model.

4.2. TMeasy tyre model - steady-state parameterisation

After discussing the basic considerations surrounding tyre modelling based on measurement data, the focus is on parameterisation of the TMeasy tyre model in this section. Therefore, because a flat track test bench seems to be the best choice for the present requirements, information about the test bench used followed by a short overview of TMeasy properties are given first.

Next, focus shifts to the parameterisation of the steady-state characteristics implemented in TMeasy as an important part in this thesis. Attention primarily goes to the described points in the previous section, for example manoeuvre selection, filtering and the parameterisation process itself.

4.2.1. Tyre test bench and sensor configuration

The tyre measurements were done on a MTS Flat-Trac® III CT (Cornering & Traction) Tyre Test System, [MTS Systems, 2019], operated by the IABG mbH company in Munich, [IABG mbH, 2019]. This system is designed to perform force and torque testing of passenger car and light truck tyres in order to gain force data for vehicle handling models. The Flat-Trac III CT supports steady-state force tests, but it is also able to handle large dynamic forces, like slip angle sweep, sinusoidal slip angle and radial deflection.

Furthermore, a stiff structure A-frame tyre carriage is provided, as seen in Figure 4.2, and a broad range of control parameters like slip angle, lateral load, longitudinal velocity, tyre camber, vertical load, slip ratio and wheel torque as well as inflation air pressure are feasible. All tyre forces and torques were measured with respect to the wheel centre c-coordinate system and automatically transformed and logged to the wheel w-coordinate system according to *International Organisation for Standardisation* (ISO) 8855, for details see Chapter Symbols.

With these control parameters and the Flat-Trac CT specification presented in Table Table 4.2, this test bench provides a good tool for investigations in this project. For

a.) MTS Flat-Trac® III CT Tyre Test System

b.) Standard temp. sensor

c.) Additional temp. sensors

Figure 4.2.: Illustrations of the used MTS Flat-Trac® III CT (Cornering & Traction) Tyre Test System used; a.) overall test bench representation, b.) mounting position of the standard temperature sensor, c.) positioning of the three additional temperature sensors

more general information, please reference the MTS website [MTS Systems, 2019] or the test bench manual [MTS Systems, 2003]. In addition to the general settings, three additional sensors were mounted aside the tyre to measure the temperature at several positions of the tyre surface area. In particular during measurements with the Pirelli Pzero 245/40 R20 99W tyre, one sensor was also used to measure within the tyre tread pattern in order to focus on the bulk temperature, see Figure 4.2 bottom right. To minimise additional external influences, all investigations were done at fixed velocity and tyre pressure levels.

Table 4.2.: Standard MTS Flat-Trac® CT (Cornering & Traction) specifications, based on manufacturer website [MTS Systems, 2019] and test bench manual [MTS Systems, 2003]

Specification	**Range**	**Unit**
Speed	± 250	kph
Vertical force	25	kN
Lateral force	± 15	kN
Spindle torque	± 2800	Nm
Slip angle	± 30	degrees
Inclination angle	-12 to 45	degrees
Tyre outer diameter	$\leq$ 910	mm
Tyre width	$\leq$ 400	mm

4.2.2. Overall concept of the TMeasy tyre model

The TMeasy tyre model is a commercial handling tyre model, based on semi-physical approaches, for applications in vehicle dynamics, see [Rill, 2012], [Rill & Hirschberg, 2012], [Rill, 2015] and [Rill, 2018]. The idea goes back to an industrial project dealing with agricultural tractor tyres where no tyre measurements were available. Later, the first applications on passenger car tyres were published in [Rill, 1994].

Overall, the model approach has consistently adhered to an *easy to use* strategy, which takes the existing insufficiencies in reliable measurement data into account. In order to fulfil the semi-physical basic ideas, parameters have a direct physical meaning, which also enables their identification in cases of unclear or even incomplete test bench data. Furthermore, the number of model parameters in TMeasy is rather limited based on its easy to use concept.

Within the TMeasy tyre model, the contact force characteristics in a lateral and longitudinal direction are described by physical parameters in which the digressive influence of decreasing tyre load is taken into account. These load influences can be easily defined by a set of parameters at a nominal and double payload. Via generated slip, the combined force characteristics can be directly taken into account.

Based on the lateral force and the implemented pneumatic trail, self-aligning torque is approximated as well. Furthermore, rolling resistance, tipping torque and bore torque, or named turn torque, is carried out. Aside from some enhancements in *multi-body system* (MBS) that have been integrated via *standard tyre interface* (STI), version 4.0 of TMeasy already included modelling concepts for dynamic tyre forces as well as approaches for dynamic parking torque. This version was also applied for the *tyre model performance test* (TMPT), organised by the Vienna University of Technology, [Lugner & Plöchl, 2009].

TMeasy is a constantly evolving tyre model, which is already at version 5.2 and provides a smooth transition from standstill to normal driving situations. The main advantage is that no optimisation or parameterisation software is needed. A skilled engineer is able to estimate a first set of appropriate parameters just by knowing the size, payload of the tyre and friction properties of the tyre. Consequently, setting up a rough default parameter file without measurement data is possible from an engineering point of view. Of course, like in this thesis, parameters can be adjusted and improved via measurement data.

In summary, the TMeasy tyre model forms a good foundation for technical research. In the next section, the focus is the parameterisation of the steady-state tyre characteristics. Clearly, this is only a small part of the overall TMeasy tyre model, but it is the most imported part for this thesis. During this project, TMeasy version 4.9 is used and fully parameterised. A validation of the overall parameterisation is presented in Appendix B for both types of tyres.

4.2.3. Steady-state modelling concept

As was already mentioned before, the steady-state tyre characteristics play an important role in the tyre-modelling concept. Not only because it presents the main information to work with, it moreover affects additional characteristics. Therefore, in this subsection the parameterisation and validation process is presented in detail. The implementation starts with the modelling concept of the TMeasy tyre model, followed by a manoeuvre selection and the parameter setting process, and finally the model validation.

For parameterising steady-state tyre behaviour, it is common to divide up the force characteristics into purely longitudinal and lateral parts, and this strategy is used in TMeasy as well. For interacting longitudinal and lateral force properties, combined slip is defined and applied to a suitable semi-physical approximation.

As a foundation for the mechanism generating tyre forces in a longitudinal direction, we consider a tyre on a flat track test bench. For this, the tyre rotates with an angular velocity ω and the flat track with a speed v_x, see Figure 4.3 on the left.

In a first step, we consider just one section in the contact patch where only adhesion between the element and the track is given, as seen on the right in Figure 4.3. After entering the contact patch, the top of the section will run with the bed velocity v_x and the bottom with the average travel velocity $v_\mathrm{t} = r_\mathrm{e}\,\omega$, where r_e is defined as the dynamic tyre radius. So depending on the velocity differences $\Delta v = r_\mathrm{e}\,\omega - v_x$, a deflection in longitudinal direction is generated, with

$$u = (r_\mathrm{e}\,\omega - v_x)\,t\,. \tag{4.1}$$

The amount of time that a section spends in the contact patch is dependent on the length itself l_cp and furthermore on the angular velocity $T = l_\mathrm{cp}/(r_\mathrm{e}\,|\omega|)$. A maximum

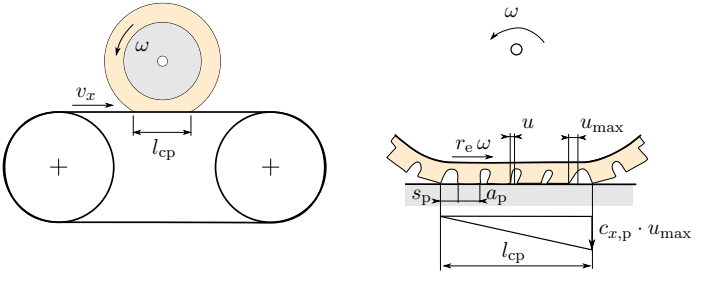

Figure 4.3.: Tyre tread section investigation concept; left, assumed tyre velocities on a flat track test rig; right, simplified shear stress distribution depending on the tyre contact length position, adapted from [Rill, 2015]

deflection of the section occurs at the end of the contact patch at time $t = T$ with

$$u_{\max} \;=\; u(t=T) \;=\; (r_{\mathrm{e}}\,\omega - v_x)\,T \;=\; (r_{\mathrm{e}}\,\omega - v_x)\,\frac{l_{\mathrm{cp}}}{r_{\mathrm{e}}\,|\omega|}\,. \tag{4.2}$$

This applied deformation of the section element applies a force to the tyre, and in a first approximation we get

$$F_{x,\mathrm{p}} \;=\; c_{x,\mathrm{p}}\,u\,, \tag{4.3}$$

where $c_{x,\mathrm{p}}$ is defined as the stiffness of one tread section. But under normal conditions, more than one element is in contact with the track, as seen in Figure 4.3 on the right. Herein, the number of sections can be estimated with $n_{\mathrm{p}} = l_{\mathrm{cp}}/(s_{\mathrm{p}} + a_{\mathrm{p}})$, where s_{p} is defined as the length of a section and a_{p} as the distance in between. If several sections are considered, this results in a linear force distribution related to the contact length, see Figure 4.3 right, whereby the resulting force in the longitudinal direction is then with

$$F_x \;=\; \frac{1}{2}\,n_{\mathrm{p}}\,c_{x,\mathrm{p}}\,u_{\max}\,. \tag{4.4}$$

Implementing Equation (4.2) and the number of sections, it yields

$$F_x \;=\; \frac{1}{2}\,\frac{l_{\mathrm{cp}}}{s_{\mathrm{p}} + a_{\mathrm{p}}}\,c_{x,\mathrm{p}}\,(r_{\mathrm{e}}\,\omega - v_x)\,\frac{l_{\mathrm{cp}}}{r_{\mathrm{e}}\,|\omega|}\,. \tag{4.5}$$

By using an approximation of the contact length l_{cp} with

$$l_{\mathrm{cp}}^2 \;=\; 4\,r_0\,\frac{F_z}{c_z}\,, \tag{4.6}$$

where r_0 is defined as the unloaded tyre radius, F_z as normal force and c_z as vertical tyre stiffness, now Equation (4.4) can be written as

$$F_x \;=\; 2\,\frac{r_0}{s_{\mathrm{p}} + a_{\mathrm{p}}}\,\frac{c_{x,\mathrm{p}}}{c_z}\,F_z\,\frac{r_{\mathrm{e}}\,\omega - v_x}{r_{\mathrm{e}}\,|\omega|}\,. \tag{4.7}$$

Now the longitudinal slip, which is the non-dimensional relation between the sliding velocity of the tread element in longitudinal direction and the average travel velocity is defined by

$$s_x \;=\; \frac{-(v_x - r_{\mathrm{e}}\,\omega)}{r_{\mathrm{e}}\,|\omega|}\,. \tag{4.8}$$

Hence, this correlation shows that the longitudinal slip implementation in the TMeasy tyre model is not simply defined in order to achieve an appropriate dimensionless quantity; rather, from a physical approach. When the tyre properties r_0, s_{p}, a_{p}, $c_{x,\mathrm{p}}$ and c_z are furthermore summarised in constant k, Equation (4.7) is simplified to

$$F_x \;=\; k\,F_z\,s_x\,. \tag{4.9}$$

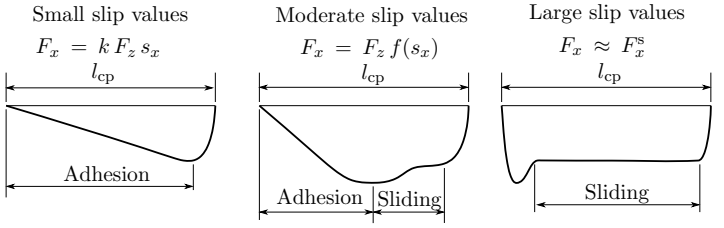

Figure 4.4.: Longitudinal force stress distribution for different slip values; areas where more adhesion and sliding condition is present are noted, adapted from [Rill, 2015]

Hence, from this equation it is clearly recognisable that the longitudinal force F_x depends on the tyre properties, summarised in k, the tyre slip s_x and the normal force F_z in this first approximation. Nonetheless, Equation (4.9) is only valid as long as all tread elements stick to the track. Therefore, at moderate slip conditions, sections at the end of the contact patch start sliding, whereas at high slip conditions only elements at the beginning of the contact area still stick to the road, see Figure 4.4.

This means Equation (4.9) only holds for very small slip areas, whereby a smooth transition from adhesion to sliding characterises the non-linear slip dependencies. To parameterise this behaviour, five semi-physical parameters have to be defined: the initial inclination (driving stiffness) dF_x^0, location $s_x^{\max}$ and magnitude of the maximum force $F_x^{\max}$ and slip value s_x^s where the sliding force F_x^s is achieved, see Figure 4.5.

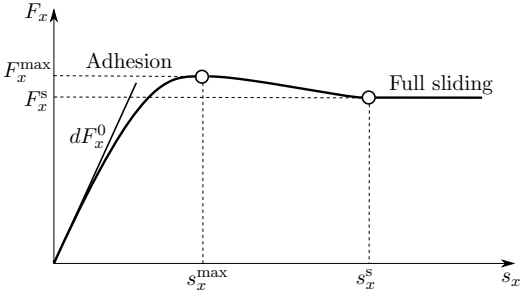

Figure 4.5.: Typical longitudinal tyre force characteristics implemented in the TMeasy tyre model, based on five parameters: the initial inclination (driving stiffness) dF_x^0, location $s_x^{\max}$ and magnitude of the maximum force $F_x^{\max}$ and slip value s_x^s where the sliding force F_x^s is achieved, adapted from [Rill, 2015]

A close contemplation is given in lateral direction. Hereby, the slip s_y is defined by

$$s_y = \tan \alpha = \frac{-v_y}{r_\mathrm{e} \, |\omega|} , \tag{4.10}$$

where α defines the tyre slip angle and v_y the lateral component of the contact point velocity. Like in longitudinal direction, as long as the tread sections stick to the road (with a small amount of slip) a close linear distribution of the force is applied along the length of the contact patch. Also, at moderate slip values, sections at the end of the contact patch start to slide. Meanwhile at high slip values, nearly all sections slide through the contact patch, see Figure 4.6.

This similar shear stress distribution assumption between longitudinal and lateral sections makes it clear that similar lateral slip versus force characteristics like in Figure 4.5 are given. Therefore, it can be described by initial inclination (cornering stiffness) dF_y^0, location $s_y^{\max}$, magnitude of the maximum force $F_y^{\max}$ and slip value s_y^s where the sliding force F_y^s is achieved. Furthermore, the distribution of the lateral force also defines the position of the resulting lateral force F_y. By using the product of this offset, also called pneumatic trail n, and the resulting force itself the self-aligning torque is implemented in TMeasy, for details see [Rill, 2015].

From this point on the tyre force characteristics, depending on the longitudinal or rather the lateral slip, can be parameterised from measurement data. In practice, the tyre characteristics are not just a product of the wheel load as in Equation (4.9), instead they affect the forces in a much more complicated way. Hence, the distribution of pressure over the contact area becomes more uneven with increasing load. Furthermore, force distribution in the contact patch depends on the wheel load as well as on the deflection.

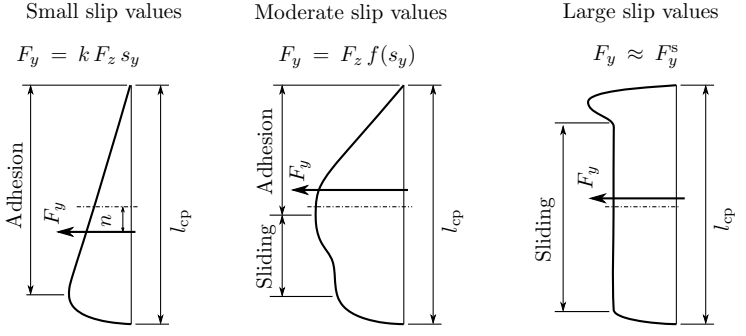

Figure 4.6.: Lateral force stress distribution for different slip values; areas where more adhesion and sliding condition is present are marked, and additionally pneumatic trail n is used to calculate the self-aligning torque, adapted from [Rill, 2015]

This means that the pressure peak at the entry of the patch cannot be used because of the small deflection and vice versa: the pressure drop in the rear leads to a reduction in the maximally transmittable friction force. In summary, with increasing pressure distribution over the contact area, the capacity to transmit forces of friction between road and tyre decreases in a non-linear way. This means that this digressive effect also has be implemented in the tyre model.

In the TMeasy tyre model, all normal force tyre characteristics can be parameterised by the five values represented in Figure 4.5, respectively in lateral and longitudinal direction. Consequently an interpolation between these normal force parameters has to be given. Therefore, based on different normal force tyre parameter setups, a parameter setup is recalculated at a defined payload $F_{z,1} = F_z^{\mathrm{N}}$ and its double $F_{z,2} = 2\,F_z^{\mathrm{N}}$ in order to take the non-linear wheel load influence into account, see Figure 4.7. In summary, regardless how much wheel load characteristics are measured, the final parameter set is defined by doubling the five mentioned parameters at payload $F_{z,1}$ and $F_{z,2}$.

Furthermore, after parameterising the longitudinal and lateral characteristics at two payloads and using the assumption that at $F_z = 0\,\mathrm{N}$, no force can be transmitted. The initial inclinations, the maximal forces and the sliding forces for arbitrary wheel loads F_z can be interpolated or extrapolated quadratically by

$$Y(F_z) \;=\; \frac{F_z}{F_z^{\mathrm{N}}}\left[2\,Y(F_z^{\mathrm{N}}) - \frac{1}{2}\,Y(2\,F_z^{\mathrm{N}}) - \left(Y(F_z^{\mathrm{N}}) - \frac{1}{2}\,Y(2\,F_z^{\mathrm{N}})\right)\frac{F_z}{F_z^{\mathrm{N}}}\right], \tag{4.11}$$

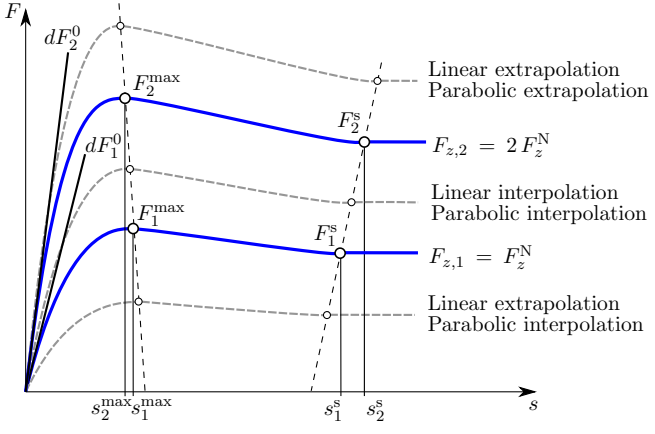

Figure 4.7.: Generic tyre model characteristics with five representative parameters, each at a defined payload $F_{z,1} = F_z^{\mathrm{N}}$ and doubled $F_{z,2} = 2\,F_z^{\mathrm{N}}$, adapted from [Rill, 2015]

where Y stands for dF_x^0, dF_y^0, $F_x^{\max}$, $F_y^{\max}$, F_x^{s} and F_y^{s}. Because the location of the maximum and slip values at which full sliding will occur cannot be zero, only a linear interpolation or extrapolation is possible. Therefore, the implementation is given with

$$X(F_z) \;=\; X(F_z^{\mathrm{N}}) + \left(X(2\,F_z^{\mathrm{N}}) - X(F_z^{\mathrm{N}})\right)\left(\frac{F_z}{F_z^{\mathrm{N}}} - 1\right), \tag{4.12}$$

by using X as a placeholder for $s_x^{\max}$, $s_y^{\max}$, s_x^{s} or s_y^{s}.

Finally, the steady-state characteristics are defined in a stepless manner depending on the slip and normal force variation. As a next step, a useful manoeuvre has to be defined to identify the mentioned parameters.

4.2.4. Steady-state manoeuvre definition

To parameterise the steady-state tyre characteristics, manoeuvres with various tyre loads and slip angles along with longitudinal slip changes have to be performed. As the name indicates, smooth manoeuvres without dynamic effects are preferred. If procedures take a long time, increasing tyre temperature and wear effect are caused which influence the overall characteristics, as presented in Section 3.2. Additionally, several normal loads are preferred with a wide slip range. Nonetheless, many different load levels increase measurement time, which means greater financial costs, while high slip levels also lead to high temperatures and wear problems.

Defining a good steady-state manoeuvre set also means dealing with a lot of compromises; this requires technical knowledge and experience in this field. Maybe the most common and well-known manoeuvres are periodic sine and triangle procedures. They sound typical and uncomplicated at first, but details can change the procedure and bring advantages in the parameterisation process. Questions like maximum amplitude, number of cycles, manoeuvre frequency or slip changes per second are only a few basic examples.

A commonly applied steady-state manoeuvre approach in lateral direction is presented in Figure 4.8 on the upper left. Here, a triangular manoeuvre with three periods and slip angle changes of $\mathrm{d}\alpha/\mathrm{d}t = 3\,\mathrm{deg/sec}$ is used. The maximum slip angle amplitude is defined with $\alpha_{\max} = 12\,\mathrm{deg}$ which turned out to be a good compromise between being high enough to reach the peak and not heating the tyre too much in the sliding area.

Before validating the manoeuvre in detail, a short overview of the filtering process is given by applying the lateral movement to the UR3 tyre at wheel load $F_z = 6000\,\mathrm{N}$ and $v_x = 60\,\mathrm{kph}$, see Figure 4.8. The measured lateral tyre force is presented in the lower left figure, wherein some information is already obvious. First, high force variation is given around the peak areas, which leads to the understanding that filtering is recommended.

Based on the lateral force, measured with a sample rate of $f_{\mathrm{s}} = 100\,\mathrm{Hz}$, a *Fast Fourier transformation* (FFT) is applied and the results are presented in the two right plots of Figure 4.8. On the upper right, two main amplitude areas are presented, the first around

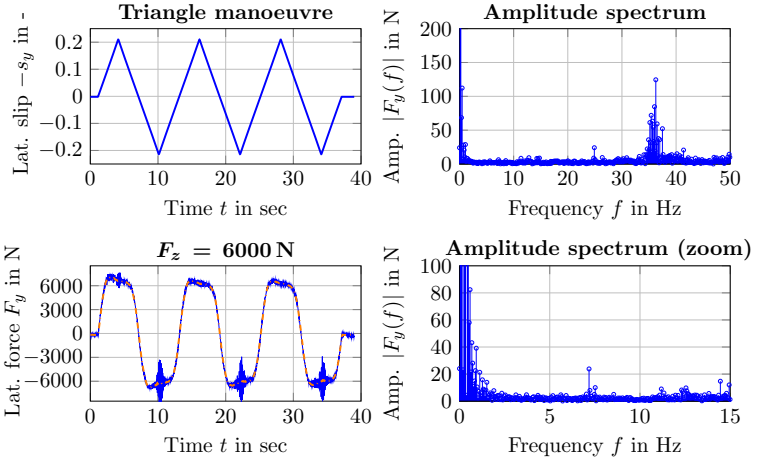

Figure 4.8.: *Fast Fourier transformation* (FFT) analysis of a steady-state lateral manoeuvre to define the right filter frequency; left, slip angle target as well as measured unfiltered and filtered lateral tyre force signal with $f_\mathrm{f} = 5\,\mathrm{Hz}$ from the UR3-tyre; right, the amplitude spectrum versus the frequency applied to the lateral tyre force

$f \approx 0\,\mathrm{Hz}$ and the second having $f \approx 35\,\mathrm{Hz}$. The first area represents the signal itself, whereby the second frequency represents the *fore-aft* tyre mode. This mode is produced by the vibration of the tyre tread in relation to the fixed tyre bead and is normally between 30 and 40 Hz, [Leister, 2015].

The zoomed spectrum on the bottom right of Figure 4.8 shows the main amplitudes until approximately 2 Hz. A tight filter frequency of $f_\mathrm{f} = 3\,\mathrm{Hz}$ would be possible, but the decision was made to use a more safe frequency. In summary, this means that because of various manoeuvre investigations, as presented in Figure 4.8, filtering for signals during non-dynamic manoeuvres by using a Butterworth filter with $f_\mathrm{f} = 5\,\mathrm{Hz}$ is applied. The comparison between unfiltered and filtered signals is shown on the lower left. A additional information which can be already seen in the measured lateral force is the changing overall amplitude over time, and furthermore the asymmetry around the peak force, whereby, both indicate a temperature influence that should be investigated in more detail.

Therefore, an evaluation of the triangle-manoeuvre, i.e. the orange dash-dotted lines, with two further evaluations are carried out in a next step and presented in Figure 4.9. The first additional manoeuvre is also a common sine procedure with frequency period of $f = 0.125\,\mathrm{Hz}$, see blue dashed lines. Both show disadvantages in dynamic influences

- the hysteresis effect in the upper right figure - as well as in the temperature influence, as seen in the hysteresis effect at high lateral slip values in the bottom right figure. Of course, higher periods of time decrease the dynamic effect but also increase time at higher slip values and therefore temperature influences.

Therefore, a new target procedure is introduced that is based on the basic idea that the focus is on small lateral slip values while only a short period of time is spent on the high values. Mathematically explained, an exponential function is defined with

$$s_{y,\mathrm{tar}} \;=\; \tan\left(\alpha_{\mathrm{tar}}\right) \;=\; A\,\mathrm{e}^{k\,t} - C\,, \tag{4.13}$$

where the parameters A, k and C are constant values and t represents the manoeuvre time which is parameterised depending on the process boundaries and referred to as the *Hirschberg* manoeuvre in this work.

The improvements in transient behaviour and hysteresis effects can be caused by force as well as by temperature behaviours, red solid line in Figure 4.9. In summary this implies that there is only a small change in the manoeuvre target, and this provides an advantage in the parameterisation process through the smaller effects on dynamic

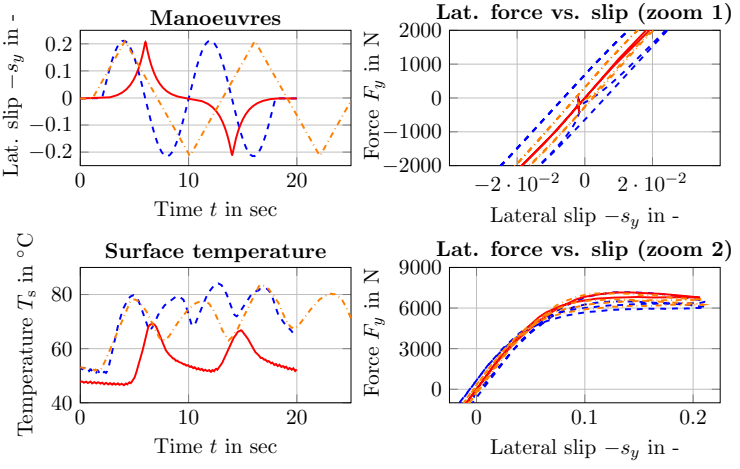

Figure 4.9.: Steady-state manoeuvre validation by means of dynamic and temperature effects using the UR3 tyre at wheel load $F_z = 6000\,\mathrm{N}$ and $v_x = 60\,\mathrm{kph}$; upper left, lateral slip value targets of the three different applications; right, dynamic and temperature effects on lateral force versus slip behaviour; bottom left, surface temperature during manoeuvre execution

and temperature. Therefore, the *Hirschberg* setup is recommended as a manoeuvre for steady-state parameterisation, in both lateral as well as longitudinal direction.

As theoretical investigations do not always apply to practical use cases, the test bench had problems with the longitudinal slip control during the *Hirschberg* manoeuvre with the UR3 tyre. To be in the same temperature window for steady-state parameterisation in longitudinal and lateral direction for this tyre, a triangle manoeuvre was chosen for both.

4.2.5. Steady-state parameterisation and validation process

After the definition of the measurement procedure and carrying out the measurements, the parameterisation process has to be done. This means that the five values based on Figure 4.7 have to be defined for each normal force in longitudinal and lateral direction first, and afterwards two sets of values based on a nominal normal force are calculated.

The parameterised results of the steady-state characteristics of the UR3-tyre are presented in Figure 4.10. The upper left figure represents the lateral force vs. slip characteristics depending on three chosen normal forces. The black dashed line represents the initial slopes and the black circles represent maximum forces and their positions for each normal force. Based on these three main values plus sliding area, the steady-state characteristics are defined and plotted with the solid grey lines.

Additionally, based on the temperature, plotted in the bottom figures, the hysteresis effect on high lateral slip values increase with higher normal forces. But overall, the parameterised characteristics in a lateral direction adequately fit the measurement data. In the two right figures, longitudinal force versus slip characteristics is presented. Because problems with the test bench slip control on high normal forces occurred, only manoeuvres of up to $F_z = 6000\,\mathrm{N}$ were feasible.

As already described, the triangular manoeuvre brings a higher dynamic as well as temperature hysteresis effect, which can be seen for each normal load. Furthermore, tyre behaviour changes under temperature and wear conditions so perfect test bench slip control seems to be difficult and leads to greater measurement noise. Because for passenger car tyres, in most cases, asymmetric characteristics may differ slightly between driving or braking, a small amplification factor that scales the initial slope, maximum force and position is implemented in the TMeasy tyre model. This can be seen in the longitudinal force versus slip characteristics because the model curve does not intersect exactly at the chosen points.

In summary, a good overlap between simulated and measured behaviour is presented. Based on these results, values for a defined nominal force at $F_z^{\mathrm{N}} = 4500\,\mathrm{N}$ and its double $2\,F_z^{\mathrm{N}} = 9000\,\mathrm{N}$ are calculated and presented in Table 4.3. These parameter setups describe the steady-state behaviour depending on slip and normal force and are used for further investigations.

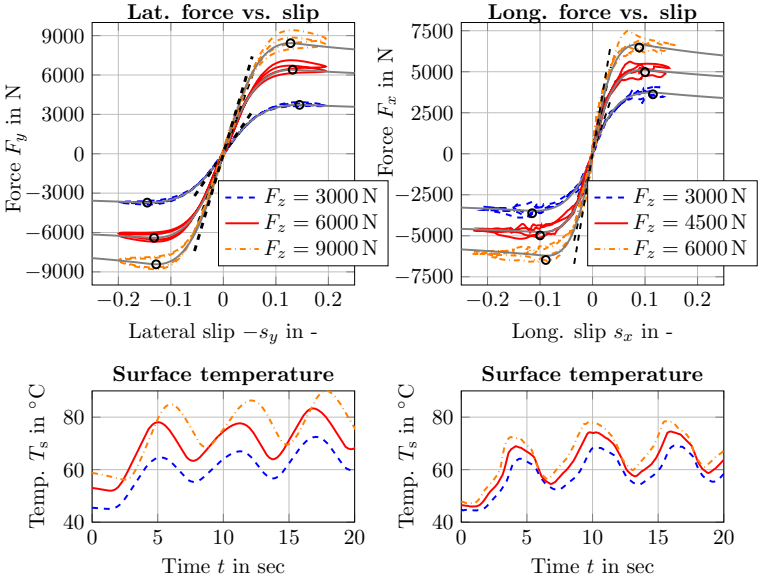

Figure 4.10.: Parameterisation of the steady-state tyre characteristics of the UR3 tyre at $v_x = 60\,\mathrm{kph}$; the two left figures show the parameterisation results of the lateral force versus slip, and the two right figures show the longitudinal results; based on the defined values shown in black, the model characteristics in grey are defined

In short, the overall parameterisation process based on the steady-state characteristics for the tyre UR3 was shown in this section. This includes the modelling concept, manoeuvre definition, parameterisation process and setup validation. Within this process, the whole TMeasy model is parameterised, based on previously mentioned literature. An overall validation for different manoeuvres for the tyres used is presented in Appendix B.

Table 4.3.: Defined longitudinal and lateral force parameter of the UR3 tyre at the payload $F_z^{\mathrm{N}} = 4500\,\mathrm{N}$, its double and a tyre velocity of $v_x = 60\,\mathrm{kph}$

Parameter	**Value**	**Description**
$dF_{x,1}^0$	146530	Initial slope at F_z^{N} in N
$F_{x,1}^{\max}$	5076	Maximum force at F_z^{N} in N
$s_{x,1}^{\max}$	0.101	Slip s_x where $F_x = F_{x,1}^{\max}$ in -
$F_{x,1}^{\mathrm{s}}$	4452	Sliding force at F_z^{N} in N
$s_{x,1}^{\mathrm{s}}$	0.499	Slip s_x where $F_x = F_{x,1}^{\max}$ in -
$dF_{x,2}^0$	285140	Initial slope at $2\,F_z^{\mathrm{N}}$ in N
$F_{x,2}^{\max}$	8664	Maximum force at $2\,F_z^{\mathrm{N}}$ in N
$s_{x,2}^{\max}$	0.062	Slip s_x where $F_x = F_{x,2}^{\max}$ in -
$F_{x,2}^{\mathrm{s}}$	7502	Sliding force at $2\,F_z^{\mathrm{N}}$ in N
$s_{x,2}^{\mathrm{s}}$	0.450	Slip s_x where $F_x = F_{x,2}^{\max}$ in -
$dF_{y,1}^0$	86181	Initial slope at F_z^{N} in N
$F_{y,1}^{\max}$	5170	Maximum force at F_z^{N} in N
$s_{y,1}^{\max}$	0.139	Slip s_y where $F_y = F_{y,1}^{\max}$ in -
$F_{y,1}^{\mathrm{s}}$	4800	Sliding force at F_z^{N} in N
$s_{y,1}^{\mathrm{s}}$	0.491	Slip s_y where $F_y = F_{y,1}^{\max}$ in -
$dF_{y,2}^0$	13581	Initial slope at $2\,F_z^{\mathrm{N}}$ in N
$F_{y,2}^{\max}$	8404	Maximum force at $2\,F_z^{\mathrm{N}}$ in N
$s_{y,2}^{\max}$	0.126	Slip s_y where $F_y = F_{y,2}^{\max}$ in -
$F_{y,2}^{\mathrm{s}}$	7589	Sliding force at $2\,F_z^{\mathrm{N}}$ in N
$s_{y,2}^{\mathrm{s}}$	0.473	Slip s_y where $F_y = F_{y,2}^{\max}$ in -

4.3. Comparative conclusion for the TMeasy steady-state parameterisation process

Before detailed investigations of temperature influences and transient effects can be carried out, a standard tyre model setup is needed. Defining a preferred test bench setup depending on the requirements turned out to be an important part of the overall process.

Different test bench setups, including advantages and disadvantages, were presented in this chapter. Using an indoor flat track test bench seemed to be the best compromise for basic research on temperature and transient tyre effects. After defining the test bench approach, the focus shifted to the parameterisation process in theoretical and practical aspects.

The process started with a presentation of the overall TMeasy concept and was followed by describing how the steady-state modelling configuration is implemented. The focus was on the force stress distribution, depending on longitudinal and lateral slip characteristics. Based on this assessment, a force behaviour with only two times five parameters at normal payload and its double are needed.

Furthermore, different manoeuvres were discussed and validated in order to parameterise the steady-state characteristics from a technical point of view. Finally it was shown how a TMeasy parameter setup for longitudinal and lateral characteristics is generated. Within this process, the whole TMeasy model is parameterised, based on previously mentioned literature. An overall validation for different manoeuvres with the tyres used is presented in Appendix B.

In summary, the foundation for further research is given in this chapter. Test bench measurements were done and the standard version of the TMeasy tyre model has been parameterised. Based on this structure the extension to temperature influence on tyre force characteristics is carried out in the next Chapter 5.

5

Tyre temperature and its impact on tyre forces

After theoretical investigations of the influence of temperature on steady-state tyre characteristics in Chapter 3 and the parameterisation of the standard TMeasy tyre model in Chapter 4, modelling the tyre temperature and its impact on tyre forces is the topic of this chapter.

Based on already published experimental investigations of temperature modelling, presented in Chapter 3, a model structure which works most practically with handling model approaches is given as introduction of this chapter. Within this model decision, assumed simplification and prerequisites are then presented, which generalise the detailed modelling process for further applications.

Based on the model decision, as a next step the focus is on the fundamentals of temperature model design based on the first law of thermodynamics. Different implemented heat phenomena are discussed and the mathematical implementation is described in detail. Next, the parameterisation process, including manoeuvre description and model validation, is presented for both tyres as a conclusion of the first part.

The second part of this chapter deals with the impact of temperature on tyre force behaviour. Different tyre layer temperatures are used as input for the temperature model and applied to the TMeasy tyre model. After the description of the mathematical implementation, the parameterisation process is presented, followed by a model validation as in the first part.

Finally, different manoeuvres are used to evaluate the enhanced TMeasy tyre model. Deviations in temperature and force behaviour are presented and discussed in detail. Furthermore, the implemented enhancements regarding temperature are summarised and a conclusion is given. In addition, all longitudinal and lateral model parameters for the tyres used are summarised in Appendix D. The presented model will be used for further investigations of transient tyre behaviour in the next chapter.

5.1. Tyre temperature modelling

The model of the temperature dependence between different tyre layers forms the basis of a solid overall tyre model that includes the influence of temperature. However, the foundation of this purpose is given by the complexity and requirements of the tyre model used, and this once again leads to a trade-off between accuracy, calculation time and parameterability based on the standard tyre model.

Hence, a summary of defined properties worked out in previous chapters is presented first, before simplifications are defined and the model used is described in detail.

Temperature influence As a final conclusion from Section 3.4, different layer-dependent temperatures influence tyre behaviour in different ways. Here, the thermal approach should be able to handle various temperature regions. In other words, a multi-layer model or a model based on a partial *differential equation* (DE) is recommended.

Literature results Most research in the literature has been carried out on influences on overall friction behaviour. Especially [Angrick et al., 2014] and [Corollaro, 2014] show that cornering stiffness is directly influenced by the bulk temperature of the tyre.

Heat generation through hysteresis effect The temperature dependent ratio between storage and loss modulus $\tan\delta$ in the carcass region is the dominant factor in terms of hysteresis friction. The reliable prediction of the temperature inside this rubber bulk is thus of great importance. Therefore, a subdivision of the tyre into belt and bulk is recommended.

Parameterisation using infrared sensors The parameterisation of the model is mostly carried out using measurements from infrared sensors. These sensors only scan the outermost region of the tyre, and they only measure extreme temperature changes. For this reason, a very reactive layer on the tyre's surface is needed, which can be only achieved through a separation between bulk and surface. Therefore, a surface layer consisting of a thin layer of rubber should be used.

Section measurements Results from section measurements have shown that influences on friction not only depend on velocity but also on section temperature. This effect is confirmed in the literature, indicating that tyre temperature has an influence on the position and absolute value of the maximum coefficient of friction.

Handling model based approach The TMeasy tyre model is categorised as a handling tyre model approach. Therefore, a physical-based temperature model application with high computation time does not work very satisfactorily with a semi-physical approach.

As a summary of these description points, a multi-layer model with three different layers (belt, bulk and surface), where each layer is assessed based on the first law of thermodynamics, seems to be a good compromise in terms of the application of the TMeasy tyre model.

To confirm this decision, a model comparison was done, see [Hackl et al., 2017c] and [Hackl et al., 2018]. Thereby, a single-layer based on [Sorniotti, 2009], a multi-layer model according to [Büttner et al., 2015] and partial model related to [De Rosa et al., 2008] were compared with respect to accuracy, parameterability and computation effort for various manoeuvres and different types of tyres. Based on these results, it has been confirmed that a multi-layer model functions with handling tyre models in a satisfactory way. Before special focus goes to the mathematical implementation of the thermal model, a few simplifications have to be defined for further clarity.

5.1.1. Temperature model simplifications

To keep the parameterisation effort as well as the overall complexity of the model as low as possible, assumptions and model prerequisites have to be applied. These simplifications are carried out based on the knowledge that measurement data used for parameterisation are obtained from a flat track test bench.

In summary, these simplifications consist of the following:

Heat generation due to hysteresis Neglecting the tyre's sidewalls, the heat generation due to hysteresis is considered to be dependent only on the vertical load. This is done because the deformation-based hysteresis effect of the contact patch from longitudinal and lateral forces is assumed to be of minor importance.

Shape of contact patch The tyre is characterised by having a cylindrical form and a rectangular contact patch with length and width depending on the tyre's normal stiffness and vertical load.

Road surface properties The road surface is assumed to be rigid, homogeneous and isotropic. It can be seen as a geometric plane, which is applicable for measurements on the surface of the flat track test bench.

Driving velocity dependent convection coefficient For reasons of constant driving velocity, the convection coefficient with the filling medium as well as the heat exchange between tyre and road are considered to be constant. The convection between tyre and ambient air is assumed to be velocity-dependent only, using a linear approach.

Camber influences The effects of changes in camber angle are excluded. Therefore, without influences on changing camber in combination with the chosen approach, the simulated temperature is uniform over the tyre width and circumference of the tyre.

Filling medium as ideal gas The temperature of the filling medium is calculated by means of the ideal gas equation.

Radiating heat flows All radiating heat flows are neglected.

Furthermore, to model the temperature of a tyre in use with an approach based on the first law of thermodynamics, it is necessary to identify certain tyre properties in terms of mass distribution, tread design and tread dimensions beforehand.

In terms of tread design, a section of the tyre was cut out, coloured and used to generate a two-coloured picture of the footprint. This footprint was used to determine the defined *groove factor* g_f, which indicates the ratio between the effective contact area (positive tread design) and the dimension of the contact patch in general (positive + negative tread design). With this information, the surface areas used for heat exchange can be described precisely.

The required dimensions of the tyre, for example unloaded radius and contact patch width, are provided by the TMeasy tyre model. In addition, further tyre sections were cut out to identify the thickness of each layer and the composition of the supporting structure in terms of the ratio between steel cords and filling material.

Regarding mass distribution, the observed tyre was weighed in its initial state. Measurements on the flat track test bench result in a profile loss of a few millimetres, so the tyre was weighed again and the mass loss per millimetre of rubber was obtained. This parameter was verified by weighing the tyre after all measurements were done and by comparing the calculated mass loss to the measured loss in mass. Since the goal of the thermal model is to simulate tread temperatures, the sidewalls are not included in this thesis approach. For this reason, a section of the tyre was used to identify the mass distribution between the tread and the sidewalls and subsequently the mass distribution between the supporting structure and the rubber inside the tread.

In summary, the model is able to use the correct mass for each layer rather than calculating temperature changes per kilogram. To calculate the correct mass of the rubber without the tread pattern, the groove factor was used to scale the mass per thickness accordingly.

5.1.2. Modelling concept of the temperature model

After defining the assumed simplifications, including mass distribution and tread design, the modelling concept can be presented based on the properties mentioned. Here, the basis of the implemented multi-layer temperature model forms the thermal equation based on the first law of thermodynamics, applied on each layer j, with

$$\sum_i \dot{Q}_{i,j} \frac{\Delta t}{m_j \, c_{p,j}} = \Delta T_j \,, \tag{5.1}$$

where $\dot{Q}_{i,j}$ describes the heat phenomena applied to each layer, Δt the time step, m_j the layer mass, $c_{p,j}$ the specific heat capacity and ΔT_j the temperature changes per time period. A detailed derivation of the first law of thermodynamics applied to a tyre in use is given in Appendix C.

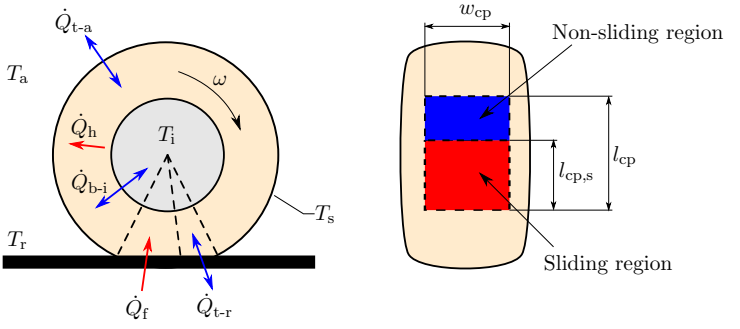

Figure 5.1.: Different heat phenomena occurring in a tyre during operation, presented left, and size of the contact patch with defined sliding and non-sliding region right, adapted from [Hackl et al., 2018] based on [Tremlett & Limebeer, 2016]

In the specific example of the implemented thermal model, the procedure described in Equation (5.1) is applied to all three layers, taking into account their individual thermal inputs and outputs. An overview of the heat phenomena evaluated can be seen in Figure 5.1.

Therein, $\dot{Q}_{\text{f}}$ represents the heating from frictional power and $\dot{Q}_{\text{h}}$ the heat generation from continuous deformations due to the vertical load. The convective heat exchange between the tyre and the ambient air is shown as $\dot{Q}_{\text{t-a}}$, whereas $\dot{Q}_{\text{b-i}}$ expresses the heat exchange from the belt layer with the inner filling medium. The heat exchange between the tyre and the road is displayed via $\dot{Q}_{\text{t-r}}$. The areas of heat generation and exchange inside the contact patch can be seen on the right side of Figure 5.1, where the non-sliding region corresponds to the heat exchange between tyre and road $\dot{Q}_{\text{t-r}}$, and the sliding region is responsible for the heat generation due to friction $\dot{Q}_{\text{f}}$.

Furthermore, heat phenomena acting upon all layers of the thermal model are given in detail in Figure 5.2 on the left. It shows the corresponding cross section, whereby the different regions of the tyre are implemented as lumped masses m_i with intermediate thermal resistors based on the tyre tread profile δ_j and A_j of each layer j, see Figure 5.2 right. Regarding heat transfer, it can be seen that in addition to the convective heat exchange of the surface layer $\dot{Q}_{\text{s-a}}$, the inner belt regions of the tyre are thermally related to the environment through the groove area of the profile design A_{belt}, and therefore also convection with the ambient air is given with $\dot{Q}_{\text{b-a}}$. At the innermost layer, the belt layer, there is heat generation due to hysteresis $\dot{Q}_{\text{h}}$. Experimental validation indicates this effect to be most pronounced at the tyre's sidewalls and the carcass. For this reason, and to keep the number of parameters needed as low as possible, this heat generation is neglected inside the bulk layer.

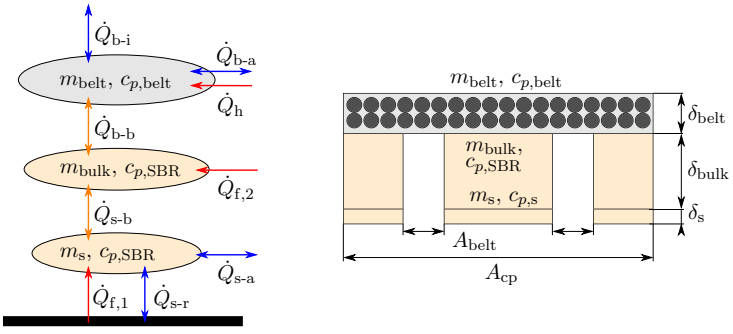

Figure 5.2.: Energy balance of lumped mass layers during a tyre in use on the left, and schematic representation of the tyre tread with the different layer thicknesses on the right

Hence, after defining the overview of heat phenomena in each layer, the focus is on a detailed mathematical description.

Heating generation from frictional power $\dot{Q}_{\text{f}}$

To calculate the heat generation from frictional power, two main components are involved, the force in longitudinal and/or lateral direction $F_{x/y}$ and the sliding velocities $v_{\text{s},x/y}$. Based on considerations from Subsection 4.2.3, sections in the contact patch are simplified in the adhesion and sliding region. This separation therefore has to be included in the friction power calculation.

In this thesis, separation is carried out by using a linear approach based on [Tremlett & Limebeer, 2016]. The sliding region is scaled separately between two dimensionless parameters $c_{\text{s},1}$ and $c_{\text{s},2}$ longitudinally $c_{\text{s},x}$ and laterally $c_{\text{s},y}$. Then the length of the sliding region is defined by the ratio of the current $s_{x/y}$ and the peak slip $s_{x/y}^{\max}$ in both directions with

$$c_{\text{s},x/y} = \frac{s_{x/y}}{s_{x/y}^{\max}} \left(c_{\text{s},2} - c_{\text{s},1}\right) + c_{\text{s},1}\,, \tag{5.2}$$

whereby the larger area in longitudinal or lateral direction defines the length $l_{cp,\text{s}} = \max\left(c_{\text{s},x}, c_{\text{s},y}\right)$ of the sliding area in the contact patch. The reference values describe the slip quantities at which maximum force is achieved. At these maximal values the sliding region of the contact patch is expected to consist of 80 % of the total area, described by parameter $c_{\text{s},2} = 0.8$. When the tyre is experiencing no slip, 30 % of the contact patch is still in a sliding state, described by $c_{\text{s},1} = 0.3$. Although these values were obtained from [Tremlett & Limebeer, 2016] for motorsports applications, experimental validation also shows satisfactory results when used for passenger car tyres, see [Hackl et al., 2018].

Besides the product of the occurring forces $F_{x/y}$ and the corresponding sliding velocity $v_{\mathrm{s},x/y}$, the parameters describing the distribution inside the contact patch $c_{\mathrm{s},x/y}$ are used to divide the measured forces according to their origin, either from the sliding or the non-sliding region of the contact patch. By using this approach in the calculation, this heat flow describes the total power generated in the tyre-road interface. Therefore, this power has to be scaled to determine the energy distribution between the tyre and the road, depending on the current temperature ratio. To do so, the ongoing surface temperature of the tyre T_s is compared to a reference temperature T^N at which the power is distributed equally, 50 % entering the road and 50 % the tyre.

Finally the heating generated from friction power can be described by

$$\dot{Q}_{\mathrm{f},x/y} = c_{\mathrm{s},x/y}\,\frac{T^\mathrm{N}}{2\,T_\mathrm{s}}\,F_{x/y}\,v_{\mathrm{s},x/y}\,, \tag{5.3}$$

where the longitudinal and lateral sum is defined as the product with $\dot{Q}_\mathrm{f} = \dot{Q}_{\mathrm{f},x} + \dot{Q}_{\mathrm{f},y}$.

Through preparatory measurements and experimental validation of the thermal model, it was found that the surface layers need to be responsive in order to cope with the temperature changes measured by the infrared sensors. To do so, a very thin layer is needed. Furthermore, studies, for example from [Persson et al., 2005], show that the penetration depth of the heat input from frictional heating is dependent on the surface texture of the roadway. Different sizes of asperities induce heat, not only in the tread region in contact with the road, but also in internal regions in a decreasing manner. Therefore, a temperature gradient along the tyre depth can be observed when the tyre is skidding over the road surface. To show this effect and enable the temperature model to cope with different road surfaces satisfactorily, the heat generated from friction is divided evenly between the surface and bulk layer, each half with $\dot{Q}_{\mathrm{f},1} = \dot{Q}_{\mathrm{f},2} = \dot{Q}_\mathrm{f}/2$, see Figure 5.2. The thickness of the surface layer can be parameterised to generate the temperature gradient resulting from this heat source. In this case, a thinner surface layer would be characterised by a surface texture with small asperities and therefore similar excitation wavelengths. With this approach, it is possible to adjust the mass and therefore the thermal responsiveness of the surface layer in a way that fast temperature changes in the surface region can be shown.

Heat generation due to hysteresis $\dot{Q}_\mathrm{h}$

The second heat generation effect assumed in the temperature model approach is heat generation due to hysteresis, which means internal heating when the tyre is periodically deformed by vertical load. This deflection of the tyre structure and the transition to its original state induces energy in the tyre and furthermore generates heat.

As mentioned above, this effect is situated at the innermost layer, because experimental validation indicates this effect to be most pronounced at the tyre's sidewalls and the carcass, as shown in Figure 5.2. Furthermore, to keep the amount of parameters needed as low as possible, this heat generation is neglected inside the bulk layer.

To calculate the hysteresis heat flow $\dot{Q}_{\mathrm{h}}$ in the tyre, vertical load F_z and the travelling velocity $|\omega|\, r_{\mathrm{e}}$ are used with

$$\dot{Q}_{\mathrm{h}} = p_z\, |\omega|\, r_{\mathrm{e}}\, F_z\,, \tag{5.4}$$

where a parameter p_z is needed to scale the generated heat correctly for different tyre construction, and enabling a fast and easy way to model this phenomenon by defining only one additional coefficient.

Heat exchange due to the environment

To describe the heat exchange with the environment, four different effects have to be discussed. As already described and also shown in Figure 5.2, two main convective heat flows couple the tyre with the environment air due to rotation. Beside the convective heat exchange of the surface layer $\dot{Q}_{\text{s-a}}$, the inner regions of the tyre are thermally coupled with the environment through the groove area of the profile design A_{belt} and therefore also convection with the ambient air is given with $\dot{Q}_{\text{b-a}}$.

Another heat exchange is given by the filling medium inside the tyre and the belt layer of the tyre. Due to the fact that the tyre pressure is constantly regulated due to test bench setup, an exchange of airflow between the tyre and the test facility is given. This furthermore leads to the effect that the filling medium inside the tyre rotates with a different speed than the tyre layer. Because of this speed difference, a convective heat exchange between belt layer of the tyre and filling medium inside the tyre $\dot{Q}_{\text{b-i}}$ is given as well.

Finally, the last heat exchange phenomenon is the heat transfer between the surface layer and the road within the adhesive area of the contact tread $\dot{Q}_{\text{s-r}}$. Because measurements on an indoor test bench were performed, the road is characterised by a sandpaper mounted on a water cooled steel belt. This means that in detail, an overall heat transfer coefficient based on a series of conductive and convective heat transfer should be used for this approach. To simplify this approach, it is assumed that the high conductivity of steel leads to negligible thermal resistance in comparison to the convective heat flow. Therefore, the heat transfer between the tyre surface layer and the water-cooled test bench road is given as a convective model application.

In summary, with these simplifications all four effects are modelled via heat transfer and mathematically described with

$$\dot{Q}_i \;=\; h_i\, A_i\, \Delta T\,, \tag{5.5}$$

where h_i describes the heat transfer coefficient, A_i the surface area where the heat transfer takes place and ΔT the difference in temperature. With this distinction and the already defined sliding and non-sliding area in the contact patch, all heat exchange areas can be described.

Thus, the overall size of the contact patch is calculated by

$$A_{\mathrm{cp}} = w_{\mathrm{cp}}\, l_{\mathrm{cp}}\, g_f\,, \tag{5.6}$$

where the g_f describes the percentage of the tread area without grooves, w_{cp} the width and l_{cp} length of the contact area, see Figure 5.1. Moreover, the size of the sliding region of the contact patch is determined by

$$A_{\mathrm{cp,s}} = w_{\mathrm{cp}}\, l_{\mathrm{cp}}\, g_f\, \max\left(c_{\mathrm{s},x}, c_{\mathrm{s},y}\right)\,, \tag{5.7}$$

and the area of heat exchange of the surface layer $A_{\mathrm{s,a}}$ with the ambient air is calculated by

$$A_{\mathrm{s,a}} = A_{\mathrm{t}}\, g_f - A_{\mathrm{cp}}\,, \tag{5.8}$$

where is A_{t} representing the whole surface area of the tyre and is calculated via information based on the type of tyre and the unloaded radius r_0. Finally the convective cooling inside the tread grooves is attributed to the belt layer and the area is calculated by

$$A_{\mathrm{belt}} = A_{\mathrm{t}}\left(1 - g_f\right). \tag{5.9}$$

Since the size of the heat exchange area of the bulk region is not only dependent on the profile design but also the profile depth, it cannot be defined in a simple manner, which means this effect is neglected. In the next step, the temperature of the filling medium T_{i} is calculated by means of the ideal gas equation via the pressure ratio between the current internal pressure p_{i} and the initial starting pressure p_0 at starting temperature T_0 by

$$T_{\mathrm{i}} = T_0\, \frac{p_{\mathrm{i}}}{p_0}\,. \tag{5.10}$$

Using this defined information, the heat exchanges due the environment can be calculated. Therefore, the heat exchange between the surface layer and the road $\dot{Q}_{\mathrm{s\text{-}r}}$ is described through

$$\dot{Q}_{\mathrm{s\text{-}r}} = h'_{\mathrm{s\text{-}r}}\, \left(A_{\mathrm{cp}} - A_{\mathrm{cp,s}}\right)\, \left(T_{\mathrm{r}} - T_{\mathrm{s}}\right)\,, \tag{5.11}$$

where $h'_{\mathrm{s\text{-}r}}$ describes the overall heat transfer coefficient between tyre surface and road, and T_{r} defines the current road (respectively the steal belt) temperature. The superscript $'$ is used because the heat transfer coefficient includes a combination of conductive and convective heat phenomena. As constant driving velocity v_x is used for the test bench, this coefficient for heat exchange is considered constant.

Because a standstill is given between test manoeuvres, which automatically means a cooling phases via convective heat exchanges, a speed-dependent heat transfer coefficient between tyre and ambient air $h_{\mathrm{t\text{-}a}}$ is used as

$$h_{\mathrm{t\text{-}a}} = h_0 + h_{\mathrm{v}}\, v_x\,, \tag{5.12}$$

where h_0 describes the transferable heat per area at standstill and h_{v} the velocity-

dependent portion of this heat flow. Due to the pronounced influence of the profile design on these coefficients, the parameters have to be defined during the parameterisation process within a justifiable range.

With this approach, all convective heat flows related to the tyre and its surroundings can be expressed with

$$\dot{Q}_{\text{s-a}} = h_{\text{t-a}}\, A_{\text{s,a}}\, (T_{\text{a}} - T_{\text{s}}) \quad \text{and} \tag{5.13}$$

$$\dot{Q}_{\text{b-a}} = h_{\text{t-a}}\, A_{\text{belt}}\, (T_{\text{a}} - T_{\text{b}})\,, \tag{5.14}$$

where T_{a} represents the ambient air temperature.

To describe the heat flow between the belt layer and the filling medium with temperature T_{i}, an additional convection coefficient $h_{\text{b-i}}$ is used. Due to the diffusion stopping sealing on the inside of the tyre, this parameter is situated at the bottom end of the convection coefficients found in the literature and is considered constant. Finally, the heat exchange via the filling medium is calculated with

$$\dot{Q}_{\text{b-i}} = h_{\text{b-i}}\, A_{\text{t}}\, (T_{\text{i}} - T_{\text{b}})\,. \tag{5.15}$$

At this point, all heat exchange via the environment and furthermore all heat generation effects are defined. In the next step, heat interactions between the layers will be investigated in detail.

Heat interaction between the layers

The different regions of the tyre are considered to be lumped masses with intermediate thermal resistors. This is done to thermally couple each region with the adjacent ones. A schematic of how this adapted form of the stationary heat conduction is implemented is shown in Figure 5.3. Thereby, $\dot{Q}_{\text{s-b}}$ represents the heat flow between the surface and the bulk layer, and $\dot{Q}_{\text{b-b}}$ represents the heat flow between the bulk and belt layer.

In this approach, the thickness of each layer δ_j, the thermal conductivity λ_j and the overall surface area times groove factor $A_{\text{t}} \cdot g_f$ are used to properly model the resistors. The geometry used corresponds to the cross section displayed in Figure 5.2 on the right.

Thus, the thermal resistance between the surface and the bulk layer $R_{\text{th,s-b}}$ via the current tread depth δ_{t} and the thermal conductivity of *styrene-butadiene rubber* (SBR) λ_{SBR} is calculated using

$$R_{\text{th,s-b}} = \frac{\delta_{\text{t}}/2}{\lambda_{\text{SBR}}\, A_{\text{t}}\, g_f}\,. \tag{5.16}$$

Furthermore, the thermal resistance between the bulk and belt layer $R_{\text{th,b-b}}$ can be

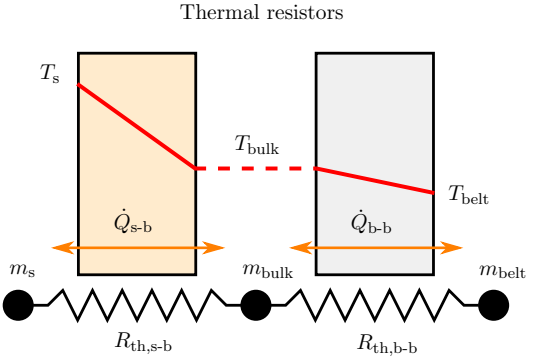

Figure 5.3.: Multi-layer model described as lumped masses with thermal resistors, adapted from [Hackl et al., 2017c]

expressed by

$$R_{\text{th,b-b}} = \left(\frac{(\delta_t - \delta_s)/2 + \delta_{SBR}}{\lambda_{SBR}} + \frac{\delta_{belt}/2}{\lambda_{belt}} \right) \frac{1}{A_t \, g_f} , \tag{5.17}$$

where δ_{SBR} represents the amount of rubber without grooves between the carcass and the usable rubber. Additionally, the thickness δ_{belt} and the thermal conductivity of the belt λ_{belt} are needed. In terms of the latter, due to the carcass design, the thermal conductivity of steel is used.

Using all of the above information, the internal heat flow between the surface and the bulk $\dot{Q}_{s\text{-}b}$ as well as the bulk and the belt layer $\dot{Q}_{b\text{-}b}$ can be expressed by

$$\dot{Q}_{s\text{-}b} = \frac{1}{R_{\text{th,s-b}}} \left(T_{bulk} - T_s \right) \quad \text{and} \tag{5.18}$$

$$\dot{Q}_{b\text{-}b} = \frac{1}{R_{\text{th,b-b}}} \left(T_{belt} - T_{bulk} \right) , \tag{5.19}$$

where T_s represents the current temperature of the surface layer, T_{bulk} the temperature of the bulk and T_{belt} the temperature of the belt layer.

Temperature changes within each layer

Before the final temperature change for each layer can be defined, the mass distribution has to be given. This is done by means of the current profile depth δ_t with

$$m_{SBR} = \delta_t \, m'_{SBR} , \tag{5.20}$$

describing the mass of usable rubber on the tyre m_{SBR}. The parameter m'_{SBR} represents the rubber profile mass in the grooved section of the tyre per tread depth in millimetre. In the same matter, the mass of the surface layer m_{s} is calculated by using the thickness of the surface layer δ_{s} and the mass per tread depth by

$$m_{\mathrm{s}} = \delta_{\mathrm{s}}\, m'_{\mathrm{SBR}}\,. \tag{5.21}$$

The mass of the bulk layer m_{bulk}

$$m_{\mathrm{bulk}} = m_{\mathrm{SBR}} - m_{\mathrm{s}}\,, \tag{5.22}$$

is calculated by means of the previously identified masses. Then, the mass of the innermost layer m_{belt} can be expressed from the overall tyre mass as

$$m_{\mathrm{belt}} = m_{\mathrm{t}} - m_{\mathrm{SBR}}\,, \tag{5.23}$$

where m_{t} is representative of the tyre's mass without the sidewalls.

With all this information gathered, the temperature changes $\Delta T_{\mathrm{s/bulk/belt}}$ per time step Δt for each layer can be calculated using the discussed heat phenomena $\dot{Q}_i$, the specific mass $m_{\mathrm{s/bulk/belt}}$ of each layer and the corresponding thermal heat capacities $c_{p,\mathrm{SBR/belt}}$ by

$$\Delta T_{\mathrm{s}} = \frac{\Delta t}{m_{\mathrm{s}}\, c_{p,\mathrm{SBR}}} \left(\dot{Q}_{\text{s-r}} + \dot{Q}_{\text{s-a}} + \dot{Q}_{\mathrm{f},1} + \dot{Q}_{\text{s-b}}\right)\,, \tag{5.24}$$

$$\Delta T_{\mathrm{bulk}} = \frac{\Delta t}{m_{\mathrm{bulk}}\, c_{p,\mathrm{SBR}}} \left(-\dot{Q}_{\text{s-b}} + \dot{Q}_{\mathrm{f},2} + \dot{Q}_{\text{b-b}}\right) \text{ and} \tag{5.25}$$

$$\Delta T_{\mathrm{belt}} = \frac{\Delta t}{m_{\mathrm{belt}}\, c_{p,\mathrm{belt}}} \left(-\dot{Q}_{\text{b-b}} + \dot{Q}_{\mathrm{h}} + \dot{Q}_{\text{b-a}} + \dot{Q}_{\text{b-i}}\right)\,. \tag{5.26}$$

With these equations, the temperature trend from the initial value can be calculated. When the tyre comes to a standstill, the same procedure can also be applied to the evaluation of the mechanisms of heat generation, enabling the model to describe the cooling process.

In summary, this section described the modelling process of a multi-layer lumped mass temperature model. A three-layer approach based on surface, bulk and belt layer was chosen in this work. Based on this approach, a wide set of parameters have to be defined in order to parameterise the presented temperature model to describe the behaviour in an accurate way, depending on a tyre of interest. Therefore, in the next subsection a parameterisation strategy based on parameters found in the literature and defined from measurement data is presented.

5.1.3. Parameterisation strategy and manoeuvre selection based on the temperature model

After defining the structure of the temperature model, the focus is on the parameterisation process in this subsection. However, in order to meet the requirements of semi-physical model approaches using physical parameters and to ensure accuracy between simulation and measurement data, a compromise has also been reached here. Therefore, a subdivision into three different types of parameters was chosen in this thesis:

General parameters are more or less material parameters and independent of the dimensions of tyre

Tyre based parameters are measured or defined for each type of tyre

Optimised parameters are set from measurement data by minimising the *root mean square* (RMS) deviation between measured and simulated data

The presented parameter subdivision has been found as result of a study of the experimental validation with different types of tyres. Hence, a higher number of optimisation parameters provide a higher degree of freedom, but also a more complex parameterisation process. This leads once again to a trade-off for different types of application, and makes space for more detailed investigations. Finally, a subdivision based on the results from the *Pirelli Pzero 245/40 R20 99W* (PP0) tyre is given in detail and values are presented in the next subsections.

General parameters

General parameters are chosen independent of the tyre and more or less material and model design oriented. Because the possibility to measure the inner layer or belt temperature during this project was unavailable, more literature-based general parameters are defined for this layer and the focus is on optimised values around the surface area.

The heat capacity $c_{p,\mathrm{steel}}$ and thermal conductivity λ_{steel} were thus first defined as general parameters from the literature. Because a wide range of values dependent on specific metal alloys are found in the literature, and furthermore detailed information about the carcass steel material is not known, an average of the found parameters is used. In addition, thermal material properties from SBR with $c_{p,\mathrm{SBR}}$ and λ_{SBR} are set, based on information from [Saxena et al., 1999], [Jayasree et al., 2006] and [MakeltFrom, 2018].

Due to the carcass design and the low proportion of SBR, the conductivity of steel is used for the belt with $\lambda_{\mathrm{belt}} = \lambda_{\mathrm{steel}}$. To define the overall specific heat capacity of the lumped belt mass, the average between the specific heat capacity of steal and SBR is used with $c_{p,\mathrm{belt}} = (c_{p,\mathrm{steel}} + c_{p,\mathrm{SBR}})/2$.

By means of the heat transfer coefficient between the belt and filling medium, $h_{\mathrm{b\text{-}i}}$ is the next thermal-based value which is defined as constant. Because of the unknown inner belt temperature as well as properties of the diffusion stopping sealing on the inside of

the tyre, this parameter is situated at the lower end of convection coefficients found in the literature and is considered to be constant.

The second main parameter setup, which was chosen to be constant are the values which define the boundaries of the sliding and non-sliding region of the tyre contact patch. After experimental investigations with different measurement and tyre data, the decision was made that the values, given from [Tremlett & Limebeer, 2016], are suitable and were used for further investigation.

In summary, the decision to keep these values constant was done during various investigations with the background of keeping as many parameters as possible constant. By using a different measurement or test bench setup, this decision may have to be revised. The selected general parameters are summarised in Table 5.1.

Tyre-based parameters

The second group forms the tyre-based parameter depending on type of tyre and layer structure. The type-dependent parameters like tyre circumference s_{circ} and tyre width w_{t}, and therefore the tyre tread area A_{t} with $A_{\mathrm{t}} = s_{\mathrm{circ}}\, w_{\mathrm{t}}$, are given in the tyre's dimension by Pirelli Pzero 245/40 R20 99W.

Furthermore, the already mentioned groove factor g_f, which indicates the ratio between the effective contact area (positive tread design) and the dimension of the contact patch in general (positive + negative tread design), is defined by the tyre tread itself. To get this ratio, a footprint is made and the ratio is calculated with the free and open source image editor GIMP [GIMP, 2019]. By applying this procedure for the PP0 tyre, the dimensionless value is calculated with $g_{f,\mathrm{PP0}} = 0.822$, see Figure 5.4 on the left.

Table 5.1.: General tyre temperature model parameters, based on a literature review and technical assumptions for the Pirelli Pzero 245/40 R20 99W tyre

Parameter	Value	Description
$c_{p,\mathrm{steel}}$	450	Specific heat capacity of steel in J/(kg K)
$c_{p,\mathrm{SBR}}$	1800	Specific heat capacity of SBR in J/(kg K)
$c_{p,\mathrm{belt}}$	1125	Specific heat capacity of belt in J/(kg K)
λ_{steel}	10	Thermal conductivity of steel in W/(m K)
λ_{SBR}	0.275	Thermal conductivity of SBR in W/(m K)
$h_{\mathrm{b\text{-}i}}$	1	Heat transfer coefficient of the filling medium in W/(m^2 K)
$c_{\mathrm{s},1}$	0.3	Scaling value for contact patch, lower boundary in -
$c_{\mathrm{s},2}$	0.8	Scaling value for contact patch, upper boundary in -

Based on tyre wear, the parameter m'_{SBR}, which represents the rubber profile mass in the grooved section of the tyre depth per millimetre, was defined by weighing the tyre and measuring the tread pattern depth before and after usage. Further tyre layer parameters, namely the thickness of the belt δ_{belt} and the SBR part which belongs to the belt δ_{SBR}, are measured by cutting the tyre after use.

The last tyre-based parameter defined is the tread pattern depth δ_{t}, but this is not used as a constant in this thesis. After most of the manoeuvres, the tread depth was measured by hand and documented, see Figure 5.4 on the right. Note that the increased depth after manoeuvre $n = 21$ means a change to a new tyre. Furthermore, the tread depth was measured after every manoeuvre due to the lack of time, e.g. between manoeuvre $n = 33$ to $n = 50$, which explains the constant areas. Nevertheless, this profile thickness can directly be used as input in the temperature model and is directly linked with a tyre wear model.

Because not all manoeuvres are within the defined boundary limits, e.g. camber or different pressure, only defined manoeuvres can be used for the parameterisation process. The solid blue line represents the tread pattern depth relative to on all manoeuvres, whereby the red asterisks define the manoeuvres that are used within the optimisation process in the next step. A summary of the tyre based parameters for the PP0 tyre is given in Table 5.2.

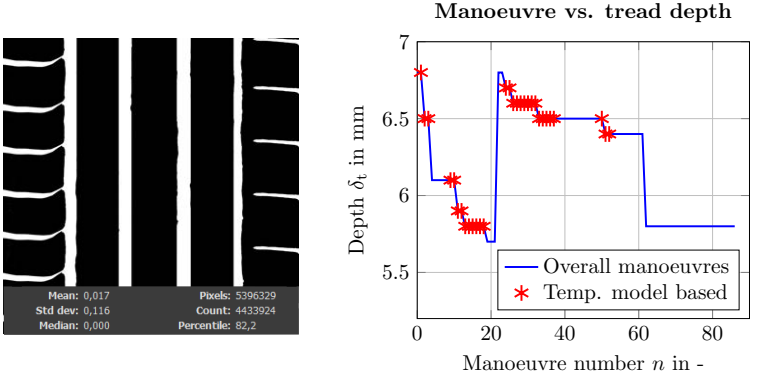

Figure 5.4.: Definition of tyre based parameters for the Pirelli Pzero 245/40 R20 99W tyre; left, a footprint picture to get groove factor g_f, which indicates the ratio between contact and patch area in general; right, measured tread pattern depth depending on the manoeuvre numbers and used as an input for the temperature model

Table 5.2.: Tyre-based temperature model parameters for the Pirelli Pzero 245/40 R20 99W tyre

Parameter	Value	Description
s_{circ}	2.227	Tyre circumference in m
w_{t}	0.245	Tyre width in m
A_{t}	0.5457	Tyre tread area in m^2
g_f	0.822	Groove factor in -
m_{tyre}	7.5	Mass tyre tread (without side walls) in kg
m'_{SBR}	0.33	Rubber SBR mass in kg/mm
d_{belt}	5	Thickness belt (steel/SBR) in mm
d_{SBR}	2	Thickness SBR without profile in mm

Optimised tyre based parameters

The last group of parameters, which are needed for the temperature model, are formed by the optimised tyre based group. To gain experience in using this model and because of the broad range of parameters found in the literature, some parameters are defined by minimising the deviation between measurement and simulation data.

To do so, different measurements carried out on the flat track test bench were used, see Section 4.1.2. The testing procedure includes steady-state as well as transient manoeuvres with changes in slip angle, slip ratio, vertical load and combinations of these. Because not all manoeuvres are within the boundary condition of this thesis, only specific ones are used for the parameterisation process, see Figure 5.4 on the right. Besides measuring the temperature along the tyre's width, one sensor was used to scan the temperature inside of one of the tyre's grooves.

When working with *infrared* (IR) sensors, they only scan the outermost elements of the measured surface. Therefore, observed temperature changes are very high and occur over short periods of time. For this reason, it is necessary to model the surface temperature in a responsive way that can cope with these trends. To do so, the thickness of the surface layer δ_{s} is optimised within the fitting process, and as a result the internal heat flows as well as the mass distribution between the layers are adapted.

Based on a literature review, a linear speed-dependent convective heat exchange modelling approach was chosen to adequately describe the needs for this kind of application, as can be seen in Equation (5.12). In reality, this mechanism of heat transfer is influenced by various factors like profile design and the nature of incidental airflow , which in turn is affected by the design of the car itself. Therefore, no explicit approach can be found for describing this parameter; possibilities range from linear functions to full physical approaches found in fluid dynamics with an immense effort in terms of parameterisation. Because the measurements used were carried out on a test bench with constant airflow from a demister, an approach solely based on the travelling velocity of the tyre is rea-

sonable. Therefore, a parameter h_0 concerning the transferable energy when the tyre is at a standstill and a velocity dependent parameter h_v are optimised within a physically justifiable range. This yields the advantage of modelling this heat exchange in an easy manner for different tyre designs.

Because of the wide range of values from various authors regarding the conductive heat exchange between rubber and roadway as well as the lack of investigations on the effects influencing this parameter, coefficient $h_\mathrm{s\text{-}r}$, is considered constant in the course of this thesis. Optimising this value enables a fast parameterisation for different tyre/roadway pairings.

For similar reasons, a reference temperature T^N is optimised as well, as seen in Equation (5.3). At this temperature, the distribution of heat generated by friction is in a thermal state of equilibrium between the tyre and the road. This means that half of the energy generated is entering the tyre and the other half is being absorbed by the road. This brings the advantage of not knowing specific material-related properties regarding the road, which are vague or non-existent in most cases, while being able to distribute the generated heat depending on the current surface temperature.

The last parameter approved for the fitting process p_z is used to scale the heat generation from hysteresis due to the constant deformations when the tyre is rolling, as can be seen in Equation (5.4). Modelling this heat phenomenon with a full physical approach would require specific information about the tyre's supporting structure, the materials used as well as the chemical composition. Such data are mostly not available or not attainable without explicit material measurements. Therefore, using a constant coefficient, by combining all mentioned uncertainties, enables an easy parameterisation for different tyre designs.

Finally, the results of the parameterisation process, based on various different manoeuvres for the PP0 tyre, is given in Table 5.3. In summary, the initial values for the optimisation process as well as their final values are validated by a comparison with the literature. A detailed discussion of the comparison between simulated and measured data for various manoeuvres is given in the next subsection. Furthermore, a summary of all parameters, including validation plots for the tyres used is presented in Appendix D. All additional information, like temperatures, forces and so on, are measured and directly used as an input for the temperature model.

5.1.4. Temperature model validation

By defining, measuring and optimising all needed parameters, a validation of the parameterised temperature model is presented in this subsection. Within the acquired dataset, all manoeuvres done during testing can be simulated and validated. In addition to the measurement data from the infrared sensors, scanning the tyre's surface, measurements from the additional sensor, and observing the groove temperature $T_\mathrm{belt,meas}$ were used to validate the simulated internal temperatures for different types of manoeuvres.

Table 5.3.: Optimised temperature model parameters for the Pirelli Pzero 245/40 R20 99W tyre

Parameter	Value	Description
$h'_{\text{s-r}}$	492.8	Heat transfer coefficient of surface-road in $\text{W}/(\text{m}^2\,\text{K})$
h_0	3.63	Speed independent value of $h_{\text{t-a}}$ in $\text{W}/(\text{m}^2\,\text{K})$
h_{v}	2.98	Speed dependent value of $h_{\text{t-a}}$ in $(\text{W}/(\text{m}^2\,\text{K}))$ / (m/s)
p_z	0.0024	Dimensionless scaling value due to hysteresis in -
T^{N}	90.17	Power distributed nominal temperature in degC
δ_{s}	0.26	Thickness of tyre surface layer in mm

The first manoeuvre used is a warm-up procedure with moderate lateral slip sweeps at different vertical loads while no activities in longitudinal direction are given, see Figure 5.5. The slip targets as well as the measured forces are presented in the two plots on the left side of the figure. By starting from the initial temperature, the surface layer is able to model the measured temperatures satisfactorily, as shown in the upper right plot. It can be seen that vertical loads influence the accuracy of the thermal model, whereby the lowest temperature deviation is given at the nominal load F_z^{N}. This can be attributed to the fact that most measurements used for parameterisation were carried out at this load, therefore the constant parameter p_z is mainly optimised for this state. When comparing the measured groove temperature of the belt layer with the two simulated temperatures from bulk and belt, a correlation can be observed, see bottom right. This indicates the accuracy of the modelled internal temperatures and validates the subdivision of the tyre into different layers.

The second manoeuvre is used to validate the cooling effect of the temperature model. In a first step, the tyre is heated by using a lateral sine warm-up manoeuvre within a constant normal force and tyre velocity, see Figure 5.6. After finishing the heating procedure at around $t = 150$ sec, the tyre velocity is set to zero and additionally the tyre is lifted up. When the tyre comes to a standstill, the surface and the bulk layer start cooling down in a coupled manner while the belt region is still heated from the stored energy in the outer layers. After the rubber falls below the belt temperature, all layers are cooling down with a decreasing slope towards lower temperatures. These effects can be observed on the measured as well as on the simulated temperature.

In summary, the coupled behaviour of the surface and bulk layer is able to achieve accurate temperature trends for both heating and cooling operation points. Additionally, the high mass of the belt layer and therefore its inert behaviour ensures a stable temperature estimation for all input variations carried out on the flat track test bench. In general, the implemented approach delivers good results for all investigated manoeuvres, is quite easy to use in terms of parameterisation and comes with a low computational load. The summarised values as well as the further validation figures are given for both tyres in Appendix D.

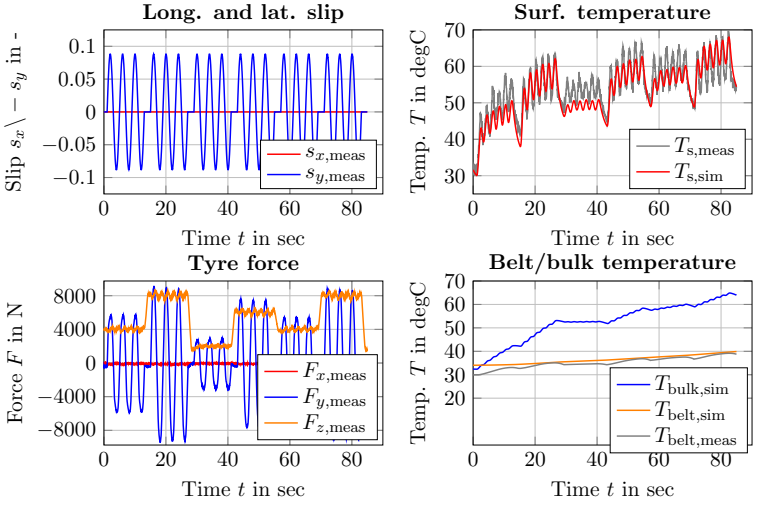

Figure 5.5.: Temperature model validation for the Pirelli Pzero 245/40 R20 99W tyre for a warm-up procedure in lateral direction

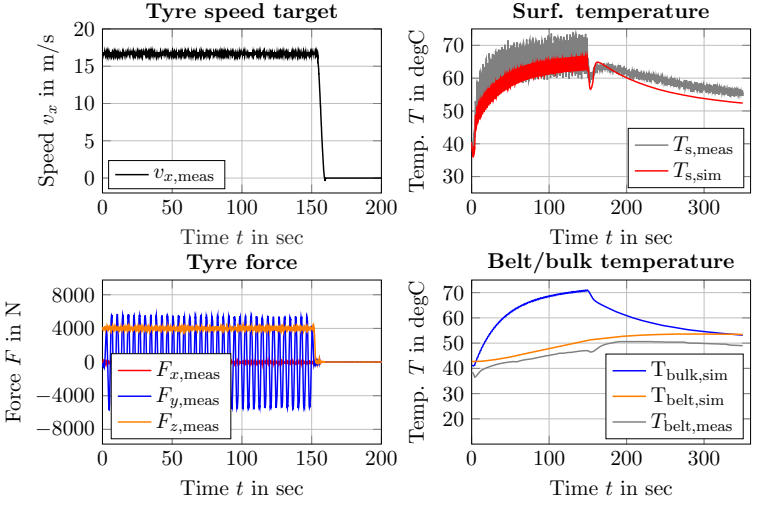

Figure 5.6.: Temperature model validation for the Pirelli Pzero 245/40 R20 99W tyre with special focus on cooling behaviour

5.1.5. Comparative analysis of the tyre temperature model

In this section, a temperature model approach based on the first law of thermodynamics was presented, discussed and evaluated for different types of tyres. Moreover, model properties and simplifications were presented to model the temperature behaviour in the sense of a semi-physical approach.

In a next step, the modelling concept based on various heat phenomena was given and followed by the parameterisation strategy. Within this process, different parameter subdivisions were used to identify the temperature model values. Thereby, the general parameters are more or less defined as material values, the tyre-based parameters have been obtained from the tyre dimensions and furthermore some parameters were optimised dependent on the manoeuvres performed.

Finally, a model validation for the Pirelli Pzero 245/40 R20 99W tyre was presented and discussed in which the summarised parameter table as well as further validation figures for all tyres are given in Appendix D. It was shown that the chosen multi-layer model represents a satisfactory simulation regarding all three temperature layers.

In order to reduce the number of optimisation parameters, two ideas are mentioned at this point. First, by defining the layer thickness as a constant of $\delta_s \approx 0.25\,\text{mm}$ seems to be a good choice for reducing optimisation parameters. Second, using a speed ramp manoeuvre, the speed dependent convection coefficient can be defined separately. This would result in saving two further parameters.

In summary, the implemented approach delivers good results for all investigated manoeuvres, is quite easy to use in terms of parameterisation and requires low computational effort. In the next step, the generated temperature characteristics are used to investigate the impact on the tyre forces, which is the goal of Section 5.2.

5.2. Temperature impact on tyre force behaviour

After definition and validation of the temperature model application, the influence on tyre force characteristics is the focus of this section. Depending on different tyre layer temperatures, the effects on the steady-state force behaviour are investigated in detail. Thereafter, the measured and simulated tyre temperatures are used to adapt the steady-state behaviour.

Here a general parameter dependency on tyre temperature is calculated first. Afterwards, a semi-physical model approach is presented which is able to model the temperature-based steady-state tyre characteristics. The main modelling focus is on one normal force, but extensions can be calculated with standard TMeasy functionality.

Finally, the implemented model is validated with different manoeuvres longitudinally and laterally for the PP0 tyre. Moreover, model values as well as evaluation plots for the types of tyres used are summarised and presented in Appendix D.

5.2.1. Temperature influence on steady-state tyre characteristics

The effect of tyre temperature on lateral and longitudinal force characteristics seems to be an influence that is not to be neglectable. As already presented during the literature review in Chapter 2, most implementations focus on influences on cornering stiffness and maximum road friction. Nevertheless, changing the value of $\mu_{\max}$ also influences the longitudinal and lateral sliding velocity, especially at the peak point of the road friction.

Information about the cornering stiffness and maximum road friction are merged into the steady-state model. The evaluation of the influence of temperature on the tyre force behaviour leads to an investigation of the steady-state characteristics, including its parameters. To do so, manoeuvres done on the test bench are chosen and subdivided into temperature-related areas, and then the steady-state behaviour is recalculated. Based on these results, a model description that includes temperature effects can be defined.

The stepwise procedure for recalculating the temperature-dependent steady-state characteristics based on a lateral manoeuvre is presented in Figure 5.7. Here, in the upper left plot, the slip target section with constant normal force conditions can be seen, and in the lower left plot, measured and simulated temperatures are presented. As a first step, for each zero crossing within the *Hirschberg* and triangle sequences, slip targets are defined and so each manoeuvre period is given.

In the next step, temperature information for each manoeuvre period can be calculated. To do so, the mean values of the simulated bulk temperature $T_{\mathrm{bulk,sim,m}}$, belt temperature $T_{\mathrm{belt,sim,m}}$ and peak values of the measured surface layer temperature per period are defined. The peak values of the measured surface layer temperatures are used, because they are established when reaching the peak of the force characteristics. Furthermore, the decision not to use the simulated surface temperatures was made in order to present results based on measured information. To use the simulated data is still possible, but it's not that accurate.

In the following step, the recalculation process can be carried out for each period. Representatively, only the fifth period is used for the detailed description and presented in the upper right figure. Based on this measured lateral force period $F_{y,\mathrm{meas}}$, the modelled TMeasy steady-state characteristics $F_{y,\mathrm{init}}$ can be calculated and compared with the measurement data. A correlation can be seen at small slip values, but around the peak force area the simulated behaviour seems too high, which can be due to a higher surface temperature in this period. Based on the initially modelled force parameterisations, the characteristics can be recalculated based on this temperature point. Because no manoeuvres with pure sliding areas were carried out, the ratio of the initial model behaviour with $F^{\mathrm{s}}_{\mathrm{init}}/F^{\mathrm{max}}_{\mathrm{init}}$ and $s^{\mathrm{s}}_{\mathrm{init}}/s^{\mathrm{max}}_{\mathrm{init}}$ are used to recalculate the temperature-dependent sliding $F^{\mathrm{s}}_{\mathrm{opt}}$ and $s^{\mathrm{s}}_{\mathrm{opt}}$ values based on the optimised ones. A representative parameter example from period number five is given in Table 5.4.

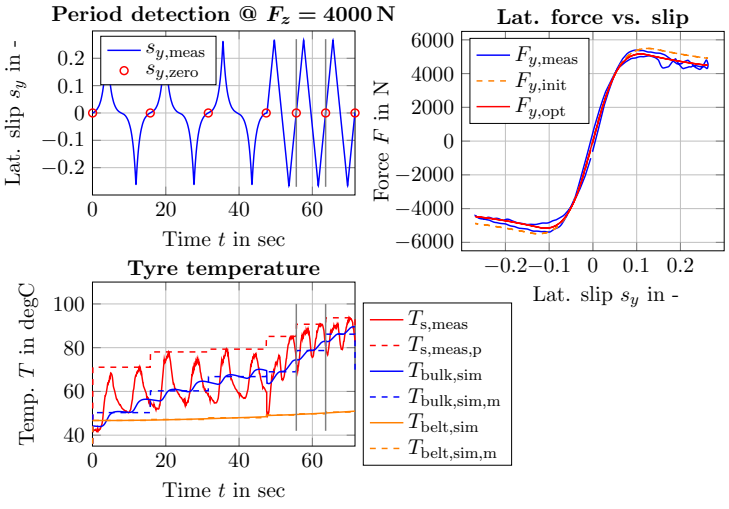

Figure 5.7.: Steady-state model parameter adjustment procedure based on measured and simulated tyre layer temperatures, applied for a manoeuvre by using the Pirelli Pzero 245/40 R20 99W tyre; left, period and temperature detection based on one period and within constant normal force; right, recalculation of the steady-state values based on the defined operating point

From the results in Table 5.4, it can be seen that the differences from the initial state and optimised initial slope dF_y^0 are small. This means that the inner (bulk/belt) temperature conditions during the standard parameterisation process and the time when this manoeuvre was carried out were similar. Regarding the peak force $F_y^{\max}$, it seems that especially after repeating this manoeuvre several times, the surface temperature is higher than the average temperature during parameterisation, see Figure 5.7. This leads to a lower absolute value, which automatically tends toward a smaller maximum position value $s_y^{\max}$ when using constant initial slope. Because no measurements were done in very high slip areas, sliding behaviour is recalculated from the temperature-optimised peak values. In the end, this procedure seems to be useful and can be done with all periodic manoeuvres carried out on the test bench with the same type of tyre. In addition, to investigate the influence of the normal force as well, a subdivision based on wheel load is recommended.

The results of applying this procedure to a wide manoeuvre spectrum is given in Figure 5.8. Based on literature studies, experience with the sections test bench and investigations during this project, the bulk temperature is useful as an influencing factor for the

Table 5.4.: Steady-state model parameter adjustment influenced by measured and simulated tyre layer temperature, shown for a manoeuvre applied to the Pirelli Pzero 245/40 R20 99W tyre; operating point conditions used are given with normal force $F_z = 4000\,\mathrm{N}$, measured peak surface temperature $T_{\mathrm{s,peak}} = 90.72\,\mathrm{degC}$, simulated mean bulk temperature $T_{\mathrm{bulk,mean}} = 78.69\,\mathrm{degC}$ and belt temperature $T_{\mathrm{belt,mean}} = 49.77\,\mathrm{degC}$

Parameter	**Initialised**	**Optimised**
dF_y^0 in N	102159	97552
$F_y^{\max}$ in N	5490	5160
$s_y^{\max}$ in -	0.125	0.109
F_y^{s} in N	4521	4250
s_y^{s} in -	0.479	0.416

initial slope. Thereby, the initial and optimised values of the initial slope dF_y^0, depending on three different wheel loads $F_{z,i} = \{2000, 4000, 6000\}\,\mathrm{N}$, are given and contrasted with the simulated bulk temperature $T_{\mathrm{bulk,sim}}$ in the upper plot. Hence, the belt temperature or a combination between the bulk and the belt temperature may also be possible.

Furthermore, the maximum force value $F_y^{\max}$ and its position $s_y^{\max}$ is given as an initial and an optimised value, depending on the normal force versus the measured surface temperature $T_{\mathrm{s,meas}}$ in the middle and lower plot in Figure 5.8. Based on the results from the section test bench, it was shown that only the tyre temperature and not the surface temperature influences the marked dependency of the maximum tyre force. Therefore, temperature information from the tyre has to be taken into account. Using the bulk temperature or a combination of both is a possibility because they are constantly interacting. Nonetheless, experimental investigations have shown that, especially on high slip manoeuvres, dynamic force effects occur; see the hysteresis effect, e.g. in Figure 4.9 or Figure 4.10 or in Appendix B. To simulate these effects a dynamic variation of the temperature is also needed. For this reason, the surface temperature seems to be the more practical choice.

In a next step, the results in Figure 5.8 are discussed in detail as a foundation for the modelling process.

Initial slope dF_y^0 At the first glance, the evaluation of the initial slope shows consistent behaviour that is dependent on the bulk temperatures, especially in areas higher than $T_{\mathrm{bulk}} > 65\,\mathrm{degC}$. On closer inspection, increasing initial slope behaviour in terms of lower bulk temperature is given by a non-linear characteristic. It seems at colder bulk layer temperatures, the carcass and bulk show stiffer behaviour which

leads to higher values around this area and also corresponds with results from the literature, see Section 3.4. By comparing this behaviour with respect to the lowest normal force $F_{z,1}$, a similar characteristic is given. Therefore, independent wheel load influence is assumed for this behaviour. Due to the fact that the tyre was already warm during measurements with high wheel loads $F_{z,3}$, no operating points could be generated at low bulk temperatures. In summary, a steep descent at the beginning which leads to a saturation behaviour around $T_\mathrm{b} \approx 65\,\mathrm{degC}$ influences the initial slop in a way that is dependent on the bulk temperature. Furthermore, it seems that there is no direct influence from normal force, which means that this effect can be parameterised by the basic TMeasy implementation.

Maximal force $F_y^{\max}$ The characteristic of the maximum force value shows an increase up to a peak value, followed by a decreasing behaviour that is dependent on the measured surface temperature, which correspondents with the literature, see Section 3.4. Especially for the second normal force $F_{z,2}$, where a few more operating points are given, a significant peak formation around $T_\mathrm{s} \approx 75\,\mathrm{degC}$ is presented. Additionally, the temperature-based peak position of the maximum force values increases with greater normal force. During investigations, it was shown that a linear position dependency based on the normal force seems to be an accurate and furthermore easy to implement model approach. This proves the fact that a peak force dependency is given by the surface temperature. Furthermore, the linear dependency on peak position is assumed to be dependent on the normal force. The influence of the normal force itself can be modelled in a way that is based on the basic TMeasy application.

Position of maximum force $s_y^{\max}$ Depending on the surface temperature, the position of the maximum force also shows a similar behaviour to the maximal force. The peak value of the position is likewise given around the peak value from the force and followed by a saturation effect. In addition, the high dispersion of the optimised values at low normal forces shows that at smaller wheel loads, the temperature effects have less influence. Furthermore, at high normal forces and high surface temperature areas, the TMeasy model runs into a boundary condition with $dF_y^0 \geq 2\,F_y^{\max}/s_y^{\max}$, which is the reason why the optimisation points are not on a lower position level. Therefore, more focus should go to wheel loads $F_{z,1}$ and $F_{z,2}$ during modelling. Nevertheless, the similar behaviour of the maximum force and the maximum force position leads to the idea to use the same semi-physical model approach for both.

In summary, a significant influence on tyre temperature on steady-state characteristics was shown within these investigations. Influences from bulk temperature on initial slope as well as surface temperature on maximum force were presented, and there is consistency with the literature investigationed. As a next step, these temperature-based parameter dependencies are modelled by means of a semi-physical model approach. This process, together with the implementation of the TMeasy tyre model, is presented in the following section.

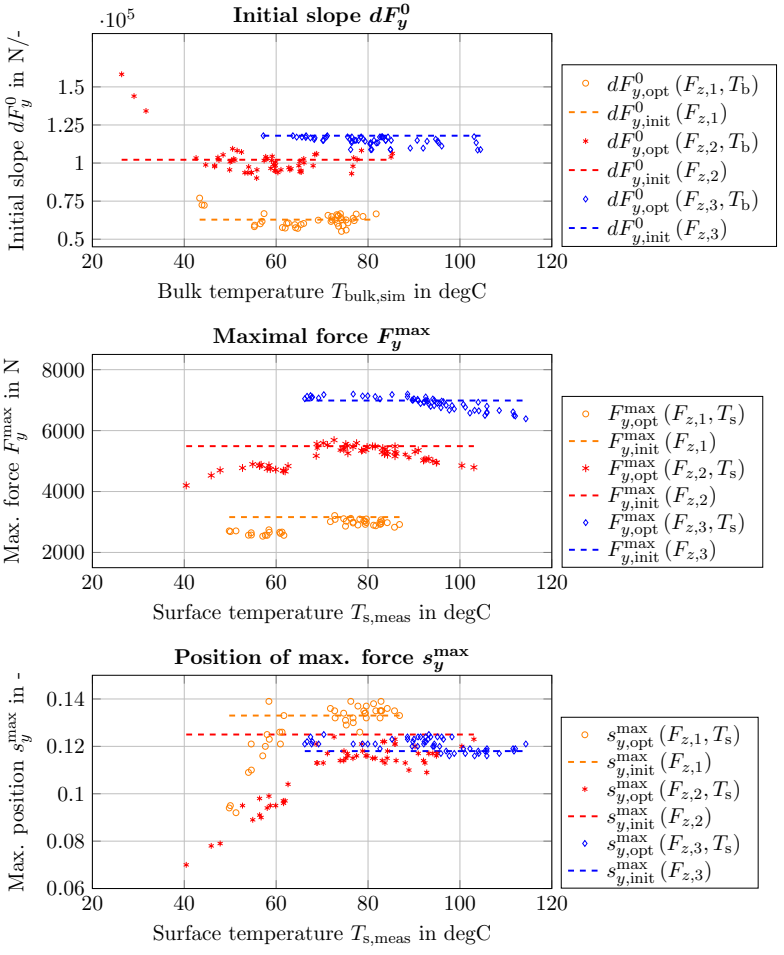

Figure 5.8.: Steady-state model parameter adjustment results based on measured and simulated tyre layer temperatures applied to the Pirelli Pzero 245/40 R20 99W tyre with $F_{z,i} = \{2000, 4000, 6000\}$ N; above, the initial slope versus the bulk temperature is given, whereby in the middle and bottom plot the maximum force value including its position are presented

5.2.2. Modelling and parameterisation process of the temperature-influenced steady-state tyre characteristics

To generate an approach based on the results presented in the previous subsection, the TMeasy tyre model has to be enhanced in order to be able to model temperature dependency. To do this, a semi-physical application that interacts well with the standard tyre model is preferred and defined as a goal for this approach. Furthermore, functionality and fundamentals from TMeasy should be used and implemented, and parameters with physical significance should be preferred for the parameterisation process.

Therefore, the temperature dependency of the initial slope dF_y^0 is modelled and the implementation presented in a first step. The maximum force value $F_y^{\max}$ and its position $s_y^{\max}$ follow from this.

Model approach for the initial slope

Based on the result from Figure 5.8, some form of exponential function seems to be suitable for the modelling process. Furthermore, parameterisation of the bulk temperature behaviour is based on results from one constant normal force. Hence, for the PP0 tyre, the second normal force with $F_z^{\mathrm{T}} = F_{z,2} = 4000\,\mathrm{N}$ is chosen because most manoeuvres were done at this normal force. The normal force-related change is calculated directly by using the application implemented within the standard TMeasy tyre model. This brings the main advantage that only one characteristic has to be parameterised, which leads to a small number of parameters, and furthermore to the usage of an already implemented normal force-dependent function.

The main equation that describes the bulk-dependent initial slope condition dF_y^{T} is proposed by

$$dF_y^{\mathrm{T}} = dF_{y,F_z}^{\mathrm{T}} + B\ \mathrm{e}^{-C\,T_{\mathrm{b}}}\,, \tag{5.27}$$

where $dF_{y,F_z}^{\mathrm{T}} = f(F_z)$ describes the normal force dependent value and B and C are function parameters which have to be defined.

By using the boundary conditions with

$$dF_{y,0}^{\mathrm{T}} = dF_y^{\mathrm{T}}\left(T_y^0\right)\,, \tag{5.28}$$

$$dF_{y,\mathrm{N}}^{\mathrm{T}} = dF_y^{\mathrm{T}}\left(T_y^{\mathrm{N}}\right) \text{ and} \tag{5.29}$$

$$dF_{y,\infty}^{\mathrm{T}} = dF_y^{\mathrm{T}}\left(T_y^{\infty} = \infty\right)\,, \tag{5.30}$$

where T_y^0 is defined as the minimum, T_y^{N} as the nominal temperature where $F_y^{\max}(F_z^{\mathrm{T}})$ achieves its peak value and T_y^{∞} as the infinite temperature. Thus, Equation (5.27) can

be fully defined with physical parameters by

$$B = \frac{dF_{y,\mathrm{N}}^{\mathrm{T}} - dF_{y,\infty}^{\mathrm{T}}}{\mathrm{e}^{-C\,T_y^{\mathrm{N}}}} \quad \text{and} \tag{5.31}$$

$$C = \ln\left(\frac{dF_{y,\mathrm{N}}^{\mathrm{T}} - dF_{y,\infty}^{\mathrm{T}}}{dF_{y,0}^{\mathrm{T}} - dF_{y,\infty}^{\mathrm{T}}}\right) \frac{1}{dF_{y,\mathrm{N}}^{\mathrm{T}} - dF_{y,0}^{\mathrm{T}}}\,. \tag{5.32}$$

Finally, by calculating the normal force dependency dF_{y,F_z}^{T} with

$$dF_{y,F_z}^{\mathrm{T}}\left(F_z\right) = dF_{y,\infty}^{\mathrm{T}} + dF_y^0\left(F_z\right) - dF_y^0\left(F_z^{\mathrm{T}}\right)\,, \tag{5.33}$$

where $dF_y^0 = f(F_z)$ is directly used as the standard normal force TMeasy function, the bulk temperature and force dependent initial slope $dF_y^{\mathrm{T}} = f(F_z, T_{\mathrm{b}})$ is fully defined. By using the same nominal temperature values for the bulk and surface with $T_y^{\mathrm{N}} = T_{y,\mathrm{b}}^{\mathrm{N}} = T_{y,\mathrm{s}}^{\mathrm{N}}$, the defined values for parameterising the temperature-based initial slope are given in Table 5.5. By incorporating these values into Equations (5.27) to (5.33), the model approach can be defined and compared with the value points, see Figure 5.9.

As was already mentioned, the main focus was on the two lower normal forces because the highest one is already close to the implemented boundary condition with $dF_y^0 \geq 2\,F_y^{\max}/s_y^{\max}$. Furthermore, a more conservative increase in behaviour at the low bulk temperature area was chosen because only a few points were available. Nevertheless, a model approach with only five physically meaningful parameters is given, which fits the optimised values in a satisfactory manner.

Table 5.5.: Simulated bulk temperature based lateral initial slope model parameters for the tyre Pirelli Pzero 245/40 R20 99W

Parameter	**Value**	**Description**
F_z^{T}	4000	Temperature based nominal tyre load in N
T_y^0	46	Minimal temperature in degC
T_y^{N}	76	Nominal temperature in degC
$dF_{y,0}^{\mathrm{T}}$	107500	Initial slope at T_y^0 in N
$dF_{y,\mathrm{N}}^{\mathrm{T}}$	97500	Initial slope at T_y^{N} in N
$dF_{y,\infty}^{\mathrm{T}}$	95000	Initial slope at T_y^{∞} in N

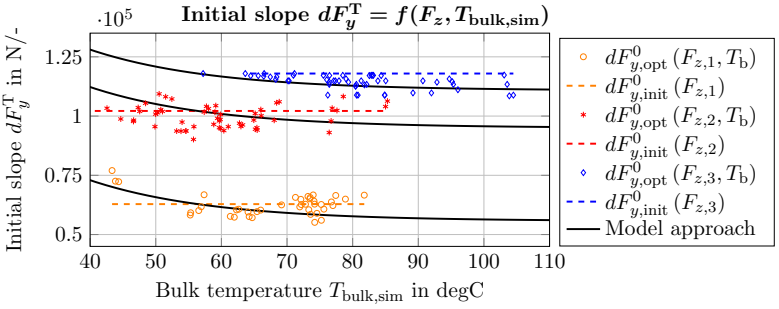

Figure 5.9.: Model validation of the lateral initial slope characteristics dF_y^{T} depending on the normal force F_z and the simulated bulk temperature, $T_{\mathrm{bulk,sim}}$ based on the PP0 tyre

Model approach of maximum force and peak position

In a next step, the model approach for the maximum force has to be defined, which is dependent on normal force and surface temperature. Because the same model application is used for both maximum force F_y^{T} and its position s_y^{T}, the approaches are presented together. As for the initial slope, the main parameterisations are given for the normal force $F_{z,2}$. Wheel load dependency is also implemented based on the standard TMeasy implementation as well. Furthermore, one additional property is defined with the linear normal force dependent temperature based peak of the maximum force value. As the main implementation, a cosine function approach with two different areas ($T_{\mathrm{s}} < T^{\mathrm{N}}$ and $T_{\mathrm{s}} > T^{\mathrm{N}}$) is used for both applications. The focus of the model description is on the maximum force value, but the same approach can directly be used for the position.

The main equation which describes the maximum force characteristics F_y^{T}, which is dependent on the surface temperature T_{s}, is proposed with

$$F_y^{\mathrm{T}} = \frac{F_{y,\mathrm{N}}^{\mathrm{T}} - F_{y,0/\infty}^{\mathrm{T}}}{2} \left[\cos\left(\pi \frac{|T_y^{\mathrm{N}} - T_{\mathrm{s}}|}{|T_y^{\mathrm{N}} - T_y^{0/\infty}|} \right) - 1 \right] + F_{y,F_z}^{\mathrm{T}}\,, \tag{5.34}$$

where $F_{y,\mathrm{N}}^{\mathrm{T}}$ defines the maximum force value at T_y^{N}, $F_{y,0}^{\mathrm{T}}$ at T_y^0 and $F_{y,\infty}^{\mathrm{T}}$ at $T_{\mathrm{s},\infty}$, whereby the two areas are defined with

$$T_{\mathrm{s}} \leq T_y^{\mathrm{N}} \quad \text{with} \quad F_{y,0/\infty}^{\mathrm{T}} = F_{y,0}^{\mathrm{T}} \quad \text{and} \quad T_y^{0/\infty} = T_y^0 \text{ or} \tag{5.35}$$

$$T_{\mathrm{s}} > T_y^{\mathrm{N}} \quad \text{with} \quad F_{y,0/\infty}^{\mathrm{T}} = F_{y,\infty}^{\mathrm{T}} \quad \text{and} \quad T_y^{0/\infty} = T_y^{\infty}\,. \tag{5.36}$$

Furthermore, $T_y^{\mathrm{N}} = f(T_1^{\mathrm{N}}, T_2^{\mathrm{N}}, F_z)$ defines the linear dependency of the normal force-

dependent position of the maximum force value, which is calculated via the TMeasy basic function presented in Equation (4.12), whereby T_1^{N} and T_2^{N} are constant values and is F_z the normal force, e.g. $T_y^{\mathrm{N}} = f(T_1^{\mathrm{N}}, T_2^{\mathrm{N}}, F_{z,2}) = 76\,\mathrm{degC}$.

Finally, by calculating the normal force dependency within the parameter $F_{y,F_z}^{\mathrm{T}} = f(F_z)$ with

$$F_{y,F_z}^{\mathrm{T}} = \frac{F_y^{\max}(F_z)}{F_y^{\max}(F_z^{\mathrm{N}})}\, F_{y,\mathrm{N}}^{\mathrm{T}}\,, \tag{5.37}$$

where $F_y^{\max} = f(F_z)$ is defined as normal force dependency and is directly used from the standard TMeasy application, the surface temperature and normal force-dependent maximum force application $F_y^{\mathrm{T}} = f(F_z, T_{\mathrm{s}})$ are fully defined.

In summary, note that just force and temperature values at three different points, namely lower and upper boundary as well as at the nominal temperature, are required to parameterise the temperature-based maximum force as well as its position. In addition, the normal force dependency is calculated directly with information from the standard TMeasy application. Finally, the defined values for the two applications are given in Table 5.6.

By implementing the defined parameter setup from Table 5.6, the model characteristics presented in Figure 5.10 is generated. In the upper figure, the model characteristic of the maximum force is shown, and in the lower figure the maximum force position is shown. Especially for the maximum force characteristics, the correlation between

Table 5.6.: Extended maximum force and position model parameter based on the surface temperature influence in lateral direction for the tyre Pirelli Pzero 245/40 R20 99W

Parameter	**Value**	**Description**
F_z^{T}	4000	Temperature based nominal tyre load in N
$T_{y,1}^{\mathrm{N}}$	76	Nominal temp. at F_z^{T} in degC
$T_{y,2}^{\mathrm{N}}$	78	Nominal temp. at $2\,F_z^{\mathrm{T}}$ in degC
T_y^0	46	Lower temp. boundary at F_z^{T} in degC
T_y^∞	106	Upper temp. boundary at F_z^{T} in degC
$F_{y,\mathrm{N}}^{\mathrm{T}}$	5490	Maximum force at $T_{y,1}^{\mathrm{N}}$ and F_z^{T} in N
$F_{y,0}^{\mathrm{T}}$	4690	Force boundary at T_y^0 and F_z^{T} in N
$F_{y,\infty}^{\mathrm{T}}$	4690	Force boundary at T_y^∞ and F_z^{T} in N
$s_{y,\mathrm{N}}^{\mathrm{T}}$	0.125	Maximum position at $T_{y,1}^{\mathrm{N}}$ and F_z^{T} in -
$s_{y,0}^{\mathrm{T}}$	0.090	Position boundary at T_y^0 and F_z^{T} in -
$s_{y,\infty}^{\mathrm{T}}$	0.120	Position boundary at T_y^∞ and F_z^{T} in -

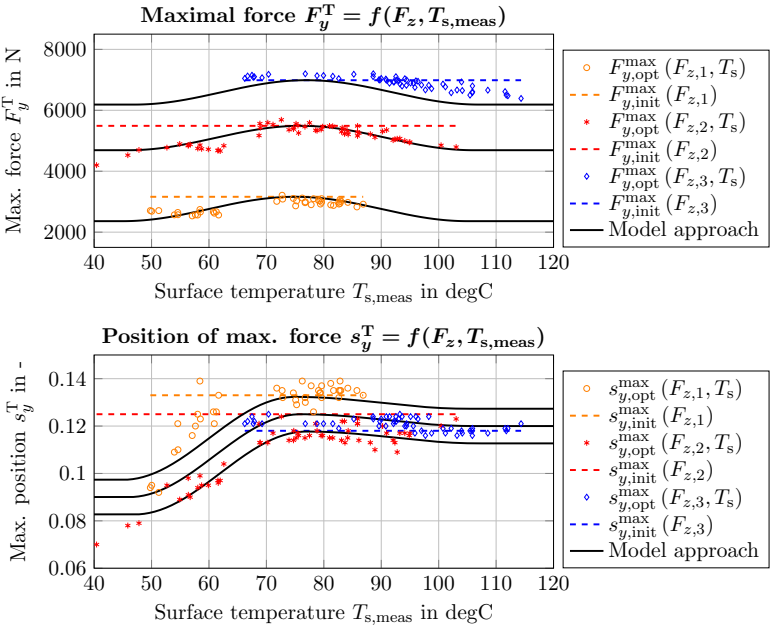

Figure 5.10.: Model validation of the maximum force F_y^{T} (upper plot) including their position s_y^{T} (bottom plot) characteristics in lateral direction, dependent on the normal force F_z and the surface temperature $T_{\mathrm{s,meas}}$ presented for investigations of the tyre PP0

simulated behaviour and optimised value is not that bad. At the highest normal force some inaccuracies can be seen, but around this area the already mentioned boundary condition from the standard TMeasy tyre model is also influencing the optimisation results in some way.

Hence, for the position of the maximum force, a less sensitive behaviour is given because of the higher dispersion of the optimisation points. Nevertheless, a quite good modelling behaviour with only three more model parameters is presented. For parameterising the initial slope, a conservative decreasing behaviour around small surface temperature values was chosen because there are then fewer operating points.

In conclusion, a semi-physical model approach for all three main TMeasy parameters, which represent the steady-state behaviour of the tyre, was presented and implemented. The focus was on a small number of parameters and also on the physical meaning of those parameters. A satisfactory consistency between the model approach and the de-

fined temperature-based operating points was shown. In the next step, the focus is on manoeuvre validation of the overall model with temperature modelling and related effect. Because the model process was presented in lateral direction, the focus is on manoeuvre validation in the same manner. The summarised parameter overview as well as result validation in lateral and longitudinal direction is given in Appendix D.

5.3. Validation of the enhanced temperature-based TMeasy tyre model

After modelling the temperature and its influences on the steady-state characteristics separately, the two parts are implemented into the standard TMeasy tyre model to enhance it with the influence of temperature, see Figure 5.11. Additionally, as a constant parameter setup is being defined for the temperature model as well as for the tyre model itself, the interaction of information is given contentiously. The final output is defined by the temperature-influenced force characteristics. To validate this implementation, two different lateral manoeuvres are chosen and evaluated in detail.

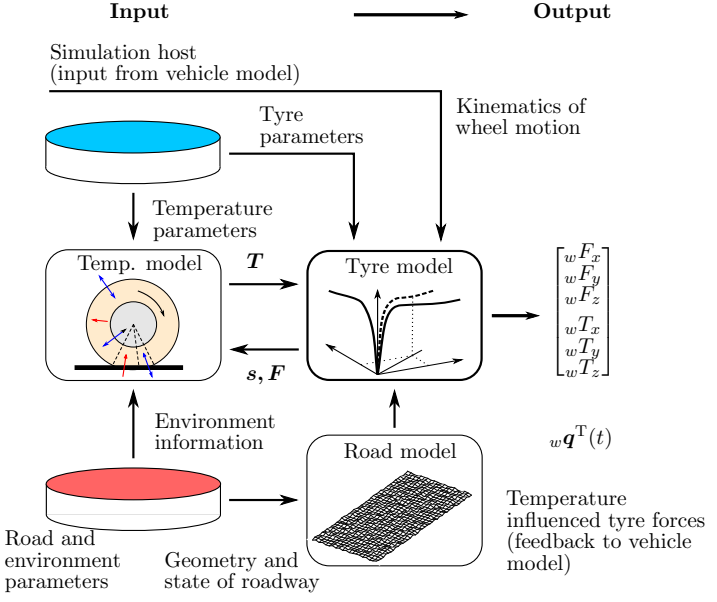

Figure 5.11.: Schematic representation of the temperature enhanced TMeasy tyre model, based on the standard tyre interface (STI)

The first one represents a section of a warm-up manoeuvre which was done at the beginning of the overall test series and presented in Figure 5.12. Slip angle targets as well as measured tyre forces are presented in the two upper left plots. It can be seen that a sinusoidal manoeuvre with moderate amplitude and frequency values was chosen by using a series of different normal forces. Furthermore, measured and simulated tyre layer temperatures are given in the two upper right plots. Regarding the evaluation of the temperature model, it can be seen that the modelled surface layer temperature fits satisfactorily, but improvements can be made, in particular for small normal forces. Furthermore, modelled bulk and belt temperatures show good correlation with the measured groove temperature.

Additionally, detailed views are presented within the remaining four images. A comparison of the lateral force versus time of the measured standard TMeasy model and the enhanced implementations are given in the two bottom left plots with two different wheel load sections. Because the warm-up procedure starts at low temperatures, the basic TMeasy implementation simulates excessive lateral force characteristics, whereby the enhanced one performs in a way that is closer to the measured characteristics for both normal force applications.

Furthermore, a different view of the lateral forces versus slip behaviour is shown in the two bottom right plots. Here as well, the same conclusion is given by comparing the standard versus the enhanced TMeasy model. In summary, a significant improvement in warm-up behaviour is given with the enhanced temperature model.

In the second manoeuvre, a section for parameterising the steady-state characteristics is presented in Figure 5.13. As in the first figure, the two upper left plots present the slip target and the measured forces, and furthermore the two upper right plots show the measured and simulated tyre layer temperatures. It is clearly visible that, during this manoeuvre, high surface temperatures are generated, especially at high normal forces. Furthermore, a good fit for the surface temperatures is given for all normal force conditions.

The four lower plots represent the validation of the lateral force versus time in regard to force versus slip characteristics. A clear improvement is also seen for both sections. Especially at higher normal forces, a temperature-based hysteresis effect similar to the measured behaviour is generated by the enhanced model, while with the standard version the forces that arise are too high.

In summary, the temperature model forms the foundation for a well-implemented model extension. The tyre layer temperatures are used as input to adjust the three main parameters, which characterise the steady-state tyre behaviour. Surface and bulk temperatures are used to model the temperature-based behaviour changes. By implementing an exponential-dependent initial slope characteristic based on the bulk, and a surface temperature-based force and position characteristic, a clear improvement of force modelling is generated. The same stepwise process is done in longitudinal direction, and the associated parameter results as well as validation plots are presented in Appendix D.

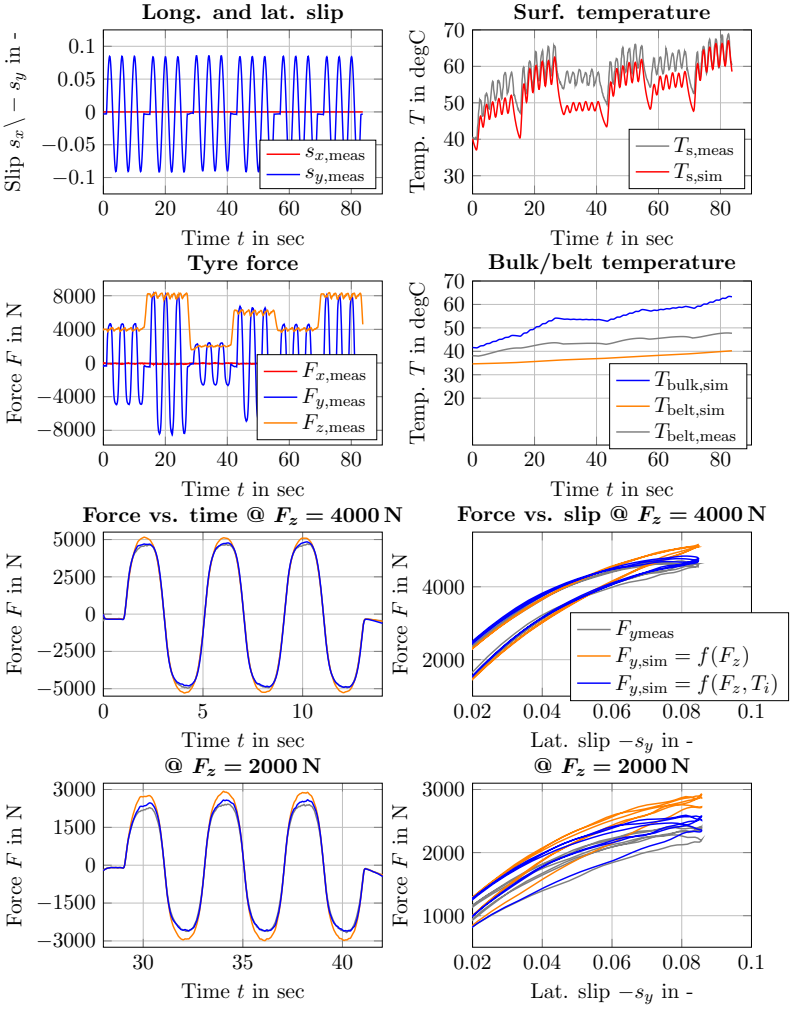

Figure 5.12.: Validation of the temperature-enhanced TMeasy tyre model in lateral direction by using a warm-up manoeuvre; the two upper left plots shown the target values including the measured forces, while in the upper two right plots the measured and simulated temperatures are given; the four bottom plots present the force comparison of the standard versus the enhanced TMeasy tyre model based on investigation of the PP0 tyre

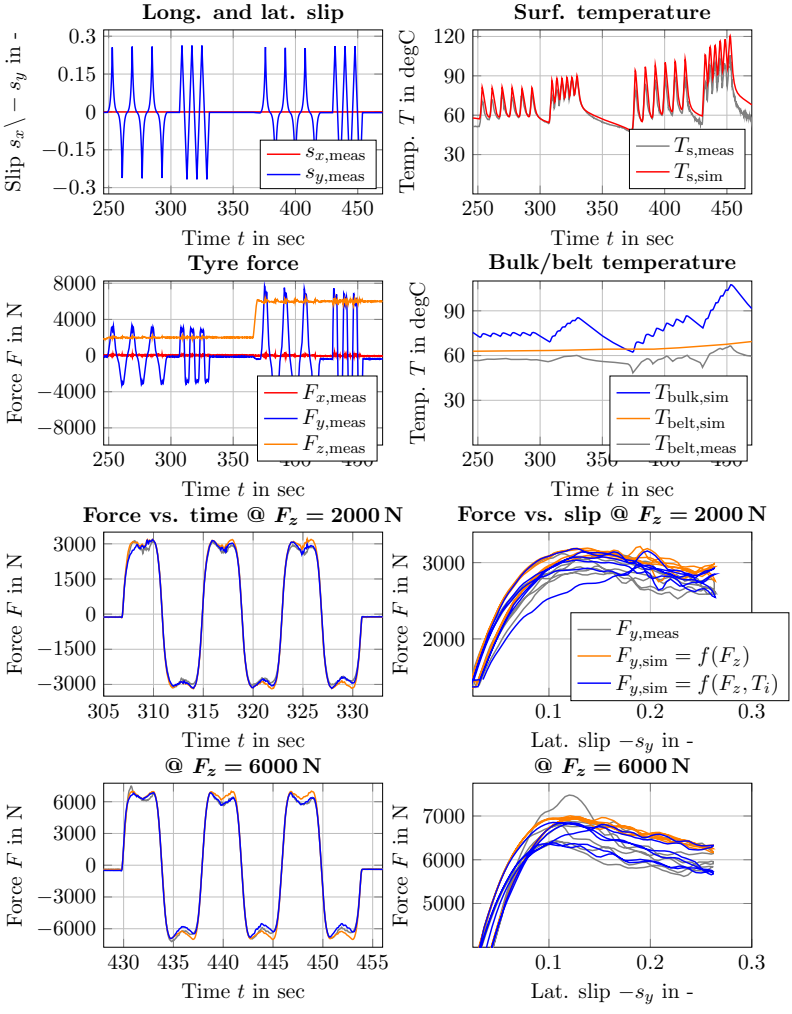

Figure 5.13.: Validation of the temperature-enhanced TMeasy tyre model in lateral direction by using a typical steady-state characteristic manoeuvre; the two upper left plots show the target values including the measured forces, while in the upper two right plots the measured and simulated temperatures are given; the four bottom plots represent the force comparison of the standard versus the enhanced TMeasy tyre model based on investigation of the PP0 tyre

5.4. Comparative conclusion of the temperature enhanced TMeasy tyre model

To investigate the tyre behaviour based on applied basic research, a wide range of influencing factors has to be taken into account. To this end, tests are often done under laboratory conditions in a first step because the environment is known and external influences can be minimised or controlled in most cases. Nevertheless, not all physical tyre effects can be reduced in size under laboratory conditions. The most common effect that should be considered is the tyre temperature. Therefore, based on a review of the literature covering the influences on tyre behaviour in Chapter 3 and the characteristics of the standard TMeasy tyre model in Chapter 4, the modelling of the tyre temperature and its impact on tyre forces was presented in this chapter as a foundation for further investigations.

Based on a literature study, preliminary investigations of different types of temperature models and measurements with the tyre section, a multi-layer model based on the first law of thermodynamics was chosen. Next, a definition of simplifications made to the temperature model concept was presented in detail. Different heat phenomena are used to describe temperature changes based on different types of parameter sets. After presenting the parameterisation process of the temperature model, different manoeuvres were used to validate the developed model. It was shown that a satisfactory match between measured and simulated data is given for warm-up as well as cooling manoeuvres. The defined inner layer was able to describe the smoothly increasing temperature behaviour and furthermore the surface layer for the high oscillating surface temperature changes for dynamic manoeuvres. Implementing the hysteresis effect in a more semi-physical approach provides possibilities for further investigations. Nevertheless, the implemented multi-layer model forms a good implementation to investigate the impact on tyre forces.

A method was presented to model the influences of tyre temperature on steady-state tyre forces in the second part of this chapter. The initial parameter setup generated in Chapter 4 is recalculated based on the current temperature. In a next step, influences from bulk temperature on initial slope and surface temperature on maximum force and its slip-dependent position were discussed in detail and confirmed with results from the literature. Based on these temperature-dependent behaviours, a model approach was presented by using physically meaningful parameters. Furthermore, the same model approach was used to describe influences on peak force and their position to reduce complexity and parameterisation effort.

After validation of both model parts, an implementation in the standard TMeasy model was carried out, followed by a detailed validation. By means of various lateral and longitudinal manoeuvres, the standard and temperature-enhanced TMeasy models were compared with measurement data. It was shown that the extended approach is able to handle low as well as high temperature conditions with different manoeuvres and normal force applications. Parameter sets as well as validation plots for both tyres, in lateral and longitudinal direction, are presented in Appendix D. This leads to the final

conclusion that the enhanced TMeasy model is able to handle temperature influences in a satisfactory manner, and it can be used for detailed investigations into further applications.

6

Semi-physical transient tyre model approaches

An experimental validation including a frequency-dependent extension of transient tyre model behaviour is given based on the previous investigations and presented in this chapter. The TMeasy-based extended temperature tyre model evaluated in Chapter 5 serves as a platform for these investigations.

Investigations presented in Chapter 2 have shown that for semi-physical model approaches in particular, first-order and second-order applications are widely used. First-order approaches in particular deal with the implementation of a time constant τ, which is mostly related to the relaxation length σ respectively the cornering stiffness c_α and the tyre stiffness c_y in lateral direction. In contrast, second-order applications using tyre mass are not easy to parameterise and furthermore show negative effects in terms of simulation time. In addition, possible normal force dependent relaxation length extensions are suitable, but the parameterisation process seems to be easier if the effect is directly related to spring and/or damper behaviour.

In summary, different transient approaches are implemented in state of the art tyre modelling applications, but they are either disadvantageous in terms of handling simulation in critical driving situations, which means for high frequency demands, or they are solely mathematical approaches without the physical background for practical application, making them too complex for semi-physical and real-time operations. In conclusion, in the field of semi-physical tyre modelling, first off a model is needed that is able to cover transient influences with high frequency areas, and second, the model has to be able to adhere to the conditions of short calculation time, parameterability and physical practicality. Therefore, further attention goes to the following:

- Normal force dependent model parameter investigations to increase accuracy and represent the normal force dependency
- The influence of the manoeuvre frequency to model the visco-elastic mechanism of tyre deformation

To achieve this goal, investigations are split into two main parts, whereby focus is on a non-rolling tyre in the first part. During these investigations, a special test bench construction is used to investigate tyre behaviour within different tyre displacement targets and normal force applications. This enables measuring the tyre displacement

and the influence on tyre behaviour directly. Additional focus goes to high displacement areas as well as different frequency and amplitude manoeuvres. The results of these investigations show that manoeuvre frequency clearly influences tyre behaviour, which confirms the decision to implement the previously mentioned characteristics in transient tyre modelling.

The second part focuses on the evaluation and implementation process of the mentioned characteristics using an industrial flat track test bench. In a first step, common manoeuvres for tyre dynamics parameterisation are presented and evaluated. Based on this evaluation, a primary manoeuvre is chosen and used for parameterising the standard transient model implemented in the TMeasy tyre model. In addition, the normal force dependency is directly presented within this parameterisation process.

In a next step, more attention is given to a more detailed look at frequency dependency. Relatedly, the apparent increase in tyre stiffness behaviour leads to a dynamic hardening effect of the tyre. Based on these results, a Maxwell element is used to model the tyre hardening effect. Because damper parameters are hard to determine in general, a semi-physical approach based on the frequency is given. This application will be implemented into the temperature-based tyre model in lateral and longitudinal directions and parameterised for both type of tyres used in this thesis.

Next, a model validation based on the standard TMeasy implementation as well as on measurement data is presented. Finally, the chapter ends with a comparative conclusion.

6.1. Fundamental analyses of a non-rolling tyre

Before a detailed investigation on transient semi-physical model approaches by means of an industrial flat track test bench was carried out, fundamental analyses of a non-rolling tyre were carried out on an adapted brake and suspension test bench at the Institute of Automotive Engineering, Graz University of Technology. The goal of this step was to gain basic knowledge about the main influencing effects on dynamic tyre behaviour within a known environment. In addition, the test bench facility was used to evaluate the basis as well as first extensions of the transient tyre model. In summary, these investigations are used as a foundation for the final modelling process presented in Section 6.3. In this thesis, only the main results and outcomes are presented. For a detailed overview of the whole measurement matrix as well as investigations of a rolling tyre within this test facility, please reference [Hackl et al., 2016a] and [Hackl et al., 2016b].

In the next subsection, an overview of the basic as well as the adapted assembly of the brake and suspension test bench is given first, followed by the results on non-linear spring and transient influencing characteristics. Because of financial restrictions, the focus was on measurements in lateral direction.

6.1.1. Test bench setup description

The fundamental non-rolling tyre investigations have been conducted on a brake and suspension test rig which is mainly used for investigations of durability and fatigue of components of quarter vehicle suspensions, [Harrich et al., 2006], located at the Institute of Automotive Engineering, Graz University of Technology, [FTG, 2019].

In general, a drum with an outer diameter of 1.219 m is used as the main driving/braking component, and it is also responsible for applying forces in lateral direction. To do so, it pivots around the vertical axis and thus generates a slip angle of ± 15 deg with a maximum rotational velocity of 25 deg/s. The drum speed can be set to between 0 and $1300\,\mathrm{min}^{-1}$, and the vertical tyre load is controlled by means of a hydraulic cylinder with a maximum force of 25 kN. Depending on the weight of the test assembly and the required travel range, a maximum pulse frequency of 35 Hz can be achieved. The maximum actuator speed is 1.1 m/s while the peak acceleration is $10\,\mathrm{m/s}^2$. The resulting forces and torques in the wheel hub are measured using a high-precision *wheel force transducer* (WFT) from [Kistler GmbH, 2019], which can be applied to different types of tyre sizes. For the presented experiments the wheel assembly - consisting of tyre, rim and wheel carrier - were mounted on the test bench using a rigid suspension. This means that elastic deflection between wheel and test bench sledge are negligible, see Figure 6.1 left.

Nevertheless, because of the fact that the available test bench setup is only able to move in vertical direction on a highly dynamic level, the mechanical assembly has to be rotated. Therefore, to transform the vertical movement of the sledge into a motion which can cause a lateral tyre force, a special arrangement had been designed, see Figure 6.1 right. It can be seen that the stiff bracket for the WFT means very stiff wheel suspension due to the fact that no external deflection influences the measurements. In order to compare the results to measurements of the rolling tyre on the drum, a curved mount with the same radius as the drum is used. To investigate the behaviour at different tyre loads, a hydraulic device is installed to change it continuously up to $F_{z,\mathrm{max}} = 10000\,\mathrm{N}$.

For the parameterisation of spring and damper values of the Voigt-Kelvin model, dynamic sinusoidal excitation is applied. Thereby, tests were carried out in a frequency range in steps from 0.125 to 12 Hz and an amplitude range of lateral deflection from 1.25 to 15 mm. With respect to the two manoeuvre ranges, a deflection frequency matrix was defined for the parameterisation.

In summary, for the modified test bench setup, high lateral deflection up to sliding effects as well as high frequency manoeuvres for transient behaviour can be applied and investigated in a next step.

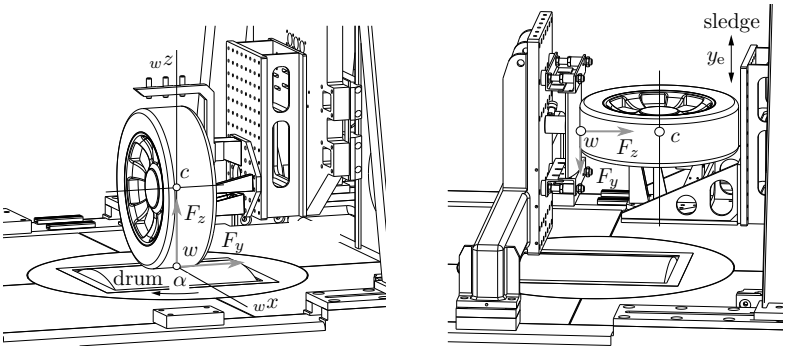

Figure 6.1.: Schematic representation of the brake and suspension test facility at the Institute of Automotive Engineering, Graz University of Technology, [FTG, 2019]; left, general setup wherein fundamental investigations of tyres are feasible; right, adapted construction to analyse the lateral tyre dynamics of a non-rolling tyre, adapted from [Hackl et al., 2016a]

6.1.2. Non-linear spring characteristics

As most of the semi-physical transient tyre model approaches use linear spring characteristics, see Chapter 2.3, dealing with properties of the lateral deflection versus force characteristics was the first fundamental investigation which was done on the modified setup of the suspension test bench. Therefore, the setup presented in Figure 6.1 right was used with a test tyre of type Continental 205/55 R16 91V. First, a vertical tyre load F_z was set followed by moving the test bench sledge slowly up or down. While moving, the force that acts in lateral direction to the tyre was measured until the tyre started sliding. Hence, at small lateral deflection areas a nearly linear characteristic is given until the tyre starts sliding. From this point, on the linear behaviour becomes non-linear up to a point where full sliding occurs, see Figure 6.2. This behaviour is confirmed by investigations from [Einsle, 2010].

Due to the very slow lateral movement, a quasi-stationary behaviour could be assumed, whereby the related characteristics can be described by a non-linear spring force

$$F_y \;=\; c_y\, y_\mathrm{e} + c_y\, p_y\, |y_\mathrm{e}|\, y_\mathrm{e}\,, \tag{6.1}$$

where c_y defines the linear spring and p_y the intensity of the non-linearity. By defining $p_y = 0$ the linear implementation can be used. A comparison of both implementations is given in Figure 6.2. Thereby, a sufficient conformity up to ± 20 mm deflection is given, while the non-linear characteristics performs better at higher deflections until full sliding is reached.

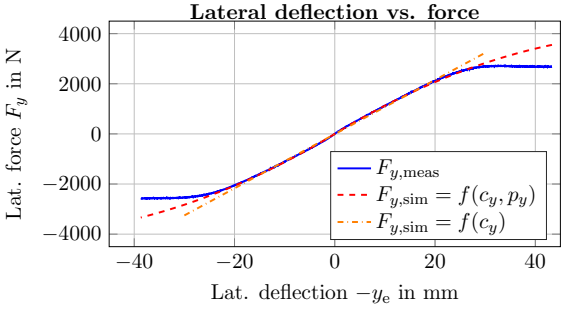

Figure 6.2.: Validation of the identified linear and non-linear lateral spring characteristics based on measurements by using the extended construction setup presented in Figure 6.1 right and a normal force of $F_z = 3600\,\mathrm{N}$, adapted from [Hackl et al., 2016b]

In summary, by using this extended test bench setup, there is a possibility to parameterise the linear spring characteristics and its non-linear extension. Such a method is also common for parameterising spring values at other test facilities.

Nevertheless, a small improvement within high displacement areas results from great effort. Specifically, this means that in order to get the non-linear behaviour, an extended test bench setup or a separate test bench facility has to be used, while with high deflection areas, changes in dynamic forces are low anyway. In conclusion, a non-linear spring may increase accuracy for high deflection areas, but the ratio of accuracy to effort is too low to use it with a practical application. The outcome: a linear spring is used for further investigations. Note that a method to get the non-linear spring characteristics from a manoeuvre on a flat test track is presented in [Hackl et al., 2017a], and evaluated within virtual measurements from the FTire tyre model, [cosin, 2018a], [cosin, 2018b].

6.1.3. Manoeuvre influences on dynamic force behaviour

In the second part of the fundamental investigations, influences on manoeuvre amplitude and frequency on the behaviour of the Voigt-Kelvin model were carried out. Therefore, the same setup that was presented in Figure 6.1, was used, wherein various sine manoeuvres within different tyre loads, tyre pressure, deflection amplitudes and manoeuvre frequencies were applied, [Hackl et al., 2016a].

For this evaluation, a defined setup with tyre load $F_z = 3600\,\mathrm{N}$, deflection amplitude of $A_{\mathrm{sine}} = 5\,\mathrm{mm}$ and a frequency of $f_{\mathrm{sine}} = 1\,\mathrm{Hz}$ was chosen to parameterise the spring and damper value of the Voigt-Kelvin model. Comparing the model approach with measurement data, good conformity is given for force over time as well as force over deflection, see Figure 6.3.

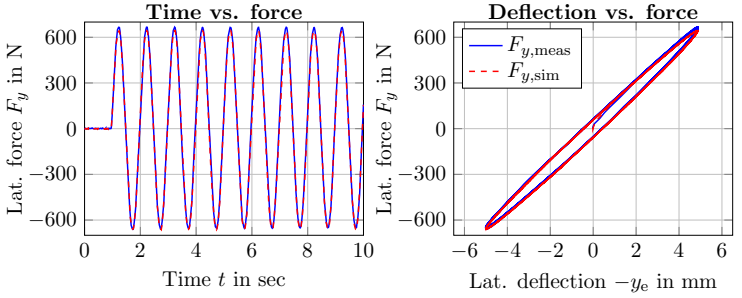

Figure 6.3.: Validation of the parameterised Voigt-Kelvin model with measurements of a deflection sine manoeuvre for the non-rolling tyre with tyre load $F_z = 3600\,\mathrm{N}$, deflection amplitude of $A_{\mathrm{sine}} = 5\,\mathrm{mm}$ and a frequency of $f_{\mathrm{sine}} = 1\,\mathrm{Hz}$, adapted from [Hackl et al., 2016a]

In a next step, the defined parameter setup of the Voigt-Kelvin model is used and the model performance is compared at different amplitudes and frequency manoeuvres, see Figure 6.4. Thereby, in the upper left plot a smaller manoeuvre amplitude was used, and on the upper right a higher amplitude was used. Small deviations around maximum deflection occur, but overall a good correlation is given because both manoeuvres are working within the linear spring area, see Figure 6.2.

For the second variation, different manoeuvre frequencies with constant amplitudes are used and validated, as can be seen in both lower plots. It is clearly evident that within smaller as well as higher frequencies, deviations between simulation and measurements result.

In summary, this allows us to conclude that a linear spring behaviour seems to be a satisfying model approach with a practical tyre operating point. Furthermore, the Voigt-Kelvin model works well at a fixed operating point, but provides a remarkable lack of accuracy when dealing with broad frequency ranges. Therefore, an approach that is able to model frequency influences has to be found for a more accurate model description.

Parameterisation and validation of the frequency dependent model approach has to be feasible without a special device for practical usage. In addition, parameterisation and validation of the frequency-dependent model approaches on rolling tyres are more practical. Therefore, focus on measurements from an industrial flat track test bench is given for further consideration. The next section starts with a manoeuvre validation for transient model characteristics for parameterising of the standard TMeasy Voigt-Kelvin model, followed by parameter influences on tyre load. Thereafter, Section 6.3 focuses on frequency influences on a rolling tyre, followed by presenting and validating an extended transient model approach.

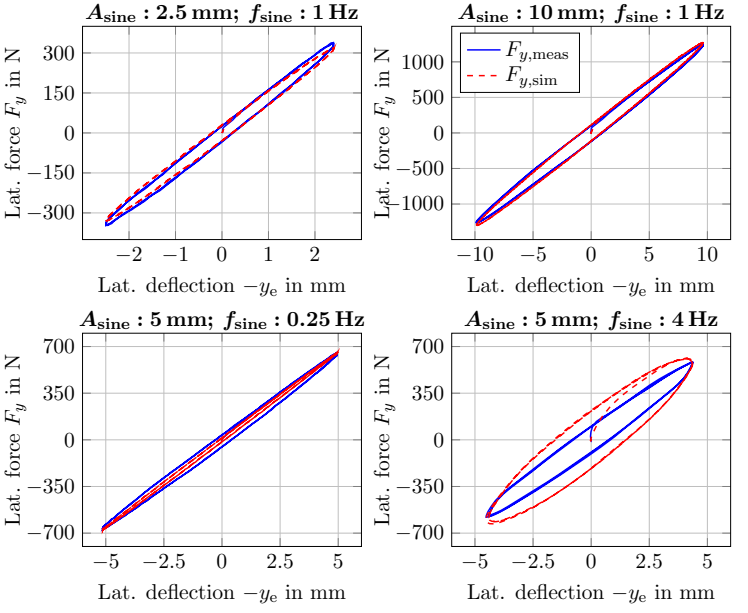

Figure 6.4.: Validation of the parameterised Voigt-Kelvin model with measurements of a non-rolling tyre with different manoeuvre amplitude and frequency settings; the upper two plots show changes of the deflection amplitude while the bottom two plots show a comparison by changing the manoeuvre frequency, adapted from [Hackl et al., 2016a]

6.2. Voigt-Kelvin parameterisation based on tyre load

Before detailed focus is given to the influences of frequency on tyre behaviour, the focus is manoeuvre choice followed by parameterising of the basic Voigt-Kelvin model as a benchmark for further comparison in this section. Therefore, an evaluation of the most common manoeuvres to parameterise transient tyre models is given, and finally a manoeuvre for frequency-based investigation is selected.

6.2.1. Transient modelling for manoeuvre validation

The most common method to parameterise transient tyre models in lateral directions is step-steer slip angle changes, or some kind of modification of this. During constant wheel load, steps from zero up to a defined slip angle value and back again are applied and the lateral force is measured. Based on an optimisation, the spring and damper values can be defined, see for example [Dessort et al., 2016], for parameterising the Voigt-Kelvin spring for the TMeasy tyre model. A further approach uses step-steer inputs to parameterise the transient-based transfer function in the frequency domain, see [Einsle, 2010]. Therein, initial values unequal to zero are also investigated to simulate influences of toe angles.

Nevertheless, in most literature-based approaches, small slip angle step values are used to stay within the linear region of the tyre force characteristics. This presents the advantage that linear transfer functions can be used for modelling as well as for parameterisation. Although these slip areas around zero are of major interest, evaluation at higher slip angle values should minimally be carried out. A possible manoeuvre example can be seen in Figure 6.5 on the left, which shows a sequence of randomly generated slip angle steps. Step-steer manoeuvres thus involve two main disadvantages.

The first disadvantage depends on possible slip angle changes of the test bench facility. An ideal step-steer manoeuvre can only be defined theoretically, which leads to practical limitations. This means parameterisation with a step-steer input based on transfer function always means making a compromise. Furthermore, results are manoeuvre dependent, which means the test bench behaviour influences the parameterisation. To counteract this characteristic, adapting the step-steer signal by using a *Fast Fourier transformation* (FFT), whereby only frequencies up to a defined boundary are allowed, is one possibility, see Figure 6.5 right. This seems to be a good theoretical idea, but experimental investigations have shown that with both methods, the second disadvantage predominates.

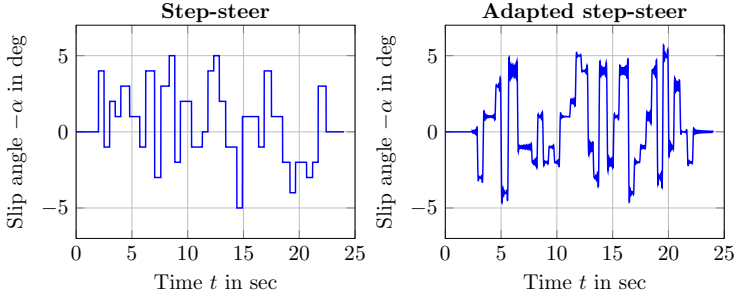

Figure 6.5.: Possible slip angle step-steer methods to parameterise lateral transient model behaviour; left, randomly generated slip angle steps within a fixed boundary; right, adapted step-steer manoeuvre with defined frequencies

The second disadvantage is based on the presented sensitivity analysis in Section 3.1. Inaccuracies around the constant slip angle areas are influencing the parameterisation of the transient model parameters. By using a transfer function where linear cornering stiffness can be directly adapted based on the operating point, a step-steer manoeuvre seems to be a good choice. But when using tyre models like TMeasy in which the transient characteristic is directly related to the steady-state behaviour, the inaccuracies should be taken into account.

The second manoeuvre category that is common for transient parameterisation is sine or sine sweep manoeuvres, as well as some modifications to these. As state of the art Voigt-Kelvin models are only feasible for one operating point, see Figure 6.4, for parameterisation cases in the literature, fixed amplitude as well as frequency is used in most cases. Nevertheless, a sweep within a broad range of frequencies is still recommended for validation, as shown in Figure 6.6 on the left. An extended version of a sine sweep is defined in Figure 6.6 on the right. For this case, a change in manoeuvre amplitude is additionally given. Therefore, a broad range of amplitudes can be validated and test bench boundaries are used in the best case. This means that when using high sine sweep amplitudes as well as frequencies, test bench boundary conditions have to be taken into account.

In summary, the experimental investigations have shown that step-steer slip angle manoeuvres are useful when using transfer function models or linear applications where the cornering stiffness can be adapted based on the operating point. When using model applications where the transient behaviour strongly interacts with the steady-state characteristics, model and parameter inaccuracies should be taken into account. When using sine or sine sweep manoeuvres, this effect can never be excluded out at all, but the dynamic behaviour is present to a higher degree. Furthermore, practical manoeuvre

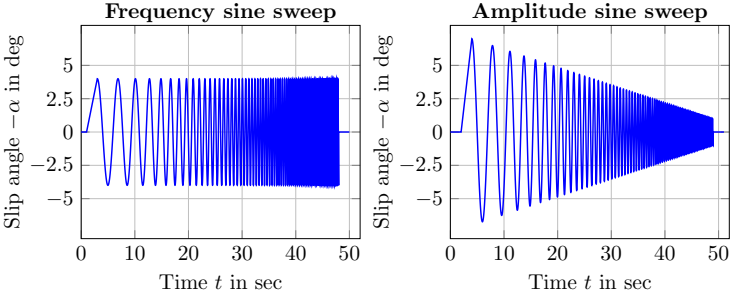

Figure 6.6.: Possible sine sweep manoeuvres to investigate lateral transient model behaviour; left, frequency based sine sweep manoeuvre from $f_{\text{sine}} = 0 \rightarrow 5\,\text{Hz}$; right, sine sweep where slip angle amplitude is also changing

investigations on flat track test benches with various tyres have shown that step-based longitudinal slip changes can be handled more poorly than sine sweeps from the control of the test bench facility. Because of these arguments and the fact that frequency investigations can more easily be done with sine manoeuvres, sweeps are used for further investigations in this thesis. Note that by comparing the results from frequency and amplitude sine sweep manoeuvres, almost the same results were achieved.

6.2.2. Parameterisation of the Voigt-Kelvin model

After defining the amplitude sine sweep manoeuvre for investigations of transient tyre behaviour, the focus in this subsection is the Voigt-Kelvin model as a standard implementation in TMeasy. In a first step, the correct filter frequency f_f has to be defined, see Figure 6.7.

As was already presented in Subsection 4.2.4, a FFT is applied on the lateral force measured with a sample rate of $f_\mathrm{s} = 1000\,\mathrm{Hz}$, see upper right plot in Figure 6.7. It is clearly visible that above a frequency range of $f > 5\,\mathrm{Hz}$, almost only signal noise is presented. By only considering this manoeuvre in lateral direction a tight filter frequency of $f_\mathrm{f} = 10\,\mathrm{Hz}$ would be possible. As for the non-dynamic filter frequency, between $f_\mathrm{f} = 10 \rightarrow 15\,\mathrm{Hz}$ are used depending on the manoeuvres in lateral and longitudinal direction, although this is a more conservative approach. Furthermore, two comparative

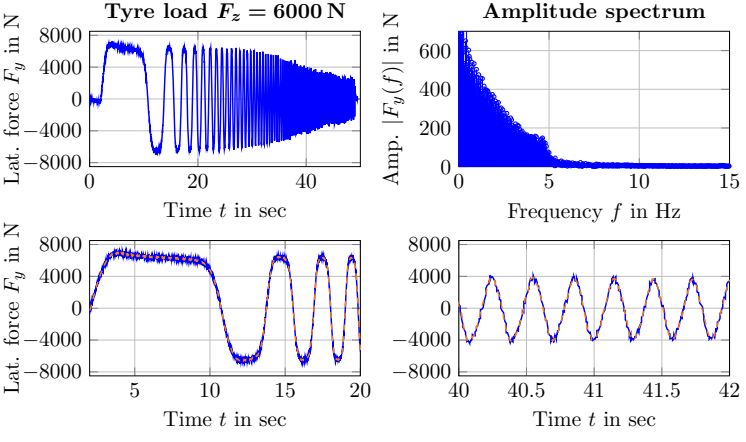

Figure 6.7.: Fast Fourier transformation analysis on a transient lateral manoeuvre to define the right filter frequency. In the upper right plot, the amplitude spectrum versus the frequency applied for the lateral tyre force (upper left) is presented, while the two bottom plots show the comparison between the raw and filtered signal

plots between raw and filtered measured lateral force are given in the two bottom plots of Figure 6.7. Like low as well as high frequency areas, a satisfactory filter effect is presented.

The filtered force can be used to parameterise the spring characteristics in lateral and longitudinal direction in a next step. For the overall spring c_y the manoeuvres based on all applied vertical tyre loads are combined and the value optimised by minimising the deviation between measured and simulated force. By separating the optimisation process that is dependent on the normal force, stiffness values based on the normal force can be calculated. Hence the results for both normal forces that are dependent and independent of spring definitions are presented in Figure 6.8. In the left plot, the lateral stiffness and on the right side the longitudinal stiffness, for both tyres Uniroyal Rainsport3 255/50 R19 107Y and Pirelli Pzero 245/40 R20 99W are presented.

The marker representing the normal force dependent optimised spring values, and the dashed and dash-dotted lines represent the values for calculating wheel load independently. Furthermore, decreasing stiffness behaviour in a lateral direction is evident, whereas increasing stiffness in longitudinal direction is clearly visible. This corresponds with literature. In addition, a higher normal force dependency is given with the high performance PP0 tyre. Because higher normal forces generate larger absolute errors, they are likewise rated higher. Therefore, this is the reason why the tyre load independent stiffnesses are closer to the values of higher normal forces.

Furthermore, a linear normal force model application, based on TMeasy, for typical values at nominal normal force F_z^{N} and its double can be implemented, see Figure 6.8, solid lines. By using these values $c_{x/y,1/2}$ given in Table 6.1, the normal force-based stiffness characteristics can be implemented into the overall tyre model. As no clear normal force dependency regarding the damping effect was visible during investigations, a constant value was used for the overall parameterisation and evaluation process.

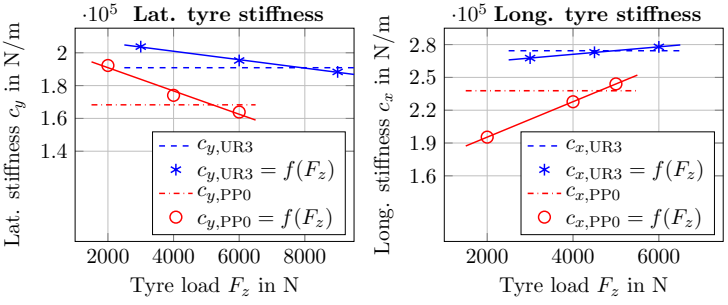

Figure 6.8.: Parameterised tyre stiffnesses in lateral (left) and longitudinal (right) direction for the tyres used; Uniroyal Rainsport3 255/50 R19 107Y (UR3) and Pirelli Pzero 245/40 R20 99W (PP0)

In summary, the parameterisation of the transient Voigt-Kelvin spring damper model shows an essential normal force dependency in lateral as well as in longitudinal direction. Based on the type of tyre, these influences are more or less pronounced. By comparing both applications based on model accuracy, the approach influenced by tyre load shows an improvement of about 5 % applied to the *root mean square* (RMS) deviation with different kinds of manoeuvres. These are just small improvements, but because of the easy implementation as well as parameterisation usage of the normal force, variation of the stiffness is recommended at this point.

Table 6.1.: Parameterised Voigt-Kelvin tyre stiffnesses in lateral and longitudinal direction for the tyres used Uniroyal Rainsport3 255/50 R19 107Y (UR3) and Pirelli Pzero 245/40 R20 99W (PP0). In addition to the normal force independent stiffnesses $c_{x/y}$ the extended linear normal force dependent values $c_{x/y,1/2}$ are also given

Parameter	Value	Description
Uniroyal Rainsport3 255/50 R19 107Y (UR3)		
d_y	268	TMeasy based lateral tyre damping in Ns/m
c_y	190900	TMeasy based lateral tyre stiffness in N/m
$c_{y,1}$	199650	Lateral tyre stiffness at F_z^{N} in N/m
$c_{y,2}$	188090	Lateral tyre stiffness at $2\,F_z^{\mathrm{N}}$ in N/m
d_x	284	TMeasy based longitudinal tyre damping in Ns/m
c_x	274380	TMeasy based longitudinal tyre stiffness in N/m
$c_{x,1}$	272820	Longitudinal tyre stiffness at F_z^{N} in N/m
$c_{x,2}$	288200	Longitudinal tyre stiffness at $2\,F_z^{\mathrm{N}}$ in N/m
Pirelli Pzero 245/40 R20 99W (PP0)		
d_y	224	TMeasy based lateral tyre damping in Ns/m
c_y	168280	TMeasy based lateral tyre stiffness in N/m
$c_{y,1}$	183830	Lateral tyre stiffness at F_z^{N} in N/m
$c_{y,2}$	162535	Lateral tyre stiffness at $2\,F_z^{\mathrm{N}}$ in N/m
d_x	238	TMeasy based longitudinal tyre damping in Ns/m
c_x	237800	TMeasy based longitudinal tyre stiffness in N/m
$c_{x,1}$	211580	Longitudinal tyre stiffness at F_z^{N} in N/m
$c_{x,2}$	260210	Longitudinal tyre stiffness at $2\,F_z^{\mathrm{N}}$ in N/m

6.3. Frequency-based Maxwell model approach

After parameterising the Voigt-Kelvin model, including investigating influences of the wheel load in the previous section, a focus on manoeuvre frequency with a model application is part of this section. Results in Figure 6.4 have already proven an effect for different manoeuvre frequencies, but for practical usage investigations and parameterisation of the extended model, this should also be possible on an industrial test bench.

To make this a reality, the already defined amplitude sine sweep is used for this investigation. This manoeuvre is divided into segments and the parameterisation of the Voigt-Kelvin model is carried out in relation to the frequency division in a first step. As a result of this process, a frequency-dependent spring characteristic can be presented. Because implementing a polynomial frequency-dependent behaviour is not desired for a semi-physical approach, a model is presented which is able to describe the expected hardening effect of a tyre. Finally, this section ends with the parameterisation and validation process of the extended transient model approach.

6.3.1. Frequency-based parameter investigations

Before investigations can be done on the frequency dependent model approach, the results of Figure 6.4 have to be confirmed with measurements on an industrial flat track test bench. The presented frequency manoeuvre as well as the amplitude sine sweep manoeuvre from Figure 6.6 can be used for these investigations, whereby comparable results are given. As the Voigt-Kelvin model has already delivered sufficient results, this model serves as a foundation for the following investigations.

The manoeuvre target is divided into segments depending on the number of periods to focus on for the frequency-dependent investigations, see the upper plot of Figure 6.9 as an example in lateral direction. Based on each division, the basis Voigt-Kelvin parameters c_y and d_y from Table 6.1 can be adapted within this range and plotted in relation to frequency and wheel load. Because a sine sweep is given, an average frequency f_m per area is calculated via FFT analysis in order to present the results within one figure. As the order of magnitude between spring and damper values represents the greater influence of the spring effect, the damper value is kept constant during this investigation. The results for both tyres in lateral and longitudinal direction are given in the bottom four plots of Figure 6.9.

In the middle two plots of Figure 6.9, the results of the normal force and frequency-dependent lateral spring parameterisation, for the UR3 tyre on the left and for the PP0 on the right, are presented. For both tyres, three different normal forces with $F_{z,\mathrm{UR3}} = \{3000, 6000, 9000\}\,\mathrm{N}$ and $F_{z,\mathrm{PP0}} = \{2000, 4000, 6000\}\,\mathrm{N}$ are used. Furthermore, because measurements for the PP0 tyre were done during a later project phase and after gaining experience with the UR3 tyre, the manoeuvre frequency was increased to $f = 7\,\mathrm{Hz}$.

As results for the parameterisation process, a nearly constant initial spring behaviour is converted into an increasing characteristics, starting at $f_\mathrm{m} > 2.5\,\mathrm{Hz}$ for all three normal forces and both types of tyres. Furthermore, for lower wheel loads, a stronger increase in the spring stiffness seems to be evident, which leads to a higher hardening effect of the tyre. Hence, the stiffness increases around $f_\mathrm{m} \approx 1.5\,\mathrm{Hz}$ is probably traceable as a cut-off test bench frequency because this effect is given for both tyres, and also for further tyres tested on this test bench.

Furthermore, in the two bottom plots, the results of the normal force and frequency dependent longitudinal spring parameterisation for the tyres are presented. Because the test facility was not able to perform longitudinal manoeuvres under high wheel load, different normal forces had to be defined with $F'_{z,\mathrm{UR3}} = \{3000, 4500, 6000\}\,\mathrm{N}$ and $F'_{z,\mathrm{PP0}} = \{2000, 4000, 5000\}\,\mathrm{N}$. Nevertheless, the results show a continuously increasing behaviour for both types of tyres. Furthermore, the UR3 tyre shows a smaller influence of the changing wheel load, which was seen already in Figure 6.8 right. Because of vibration behaviour and/or problems with the slip controller during measurements in longitudinal direction of the PP0 tyre, only the two higher wheel loads and frequencies lower than 3.5 Hz can be evaluated.

Nonetheless, based on these results the acceptance that the widely used Voigt-Kelvin model approach supplies satisfactory results for small manoeuvre frequencies or near a fixed operating point has been confirmed. Therefore, in order to describe the typical effect of dynamic frequency-dependent hardening of elastomer materials, an extended model approach has to be taken into account for highly transient manoeuvres. A mathematical polynomial frequency dependent spring implementation is suitable, but not practical for handling modelling. Therefore, a semi-physical model approach has to be defined in the next subsection to model the hardening effect of the elastomer tyre material. It is carried out by means of a Maxwell model approach.

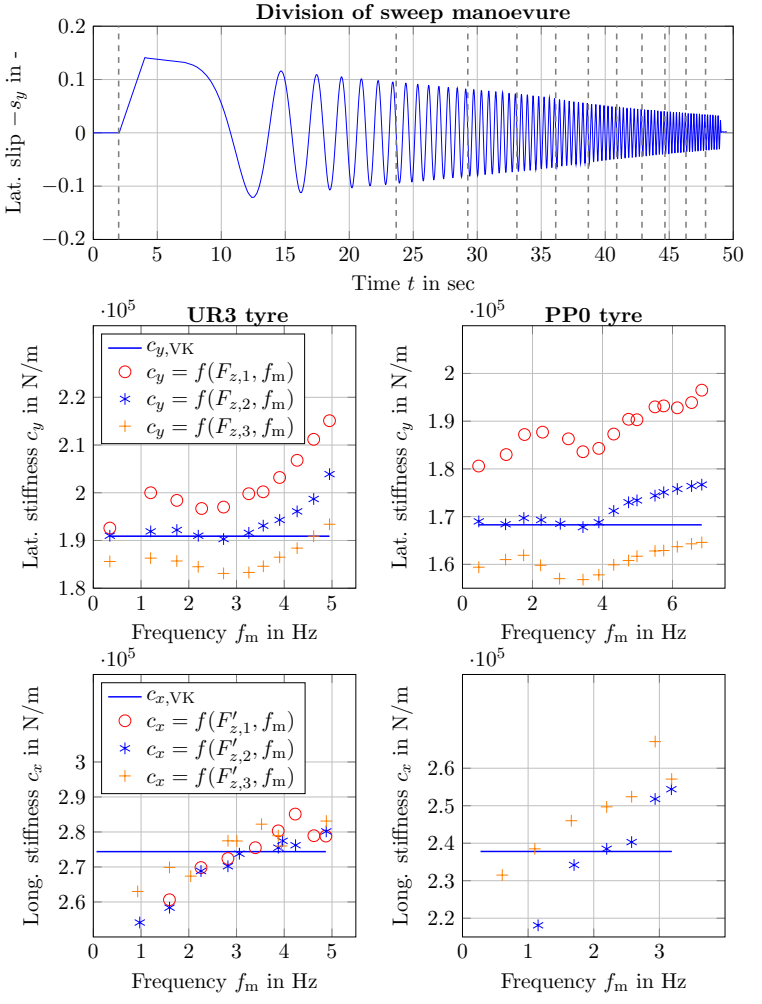

Figure 6.9.: Frequency dependent model parameter investigation; in the upper plot the division based on number of periods is shown; furthermore, in the four bottom plots the normal force and frequency-dependent lateral and longitudinal stiffness results are presented for the Uniroyal Rainsport3 255/50 R19 107Y left and Pirelli Pzero 245/40 R20 99W right

6.3.2. Enhanced tyre dynamics model approach - Maxwell model

Based on the physical characteristic that elastomer materials show hardening effects with increasing frequency, which leads to an increasing stiffness, the extended model should be able to handle a frequency-based stiffness. Furthermore, investigations of damping effects have shown that damper values are sensitive, but this decreases rapidly with increasing frequency. In summary, a model extension that mainly increases stiffness and also decreases damping behaviour with increasing frequency has to be defined in this case.

Therefore, based on fundamental investigations in [Rill, 2012] and tyre based considerations in [Hackl et al., 2016b], [Hackl et al., 2017a] and [Hackl et al., 2018], a Maxwell element approximates the desired behaviour best. This means, in detail that in addition to the already used Voigt-Kelvin spring and damper, a Maxwell element has to be used to model the dynamic hardening of elastomer materials. Hence, a Maxwell element provides nearly no stiffness and full damping in lower frequency ranges, which means this implementation brings further damping effects. Additionally, fundamental analyses in [Hackl et al., 2017a] confirmed with experimental investigations in [Hackl et al., 2017b] have shown that the Maxwell element is able to model the main tyre damping effect within low frequency areas and therefore the Voigt-Kelvin damper can be neglected. In summary, Figure 6.10 presents the Voigt-Kelvin standard implementation on the left and the extended model approach to describe the dynamic hardening effect of the tyre on the right. Therefore, based on the TMeasy implementation presented in Chapter 2, a short summary of the standard model followed by the extended version is given as a next step. Hence, a mathematical description of the model extension is given in lateral direction, but transformed into longitudinal accordingly.

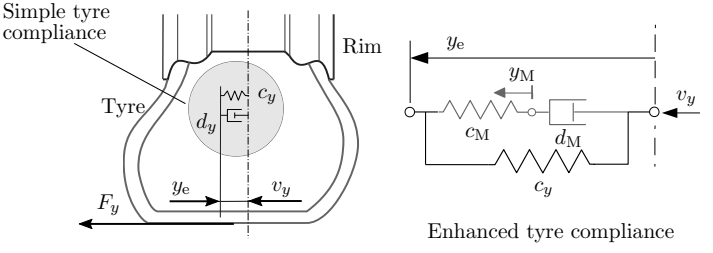

Figure 6.10.: Standard and extended model implementations describe the transient tyre behaviour in lateral direction; left, simple tyre compliance as a foundation implemented in TMeasy; right, enhanced application to model the dynamic hardening effect of a tyre, adapted from [Hackl et al., 2017b]

Mathematical implementation of the extended Maxwell model

The TMeasy tyre model describes the dynamics of the tyre forces and torques by taking tyre compliance into account. As part of this approach, the dynamic behaviour is modelled by a linear spring parallel to a linear damper, see Figure 6.10 left. This Voigt-Kelvin model is defined by a Taylor expansion of the dynamic tyre force

$$F_y^{\mathrm{D}} \;=\; F_y\,(v_y + \dot{y}_{\mathrm{e}}) \;\approx\; F_y\,(v_y) \;+\; \frac{\partial F_y}{\partial v_y}\,\dot{y}_{\mathrm{e}} \;=\; F_y^{\mathrm{S}} \;+\; \frac{\partial F_y}{\partial s_y^{\mathrm{N}}}\,\frac{\partial s_y^{\mathrm{N}}}{\partial v_y}\,\dot{y}_{\mathrm{e}}\,, \tag{6.2}$$

accompanied by the force law

$$F_y^{\mathrm{D}} \;=\; c_y\,y_{\mathrm{e}} \;+\; d_y\,\dot{y}_{\mathrm{e}}\,, \tag{6.3}$$

where F_y^{S} denotes the steady-state lateral tyre force, v_y is the lateral component of the contact point velocity, y_{e} denotes the lateral tyre deflection and c_y and d_y are the stiffness and damping constants approximating the tyre compliance in lateral direction. Combining the relation in Equation (6.2) and (6.3) results in a first-order *differential equation* (DE) for lateral tyre deflection. Taking advantage of the TMeasy tyre modelling concept, one gets

$$\left(v_{Ty}^*\,d_y \;+\; f_{\mathrm{G}}\right)\,\dot{y}_{\mathrm{e}} \;=\; -\,v_{Ty}^*\,c_y\,y_{\mathrm{e}} \;-\; f_{\mathrm{G}}\,v_{Ty}^*\,s_y\,, \tag{6.4}$$

where s_y denotes the lateral slip, $f_{\mathrm{G}} = F_{\mathrm{G}}/s_{\mathrm{G}}$ represents the global slip derivative of the generalised tyre characteristics and a modified travel velocity v_{Ty}^* through the contact patch is used to simplify the expressions. The generalised tyre characteristics, F_{G} includes information about the steady-state tyre behaviour, which is additionally influenced by the normal force.

As was already presented, this simple approach is it quite effective, but is only valid within a small frequency area. Therefore the Maxwell element is taken instead of the Voigt-Kelvin damper, see Figure 6.10 right and the force law given in Equation (6.3) has to be redefined by

$$F_y^{\mathrm{D}} \;=\; c_y\,y_{\mathrm{e}} \;+\; c_{\mathrm{M}}\,(y_{\mathrm{e}} - y_{\mathrm{M}})\,. \tag{6.5}$$

Combining this equation with Equation (6.2) finally results in

$$f_{\mathrm{G}}\,\dot{y}_{\mathrm{e}} \;=\; -\,v_{Ty}^*\,c_y\,y_{\mathrm{e}} \;-\; v_{Ty}^*\,c_{\mathrm{M}}\,(y_{\mathrm{e}} - y_{\mathrm{M}}) \;+\; f_{\mathrm{G}}\,v_{Ty}^*\,s_y\,. \tag{6.6}$$

As an extension to Equation (6.4), the time derivative of the lateral tyre deflection y_{e} now additionally depends on the stiffness c_{M}, the damping d_{M} and the internal displacement y_{M} of the Maxwell element. The force balance applied to the Maxwell element delivers

a second first-order DE with respect to y_M in the form of

$$d_\mathrm{M}\,\dot{y}_\mathrm{M} \;=\; c_\mathrm{M}\,(y_\mathrm{e} - y_\mathrm{M}) \quad \text{or} \tag{6.7}$$

$$T_\mathrm{M}\,\dot{y}_\mathrm{M} \;=\; -y_\mathrm{M} \,+\, y_\mathrm{e} \quad \text{with} \quad T_\mathrm{M} \;=\; \frac{d_\mathrm{M}}{c_\mathrm{M}}\,, \tag{6.8}$$

where this relation is driven by the lateral tyre deflection y_e and characterised by the time constant T_M, which is defined by the stiffness c_M and damping d_M parameters of the Maxwell element.

This means in summary, that the stiffness c_M and the damping d_M or the time constant by $T_\mathrm{M} = d_\mathrm{M}/c_\mathrm{M}$ characterise the Maxwell element. It provides frequency-dependent stiffness and damping properties that, according to [Rill, 2012], are characterised by the dynamic stiffness

$$c_\mathrm{dyn}\,(\Omega) = \frac{\Omega}{\sqrt{\Omega^2 + (c_\mathrm{M}/d_\mathrm{M})^2}}\,c_\mathrm{M}\,, \tag{6.9}$$

and the dissipation angle

$$\Psi\,(\Omega) = \arctan\frac{c_\mathrm{M}/d_\mathrm{M}}{\Omega} \tag{6.10}$$

where Ω denotes the circular excitation frequency. Hence, a Maxwell element provides nearly no stiffness, $c_\mathrm{dyn}\,(\Omega \to 0) = 0$ and full damping $\Psi\,(\Omega \to 0) = 90\,\mathrm{deg}$ in the lower frequency range, whereas at high frequencies it acts like a simple spring $c_\mathrm{dyn}\,(\Omega \to \infty) = c_\mathrm{M}$ and $\Psi\,(\Omega \to \infty) = 0\,\mathrm{deg}$. The ratio $c_\mathrm{M}/d_\mathrm{M}$ of the Maxwell parameter determines the transition from a lower to higher a frequency range.

Nevertheless, damping parameters are hard to estimate and to determine in general. That is why the frequency Ω_{95}, where the Maxwell element provides 95 % of its maximum stiffness, will be used instead to assess the impact of the Maxwell element on the TMeasy tyre model in a more practical way. In that case, Equation (6.9) delivers

$$c_\mathrm{dyn}\,(\Omega_{95}) = \frac{95}{100}\,c_\mathrm{M} = \frac{\Omega_{95}}{\sqrt{\Omega_{95}^2 + (c_\mathrm{M}/d_\mathrm{M})^2}}\,c_\mathrm{M}\,. \tag{6.11}$$

By using the relationship $\Omega = 2\pi f$ one finally gets

$$f_{95} = \frac{1}{2\pi}\,\frac{1}{\sqrt{\left(\frac{100}{95}\right)^2 - 1}}\,\frac{c_\mathrm{M}}{d_\mathrm{M}} = 0.4842\,\frac{c_\mathrm{M}}{d_\mathrm{M}}\,. \tag{6.12}$$

By comparing different Maxwell element parameter setups, a comparison of the standard TMeasy model is given by varying the damping in Figure 6.11 and spring values in Figure 6.12.

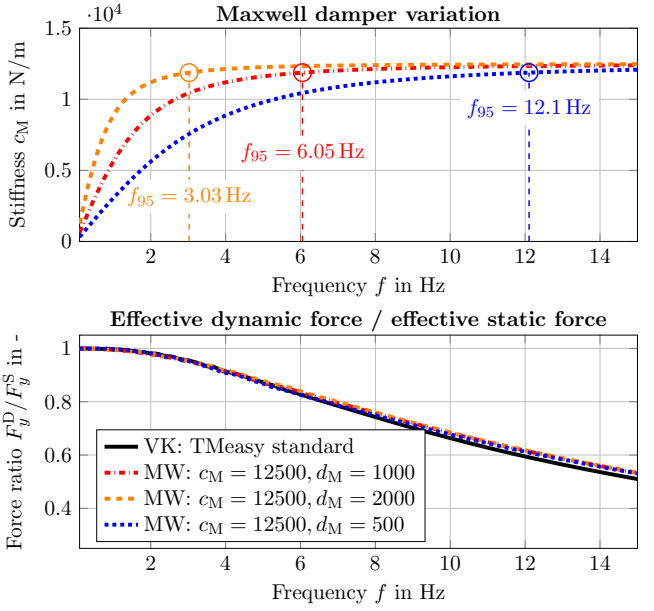

Figure 6.11.: Parameter-based Maxwell model characteristics; the upper plot presents the dynamic stiffness of the Maxwell element due to varying the damping effect versus the frequency, while the bottom plot presents the dynamic effect due to the static force of the Voigt-Kelvin (VK) as well as various Maxwell (MW) model parameter setups

Adding a Maxwell model with different parameter setups (red dot-dashed, blue dotted and orange dashed lines) affects the dynamics of the lateral force in the frequency range of $f > 1\,\text{Hz}$ in particular. By changing the damping effect, the red and orange lines in the bottom plot of Figure 6.11 correspond to two different Maxwell elements, however they do not influence the tyre dynamics in high frequency areas. Hence, in both cases the hardening effect of the Maxwell element $c_{\text{dyn}} \to c_M$ characterised by $f_{95}^{\text{orange}} = 3.03\,\text{Hz}$ and $f_{95}^{\text{red}} = 6.05\,\text{Hz}$ already takes place at frequencies $f \leq 6\,\text{Hz}$ and has no further influence in the higher frequency range. The blue line represents a Maxwell element that hardens at a higher frequency ($f_{95}^{\text{blue}} = 12.1\,\text{Hz}$) and consequently impacts the dynamics of the lateral force.

By changing the damper values in Figure 6.11, a smaller effect is given due to the force ratio than varying the spring values, see the bottom plot of Figure 6.12. With

higher spring values c_{M}, an increasing hardening effect is given for higher frequencies. Nevertheless, this behaviour confirms the conclusion to use the mentioned frequency f_{95} for the final parameterisation process. Furthermore, the Maxwell element shifts the decrease of the effective lateral force to higher frequencies in all cases (red, blue, orange). This shift strongly depends on the damper value on the one hand, see upper plot of Figure 6.11 and the magnitude of the Maxwell stiffness c_M on the other hand, as can be seen by inspecting the plots on the right side of Figure 6.12.

In summary, for parameterising the dynamic hardening of an elastomer material, the Maxwell element seems to be a suitable choice. Furthermore, by taking the frequency f_{95} instead of the damping value into account, an easier parameterisation process is given from the technical point of view. Thereby, by using the elaborated results from Figure 6.9 and additionally the properties described above, the process itself can be carried out in a next step.

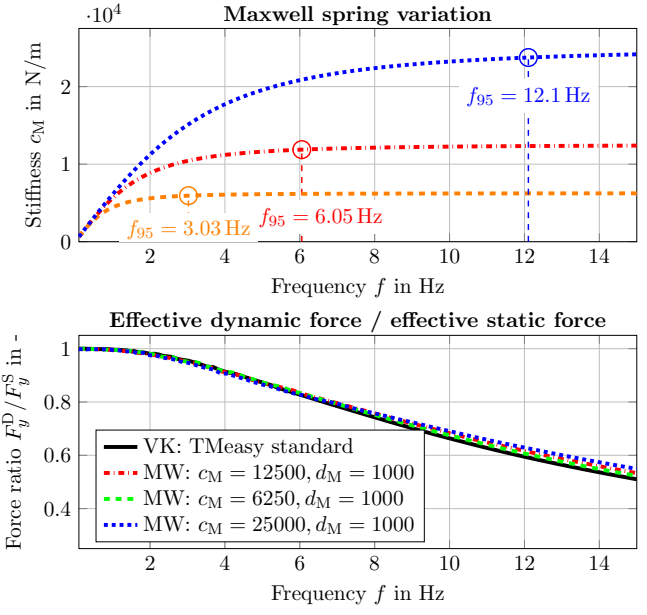

Figure 6.12.: Parameter-based Maxwell model characteristics; the upper plot presents the dynamic stiffness of the Maxwell element due to varying the spring value c_{M} versus the frequency, while the bottom plot presents the dynamic effect due to the static effective force of the Voigt-Kelvin (VK) as well as various Maxwell (MW) model parameter setups

6.3.3. Parameterisation process of the extended Maxwell model

After the confirmation of the frequency influence and the derivation of an extended transient model approach called the Maxwell model, the parameterisation process is explained in this subsection. Thereby, three model parameters in lateral as well as in longitudinal direction - namely the tyre stiffness $c_{x/y}$, the Maxwell stiffness $c_{x\mathrm{M}/y\mathrm{M}}$ and the frequency where the Maxwell element provides 95 % of its stiffness $f_{95,x/y}$ (short Maxwell frequency) - have to be defined, see Figure 6.10.

Based on the background of handling and semi-physical model approaches, a parameterisation process from the technical point of view with a low number of parameters is always preferred. Therefore, based on the results from Figure 6.9 in comparison to a fundamental investigation in Figure 6.11 and Figure 6.12, the decision was made to generalise the Maxwell frequency with $f_{95} = f_{95,x} = f_{95,y} = 10\,\mathrm{Hz}$. This was decided upon since this characteristic shows a good conformity with longitudinal and lateral results, and also gives a good boundary condition within the operating point for handling models with $f < 8\,\mathrm{Hz}$. A normal force-dependent Maxwell frequency would possible, and moreover it would be easy to implement and brings a slightly better conformity, but the decision for easier parameterability was made at this point and used further on.

In the second step the two remaining parameters, the tyre $c_{x/y}$ stiffness and the Maxwell stiffness $c_{x\mathrm{M}/y\mathrm{M}}$ are parameterised together, but separately longitudinally and laterally. Because a normal force dependency has proven to be a suitable implementation, this is used for both implementations here as well. Thereby, based on the property that the tyre spring and the dynamic stiffness c_{dyn} act in parallel, the behaviour from Figure 6.9 can be taken into account. Therefore, based on the frequency-dependent spring characteristics, a tyre stiffness at $f = 0\,\mathrm{Hz}$, named $c_{x0/y0}$, and a Maxwell stiffness for increasing frequency can be defined for each normal force in lateral and in longitudinal direction, as can be seen Figure 6.13.

In a next step, the defined normal force-dependent values can be interpolated linearly, and implemented with the standard TMeasy interpolation characteristics, see Figure 6.14, whereby the value results are given in Table 6.2. This leads to an implementation that is based on TMeasy, for each normal force application. Hence, the non-physical spring value $c_{x\mathrm{M},2}$ for the UR3 tyre results from the interpolation at high normal force application $2\,F_z^{\mathrm{N}} = 9000\,\mathrm{N}$. Therefore, a boundary condition is used with $c_{x\mathrm{M}} \geq 0$ in this thesis. Alternatively, a linearisation with $c_{x\mathrm{M},2} = 0\,\mathrm{N/m}$ is possible, but this causes worse interpolation with the defined measurement points. A non-linear interpolation is a possibility, but with only three normal force sampling points it is not taken into account within these investigations.

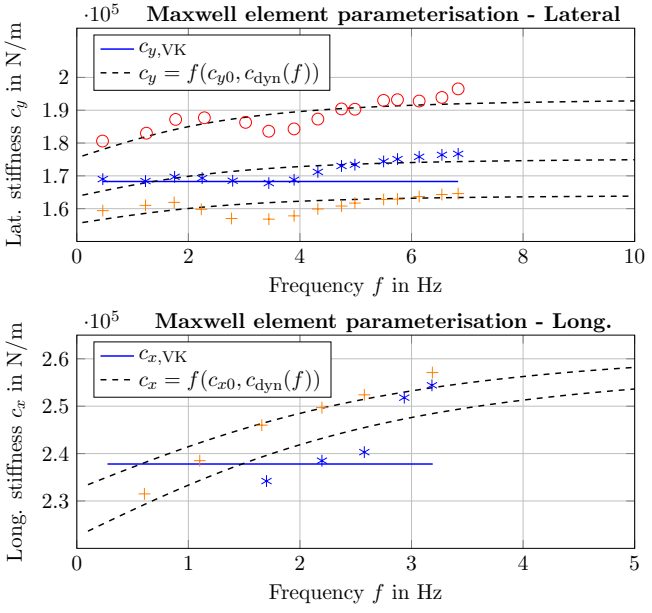

Figure 6.13.: Parameterisation of the extended Maxwell model for transient tyre behaviour; the upper plot represents results in lateral direction and the lower plot in longitudinal direction for different wheel loads for the PP0 tyre

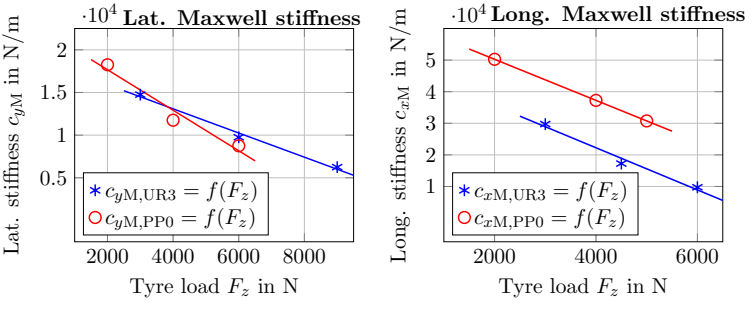

Figure 6.14.: Parameterised Maxwell stiffness in lateral (left) and longitudinal (right) direction for the tyres used, Uniroyal Rainsport3 255/50 R19 107Y (UR3) and Pirelli Pzero 245/40 R20 99W (PP0), at different wheel loads

Table 6.2.: Maxwell tyre stiffness parameters in lateral and longitudinal direction for the tyres used, Uniroyal Rainsport3 255/50 R19 107Y (UR3) and Pirelli Pzero 245/40 R20 99W (PP0); normal force dependent lateral and longitudinal tyre stiffnesses as well as Maxwell stiffnesses are used

Parameter	**Value**	**Description**
Uniroyal Rainsport3 255/50 R19 107Y (UR3)		
f_{95}	10	Frequency where Maxwell element provides 95 % of its stiffness in Hz
$c_{y0,1}$	189920	Lat. tyre stiffness at F_z^{N} in N/m
$c_{y0,2}$	181670	Lat. tyre stiffness at $2\,F_z^{\mathrm{N}}$ in N/m
$c_{y\mathrm{M},1}$	12375	Lat. Maxwell stiffness at F_z^{N} in N/m
$c_{y\mathrm{M},2}$	6000	Lat. Maxwell stiffness at $2\,F_z^{\mathrm{N}}$ in N/m
$c_{x0,1}$	265780	Long. tyre stiffness at F_z^{N} in N/m
$c_{x0,2}$	286410	Long. tyre stiffness at $2\,F_z^{\mathrm{N}}$ in N/m
$c_{x\mathrm{M},1}$	18920	Long. Maxwell stiffness at F_z^{N} in N/m
$c_{x\mathrm{M},2}$	(-11080)	Long. Maxwell stiffness at $2\,F_z^{\mathrm{N}}$ in N/m
Pirelli Pzero 245/40 R20 99W (PP0)		
f_{95}	10	Maxwell frequency in Hz
$c_{y0,1}$	169920	Lat. tyre stiffness at F_z^{N} in N/m
$c_{y0,2}$	154920	Lat. tyre stiffness at $2\,F_z^{\mathrm{N}}$ in N/m
$c_{y\mathrm{M},1}$	15290	Lat. Maxwell stiffness at F_z^{N} in N/m
$c_{y\mathrm{M},2}$	8165	Lat. Maxwell stiffness at $2\,F_z^{\mathrm{N}}$ in N/m
$c_{x0,1}$	212500	Long. tyre stiffness at F_z^{N} in N/m
$c_{x0,2}$	242500	Long. tyre stiffness at $2\,F_z^{\mathrm{N}}$ in N/m
$c_{x\mathrm{M},1}$	43750	Long. Maxwell stiffness at F_z^{N} in N/m
$c_{x\mathrm{M},2}$	24250	Long. Maxwell stiffness at $2\,F_z^{\mathrm{N}}$ in N/m

In summary, during this subsection a parameterisation process for the extended transient model approach, called the Maxwell model, was presented. Stiffness behaviour generated by a sweep manoeuvre and mathematical properties of a Maxwell element were taken into account. In addition, only two further parameters in lateral and longitudinal direction had to be defined, based on the predefined Maxwell frequency. Furthermore, a linear interpolation for the tyre as well as for the Maxwell stiffness was chosen for easy implementation with standard TMeasy characteristics. This approach presented an improvement for modelling the dynamic hardening effect of a tyre within increasing frequency response. An overall validation based on a Bode plot as well as general force deviation is given in the next subsection.

6.3.4. Validation of the extended Maxwell model

To prove the better performance of the extended Maxwell model in comparison to the standard Voigt-Kelvin approach, a validation is carried out in this subsection. For this, the magnitude ratio and phase response as well as a frequency-based accuracy comparison is done by means of the sine sweep in a first step, followed by a comparison of time-based step-steer manoeuvres in a second step. As both the standard as well the extended transient tyre characteristics implemented in the TMeasy tyre model exhibit non-linear behaviour, common methods like Bode plot generation with FFT or power and cross power spectral density estimation are not appropriate. Therefore a numerical approach by approximating each sine sweep period with a sine oscillation along with a cosine function oscillation is used. Thereby, amplitude and phase information for the simulated as well as the measured force approximation are taken into account to generate the magnitude and phase response characteristics.
Note that by assuming a linear system and using methods based on the transfer function, only small inaccuracies in comparison to the numerical methods result. This means that for a detailed investigation, for example the investigation carried out in this thesis, the numerical method along a sine sweep is recommended, but for a rough investigation linear assumptions still bring satisfactory results.

As a first validation, magnitude and phase responses based on the frequency sine sweep are performed with the PP0 tyre and three different wheel loads $F_{z,\mathrm{PP0}}$ are presented in Figure 6.15. Thereby, the measured and simulated transient steady-state force ratios $F_y^{\mathrm{D}}/F_y^{\mathrm{S}}$ are given in the upper plot and the phase response $\Delta\varphi$ in the plot below. For a normalised visualisation, the simulated steady-state force ratio serves as a basis for the measured $F_{y,\mathrm{meas}}$ in solid blue, the simulated Voigt-Kelvin $F_{y,\mathrm{VK}}^{\mathrm{D}}$ in dashed red and the simulated Maxwell $F_{y,\mathrm{MW}}^{\mathrm{D}}$ force in dot-dashed orange. Note that with increasing normal force, decreasing force ratios $F_y^{\mathrm{D}}/F_y^{\mathrm{S}}$ as well as a higher phase response $\Delta\varphi$ are given in general. Based on the solid blue line, which represents the measured force characteristics, a higher force ratio is given, especially at higher frequencies in comparison to the simulated characteristics. This corresponds to an increasing stiffness and hardening effect of a tyre. It seems this behaviour is more distinct at lower wheel loads, which corresponds with the increasing stiffness from Figure 6.9 at smaller normal force values.

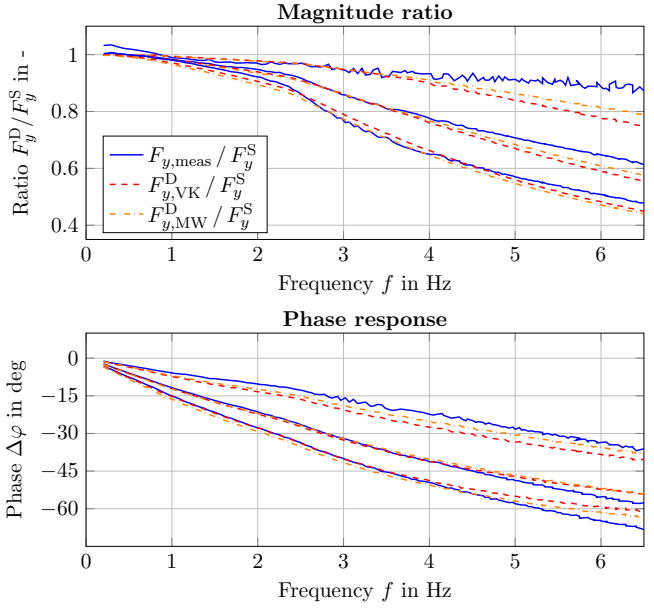

Figure 6.15.: Magnitude ratio and phase response in lateral direction for the PP0 tyre based on the frequency sine sweep for three different wheel loads $F_{z,\mathrm{PP0}}$; the simulated steady-state force serves as basis for the measured $F_{y,\mathrm{meas}}$ in solid blue, the simulated Voigt-Kelvin $F_{y,\mathrm{VK}}^{\mathrm{D}}$ in dashed red and the simulated Maxwell $F_{y,\mathrm{MW}}^{\mathrm{D}}$ force in dot-dashed orange

Hence, in lateral direction a combination of sidewall and tread rubber stiffness is given. The fact that at high normal forces the sidewall movement is more pronounced serves as possible explanation. Nevertheless, it is obvious that both models are not able to describe this behaviour in an ideal manner, but improvements are clearly present within the Maxwell model. The sharp bend at the highest wheel load of $f \approx 2.5\,\mathrm{Hz}$ is because, at this point, the test facility was not able to handle the constant amplitude of 4 deg with increasing frequency. Therefore, a decreasing slip angle results in non-linear model behaviour, which corresponds to this effect at the highest wheel load.

Furthermore, similar behaviour is given in the plot below, which represents the phase response between steady-state and dynamic tyre force. Especially for the middle normal force, both model characteristics can handle the phase response quite well up to high frequency areas. However for the highest and lowest wheel load, deviations are present.

The Maxwell model thus shows improvements, particularly at lower normal forces. In summary, a non-linear behaviour based on measurement data is presented for different normal forces and a wide range of frequencies. Both models perform satisfactorily, though an improvement in the magnitude ratio and phase response is given by the Maxwell model. Similar behaviour is given for the UR3 tyre in lateral direction.

In a next step, the model comparison based on the longitudinal frequency sine sweep manoeuvre for the UR3 tyre at three different wheel loads $F'_{z,\mathrm{UR3}}$ is shown in Figure 6.16. As in lateral direction, the steady-state longitudinal force serves as the basis ratio for the measured force $F_{x,\mathrm{meas}}$ in solid blue, the simulated Voigt-Kelvin $F^{\mathrm{D}}_{x,\mathrm{VK}}$ in dashed red and the simulated Maxwell $F^{\mathrm{D}}_{x,\mathrm{MW}}$ in dot-dashed orange.

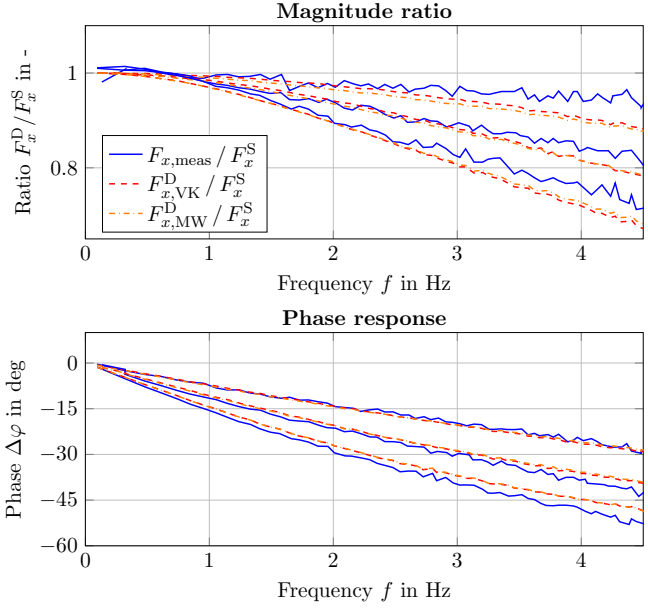

Figure 6.16.: Magnitude ratio and phase response in longitudinal direction for the UR3 tyre based on the frequency sine sweep for three different wheel loads $F'_{z,\mathrm{UR3}}$; the simulated steady-state force serves as basis for the measured $F_{x,\mathrm{meas}}$ in solid blue, the simulated Voigt-Kelvin $F^{\mathrm{D}}_{x,\mathrm{VK}}$ in dashed red and the simulated Maxwell $F^{\mathrm{D}}_{x,\mathrm{MW}}$ force in dot-dashed orange

A similar overall behaviour to the lateral direction behaviour can be seen. For all normal forces, a higher magnitude ratio than in the simulation is given, whereby the effect increases with lower wheel loads. Again, both model applications are not able to approximate the behaviour sufficiently. Furthermore, nearly no differences between the Voigt-Kelvin and Maxwell model are present. The reason for this can easily be derived from Figure 6.9. Only a very small influence in normal force dependency is given, so this model extension loses its effect. Additionally, due to the smaller hardening effect compared to the lateral direction, the improvements of the model extension are also smaller. This means, in summary, that a similar behaviour is given. By comparing the model approaches with the PP0 tyre in longitudinal direction, a better performance at higher normal force is given.

In summary, the Maxwell model is able to reduce the deviation in a satisfactory manner in comparison to the Voigt-Kelvin model. Especially improvements in lateral direction based on investigations with the magnitude ratio and phase response definitively count as an overall improvement.

Another possibility to present the increased model accuracy by means of the Maxwell model in comparison to the Voigt-Kelvin is given in Figure 6.17. The PP0 tyre, based on the frequency sine sweep and three different wheel loads $F_{z,\mathrm{PP0}}$, is used.

Thereby, the Euclidean norm ratio of the Maxwell and Voigt-Kelvin model deviation is compared with respect to each of the time periods used or frequency bands. Further on, $\boldsymbol{e}_{\mathrm{MW}}$ represents the error vector between measured and simulated Maxwell lateral

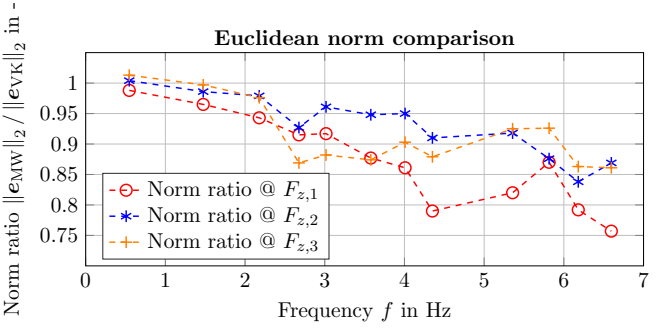

Figure 6.17.: Euclidean norm for the model comparison for the PP0 tyre based on the frequency sine sweep manoeuvre in lateral direction and three different wheel loads $F_{z,\mathrm{PP0}}$; where $\boldsymbol{e}_{\mathrm{MW}}$ represents the error vector between measured and simulated Maxwell lateral force, and $\boldsymbol{e}_{\mathrm{VK}}$ the error vector between the measured and Voigt-Kelvin model

force and $\boldsymbol{e}_{\mathrm{VK}}$ the one between the measured and Voigt-Kelvin model, whereby two main facts are given in this figure. First, the main goal that the extended model approach is also accurate with low frequency areas, and second, increasing improvements with increasing frequencies are present for all three wheel load applications. The fact that the Voigt-Kelvin spring value is rated at higher wheel loads enables the best improvements with small normal force applications. Hence, similar improvements are also given with the UR3 tyre for lateral investigations.

In longitudinal direction, overall a lower improvement of about maximum 10 % for the PP0 tyre and even lower for the UR3 tyre is given. Hence, less potential for improvement is also attributed to the effect that longitudinal investigations are harder to handle in general. Different tyre behaviour during accelerating and braking increases the overall inaccuracy from the fundamental steady-state behaviour. Furthermore, longitudinal slip control is harder to handle in a test facility, which leads to higher oscillations and measurement noise behaviour.

Finally, step-steer manoeuvres in lateral direction are used to complete the validation process. Thereby, randomly generated slip angle step-steers, as was already presented in Figure 6.5 left, are applied to a tyre under fixed wheel load conditions. To evaluate the model performance, the same target setting can be used as input for the standard and extended transient tyre model and compared with the measured force, see Figure 6.18.

Based on this process, four comparison plots are presented, in the two plots left the results for the UR3 tyre at a wheel load of $F_z = 9000\,\mathrm{N}$ and in the two plots right results from the PP0 tyre at $F_z = 6000\,\mathrm{N}$ are given. Furthermore, one positive as well as one negative step-steer manoeuvre is applied with various start and end slip angle values. First, a sufficient overall performance is seen for both types of model applications and tyres. Still, by comparing the standard Voigt-Kelvin and the extended Maxwell model in detail, an improvement is given for all four manoeuvres. This confirms the previous evaluation that modelling the dynamic hardening effect of a tyre leads to the better performance of the tyre model. Especially for manoeuvres where the steady-state force at the start and end is close to the measured one, a high conformity over all manoeuvres was observed.

In summary, this confirms the overall statement of the thesis that a model, which is able to describe the dynamic hardening effect of the tyre, allows for better performance, especially with high frequency manoeuvres. Nevertheless, extensions only bring improvements if an accurate standard model, including best possible parameters, is used.

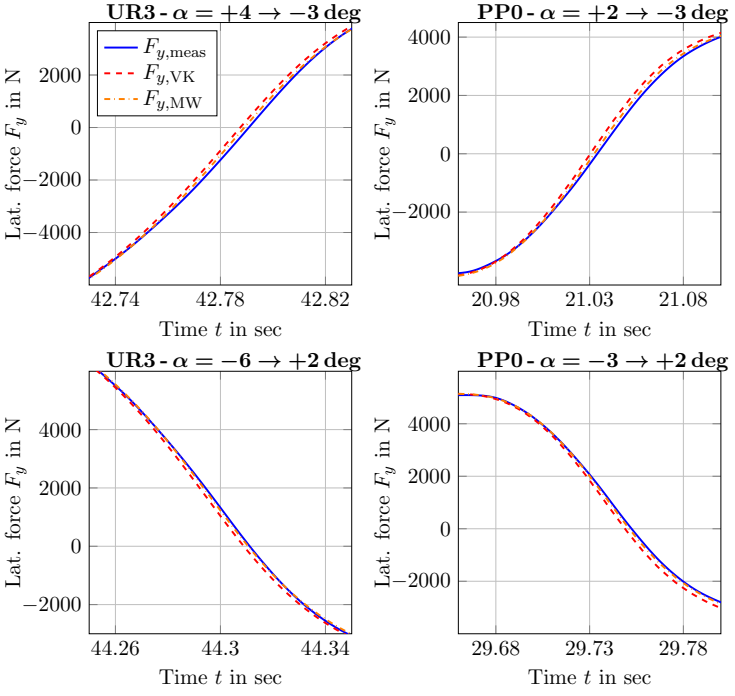

Figure 6.18.: Model validation of the Voigt-Kelvin and extended Maxwell model by means of step-steer manoeuvres for various start and end slip angle values; the two plots on the left show results for the UR3 tyre at a wheel load of $F_z = 9000\,\mathrm{N}$, and the two plots on the right show results for the PP0 tyre at $F_z = 6000\,\mathrm{N}$

6.4. Comparative conclusion on transient tyre model approach validation

Handling and semi-physical tyre model approaches are still widely used, especially within *advanced driver assistance systems* (ADAS) and *vehicle dynamics controller* (VDC) applications. Because rubber physics allow force effects that are not steady-state in nature, most model applications have a transient model approach already implemented. The review of the literature from Chapter 2 has shown that first-order applications are common and widely used for this kind of model applications, for example as implemented in the TMeasy tyre model that is used in this thesis.

Nevertheless, basic analyses of a non-rolling tyre have shown that the transient model approach based on a spring and damper element presents sufficient model accuracy with a fixed operating point, but improvement potential became apparent outside this area. Thereby, the linear spring behaviour, which is represented by a constant value for the Voigt-Kelvin application, was validated first. It has been demonstrated that overall a non-linear behaviour is more realistic, but the linear approach is suitable for most practical applications. In a second step, displacement manoeuvres with various frequency targets were applied and investigated for a non-rolling tyre. A high influence on dynamic tyre behaviour was mainly presented, while the Voigt-Kelvin application was not able to handle this influence within an accurate range. The reason is that a more detailed model approach is needed - one based on frequency influence to model the physical hardening effect of a tyre.

Based on the experience gained with the non-rolling tyre, results were confirmed with measurements on an industrial flat track test bench. Validation of the widely applied Voigt-Kelvin model was also carried out here as a first step. Increasing stiffness behaviour in longitudinal direction and decreasing in lateral direction based on increasing wheel loads was shown. By implementing this effect with a standard linear TMeasy function, a model improvement of about 5 % was achieved. Afterwards, the focus went to frequency-based investigations. To do so, a sine sweep was defined as the main applicable manoeuvre by comparing different literature-based targets. By applying this manoeuvre to a rotating tyre and various wheel loads, increasing stiffness behaviour became apparent with increasing frequencies.

Therefore, in order to model this typical effect of dynamic frequency-dependent hardening of elastomer materials, an extended model approach was taken into account for transient manoeuvres. Because a mathematical polynomial frequency-dependent spring implementation is not practical for handling modelling, a Maxwell model which is able to handle this effect was presented and parameterised by using parameters with physical background. Finally, the extended Maxwell model application was evaluated with measurement data and compared to the Voigt-Kelvin application. It has been demonstrated that the extended Maxwell model increases in accuracy in comparison to the standard Voigt-Kelvin approach, especially within high frequency areas.

In summary, this confirms the overall statement of the thesis that a model, which is able to describe the dynamic hardening effect of the tyre, allows for better performance, especially for high frequency manoeuvres. Nevertheless, extensions only bring improvements if an accurate standard model, including parameters, is used.

7

Summary and Conclusion

Modelling and simulation of safety-relevant *advanced driver assistance systems* (ADAS) and *vehicle dynamics controller*s (VDCs) has become a state of the art tool to reduce development time, limit safety risks and save costs. The growing demands for lower computation effort, higher accuracy and easier parameterability increase the expectations surrounding vehicle models and driver models as well as environment models. Therefore, the demand for higher accuracy in tyre modelling for vehicle dynamics and handling applications is a further outcome.

This thesis deals with the influences of tyre temperature as well as the modelling of transient tyre force behaviour. Special focus goes to handling and semi-physical tyre model approaches, which are still widely applied in the field of ADAS and VDC. To provide a knowledge basis, the analysis of these aspects was carried out in different chapters, which are summarised below and concluded with a final statement at the end.

Chapter 1: Introduction In the first chapter an overview of the significance of modelling and simulation for safety-relevant ADAS and VDC was presented. Moreover, the statement was made that a vehicle model alone is hardly capable of describing real world conditions. This means that, in addition to a realistic vehicle model, a description of the environment, a driver and their interactions are required to handle all conditions precisely. Furthermore, a more detailed vehicle model leads to a higher demand for accuracy in tyre modelling and vice versa. Consequently, greater focus has to go to the model description and parameterability in the field of tyre modelling.

Chapter 2: Tyre model approaches Chapter two started with an extensive literature overview of existing tyre model approaches for automotive applications. As a result, based on ADAS and VDC systems, semi-physical handling models turned out to offer a reasonable compromise between accuracy, parameterability and calculation time for further tyre investigations. Therefore, the decision to use the TMeasy tyre model for experimental investigations was made.
The focus then shifted to transient semi-physical tyre model approaches. Based on the stretched-string tyre model from *Von Schlippe and Dietrich*, state of the art applications were presented in more detail. It was shown that first-order approaches in particular are widely used, but also second-order non-linear applications exist that use a tyre mass. Concluding, different transient approaches have been implemented in tyre modelling applications already. However, such implementations are hardly able to handle simulations

in critical driving situations, they are based on mathematical approaches without any physical background or are still too complex for semi-physical modelling under real time conditions. Therefore, it is recommended that tyre modelling within higher frequency areas be covered by semi-physical tyre model approaches. Nevertheless, another main factor became clear during this study. In almost all semi-physical transient model applications, an interaction with the steady-state tyre force characteristics is implemented, so the inaccuracies of steady-state characteristics are influencing transient tyre behaviour. Therefore, the intensity of these influences and the consequences of these inaccuracies were the focus of the next chapter.

Chapter 3: External influences on steady-state characteristics The third chapter started with a sensitivity analysis, which showed that inaccuracies in steady-state behaviour influence dynamics modelling considerably and should not be neglected. Therefore, a literature study showed that nearly all external influences such as road conditions, tyre velocity and temperature changes interact and affect the steady-state characteristics. Since most of the external influences could be controlled from the test bench facility, the focus in this thesis was the influence of temperature. Consequently, a fundamental literature review covering tyre temperature behaviour and influences on tyre force was carried out. Finally, the chapter closed with the conclusion that a multi-layer temperature model best meets the technical requirements, and furthermore such a model interacts quite well with the handling and semi-physical model demands.

Chapter 4: TMeasy tyre model Before detailed investigations of temperature influences and transient effects were carried out, a basis tyre model setup was needed. Therefore, the fourth chapter described the parameterisation of the tyre model used. By comparing advantages and disadvantages of different test bench setups, the decision was made that measurements on an indoor flat track test bench is the best compromise for fundamental research of temperature and transient tyre effects. After introducing the concept of TMeasy, with a focus on steady-state modelling in longitudinal and lateral direction, the respective parameterisation process was presented and validated with measurements. This chapter then served as a basis for further investigations.

Chapter 5: Temperature and its impact on tyre forces Modelling the tyre temperature and its impact on tyre forces was the topic of the fifth chapter. Stemming from a description of different heat transfer mechanisms, a multi-layer model based on the first law of thermodynamics was formed to be a good modelling compromise. After focusing on the parameterisation process, different manoeuvres were used to validate the temperature model. Here, the agreement between measured and simulated data was satisfactory during warm-up as well as cooling manoeuvres.
Next, a method to model the influences of tyre temperature on steady-state tyre forces was presented. Impacts from bulk temperature on initial slope and surface temperature on maximum force and slip position were discussed in detail and confirmed by the literature. Based on this temperature-dependent behaviour, a model approach was presented using parameters having physical relevance. Afterwards, an implementation into the fundamental TMeasy model was done, followed by a detailed validation. By means of

various manoeuvres in lateral and longitudinal direction, it was shown that the extended approach is able to handle various conditions not only by calculating the temperature but also by calculating their impact on the tyre force characteristics in quite a sufficient manner.

Chapter 6: Transient tyre model approaches. Based on the temperature-extended TMeasy model described in Chapter 5, an experimental validation of semi-physical transient model approaches was carried out in Chapter 6. Early on, fundamental analyses of a non-rolling tyre were carried out. It was demonstrated that the transient model approach based on a Voigt-Kelvin model provides sufficient accuracy with a fixed operating point, but potential for improvement became apparent; in particular, changes in manoeuvre frequency were shown to greatly influence model accuracy. Based on the experience gained with the non-rolling tyre, a model extension was developed by means of measurements on a flat track test bench and presented.
In addition to normal force-dependent tyre stiffness in longitudinal and lateral direction, increasing stiffness behaviour became apparent at increasing frequencies. In order to model the effect of the hardening of elastomer materials that is dependent on the dynamic frequency, an extended model approach was developed to cover highly transient manoeuvres. Thus, an extended Maxwell model was presented, which has improved modelling accuracy compared to the Voigt-Kelvin model, especially in higher frequency ranges. In summary, it could be proven that a model that is able to describe the dynamic hardening effect of the tyre leads to better performance, particularly for high frequency manoeuvres.

Final statement: The presented thesis provides a well-grounded analysis of tyre model approaches, which are based on handling model applications with a focus on temperature influences and transient tyre force behaviour. Thus, the limits of conventional dynamic model first-order and higher order approaches were systematically analysed and evaluated. It could be demonstrated that steady-state tyre characteristics influence transient force modelling for most state of the art model applications. Conversely, common first-order approaches present sufficient model accuracy within a fixed operating point, but improvement potential became apparent outside this area. In order to ensure sufficiently accurate steady-state tyre characteristics, by means of external influences during test bench investigations, a temperature model including its impact on tyre force behaviour was first developed, validated and implemented in the standard TMeasy tyre model. Finally, the implementation of an extended semi-physical Maxwell model approach was shown to be able to improve performance accuracy based on practical investigations, especially for highly dynamic manoeuvres.

In summary, the extensions by means of the multi-layer based temperature model and the Maxwell model satisfactorily increase the accuracy and validity of the tyre model. This leads to higher overall model accuracy in vehicle/environment simulations and to an improvement in the representation of tyre and vehicle behaviour for various ADAS and VDC testing.

A

Basic theory of sensitivity analysis

Sensitivity analyses are often used for parameter studies when values or initial conditions of systems are not accurately known or for modelling simplification if effects can be neglected in basic models. A parameter is defined as sensitive when small changes of the value lead to big changes in the results.

Based on [Campolongo et al., 2000], sensitivity analyses can be categorised into *factor screening*, *local* and *global methods*. Factor screening is especially useful for complex models with a large number of input variables. This method first seeks to filter the variables that have the greatest impact on the model results and sort them afterwards according to their weightings. One-at-a-time experiments are a specific type of factor screening. They analyse the effects of changes to the input quantities. The fact that this method focuses on a local point and does not consider the interaction between the factors should be taken into account for detailed investigations.

Global methods (like Monte Carlo analysis) carry out multiple evaluations with random factors to determine the overall risk of the model and the individual risk of each variable. The variability of all variables is analysed and considered simultaneously. However, the sensitivity and furthermore a ranking cannot be assigned to the parameters with this method. In addition, global methods also require a lot of simulation time.

Local methods analyse the local influence of a parameter at a given point. This leads to an easy method in which the sensitivity can be clearly assigned to an input variable. However, local methods are often modelled as initial-value *ordinary differential equation*s (ODEs), which leads to the conclusion that local methods are quite suitable for our problem. As a special case for the local method, this work focuses on a *quasi-direct approach*, where the (linear) *first-order local sensitivity coefficients* of non-linear models are calculated. This method, with the mathematical fundamentals from [Dickinson & Gelinas, 1976], was worked out and evaluated with experimental data from [Lex, 2015] in which the sensitivity influence of vehicle data on road friction estimation was investigated.

In this approach, it is assumed that the investigated model is given by a non-linear, time-dependent ODE in the form of $\dot{\boldsymbol{z}} = \boldsymbol{f}(z_1, \ldots, z_n, t, \boldsymbol{c})$ with $l = 1, \ldots, n$ elements in the state vector $\boldsymbol{z}$ and $m = 1, \ldots, o$ elemtents in parameter $\boldsymbol{c}$. The linear sensitivity of the given model is given by $\boldsymbol{p} = \frac{\partial \boldsymbol{z}}{\partial c_m}$ with respect to a parameter c_m. For each of the o parameters n, ODE have to be solved for $\boldsymbol{z}$.

By using the time integral with $\dot{p}_l = \frac{\partial}{\partial t}(p_l)$, the sensitivity p_l for the lth state variable can be calculated by

$$\dot{p}_l = \frac{\partial f_l}{\partial c_m} + \sum_{d=1}^{N} \frac{\partial f_l}{\partial z_d} \cdot \frac{\partial z_d}{\partial c_m}\,, \tag{A.1}$$

were f_l is positioned on the right-hand side of $\dot{z}_l$, [Dickinson & Gelinas, 1976]. By using the Jacobian matrix $\boldsymbol{J}$ and defining $\boldsymbol{f}_c$ as the sensitivity of the right-hand side $\boldsymbol{f}$ with respect to c_m, Equation A.1 becomes

$$\dot{\boldsymbol{p}} = \boldsymbol{f}_c + \boldsymbol{J} \cdot \boldsymbol{p}\,. \tag{A.2}$$

To solve the problem given in Equation (A.2), initial values have to be provided. Based on [Dickinson & Gelinas, 1976], the value for initial sensitivity $p_l(0)$ is defined by its limit

$$p_l(0) = \lim_{\Delta c_m \to 0} \frac{z_l\left(c_m + \Delta c_m, 0\right) - z_l\left(c_m, 0\right)}{\Delta c_m}\,. \tag{A.3}$$

Therefore, two cases can be distinguished in terms of whether a parameter is an explicit initial condition of any state variable or not. As a first case, where c_m is not an initial condition of any of the state variables, the whole numerator of Equation (A.3) becomes zero and the initial sensitivities are given as $p_l(0) = 0$. As a second case, the parameter c_m is an explicit initial condition of the n-th state variable z_n. Thus, the numerator term results in $p_l(0) = 1$. In summary, the initial sensitivities lead to

$$p_{l=n}(0) \;=\; 1\,, \tag{A.4}$$

$$p_{l\neq n}(0) \;=\; 0\,. \tag{A.5}$$

Thus, by solving the derivatives in Equation (A.2) analytically and using the boundary condition from boundary Equation (A.4) and (A.5), the sensitivity of first-order differential equations can be calculated.

For detailed descriptions and further use cases involving this method, reference [Lex, 2015].

B

TMeasy model validation

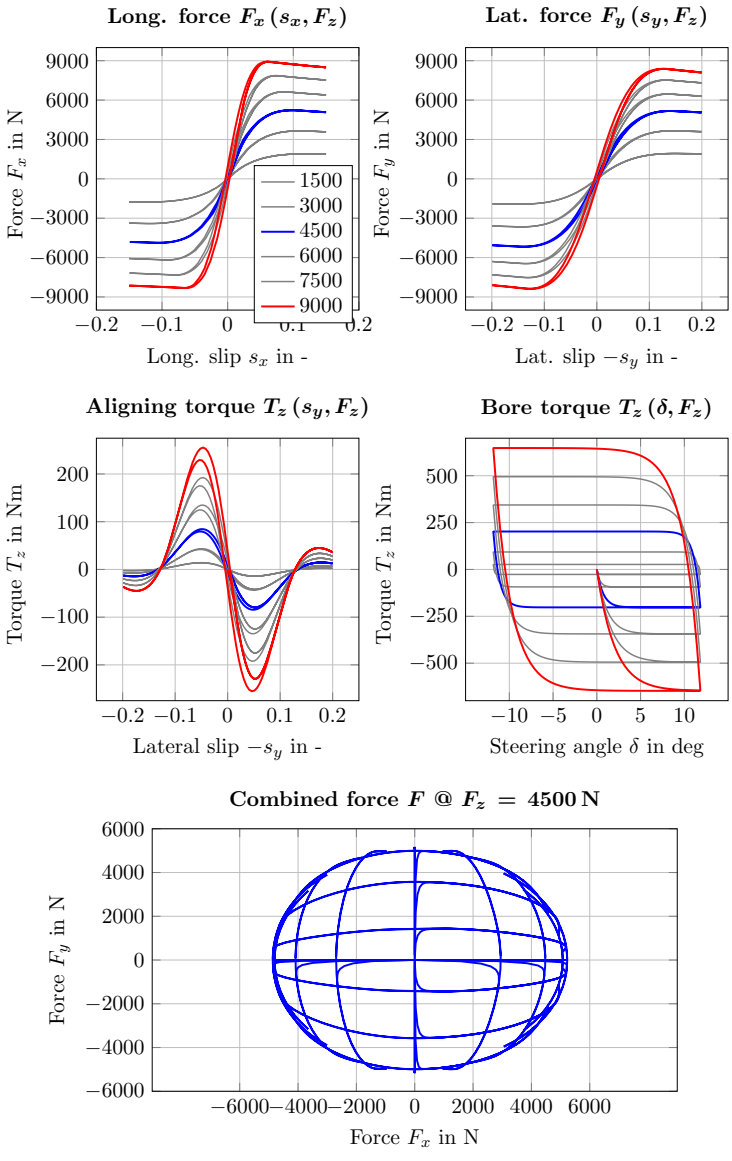

Figure B.1.: TMeasy model characteristics - Uniroyal Rainsport3 255/50 R19 107Y tyre

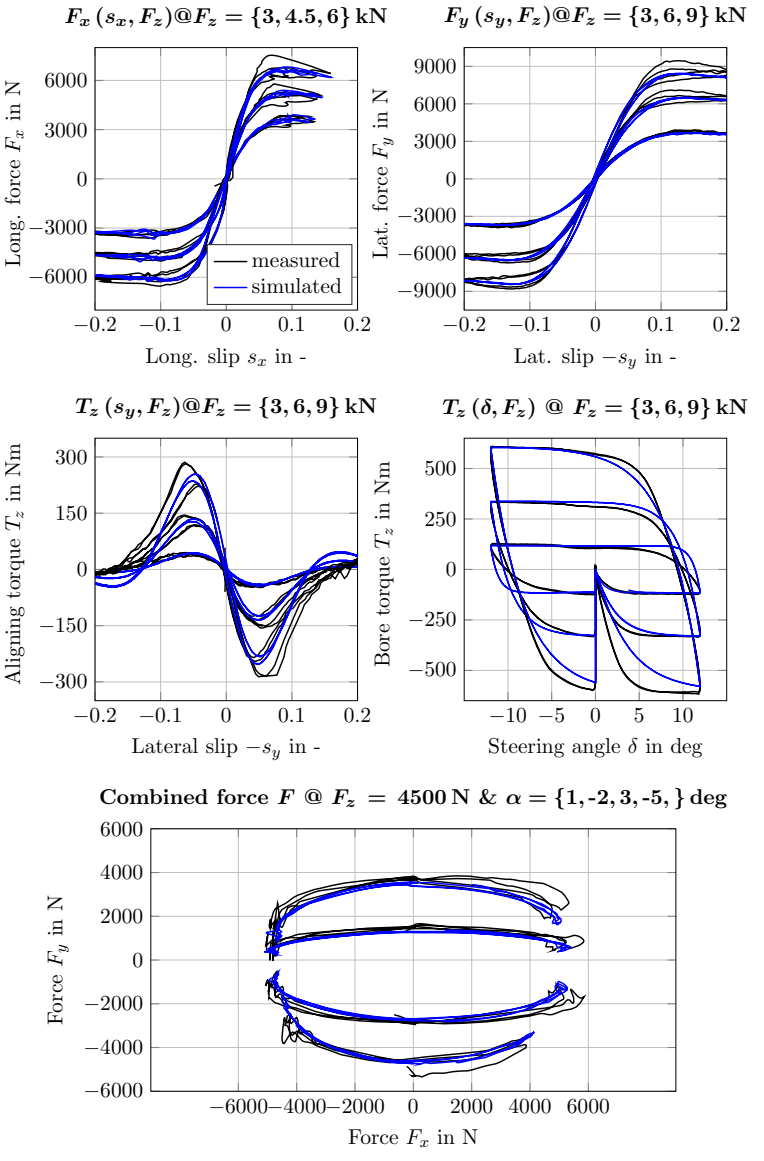

Figure B.2.: Model validation of the parameterised TMeasy characteristics for the Uniroyal Rainsport3 255/50 R19 107Y tyre

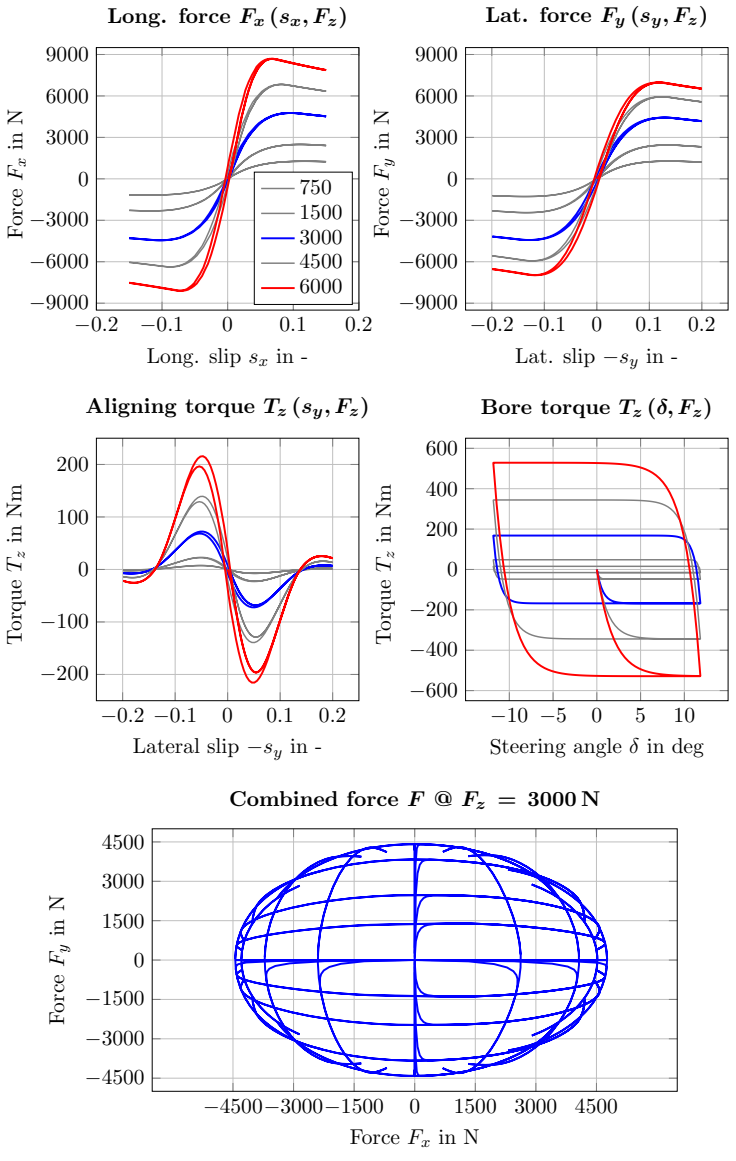

Figure B.3.: TMeasy model characteristics - Pirelli Pzero 245/40 R20 99W tyre

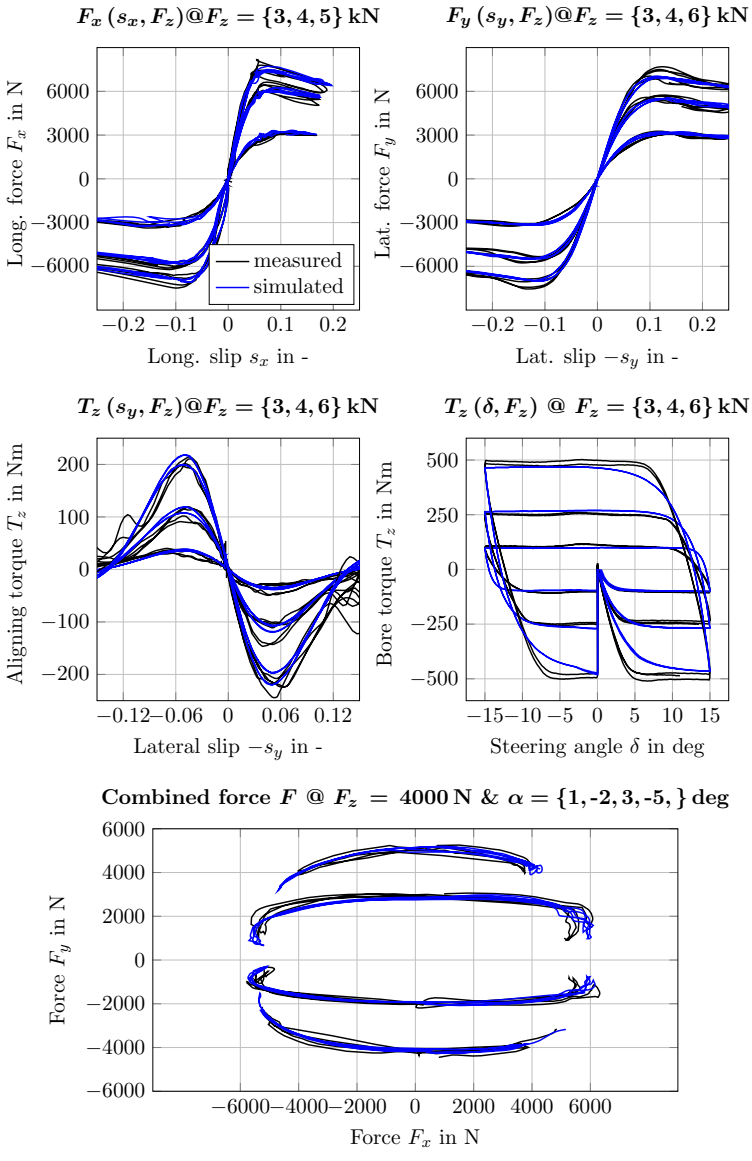

Figure B.4.: Model validation of the parameterised TMeasy characteristics for the Pirelli Pzero 245/40 R20 99W tyre

C

First law of thermodynamics applied to a tyre in use

In general, the first law of thermodynamics can be stated as

$$\delta Q + \delta W \;=\; \mathrm{d}E_a + \mathrm{d}U\,, \tag{C.1}$$

where δQ is the quantity of energy added to the system by a heating process, δW is the quantity of energy lost by the system due to work done by the system, $\mathrm{d}E_a$ is the changing potential or kinetic energy and $\mathrm{d}U$ is the change in the internal energy of the system, [Klell & Almbauer, 2015].

This equation is used on a defined system and is simplified in the process. In the case of a tyre, the system being considered is closed in nature without any entering or exiting mass flows or energy flows, as shown in Figure C.1.

Because neither potential nor kinetic energy $\mathrm{d}E_a$ is entering or leaving the system, this term is eliminated from Equation (C.1). Additionally all of the work entering the system δW is occurring as friction work, either between the tyre and the road or because of internal friction from hysteresis effects. For this reason work can be seen as irreversible

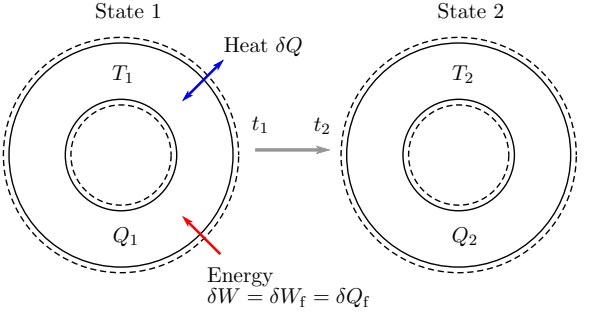

Figure C.1.: Schematic representation - first law of thermodynamics applied to a tyre in use

since the generated heat can't be converted back to work.

Therefore, the induced work

$$\delta W \;=\; \delta W_{\mathrm{f}} \;=\; P_{\mathrm{h}} + P_{\mathrm{f}}\,, \tag{C.2}$$

can be written as heat energy δQ_{f}. With these simplifications, the first law of thermodynamics can be stated as

$$\delta Q + \delta Q_{\mathrm{f}} \mathrel{\widehat{=}} \delta Q \;=\; \mathrm{d}U \tag{C.3}$$

or furthermore, regarding the mass inside the system, by

$$\delta Q \;=\; m\,\mathrm{d}u\,. \tag{C.4}$$

Since the observed system is a solid, which means the volume is almost entirely independent from temperature changes, the internal energy $\mathrm{d}u$ can be expressed by

$$c_p \;=\; \frac{\mathrm{d}u}{\mathrm{d}T}\,. \tag{C.5}$$

With all of these simplifying assumptions, Equation (C.4) can be written as

$$\delta Q \;=\; m\,c_p\,\mathrm{d}T\,. \tag{C.6}$$

With respect to the change of state displayed in Figure C.1, this equation can be integrated from the first to the second state with

$$\int_1^2 \mathrm{d}Q \;=\; m\,c_p \int_{T_1}^{T_2} \mathrm{d}T\,. \tag{C.7}$$

Therefore, the change in temperature between first and second state depends on the entering or exiting of thermal energy or heat by

$$Q_{12} = m\,c_p\,\Delta T\,. \tag{C.8}$$

Additionally this equation can be integrated over a period of time to calculate temperature changes ΔT per time Δt with

$$\int_{t_1}^{t_2} Q_{12}\,\mathrm{d}t \;=\; m\,c_p \int_{t_1}^{t_2} \Delta T\,\mathrm{d}t\,, \tag{C.9}$$

and simplified with the following mathematical steps by

$$\begin{aligned} Q_{12}\,(t_2 - t_1) &= m\,c_p\,\Delta T\,(t_2 - t_1)\,, \\ Q_{12}\,\Delta t &= m\,c_p\,\Delta T\,\Delta t\,, \\ \frac{Q_{12}}{\Delta t}\,\Delta t &= m\,c_p\,\Delta T\,, \\ \dot{Q}_{12}\,\Delta t &= m\,c_p\,\Delta T\,. \end{aligned}$$

By concluding these final steps with all occurring heat flows applied, the first law of thermodynamics can be

$$\sum_i \dot{Q}_i \,\frac{\Delta t}{m\,c_p} = \Delta T\,, \tag{C.10}$$

with the physical units

$$\left[\frac{\mathrm{J}}{\mathrm{s}}\right]\left[\frac{\mathrm{s}}{\mathrm{kg}\,\frac{\mathrm{J}}{\mathrm{kg\,K}}}\right] = [\mathrm{K}]\,. \tag{C.11}$$

D

Temperature model data

D.1. Uniroyal Rainsport3 255/50 R19 107Y

Table D.1.: Tyre temperature model parameter - UR3 tyre; subdivided into general, tyre-based and optimised values

Parameter	Value	Description
General		
$c_{p,\text{steel}}$	450	Specific heat capacity steel in J/(kg K)
$c_{p,\text{SBR}}$	1800	Specific heat capacity SBR in J/(kg K)
$c_{p,\text{belt}}$	1125	Specific heat capacity belt in J/(kg K)
λ_{steel}	10	Thermal conductivity steel in W/(m K)
λ_{SBR}	0.275	Thermal conductivity SBR in W/(m K)
$h_{\text{b-i}}$	1	Heat transfer coeff. filling medium in W/(m^2 K)
$c_{\text{s},1}$	0.3	Scaling value contact patch, lower boundary in -
$c_{\text{s},2}$	0.8	Scaling value contact patch, upper boundary in -
Tyre based		
s_{circ}	2.316	Tyre circumference in m
w_{t}	0.255	Tyre width in m
A_{t}	0.5920	Tyre of tread area in m^2
g_f	0.68	Groove factor in -
m_{tyre}	9	Mass tyre tread (without tyre walls) in kg
m'_{SBR}	0.35	Rubber SBR mass in kg/mm
d_{belt}	5	Thickness belt (steel/SBR) in mm
d_{SBR}	3	Thickness SBR without profile in mm
Optimised		
$h'_{\text{s-r}}$	185.87	Heat transfer coefficient surface-road in W/(m^2 K)
h_0	3.23	Speed independent value of $h_{\text{t-a}}$ in W/(m^2 K)
h_{v}	2.23	Speed dependent value of $h_{\text{t-a}}$ in (W/(m^2 K)) / (m/s)
p_z	0.0045	Dimensionless scaling value due hysteresis in -
T^{N}	51.82	Power distributed nominal temperature in degC
δ_{s}	0.3	Thickness of tyre surface layer in mm

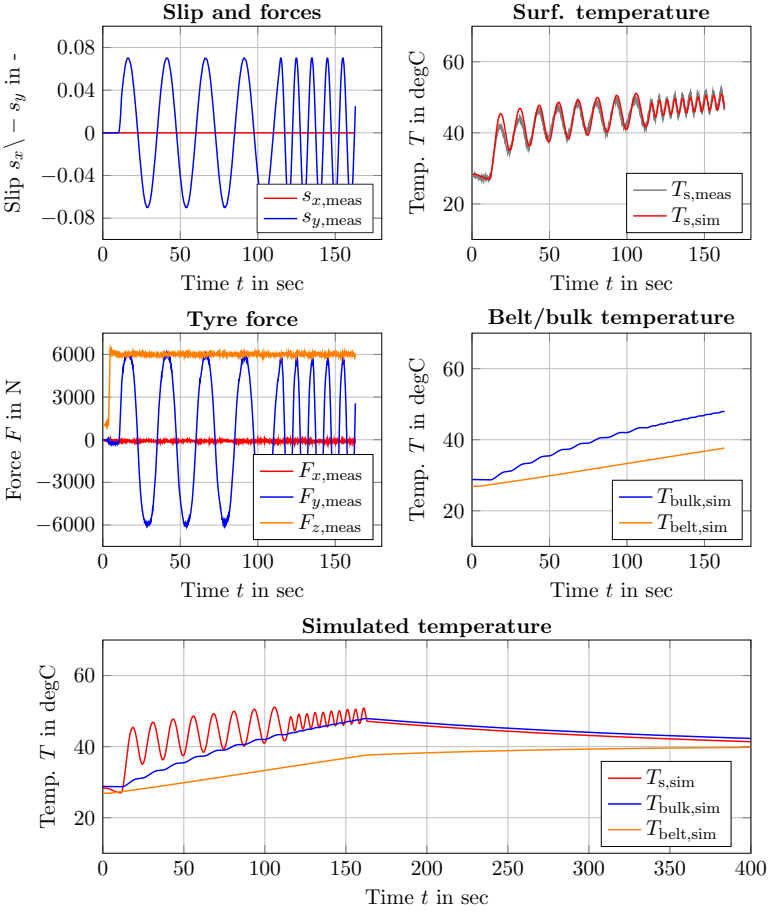

Figure D.1.: Validation of the parameterised temperature model based on the Uniroyal Rainsport3 255/50 R19 107Y tyre and a warm-up manoeuvre in lateral direction; the upper left plot shows the slip target whereby the measured forces are given in the middle left plot; the upper right plot shows the measured and simulated surface temperature, whereby in the middle plot, the belt and bulk layer temperatures are displayed; the bottom plot presents the simulated tyre layer temperature behaviour, including the cooling process for the whole manoeuvre

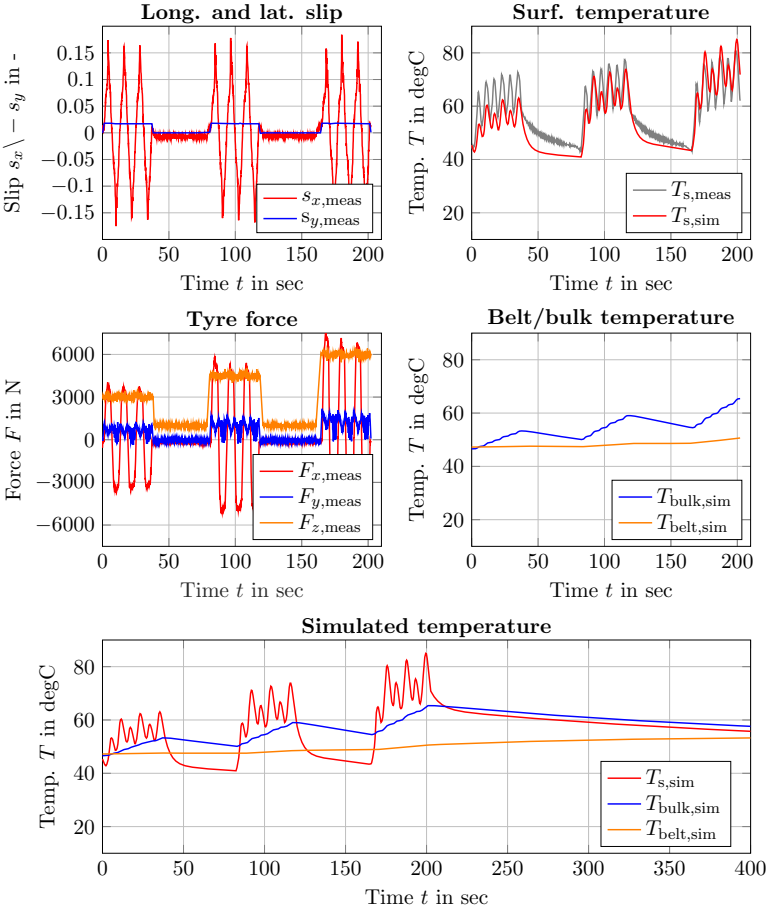

Figure D.2.: Validation of the parameterised temperature model based on the Uniroyal Rainsport3 255/50 R19 107Y tyre and a combined slip manoeuvre; the upper left plot describes the slip target whereby the measured forces are given in the middle left plot; the upper right plot shows the measured and simulated surface temperature, whereby in the middle plot the belt and bulk layer temperatures are displayed; the bottom plot presents the simulated tyre layer temperature behaviour, including the cooling process for the whole manoeuvre

Table D.2.: Extended model parameter based on temperature influence in lateral direction for the Uniroyal Rainsport3 255/50 R19 107Y tyre

Parameter	Value	Description
General		
F_z^{T}	6000	Temperature based nominal tyre load in N
$T_{y,1}^{\mathrm{N}}$	60	Nominal temp. at F_z^{T} in degC
$T_{y,2}^{\mathrm{N}}$	65	Nominal temp. at $2\,F_z^{\mathrm{T}}$ in degC
T_y^0	17	Lower temp. boundary at F_z^{T} in degC
T_y^∞	100	Upper temp. boundary at F_z^{T} in degC
Initial slope dF_y^0		
$dF_{y,\mathrm{N}}^{\mathrm{T}}$	107500	Initial slope at $T_{y,1}^{\mathrm{N}}$ in N
$dF_{y,0}^{\mathrm{T}}$	191000	Initial slope at T_y^0 in N
$dF_{y,\infty}^{\mathrm{T}}$	105000	Initial slope at T_y^∞ in N
Maximal force $F_y^{\max}$		
$F_{y,\mathrm{N}}^{\mathrm{T}}$	6875	Maximum force at $T_{y,1}^{\mathrm{N}}$ and F_z^{T} in N
$F_{y,0}^{\mathrm{T}}$	5325	Force boundary at T_y^0 and F_z^{T} in N
$F_{y,\infty}^{\mathrm{T}}$	5675	Force boundary at T_y^∞ and F_z^{T} in N
Position of maximal force $s_y^{\max}$		
$s_{y,\mathrm{N}}^{\mathrm{T}}$	0.138	Maximum position at $T_{y,1}^{\mathrm{N}}$ and F_z^{T} in -
$s_{y,0}^{\mathrm{T}}$	0.065	Position boundary at T_y^0 and F_z^{T} in -
$s_{y,\infty}^{\mathrm{T}}$	0.128	Position boundary at T_y^∞ and F_z^{T} in -

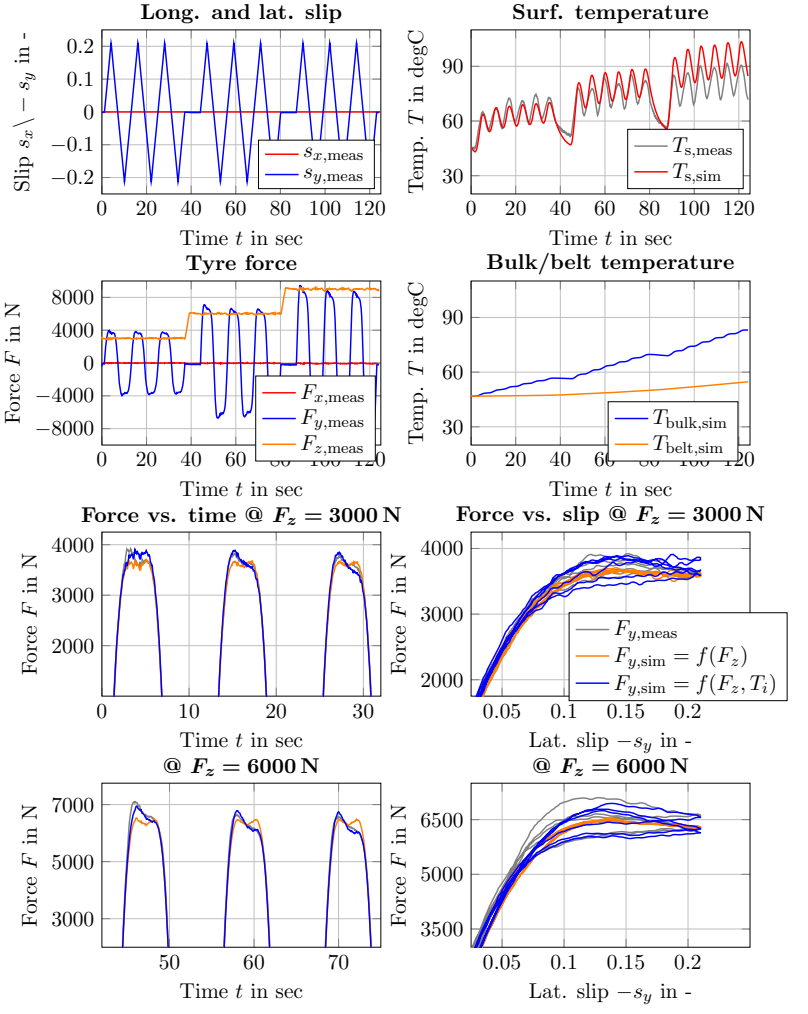

Figure D.3.: Validation of the temperature enhanced TMeasy tyre model in lateral direction; the two upper left plots characterise the target values, including the measured forces, while in the upper two right graphs the measured and simulated temperatures are given; the four bottom plots represent the force comparison of the standard versus the enhanced TMeasy tyre model based on research on the UR3 tyre

Table D.3.: Extended model parameter based on temperature influence in longitudinal direction for the Uniroyal Rainsport3 255/50 R19 107Y tyre

Parameter	Value	Description
General		
F_z^{T}	4500	Temperature based nominal tyre load in N
$T_{x,1}^{\mathrm{N}}$	52	Nominal temp. at F_z^{T} in degC
$T_{x,2}^{\mathrm{N}}$	58	Nominal temp. at $2\,F_z^{\mathrm{T}}$ in degC
T_x^0	17	Lower temp. boundary at F_z^{T} in degC
T_x^∞	92	Upper temp. boundary at F_z^{T} in degC
Initial slope dF_x^0		
$dF_{x,\mathrm{N}}^{\mathrm{T}}$	146500	Initial slope at $T_{x,1}^{\mathrm{N}}$ in N
$dF_{x,0}^{\mathrm{T}}$	200000	Initial slope at T_x^0 in N
$dF_{x,\infty}^{\mathrm{T}}$	140000	Initial slope at T_x^∞ in N
Maximal force $F_x^{\max}$		
$F_{x,\mathrm{N}}^{\mathrm{T}}$	5525	Maximum force at $T_{x,1}^{\mathrm{N}}$ and F_z^{T} in N
$F_{x,0}^{\mathrm{T}}$	4475	Force boundary at T_x^0 and F_z^{T} in N
$F_{x,\infty}^{\mathrm{T}}$	4225	Force boundary at T_x^∞ and F_z^{T} in N
Position of maximal force $s_x^{\max}$		
$s_{x,\mathrm{N}}^{\mathrm{T}}$	0.1075	Maximum position at $T_{x,1}^{\mathrm{N}}$ and F_z^{T} in -
$s_{x,0}^{\mathrm{T}}$	0.065	Position boundary at T_x^0 and F_z^{T} in -
$s_{x,\infty}^{\mathrm{T}}$	0.097	Position boundary at T_x^∞ and F_z^{T} in -

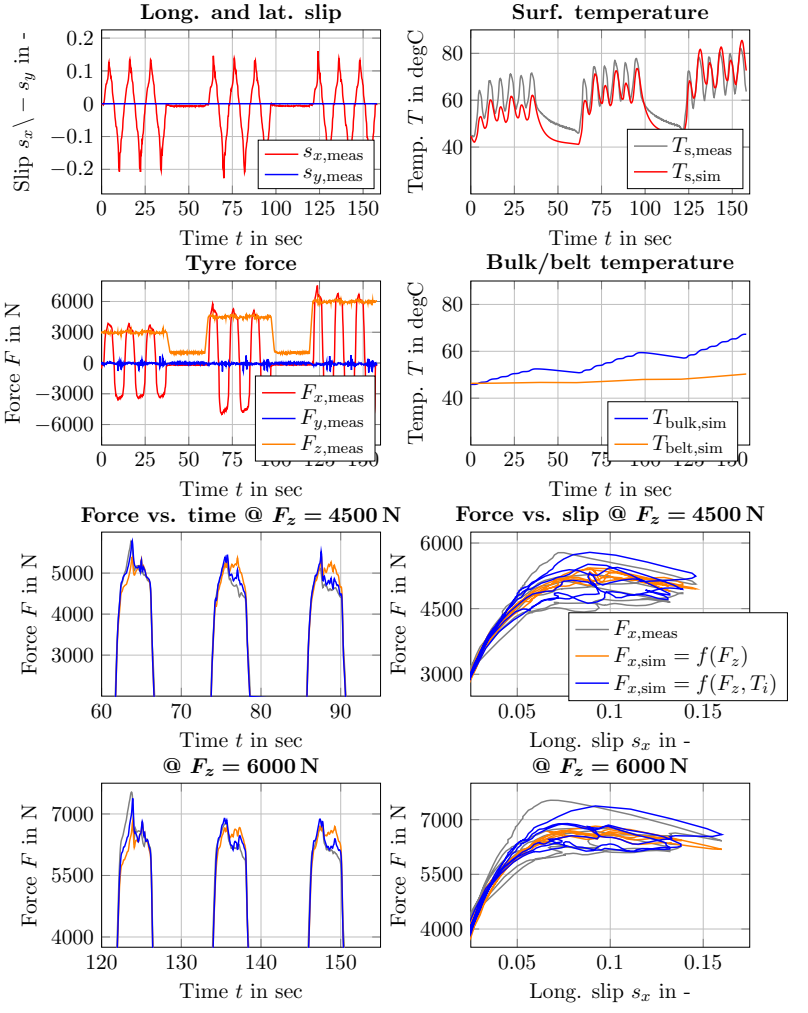

Figure D.4.: Validation of the temperature enhanced TMeasy tyre model in longitudinal direction; the two upper left plots characterise the target values, including the measured forces, while in the upper two right graphs the measured and simulated temperatures are given; the four bottom plots represent the force comparison of the standard versus the enhanced TMeasy tyre model based on research on the UR3 tyre

D.2. Pirelli Pzero 245/40 R20 99W

Table D.4.: Tyre temperature model parameter - PP0 tyre; subdivided into general, tyre-based and optimised values

Parameter	Value	Description
General		
$c_{p,\mathrm{steel}}$	450	Specific heat capacity steel in J/(kg K)
$c_{p,\mathrm{SBR}}$	1800	Specific heat capacity SBR in J/(kg K)
$c_{p,\mathrm{belt}}$	1125	Specific heat capacity belt in J/(kg K)
λ_{steel}	10	Thermal conductivity steel in W/(m K)
λ_{SBR}	0.275	Thermal conductivity SBR in W/(m K)
$h_{\mathrm{b\text{-}i}}$	1	Heat transfer coeff. filling medium in W/(m^2 K)
$c_{\mathrm{s},1}$	0.3	Scaling value contact patch, lower boundary in -
$c_{\mathrm{s},2}$	0.8	Scaling value contact patch, upper boundary in -
Tyre based		
s_{circ}	2.227	Tyre circumference in m
w_{t}	0.245	Tyre width in m
A_{t}	0.5457	Tyre tread area in m^2
g_f	0.822	Groove factor in -
m_{tyre}	7.5	Mass of tyre tread (without tyre walls) in kg
m'_{SBR}	0.33	Rubber SBR mass in kg/mm
d_{belt}	5	Thickness belt (steel/SBR) in mm
d_{SBR}	2	Thickness SBR without profile in mm
Optimised		
$h'_{\mathrm{s\text{-}r}}$	492.8	Heat transfer coefficient surface-road in W/(m^2 K)
h_0	3.63	Speed independent value of $h_{\mathrm{t\text{-}a}}$ in W/(m^2 K)
h_{v}	2.98	Speed dependent value of $h_{\mathrm{t\text{-}a}}$ in (W/(m^2 K)) / (m/s)
p_z	0.0024	Dimensionless scaling value due hysteresis in -
T^{N}	90.17	Power distributed nominal temperature in degC
δ_{s}	0.26	Thickness of tyre surface layer in mm

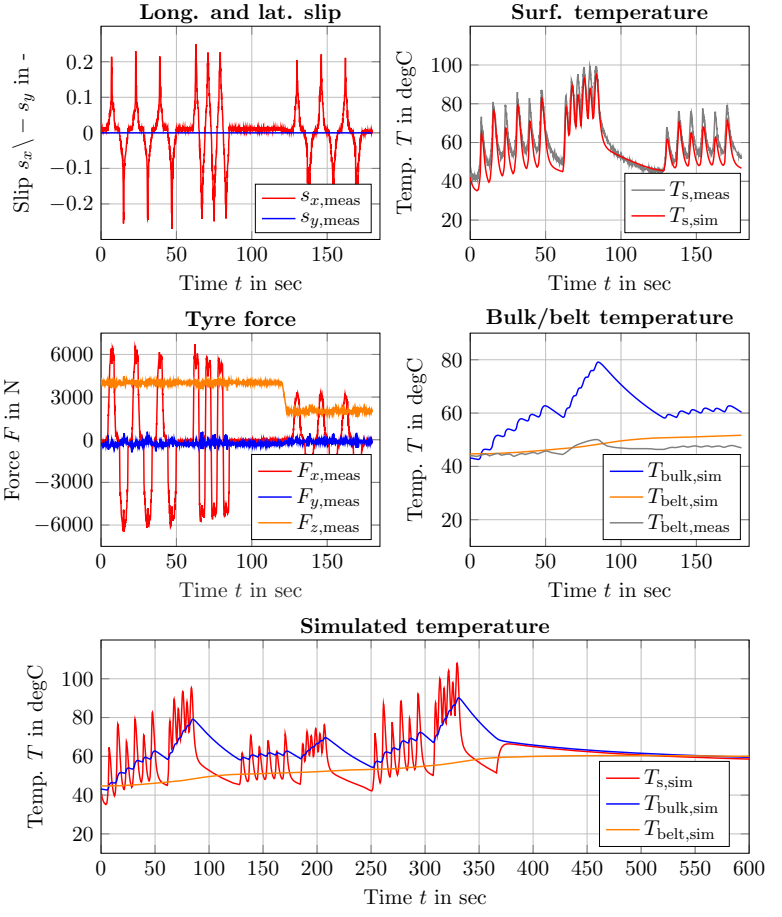

Figure D.5.: Validation of the parameterised temperature model based on the Pirelli Pzero 245/40 R20 99W tyre and a steady-state longitudinal manoeuvre; the upper left plot shows the slip target whereby the measured forces are given in the middle left plot; the upper right plot shows the measured and simulated surface temperature, whereas in the middle, the belt and bulk layer temperatures are displayed; note that for better result presentation, the upper four plots only show a section of the overall manoeuvre; the bottom plot presents the simulated tyre layer temperature behaviour, including the cooling process of the whole manoeuvre

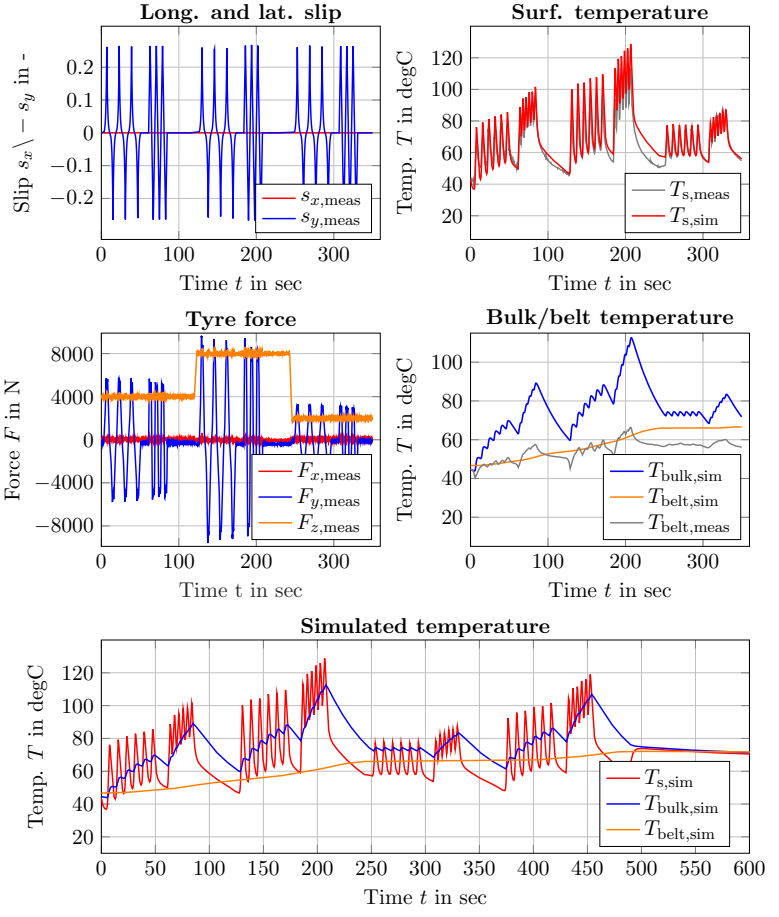

Figure D.6.: Validation of the parameterised temperature model based on tyre Pirelli Pzero 245/40 R20 99W and a steady-state lateral manoeuvre; the upper left plot shows the slip target whereby the measured forces are given in the middle left plot; the upper right plot shows the measured and simulated surface temperature, whereas in the middle, the belt and bulk layer temperatures are displayed; note that for better result presentation, the upper four plots only show a section of the overall manoeuvre; the bottom plot presents the simulated tyre layer temperature behaviour, including the cooling process of the whole manoeuvre

Table D.5.: Extended model parameter based on the temperature influence in lateral direction for the Pirelli Pzero 245/40 R20 99W tyre

Parameter	Value	Description
General		
F_z^{T}	4000	Temperature based nominal tyre load in N
$T_{y,1}^{\mathrm{N}}$	76	Nominal temp. at F_z^{T} in degC
$T_{y,2}^{\mathrm{N}}$	78	Nominal temp. at $2\,F_z^{\mathrm{T}}$ in degC
T_y^0	46	Lower temp. boundary at F_z^{T} in degC
T_y^∞	106	Upper temp. boundary at F_z^{T} in degC
Initial slope dF_y^0		
$dF_{y,0}^{\mathrm{T}}$	107500	Initial slope at T_y^0 in N
$dF_{y,\mathrm{N}}^{\mathrm{T}}$	97500	Initial slope at $T_{y,1}^{\mathrm{N}}$ in N
$dF_{y,\infty}^{\mathrm{T}}$	95000	Initial slope at T_y^∞ in N
Maximal force $F_y^{\max}$		
$F_{y,\mathrm{N}}^{\mathrm{T}}$	5490	Maximum force at $T_{y,1}^{\mathrm{N}}$ and F_z^{T} in N
$F_{y,0}^{\mathrm{T}}$	4690	Force boundary at T_y^0 and F_z^{T} in N
$F_{y,\infty}^{\mathrm{T}}$	4690	Force boundary at T_y^∞ and F_z^{T} in N
Position of maximal force $s_y^{\max}$		
$s_{y,\mathrm{N}}^{\mathrm{T}}$	0.125	Maximum position at $T_{y,1}^{\mathrm{N}}$ and F_z^{T} in -
$s_{y,0}^{\mathrm{T}}$	0.090	Position boundary at T_y^0 and F_z^{T} in -
$s_{y,\infty}^{\mathrm{T}}$	0.120	Position boundary at T_y^∞ and F_z^{T} in -

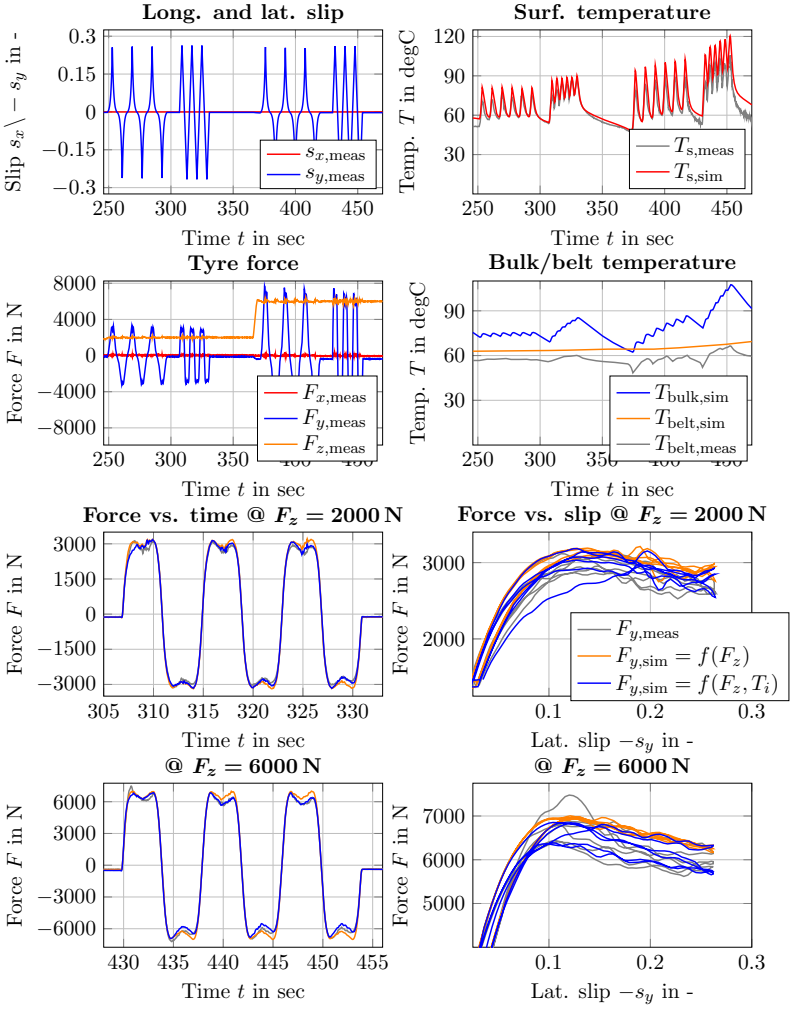

Figure D.7.: Validation of the temperature enhanced TMeasy tyre model in lateral direction; the two upper left plots show the target values, including the measured forces, while in the upper two right graphs the measured and simulated temperatures are given; the four bottom plots represent the force comparison of the standard versus the enhanced TMeasy tyre model based on research on the PP0 tyre

Table D.6.: Extended model parameter based on the temperature influence in longitudinal direction for the Pirelli Pzero 245/40 R20 99W tyre

Parameter	Value	Description
General		
F_z^{T}	4000	Temperature based nominal tyre load in N
$T_{x,1}^{\mathrm{N}}$	68	Nominal temp. at F_z^{T} in degC
$T_{x,2}^{\mathrm{N}}$	70	Nominal temp. at $2\,F_z^{\mathrm{T}}$ in degC
T_x^0	33	Lower temp. boundary at F_z^{T} in degC
T_x^∞	103	Upper temp. boundary at F_z^{T} in degC
Initial slope dF_x^0		
$dF_{x,0}^{\mathrm{T}}$	195000	Initial slope at T_x^0 in N
$dF_{x,\mathrm{N}}^{\mathrm{T}}$	155000	Initial slope at $T_{x,1}^{\mathrm{N}}$ in N
$dF_{x,\infty}^{\mathrm{T}}$	145000	Initial slope at T_x^∞ in N
Maximal force $F_x^{\max}$		
$F_{x,\mathrm{N}}^{\mathrm{T}}$	5950	Maximum force at $T_{x,1}^{\mathrm{N}}$ and F_z^{T} in N
$F_{x,0}^{\mathrm{T}}$	5450	Force boundary at T_x^0 and F_z^{T} in N
$F_{x,\infty}^{\mathrm{T}}$	4950	Force boundary at T_x^∞ and F_z^{T} in N
Position of maximal force $s_x^{\max}$		
$s_{x,\mathrm{N}}^{\mathrm{T}}$	0.090	Maximum position at $T_{x,1}^{\mathrm{N}}$ and F_z^{T} in -
$s_{x,0}^{\mathrm{T}}$	0.055	Position boundary at T_x^0 and F_z^{T} in -
$s_{x,\infty}^{\mathrm{T}}$	0.080	Position boundary at T_x^∞ and F_z^{T} in -

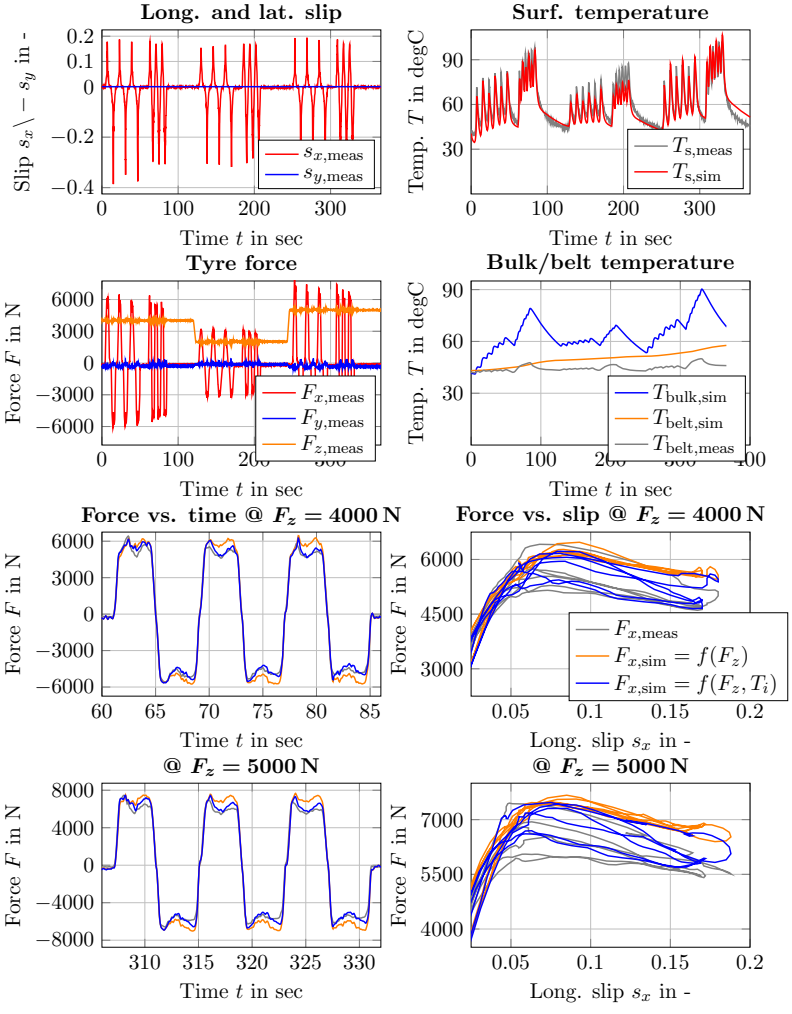

Figure D.8.: Validation of the temperature-enhanced TMeasy tyre model in longitudinal direction; the two upper left plots characterise the target values, including the measured forces, while in the upper two right graphs the measured and simulated temperatures are given; the four bottom plots represent the force comparison of the standard versus the enhanced TMeasy tyre model based on research on the PP0 tyre

List of Figures

List of Tables

Bibliography

[Acosta et al., 2018] Acosta, M., Kanarachos, S., & Blundell, M. (2018). Virtual tyre force sensors: An overview of tyre model-based and tyre model-less state estimation techniques. *Proceedings of the Institution of Mechanical Engineers, Part D: Journal of Automobile Engineering*, 232(14), 1883–1930. DOI: 10.1177/0954407017728198.

[Ammon, 2005] Ammon, D. (2005). Vehicle dynamics analysis tasks and related tyre simulation challenges. *Vehicle System Dynamics*, 43(Issue sup1), 30–47. DOI: 10.1080/00423110500141003.

[Angrick et al., 2014] Angrick, C., van Putten, S., & Prokop, G. (2014). Influence of Tire Core and Surface Temperature on Lateral Tire Characteristics. *SAE International Journal of Passenger Cars - Mechanical Systems*, 7(2), 468–481. DOI: 10.4271/2014-01-0074.

[Anupam et al., 2013] Anupam, K., Srirangam, S. K., Scarpas, A., & Kasbergen, C. (2013). Influence of Temperature on Tire - Pavement Friction: Analyses. *Transportation Research Record*, 2369(1), 114–124. DOI: 10.3141/2369-13.

[AVL, 2019] AVL (2019). AVL List GmbH. `https://www.avl.com/`. Accessed on 26 April 2019.

[Baffet et al., 2006] Baffet, G., Charara, A., & Stephant, J. (2006). Sideslip angle, lateral tire force and road friction estimation in simulations and experiments. In *2006 IEEE Conference on Computer Aided Control System Design, 2006 IEEE International Conference on Control Applications, 2006 IEEE International Symposium on Intelligent Control* (pp. 903–908). DOI: 10.1109/CACSD-CCA-ISIC.2006.4776765.

[Bernsteiner, 2016] Bernsteiner, S. (2016). *Integration of Advanced Driver Assistance Systems on Full-Vehicle Level* . PhD thesis, Graz University of Technology, Graz, Austria. ISBN: 978-3-85125-468-6.

[Besselink, 2000] Besselink, I. J. M. (2000). *Shimmy of Aircraft Main Landing Gears*. PhD thesis, Technische Universiteit Delft, Delft, Netherlands. ISBN: 90-9014104-9.

[Bhoraskar & Sakthivel, 2017] Bhoraskar, A. & Sakthivel, P. (2017). A review and a comparison of Dugoff and modified Dugoff formula with Magic formula. In *2017 International Conference on Nascent Technologies in Engineering (ICNTE)* (pp. 1–4). DOI: 10.1109/ICNTE.2017.7947898.

[Böttinger, 2018] Böttinger, S. (2018). Hohenheimer Reifenmodell. `https://reifenmodell.uni-hohenheim.de/`. Accessed on 19 November 2018.

[Braess & Seiffert, 2013] Braess, H. H. & Seiffert, U. (2013). *Vieweg Handbuch Kraftfahrzeugtechnik*. Springer Vieweg, 7 edition. DOI: 10.1007/978-3-658-01691-3.

[Braghin et al., 2006] Braghin, F., Cheli, F., Melzi, S., & Resta, F. (2006). Tyre

Wear Model: Validation and Sensitivity Analysis. *Meccanica*, 41(2), 143–156. DOI: 10.1007/s11012-005-1058-9.

[Brinkmeier et al., 2008] Brinkmeier, M., Nackenhorst, U., Biermann, J., & Von Estorff, O. (2008). Simulation and analysis of tire road noise, finite element results and validation. *The Journal of the Acoustical Society of America*, 123, 3673. DOI: 10.1121/1.2935021.

[Büttner et al., 2015] Büttner, F., Unterreiner, M., & Bortolussi, P. (2015). An effective method to identify thermodynamic tire characteristics through driving maneuvers. In M. Bargende, H.-C. Reuss, & J. Wiedemann (Eds.), *15. Internationales Stuttgarter Symposium: Automobil- und Motorentechnik* (pp. 921–936). Wiesbaden: Springer Fachmedien Wiesbaden. DOI: 10.1007/978-3-658-08844-6-62.

[Calabrese et al., 2015] Calabrese, F., Baecker, M., Galbally, C., & Gallrein, A. (2015). A Detailed Thermo-Mechanical Tire Model for Advanced Handling Applications. *SAE Int. J. Passeng. Cars - Mech. Syst.*, 8, 501–511. DOI: 10.4271/2015-01-0655.

[Campolongo et al., 2000] Campolongo, F., Saltelli, A., Sorensen, T., & Tarantola, S. (2000). *Hitchhiker's Guide to Sensitivity Analysis*. John Wiley and Sons. Sensitivity Analysis, Chapter 2.

[Chae, 2006] Chae, S. (2006). *Nonlinear finite element modeling and analysis of truck tire*. PhD thesis, Pennsylvania State University, Pennsylvania, United States of America.

[Corollaro, 2014] Corollaro, A. (2014). *Essentiality of Temperature Management while Modeling and Analyzing Tires Contact Forces*. PhD thesis, Universita degli Studi di Napoli Federico II, Ingegneria Industriale.

[cosin, 2018a] cosin, s. s. (2018a). cosin scientific software. `https://www.cosin.eu/`. Accessed on 19 November 2018.

[cosin, 2018b] cosin, s. s. (2018b). FTire-Flexible Structure Tire Model. `https://www.cosin.eu/wp-content/uploads/ftire_model.pdf`. Accessed on 19 November 2018.

[Dang & Guo, 2011] Dang, L. & Guo, K. (2011). UniTire steady state model: Overview and applications. In *2011 3rd International Conference on Advanced Computer Control* (pp. 341–345). DOI: 10.1109/ICACC.2011.6016428.

[De Rosa et al., 2008] De Rosa, R., Di Stazio, F., Giordano, D., Russo, M., & Terzo, M. (2008). ThermoTyre: tyre temperature distribution during handling manoeuvres. *Vehicle System Dynamics*, 46(9), 831–844. DOI: 10.1080/00423110701684579.

[Dessort et al., 2016] Dessort, R., Chucholowski, C., & Rill, G. (2016). Parametrical Approach for Modeling of Tire Forces and Torques in TMeasy 5. In *16. Internationales Stuttgarter Symposium, Proceedings* (pp. 435–449). DOI: 10.1007/978-3-658-13255-2.

[Dickinson & Gelinas, 1976] Dickinson, R. P. & Gelinas, R. J. (1976). Sensitivity analysis of ordinary differential equation systems – A direct method. *Journal of Computational Physics*, 21(2), 123 – 143. DOI: 10.1016/0021-9991(76)90007-3.

[Ding & Taheri, 2010] Ding, N. & Taheri, S. (2010). A Modified Dugoff Tire Model for Combined-slip Forces. *Tire Science and Technology*, 38(3), 228–244. DOI: 10.2346/1.3481696.

[Dugoff et al., 1970] Dugoff, H., Fancher, P. S., & Segel, L. (1970). An Analysis of Tire Traction Properties and Their Influence on Vehicle Dynamic Performance. In *International Automobile Safety Conference*: SAE International. DOI: 10.4271/700377.

[Einsle, 2010] Einsle, S. (2010). *Analyse und Modellierung des Reifenübertragungsverhaltens bei transienten und extremen Fahrmanövern*. PhD thesis, Technische Universität Dresden, Dresden, Germany.

[Février & Fandard, 2008] Février, P. & Fandard, G. (2008). Thermal and mechanical tyre modelling for handling simulation. *ATZ worldwide*, 110(5), 26–31. DOI: 10.1007/BF03225006.

[Frauenhofer-Institut, 2018] Frauenhofer-Institut (2018). CD-Tire - Scalable Tire Model. `https://www.itwm.fraunhofer.de/en/departments/mdf/cdtire.html#tabpanel-1`. Accessed on 19 November 2018.

[FTG, 2019] FTG (2019). Radaufhängungsprüfstand. `https://www.tugraz.at/institute/ftg/forschung/labor/fahrwerkspruefstand/`. Accessed on 02 April 2019.

[Gallrein & Bäcker, 2007] Gallrein, A. & Bäcker, M. (2007). CDTire: a tire model for comfort and durability applications. *Vehicle System Dynamics*, 45(sup1), 69–77. DOI: 10.1080/00423110801931771.

[Ghoreishy, 2006] Ghoreishy, M. H. R. (2006). Finite element analysis of steady rolling tyre with slip angle: effect of belt angle. *Plastics, Rubber and Composites*, 35(2), 83–90. DOI: 10.1179/174328906X79905.

[Ghoreishy, 2009] Ghoreishy, M. H. R. (2009). Finite Element Modelling of the Steady Rolling of a Radial Tyre with Detailed Tread Pattern. In *Iranian Polymer Journal*, volume 18: Iran Polymer and Petrochemical Institute. ISSN: 641-650.

[Giashi et al., 2015] Giashi, A., Falk, K., & Kaliske, M. (2015). *Tire Simulations Using a Slip Velocity, Pressure and Temperature Dependent Friction Law*. DOI: 10.13140/RG.2.1.2678.9203.

[GIMP, 2019] GIMP, T. (2019). GNU Image Manipulation Program. `https://www.gimp.org/`. Accessed on 12 March 2019.

[Gipser et al., 1997] Gipser, M., Hofer, R., & Lugner, P. (1997). Dynamical Tyre Forces Response to Road Unevennesses. *Vehicle System Dynamics*, 27(sup001), 94–108. DOI: 10.1080/00423119708969647.

[Gnadler et al., 2005] Gnadler, R., Huinink, H., Frey, M., Mundl, R., Sommer, J., Unrau, H.-J., & Wies, B. (2005). Kraftschluss messungen auf Schnee mit dem Reifen-Innentrommel-Prüfstand. *ATZ - Automobiltechnische Zeitschrift*, 107(3), 198–207. DOI: 10.1007/BF03221700.

[Guo & Lu, 2007] Guo, K. & Lu, D. (2007). UniTire: unified tire model for vehicle dynamic simulation. *Vehicle System Dynamics*, 45(sup1), 79–99. DOI: 10.1080/00423110701816742.

[Guo et al., 2005a] Guo, K., Lu, D., Chen, S.-k., Lin, W. C., & Lu, X.-p. (2005a). The UniTire model: a nonlinear and non-steady-state tyre model for vehicle dynamics simulation. *Vehicle System Dynamics*, 43(sup1), 341–358. DOI: 10.1080/00423110500140690.

[Guo et al., 2005b] Guo, K., Ye, Z., Dang, L., Shih-ken, C., & William, L. (2005b). A study on speed-dependent tyre-road friction and its effect on the force and the moment. *Vehicle System Dynamics*, 43(sup1), 329–340. DOI: 10.1080/00423110500140815.

[Hackl et al., 2016a] Hackl, A., Hirschberg, W., Lex, C., & Rill, G. (2016a). Experimental validation of a non-linear first-order tyre dynamics approach. In *The Dynamics of Vehicles on Roads and Tracks*, volume 24 (pp. 443).: CRC Press. ISBN: 978-1-138-02885-2.

[Hackl et al., 2016b] Hackl, A., Hirschberg, W., Lex, C., & Rill, G. (2016b). Experimental validation of the Maxwell model for description of transient tyre forces. In M. Bargende, H.-C. Reuss, & J. Wiedemann (Eds.), *16. Internationales Stuttgarter Symposium* (pp. 401 – 418). Wiesbaden: Springer Fachmedien Wiesbaden. ISBN: 978-3-658-13255-2.

[Hackl et al., 2016c] Hackl, A., Hirschberg, W., Lex, C., & Rill, G. (2016c). Tyre Dynamics: Model Validation and Parameter Identification. In C. Andreescu & A. Clenci (Eds.), *Proceedings of the European Automotive Congress EAEC-ESFA 2015* (pp. 219–232). Cham: Springer International Publishing. ISBN: 978-3-319-27276-4.

[Hackl et al., 2017a] Hackl, A., Hirschberg, W., Lex, C., & Rill, G. (2017a). Parameterization Process of the Maxwell Model to Describe the Transient Force Behavior of a Tire. In *WCX 17: SAE World Congress Experience*: SAE International. DOI: 10.4271/2017-01-1505.

[Hackl et al., 2017b] Hackl, A., Hirschberg, W., Lex, C., & Rill, G. (2017b). Tyre Type Dependent Transient Force Behaviour by Means of a Maxwell Model. In *The Dynamics of Vehicles on Roads and Tracks - Spiryagin et al. (Eds)*, volume 25: Taylor & Francis Group. ISBN: 978-1-138-03571-3.

[Hackl et al., 2017c] Hackl, A., Scherndl, C., Hirschberg, W., & Lex, C. (2017c). Experimental Validation of Various Temperature Models for Semi-Physical Tyre Model Approaches. *IOP Conference Series: Materials Science and Engineering*, 252, 012009. DOI: 10.1088/1757-899x/252/1/012009.

[Hackl et al., 2018] Hackl, A., Scherndl, C., Hirschberg, W., & Lex, C. (2018). Experimental validation of different approaches for thermodynamic simulation of passenger car tyres. In M. Bargende, H.-C. Reuss, & J. Wiedemann (Eds.), *18. Internationales Stuttgarter Symposium* (pp. 1233–1247). Wiesbaden: Springer Fachmedien Wiesbaden. ISBN: 978-3-658-21194-3.

[Harrich et al., 2006] Harrich, A., Hirschberg, W., & Anton Angelov, T. (2006). Der neue dynamische Bremsen- und Radaufhängungsprüfstand an der TU Graz. In *brake.tech*: TÜV Süd.

[Hirschberg, 2009] Hirschberg, W. (2009). *TMsimple: A simple to use tyre model*. Technical report, Institute of Automotive Engineering, Graz University of Technology.

[Hirschberg et al., 2009] Hirschberg, W., Palcak, F., Rill, G., & Sotnik, J. (2009). Reliable vehicle dynamics simulation in spite of uncertain input data. In *EAEC 2009 Europe in the Second Century of Auto Mobility (CD)* (pp. 1–15).: Slovak Society of Automotive Engineers Bratislava. ISBN: 978-80-969243-8-7.

[Hirschberg et al., 2002] Hirschberg, W., Rill, G., & Weinfurter, H. (2002). User-Appropriate Tyre-Modelling for Vehicle Dynamics in Standard and Limit Situations. *Vehicle System Dynamics*, 38(2), 103–125. DOI: 10.1076/vesd.38.2.103.5620.

[Hirschberg & Waser, 2012] Hirschberg, W. & Waser, H. (2012). Kraftfahrzeugtechnik. Lecture notes, winter term 2012/13. Institute of Automotive Engineering, Graz University of Technology.

[Hirschberg et al., 2000] Hirschberg, W., Weinfurter, H., & Jung, C. (2000). *Ermittlung der Potenziale zur LKW-Stabilisierung durch Fahrdynamiksimulation*, (pp. 167–188). VDI Verlag GMBH: Deutschland.

[Holtschulze, 2000] Holtschulze, J. (2000). Die dynamischen Seitenkrafteigenschaften von Reifen und ihre Auswirkungen auf das Lenkverhalten. In *Fachtagung Fahrwerktechnik*: Haus der Technik e.V., München.

[Horn & Doudoumas, 2004] Horn, M. & Doudoumas, N. (2004). *Regelungstechnik - Rechnerunterstützter Entwurf zeitkontinuierlicher und zeitdiskreter Regelkreise*. München, Germany: Pearson Education Deutschland GmbH. ISBN: 3-8273-7059-0.

[Hou et al., 2018] Hou, Y., Zhang, H., Wu, J., Wang, L., & Xiong, H. (2018). Study on the Microscopic Friction Between Tire and Asphalt Pavement Based on Molecular Dynamics Simulation. *International Journal of Pavement Research and Technology*, 11(2), 205 – 212. DOI: 10.1016/j.ijprt.2017.09.001, In Honor of Professor James S. Lai.

[Hüsemann, 2011] Hüsemann, T. C. (2011). *Adaption von Labor-Reifenkennfeldern an reale Fahrbahnoberflächen*. PhD thesis, RWTH Aachen University. ISBM: 978-3-940374-51-6.

[IABG mbH, 2019] IABG mbH (2019). Industrieanlagen-Betriebsgesellschaft mbH. `https://www.iabg.de/`. Accessed on 30 January 2019.

[IAT Dynamics mbH, 2018] IAT Dynamics mbH (2018). RMOD-K overview. `https://www.rmod-k.com/`. Accessed on 19 November 2018.

[ISO Central Secretary, 2011] ISO Central Secretary (2011). *Road vehicles – Vehicle dynamics and road-holding ability – Vocabulary*. International Standard ISO 8855:2011(E), International Organization for Standardization, Geneva, CH.

[Jayasree et al., 2006] Jayasree, T., Predeep, P., Agarwal, R., & Saxena, N. (2006). Thermal Conductivity and Thermal Diffusivity of Thermoplastic Elastomeric Blends of Styrene Butadiene Rubber/High Density Polyethylene: Effect of Blend Ratio and Dynamic Crosslinking. *Trends in Applied Sciences Research*, 1, 278 – 291. DOI: 10.3923/tasr.2006.278.291.

[Kelly & Sharp, 2012] Kelly, D. P. & Sharp, R. S. (2012). Time-optimal control of the race car: influence of a thermodynamic tyre model. *Vehicle System Dynamics*, 50(4), 641–662. DOI: 10.1080/00423114.2011.622406.

[Kerschbaumer, 2017] Kerschbaumer, A. (2017). *Identifikation von nichtlinearen Reifeneigenschaften mittels Fahrzustandsbeobachtung*. PhD thesis, Graz University of Technology, Graz, Austria.

[Kindt et al., 2008] Kindt, P., Sas, P., & Desmet, W. (2008). Three-dimensional Ring Model for the Prediction of the Tyre Structural Dynamic Behaviour. In *23rd International Conference on Noise and Vibration Engineering 2008*: ISMA.

[Kindt et al., 2009] Kindt, P., Sas, P., & Desmet, W. (2009). Development and validation of a three-dimensional ring-based structural tyre model. *Journal of Sound and Vibration*, 326(3), 852 – 869. DOI: 10.1016/j.jsv.2009.05.019.

[Kistler GmbH, 2019] Kistler GmbH (2019). RoaDyn S625 sp Messrad für leichte PKWs. `https://www.kistler.com/de/produkt/type-9266a1`. Accessed on 02 April 2019.

[Klaas et al., 1999] Klaas, A., Van Oosten, J., Savi, C., Unrau, H., Bouhet, O., & Colinot, J. (1999). TIME, Tire Measurements - A new standard test procedure for stationary cornering measurements of tires. *VDI-Verlag*, 1494, 398. ISBN: 3180914947.

[Klell & Almbauer, 2015] Klell, M. & Almbauer, R. (2015). Höhere Thermodynamik. Lecture notes, Winter term 2015/16. Institute of Internal Combustion Engines and Thermodynamics, Graz University of Technology.

[Klueppel et al., 2011] Klueppel, M., Busse, L., & Boubakri, I. (2011). Friction master curves for rubber on dry and wet granite experiments and simulations. *KGK-Kautschuk Gummi Kunststoffe*, 64, 35–39.

[Kollreider, 2009] Kollreider, D. (2009). *Identifikation der Reifeneigenschaften als Grundlage zur Fahrdynamikbewertung*. PhD thesis, Graz University of Technology, Graz, Austria.

[Kuiper & Van Oosten, 2007] Kuiper, E. & Van Oosten, J. J. M. (2007). The PAC2002 advanced handling tire model. *Vehicle System Dynamics*, 45(sup1), 153–167. DOI: 10.1080/00423110701773893.

[Laermann, 1986] Laermann, F.-J. (1986). Seitenführungsverhalten von Kraftfahrzeugreifen bei schnellen Radlasänderungen. In *Fortschrittberichte VDI : Reihe 12, Verkehrstechnik, Fahrzeugtechnik* Düsseldorf, Germany: VDI-Verlag. ISBN: 318147312X; 9783181473122.

[Lang & Klueppel, 2017] Lang, A. & Klueppel, M. (2017). Influences of temperature and load on the dry friction behaviour of tire tread compounds in contact with rough granite. *Wear*, 380-381, 15–25. DOI: 10.1016/j.wear.2017.02.047.

[Leister, 2015] Leister, G. (2015). *Fahrzeugräder - Fahrzeugreifen, Entwicklung - Herstellung - Anwendung*, volume 2 of *Fahrzeugtechnik*. Springer Fachmedien Wiesbaden: Springer Vieweg. DOI: 10.1007/978-3-658-07464-7.

[Lex, 2015] Lex, C. (2015). *Estimation of the Maximum Coefficient of Friction between Tire and Road Based on Vehicle State Measurements*. PhD thesis, Graz University of Technology, Graz, Austria. ISBN: 978-3-85125-422-8.

[Lex & Eichberger, 2011] Lex, C. & Eichberger, A. (2011). Der Reifen als Einflussgröße für Fahrerassistenzsysteme und Fahrdynamikregelungen. In *OEAMTC Symposium Reifen und Fahrwerk* Vienna.

[Lex & Hirschberg, 2015] Lex, C. & Hirschberg, W. (2015). Tyre - The Essential Component for Traction and Vehicle Dynamics. In *Proceedings of 15th European All-Wheel Drive Congress (EAWD)* Magna Powertrain & Magna Steyr, 16-17 April 2015, Graz, Austria.

[Lines, 1991] Lines, J. A. (1991). *The Suspension Characteristics of Agricultural Tractor Tyres*. PhD thesis, Cranfield Institute of Technology, Silsoe College, Cranfield, England.

[Lugner et al., 2005] Lugner, P., Pacejka, H., & Plöchl, M. (2005). Recent advances in tyre models and testing procedures. *Vehicle System Dynamics*, 43(6-7), 413–426. DOI: 10.1080/00423110500158858.

[Lugner & Plöchl, 2009] Lugner, P. & Plöchl, M. (2009). Tyre Model Performance Test. `http://http://tmpt.tuwien.ac.at//`. Accessed on 31 January 2019.

[Lundahl et al., 2011] Lundahl, K., Åslund, J., & Nielsen, L. (2011). *Investigating Vehicle Model Detail for Close to Limit Maneuvers Aiming at Optimal Control*.

[MakeltFrom, 2018] MakeltFrom (2018). Styrene Butadiene Rubber (SBR, Buna-S). `https://www.makeitfrom.com/material-properties/Styrene-Butadiene-Rubber-SBR-Buna-S`. Accessed on 23 February 2019.

[Mizuno et al., 2005] Mizuno, M., Sakai, H., Oyama, K., & Isomura, Y. (2005). Development of a tyre force model incorporating the influence of the tyre surface temperature. *Vehicle System Dynamics*, 43(sup1), 395–402. DOI: 10.1080/00423110500140187.

[MTS Systems, 2003] MTS Systems (2003). *MTS Flat-Trac® III CT Tire Test System*. MTS Systems Corporation. `http://www.mts.com`.

[MTS Systems, 2019] MTS Systems (2019). Flat-Trac Tire Testing Systems. `https://www.mts.com/en/products/producttype/test-systems/simulation-systems/tire/flat-trac/index.htm`. Accessed on 30 January 2019.

[Müller-Wondorf, 2017] Müller-Wondorf, R. (2017). Elektrooffensive mit Wenn und Aber. *VDI Nachrichten - Technik, Wirtschaft, Gesellschaft*, Volume 37, Page 14. Published: 15. September 2017.

[Nast et al., 1991] Nast, R., Teubert, C., & Willumeit, H. P. (1991). Messungen der Übertragungseigenschaften von Luftreifen bei zeitlich veränderten Schräglaufschaufeln und anschließende Nachbildung dieser Größen durch Approximationsgleichungen. *VDI Berichte*, 916, 329–344.

[Nuessle, 2003] Nuessle, M. (2003). *Ermittlung von Reifeneigenschaften im realen Fahrbetrieb*. PhD thesis, RWTH Aachen University. Aachen 2003. (Berichte aus der Fahrzeugtechnik.) Fak. für Maschinenbau.

[Oertel, 2018] Oertel, C. (2018). RMOD-K Formula Documentation. `https://www.rmod-k.com/formula`. Accessed on 19 November 2018.

[Oertel & Fandre, 2001] Oertel, C. & Fandre, A. (2001). Das Reifenmodellsystem RMOD-K. *ATZ - Automobiltechnische Zeitschrift*, 103(11), 1074–1079. DOI: 10.1007/BF03223462.

[Pacejka, 2012] Pacejka, H. B. (2012). *Tire and Vehicle Dynamics*. Oxford, United Kingdom: Butterworth-Heinemann, Elsevier Ltd. ISBN: 978-0-08-097016-5.

[Pacejka & Bakker, 1992] Pacejka, H. B. & Bakker, E. (1992). The magic formula tyre model. *Vehicle System Dynamics*, 21(sup001), 1–18. DOI: 10.1080/00423119208969994.

[Pacejka & Besselink, 1997] Pacejka, H. B. & Besselink, I. J. M. (1997). Magic Formula Tyre Model with Transient Properties. *Vehicle System Dynamics*, 27(sup001), 234–249. DOI: 10.1080/00423119708969658.

[Parczewski, 2013] Parczewski, K. (2013). Effect of the tyre inflation pressure on the vehicle dynamics during braking manoeuvre. *Eksploatacja i Niezawodnosc - Maintenance and Reliability*, 15 (2), 134–139.

[Pearson et al., 2016] Pearson, M., Blanco-Hague, O., & Pawlowski, R. (2016). TameTire: Introduction to the Model. *Tire science and technology, TSTCA*, 44(2), 102–119. ISSN: 0090-8657.

[Persson et al., 2005] Persson, B. N. J., Albohr, O., Tartaglino, U., Volokitin, A., & Tosatti, E. (2005). On the nature of surface roughness with application to contact mechanics, sealing, rubber friction and adhesion. *Journal of Physics: Condensed Matter*, 17(1), R1. DOI: 10.1088/0953-8984/17/1/R01.

[Rauh, 2003] Rauh, J. (2003). Virtual Development of Ride and Handling Characteristics for Advanced Passenger Cars. In *Vehicle System Dynamics*, volume 40 (pp. 135–155).: Taylor & Francis. DOI: 10.1076/vesd.40.1.135.15876.

[Rauh & Mössner-Beigel, 2008] Rauh, J. & Mössner-Beigel, M. (2008). Tyre simulation challenges. In *Vehicle System Dynamics*, volume 46 (pp. 49–62).: Taylor & Francis. DOI: 10.1080/00423110701882298.

[Rill, 1994] Rill, G. (1994). *Simulation von Kraftfahrzeugen*. Vieweg-Verlag.

[Rill, 2006] Rill, G. (2006). First Order Tire Dynamics. In *III European Conference on Computational Mechanics, Solid, Structures and Coupled Problems in Engineering* (pp. 776 –776). Dordrecht, Portugal. ISBN: 978-1-4020-5370-2.

[Rill, 2012] Rill, G. (2012). *Road Vehicle Dynamics, Fundamentals and Modeling*. Boca Raton, United States: CRC Press, Taylor & Francis Group. ISBN: 978-1-4398-9744-7.

[Rill, 2015] Rill, G. (2015). *TMeasy Extended Documentation*, version 5.0.1 edition.

[Rill, 2017] Rill, G. (2017). Sophisticated but Quite Simple Contact Calculation for Handling Tire Models. In Ambrosio J., Schiehlen W., Pombo J. (Ed.), *EUROMECH COLLOQUIUM 578, Rolling Contact Mechanics for Multibody System Dynamics* Funchal, Madeira, Portugal,.

[Rill, 2018] Rill, G. (2018). TMeasy - Tire Model easy to use. `http://www.tmeasy.de/`. Accessed on 10 November 2018.

[Rill & Hirschberg, 2012] Rill, G. & Hirschberg, W. (2012). TMeasy Tyre Model. In C.-C.-G. e.V. (Ed.), *CCG - Tyre Models in Vehicle Dynamics*, number Seminar TV 4.08 in Transport- und Verkehrssysteme Vienna University of Technology.

[SAE, 2014] SAE, I. (2014). *Taxonomy and Definitions for Terms Related to On-Road Motor Vehicle Automated Driving Systems*. DOI: 10.4271/J3016_201401.

[Saxena et al., 1999] Saxena, N., Pradeep, P., GP, M., Thomas, S., Gustavsson, M., & Gustafsson, S. (1999). Thermal conductivity of styrene butadiene rubber compounds with natural rubber prophylactics waste as filler. *European Polymer Journal*, 35, 1687–1693. DOI: 10.1016/S0014-3057(98)00247-X.

[Schlippe & Dietrich, 1942] Schlippe, B. & Dietrich, R. (1942). Zur Mechanik des Luftreifens. In *Zentrale für wissenschaftliches Berichtwesen der Luftfahrtforschung (ZWB)* Berlin, Adlershof.

[Schmeitz et al., 2007] Schmeitz, A. J. C., Besselink, I. J. M., & Jansen, S. T. H. (2007). TNO MF-SWIFT. *Vehicle System Dynamics*, 45(sup1), 121–137. DOI: 10.1080/00423110701725208.

[Seewald, 2000] Seewald, A. (2000). Integrated Vehicle Control System Technology - Steering, Braking, Suspension, and Powertrain Systems. *Technology Review Journal*, Millennium Issue.

[Sharp & Jones, 1980] Sharp, R. S. & Jones, C. J. (1980). A Comparison of Tyre Representations in a Simple Wheel Shimmy Problem. *Vehicle System Dynamics*, 9(1), 45–57. DOI: 10.1080/00423118008968614.

[Sorniotti, 2009] Sorniotti, A. (2009). Tire Thermal Model for Enhanced Vehicle Dynamics Simulation. In *SAE Technical Paper*: SAE International. DOI: 10.4271/2009-01-0441.

[Svendenius & Wittenmark, 2003] Svendenius, J. & Wittenmark, B. (2003). Brush tire model with increased flexibility. In *2003 European Control Conference (ECC)* (pp. 1863–1868). DOI: 10.23919/ECC.2003.7085237.

[TNO Automotive Safety Sol., 2018] TNO Automotive Safety Sol. (2018). MF-Tyre/MF-Swift. `http://www.tassinternational.com/delft-tyre`. Accessed on 20 November 2018.

[TNO Delft Tyre, 2013] TNO Delft Tyre (2013). *MF-Tyre/MF-Swift 6.2 - Help Manual*. `http://www.delft-tyre.com`.

[Tremlett & Limebeer, 2016] Tremlett, A. J. & Limebeer, D. J. N. (2016). Optimal tyre usage for a Formula One car. *Vehicle System Dynamics*, 54(10), 1448–1473. DOI: 10.1080/00423114.2016.1213861.

[Unrau, 2013] Unrau, H.-J. (2013). *Der Einfluss der Fahrbahnoberflächenkrümmung auf den Rollwiderstand, die Cornering Stiffness und die Aligning Stiffness von Pkw-Reifen*. PhD thesis, KIT-Karlsruher Institut für Technologie. ISBN: 978-3-86644-983-1.

[Van der Auweraer et al., 2013] Van der Auweraer, H., Anthonis, J., De Bruyne, S., & Leuridan, J. (2013). Virtual engineering at work: the challenges for designing mechatronic products. *Engineering with Computers*, 29(3), 389 – 408. DOI: 10.1007/s00366-012-0286-6.

[Van Oosten, 2003] Van Oosten, J. (2003). Swift-tyre in simpack: for comfort, ride, durability and chassis control analysis. In *SIMPACK User Meeting* Freiburg im Breisgau.

[Van Oosten et al., 1997] Van Oosten, J. J. M., UNRAU, H.-J., RIEDEL, A., & BAKKER, E. (1997). TYDEX Workshop: Standardisation of Data Exchange in Tyre Testing and Tyre Modelling. *Vehicle System Dynamics*, 27(sup001), 272–288. DOI: 10.1080/00423119708969660.

[Waser, 2009] Waser, S. (2009). *Generierung der beanspruchungsrelevanten Belastungen von Nutzfahrzeugen mittels Reifen-, Fahrbahn- und Fahrzeugmodellen*. PhD thesis, Graz University of Technology, Graz, Austria.

[Weber & Persch, 1976] Weber, R. & Persch, H.-G. (1976). Frequency Response of Tires-Slip Angle and Lateral Force. In *1976 Automotive Engineering Congress and Exposition*: SAE International. DOI: 10.4271/760030.

[Williams et al., 1955] Williams, M. L., Landel, R. F., & Ferry, J. D. (1955). The Temperature Dependence of Relaxation Mechanisms in Amorphous Polymers and Other Glass-forming Liquids. *Journal of the American Chemical Society*, 77(14), 3701–3707.

[Witzel & Böttinger, 2014] Witzel, P. & Böttinger, S. (2014). Das Hohenheimer Reifenmodell - Weiterentwicklung zu einem dreidimensionalen Ansatz und dessen Validierung. In *72. Internationale Tagung Land.Technik, Agrartechnik im Dialog mit Politik und Gesellschaft*, volume 2226: VDI-Verlag. ISSN: 0083-5560.

[Xu et al., 2016] Xu, N., Guo, K., & Yang, Y. (2016). UniTire Model for Tire Corner-

ing Properties under Varying Traveling Velocities. In *SAE 2016 Commercial Vehicle Engineering Congress*: SAE International. DOI: 10.4271/2016-01-8037.

[Zamow, 1995] Zamow, J. (1995). Measurement of the tyre behaviour on different test rigs. *VDI-Verlag*, 1224, 43–60. ISSN: 0083-5560.

[Zegelaar, 1998] Zegelaar, P. W. A. (1998). *The dynamic response of tyres to brake torque variations and road unevennesses*. PhD thesis, Technische Universiteit Delft, Delft, Netherlands.

Monographic Series TU Graz

Reihe Fahrzeugtechnik

Vol. 1 Haymo Niederkofler

Analyse radselektiv eingreifender Fahrdynamikregelsysteme für die Anwendung in Elektromechanischen Corner-Modulen
2012
ISBN 978-3-85125-220-0

Vol. 2 Andrés Eduardo Rojas Rojas

Passenger Vehicles with In-Wheel Motors
2012
ISBN 978-3-85125-234-7

Vol. 3 Daniel Wallner

Experimental and Numerical Investigations on Brake Squeal
2013
ISBN 978-3-85125-269-9

Vol. 4 Alexander Harrich

CAD-basierte Methoden zur Unterstützung der Karosseriekonstruktion in der Konzeptphase
2015
ISBN 978-3-85125- 420-4

Vol. 5 Cornelia Lex

Maximum Tire-Road Friction Coefficient Estimation
2015
ISBN 978-3-85125-422-8

Vol. 6 Stefan Bernsteiner

Integration of Advanced Driver Assistance Systems on Full-Vehicle Level
2016
ISBN 978-3-85125-468-6

Monographic Series TU Graz

Reihe Fahrzeugtechnik

Vol. 7 Patrick Rossbacher

Beitrag integrierter Konzeptmodelle zur virtuellen Gesamtfahrzeugentwicklung in der frühen Entwurfsphase

2020
ISBN 978-3-85125-730-4

Vol. 8 Andreas Hackl

Enhanced Tyre Modelling for Vehicle Dynamics Control Systems

2020
ISBN 978-3-85125-728-1